Peptide Diversification Through Hypervalent Iodine-Mediated *o*-Quinone Chemistry

Dissertation

Submitted in partial fulfilment of the requirements for the degree of
Dr. rer. nat.

Prepared at the School of Mathematics and Natural Sciences

at the University of Wuppertal

Srashti Chaudhary

20 March 2026

This page intentionally left blank

This work was carried out under the supervision of Prof. Stefan F. Kirsch at the Institute of Organic Chemistry, University of Wuppertal, between August 2022 and January 2026.

Parts of this work have been published in the following articles:

- S. Chaudhary, H. Aldemir, S. F. Kirsch and A. Gómez-Suárez, *Bioinspired Diversification of Short Peptides via Tyrosine Umpolung*, **2026**.

Parts of this work have been presented at conferences:

- A communication poster titled "Site-Selective Tyrosine Modification using Hypervalent Iodine (V) Reagents" by S. Chaudhary, H. Aldemir, A. Gómez-Suárez, and S.F. Kirsch was presented at the **EWOC Conference 2025** in Basel, Switzerland.
- A communication poster titled "Site-Selective Tyrosine Modification using Hypervalent Iodine (V) Reagents" by S. Chaudhary, H. Aldemir, A. Gómez-Suárez, and S.F. Kirsch was presented at the **ESOC Conference 2025** in Copenhagen, Denmark.

Acknowledgements

First of all, I would like to thank my doctoral supervisor, Prof. Dr. Stefan F. Kirsch, for giving me the opportunity to pursue PhD in his research group. I am honoured to have worked on fascinating topics under his guidance. His mentorship inspired me to push the boundaries of my knowledge and pursue excellence in my work. Thank you for your guidance, encouragement, and invaluable contributions to my academic journey.

I would also like to thank Prof. Dr. Felix Strieth-Kalthoff for preparing the second review, as well as Prof. Dr. Fabian Mohr and Prof. Dr. Julia Bornhorst for their participation in my examination committee.

My sincere appreciation goes to the senior academic advisors of the Kirsch research group, Dr. Adrián Gómez-Suárez, Dr. Markus Roggel, Dr. Andreas F. Kotthaus, and Dr. Hülya Aldemir, for their insightful discussions and valuable scientific guidance. Their expertise and thoughtful input significantly contributed to the development of this research.

I sincerely thank the analytical team Ilka Polanz, Boris Ihmenkamp, and Andreas Siebert, for measuring numerous samples. Without their support, this work would not have been possible.

I am also grateful to Tanja Lohr and former administrative assistant Christine Schneidereit for their invaluable assistance with organizational and administrative matters, which greatly facilitated the smooth progress of my doctoral work.

I would like to express my gratitude to the current and former doctoral students of the Kirsch working group for making my time in the laboratory a truly special experience. I especially thank Michael Tapera and Hauke Junghans for the enjoyable time in the lab. I am particularly grateful to Michael Tapera for proofreading this work and for motivating me during challenging times in the lab. I also thank Timo Zschau for proofreading this thesis. In addition, I would like to thank former lab members Dr. Fabia Mittendorf and Dr. Kevin Kunz for warmly welcoming me to the group in initial days.

Many thanks go to Malavika Krishnan, as well as to the postdoctoral researchers Dr. Venkadesh Balakrishnan and Dr. Bincy Chindan, for the pleasant time both inside and outside the lab. I would also like to thank the current group members Mohit Chotia, Timo Zschau, Cedric Meysing, Nau Jan, Antonia Gres, and my intern Siham Laroub. Furthermore, I would like to extend my thanks to the former group members Anastasiia Krupka, Federica Borghi, Kathrin Bensberg, Bastian Springer, and Athanasios Savvidis for contributing to a motivating and collegial research environment.

Finally, I would like to thanks my parents for their unconditional support and for always encouraging me in the best possible way. I am deeply grateful for their love and for always believing in me. I would also like to thank my grandparents for their love, care, and constant pride in my achievements. To my grandfather, who is no longer with us: you will always remain in my memory and in my heart. Additionally, I would like to thank my sister and my brother for their support, encouragement, and for always being there for me.

Table of Contents

Abstract

Late-stage diversification of peptides remains constrained by limited functional-group tolerance and a predominant reliance on the native nucleophilicity of peripheral side chains. In particular, most chemical approaches to tyrosine modification preserve the intrinsic polarity of the phenolic residue, thereby restricting the structural and physicochemical diversity accessible through late-stage functionalization. In contrast, biological systems transiently invert phenol polarity through enzymatic oxidative umpolung, enabling bond constructions that are difficult to achieve using conventional synthetic strategies.

This thesis demonstrates a metal-free synthetic platform that translates this oxidative strategy into a practical method for the modification of short peptides. Mild oxidation of tyrosine residues using a hypervalent iodine(V) reagent generates electrophilic *ortho*-quinone intermediates in situ under conditions compatible with a wide range of amino acid side chains. Controlled interception of these common intermediates enables two complementary modes of diversification within a unified framework: (i) formation of phenazine frameworks, and (ii) peripheral modification through site-selective tyrosine-cysteine crosslinking.This methodology operates in densely functionalized oligopeptides and enables late-stage modification without recourse to protecting-group-intensive or de novo synthetic routes.

Beyond peptide diversification, the reactivity of *o*-quinone intermediates was exploited to develop cysteine-labeling tags with fluorophores, enabling chemoselective tagging under mild conditions. In parallel, a solid-phase hypervalent iodine(V) catalyst was employed for the oxidative rearrangement of tertiary allylic alcohols under continuous-flow conditions, demonstrating the efficiency and scalability of immobilized catalysts for metal-free oxidative transformations.

Collectively, this work establishes phenolic umpolung as a generalisable design principle for peptide functionalization and extends the utility of hypervalent iodine(V) chemistry to complex biomolecular and synthetic substrates.

Chapter 1
General Introduction

General Introduction

Research in peptide and protein modification originated in the early twentieth century, marked by seminal contributions from pioneers such as Emil Fischer and R.B. Merrifield. In 1901, Fischer synthesized the first dipeptide, glycylglycine (Gly-Gly) and was awarded the Nobel Prize in Chemistry in 1902.[1] He laid the foundation of peptide chemistry by introducing the concept of the peptide bond while studying protein structure.[1,2] Several decades later, Robert Bruce Merrifield introduced solid-phase peptide synthesis (SPPS) in the 1960s, a transformative methodology that enabled the efficient and systematic assembly of peptides.[3–5] He was subsequently awarded the Nobel Prize in Chemistry in 1984.[6] Today, SPPS is an important technique in peptide science and is widely employed in both academic research and industrial peptide-based drug discovery.

Building on these foundational advances, the early twenty-first century has witnessed a rapid expansion in the discovery and development of peptides (Figure 1.1). This growth has been driven by natural product isolation, rational and de novo design strategies inspired by biological systems, as well as curiosity-driven scientific exploration.[7,8]

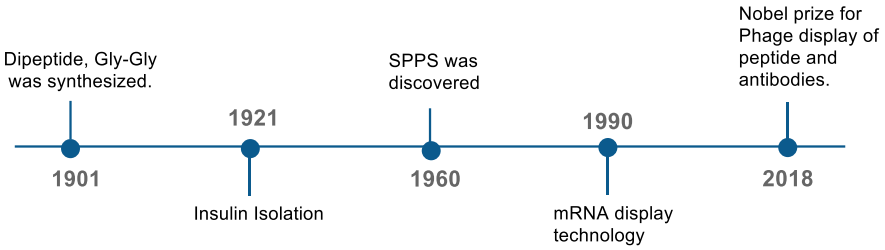

Figure 1.1: Key breakthroughs in peptide chemistry through the years.

Although over 500 amino acids exist in nature, by far the most important are the 22 α-amino acids, 20 are encoded by the standard genetic code, while two additional amino acids-selenocysteine and pyrrolysine can be incorporated by special translation mechanisms (Figure 1.2).[9,10]

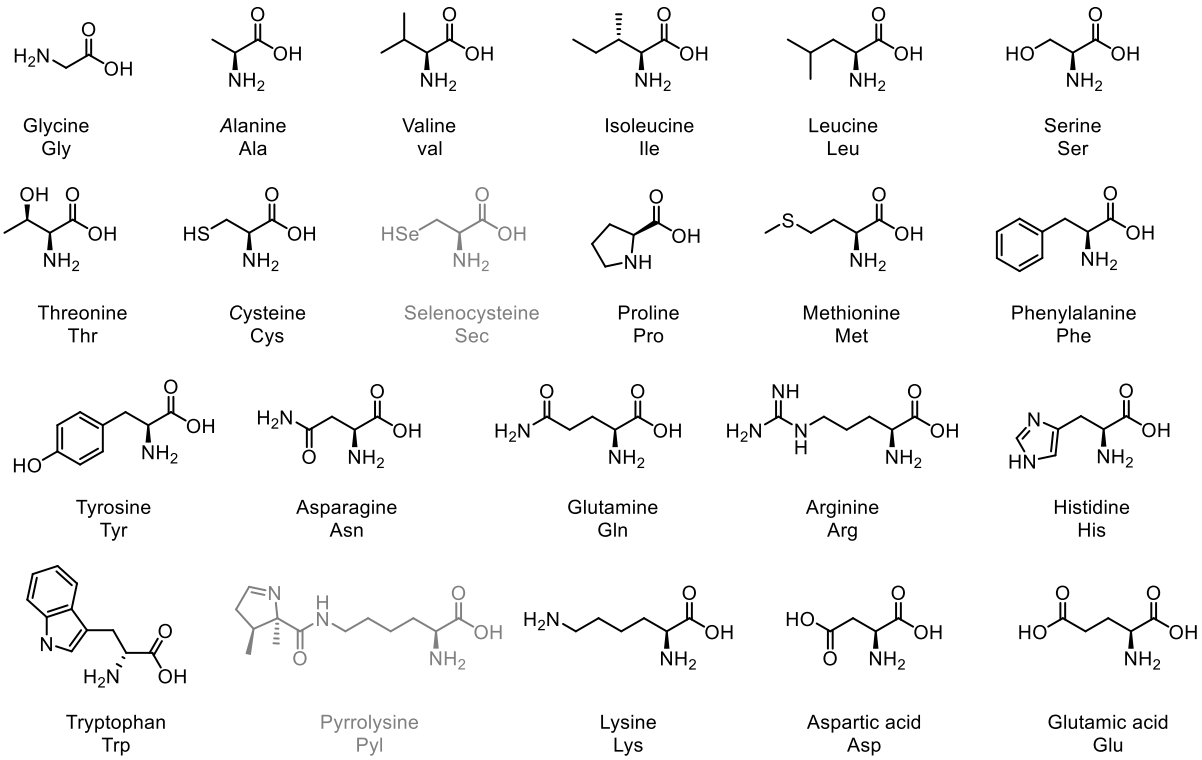

Figure 1.2: Structure of 20 standard proteinogenic amino acids, along with the two additional amino acids (in grey color).

1.1 Peptides: Biological Importance and Therapeutic Potential

Peptides are defined as short chains of amino acids linked by peptide bonds, serve as essential structural and functional components of living systems. They play critical roles in diverse biological processes, including hormonal regulation, immune defense, and cellular signaling. From a therapeutic perspective, peptide-based drugs are often characterised by high biological activity, remarkable target specificity, and relatively low toxicity compared to small-molecule drugs.[11] Moreover, the inherent conformational flexibility and three-dimensional structure of peptides make them particularly well suited for modulating protein-protein interactions, thereby positioning peptides as attractive modalities in modern medicinal chemistry.[11–15] As of 2025, approximately 80 peptide drugs are approved for clinical use, with over 150 additional peptides in clinical development.[16–18]

Native peptides exhibit considerable biological and therapeutic potential, but they often exhibit inherent limitations that restrict their broader application. These are some of the limitations: poor metabolic stability, quick enzymatic breakdown, low bioavailability, and poor physicochemical properties.[19] Furthermore, unmodified peptides often lack functional handles that can be used for imaging, tracking, or targeted delivery. As a result, chemical modification has emerged as a powerful and versatile strategy to enhance peptide properties and expand their utility (Figure 1.3).[20–28]

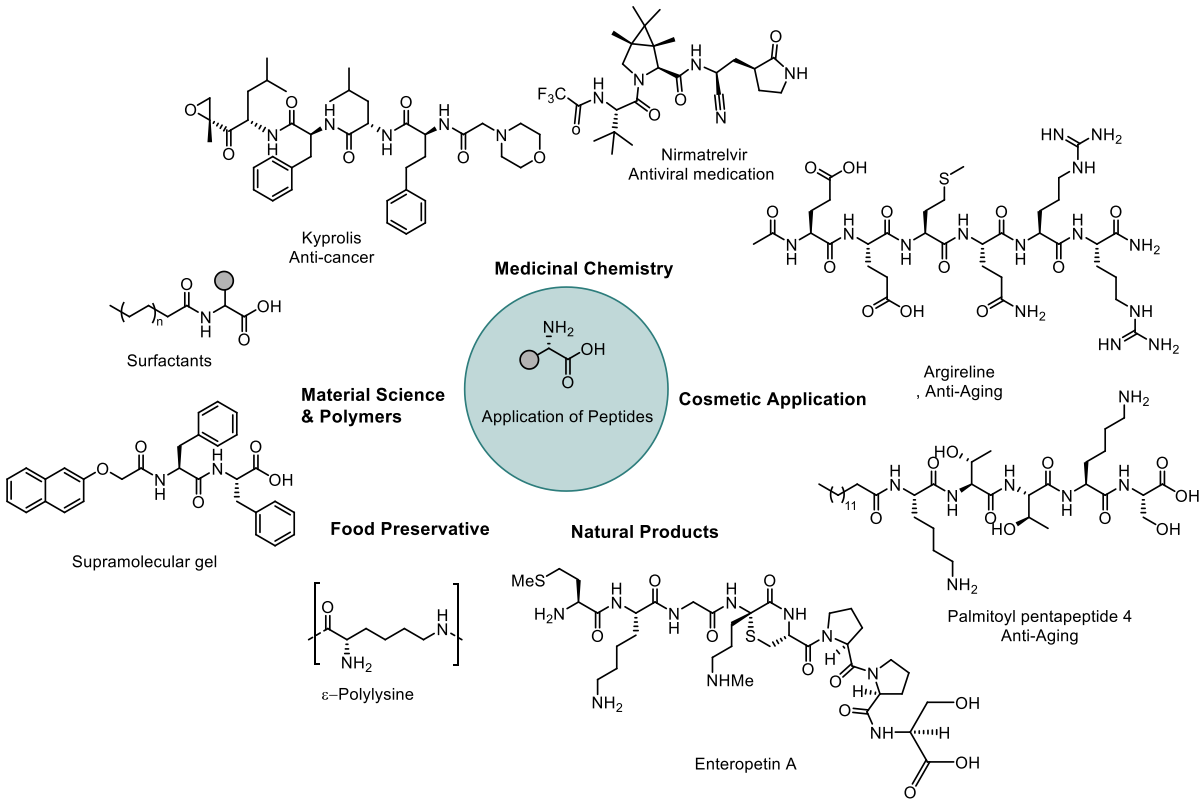

Figure 1.3: Schematic representation highlighting the diverse roles of peptides in pharmaceuticals, biomaterials, cosmetics, and related technological applications, illustrating their interdisciplinary relevance and functional versatility.

1.2 Selectivity as a Central Challenge

The engineering of peptides and proteins requires highly selective chemical transformations capable of operating within densely functionalized molecular environments. Peptides contain multiple side chains with diverse reactivities, including nucleophiles, electrophiles, aromatic systems, and redox-active groups (Figure 1.4). Within this context, peptide modification represents one of the most demanding tests of chemoselectivity, site-selectivity as reactions must proceed efficiently and predictably in the presence of numerous competing functional groups.[29]

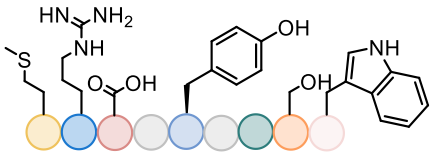

Figure 1.4: Illustration of a peptide backbone containing multiple functional groups.

This challenge becomes particularly significant for late-stage functionalization, where the peptide backbone and side chains are already fully assembled. Transformations must

therefore avoid undesired cross-reactivity while preserving peptide integrity. The growing importance of peptides as therapeutically relevant molecules have intensified the demand for robust and selective late-stage modification strategies that allow structural diversification without compromising biological function.

1.3 Peptide and Protein Modification Strategies

Peptide and protein modifications can be achieved through both enzyme-mediated and chemical approaches, each offering distinct advantages as well as intrinsic limitations. In biological systems, post-translational modifications (PTMs) generate functional diversity following ribosomal synthesis, expanding the structural and functional repertoire of proteins (Figure 1.5). These modifications regulate peptide activity, localization, stability, and intermolecular interactions.[30]

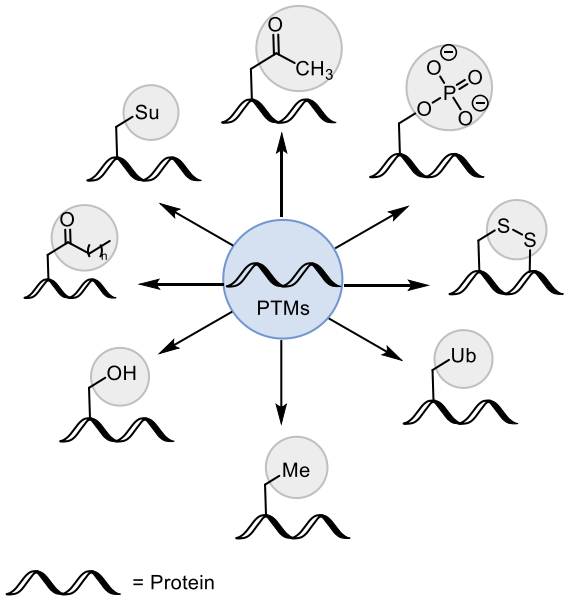

Figure 1.5: Examples of post-translational modifications.

Among the most extensively studied PTMs is phosphorylation, a reversible process in which protein kinases transfer a phosphate group to specific amino acid residues, most commonly serine, threonine, and tyrosine (Scheme 1.1). This modification can induce conformational changes that modulate protein activity and biomolecular interactions.[31]

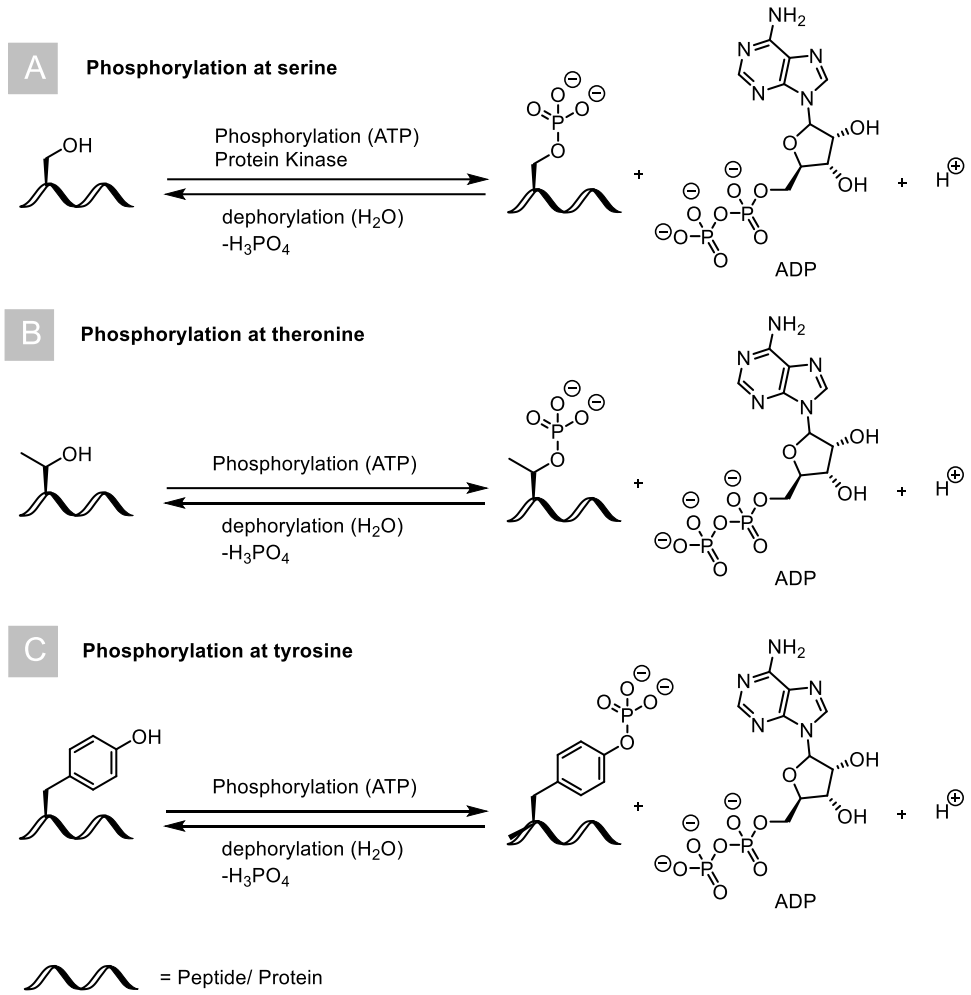

Scheme 1.1: Phosphorylation of proteinogenic amino acid residues: (A) serine, (B) threonine, and (C) tyrosine.

Glycosylation represents another important PTM involving the covalent attachment of carbohydrate moieties to defined amino acid side chains. *N*-linked glycosylation typically occurs at asparagine residues, whereas *O*-linked glycosylation is observed at serine or threonine residues (Scheme 1.2). These modifications play critical roles in protein folding, stability, and cellular recognition.[32,33]

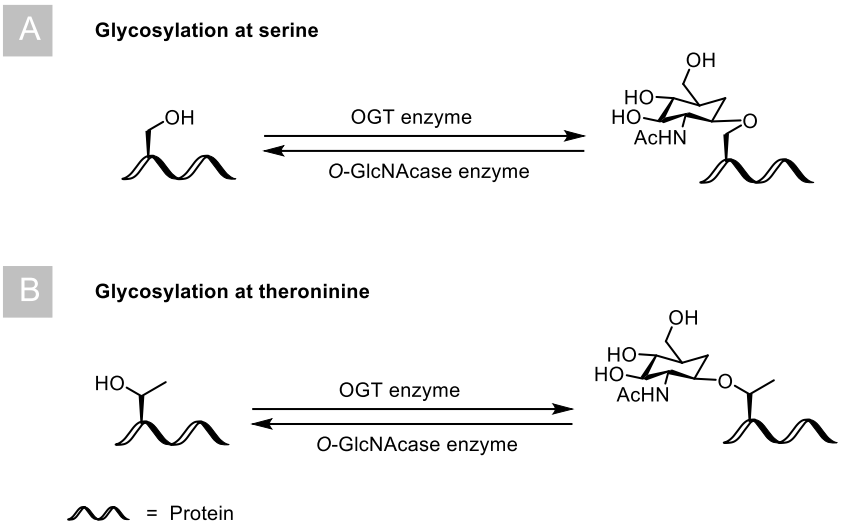

Scheme 1.2: *O*-Glycosylation at hydroxyl-containing residues: (A) serine and (B) threonine.

Disulfide bond formation between cysteine residues further contributes to protein stability by reinforcing tertiary and quaternary structures and ensuring correct folding.[34] Collectively, PTMs provide a versatile biological toolkit for fine-tuning protein structure and function within complex cellular environments.

Due to their high selectivity and efficiency under mild physiological conditions, enzymatic processes have gained increasing attention in both academic research and industrial applications. Recent advances in biocatalysis and enzyme immobilization have improved enzyme stability, reusability, and cost efficiency, further supporting their use in peptide and protein functionalization.[35–37]

Despite these advantages, several challenges continue to limit the broader application of enzymatic strategies. Only a small fraction of naturally occurring enzymes have been functionally and structurally characterized, often due to difficulties associated with heterologous expression, improper folding, or limited substrate accessibility under laboratory conditions.[38] Moreover, many enzymes have not been systematically evaluated against non-native substrates, restricting their utility in diverse chemical context.[39,40] As a result, the adoption of enzymatic strategies remains limited in many chemical laboratories.

In parallel, chemical approaches have been extensively developed to overcome these limitations and expand the accessible chemical space beyond naturally occurring PTMs. Chemical methods enabled site-specific functionalization without reliance on enzymatic activity; however, achieving high selectivity and compatibility with complex biomolecular structures remains a central challenge.[41]

Accordingly, enzyme-mediated and chemical approaches are complementary and together enable efficient peptide and protein modification.

1.4 Chemical Modification Strategies

Among the diverse strategies developed for peptide and protein modification, significant attention has been devoted to (i) the incorporation of unnatural amino acids followed by derivatization, and (ii) direct late-stage functionalization of native peptides, alongside enzymatic and tag-based approaches.

The first approach involves the incorporation of unnatural amino acids bearing reactive handles, such as azides, alkynes, ketones, or strained alkenes. These functionalities serve as bioorthogonal sites for subsequent derivatization through reactions such as copper-catalyzed or strain-promoted azide-alkyne cycloaddition (click chemistry), Staudinger ligation, or oxime formation (Scheme 1.3).[42–46] Such approaches enable highly selective conjugation of fluorophores, affinity tags, polymers, or drug molecules at predetermined positions within a peptide sequence. However, the incorporation of unnatural amino acids often requires advanced SPPS or genetic code expansion techniques in recombinant systems. These methods can be technically demanding, time-intensive, and may suffer from limitations in efficiency, scalability, or expression yield.[47]

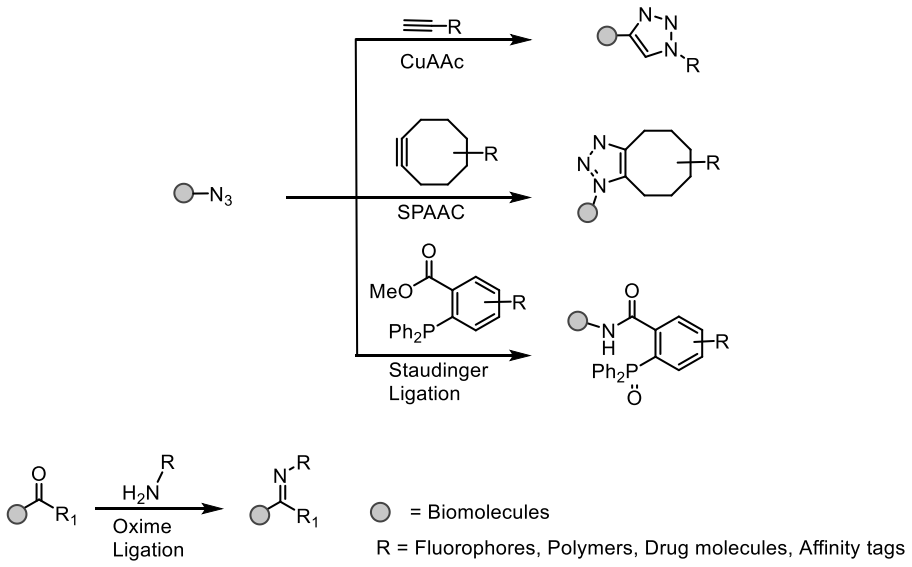

Scheme 1.3: Examples of bioorthogonal reactions.

In contrast, late-stage functionalization (LSF) refers to the chemical modification of peptides and proteins at advanced stages of synthesis, or directly on fully assembled biomolecules. This approach allows functional groups such as reactive handles, imaging probes, affinity tags, or therapeutic payloads to be introduced without the need for complete de novo synthesis.[48]

When performed on native peptides, LSF offers a practical alternative, provided that the reactions proceed under mild conditions and exhibit high chemoselectivity.[49]

Recent advances in catalysis have substantially expanded the scope of late-stage peptide modification.[50] Transition-metal-catalyzed methodologies have enabled selective bond formation on amino acid side chains. Palladium, copper, and nickel catalysts are commonly employed for C-heteroatom bond formation, facilitating coupling reactions at sulfur, selenium, and nitrogen-containing residues. Nickel catalysts have also been utilized in decarboxylative coupling strategies, while iron, palladium, and copper-mediated C-H functionalization offers powerful routes for the direct modification of peptide frameworks.[51,52] Photocatalytic approaches further allow transformations under mild conditions with improved control over reactivity.[53] In parallel, biorthogonal reactions have been optimized to proceed selectively in complex biological functionality, allowing conjugation in aqueous and physiologically relevant media.

Despite these advances, achieving high chemoselectivity within peptide frameworks remains a significant challenge. Peptides often contain multiple reactive residues-including lysine, cysteine, that may compete under similar reaction conditions. Consequently, the design of chemical transformations that operate under mild conditions while preserving peptide integrity continues to be a central objective in peptide modification research. In parallel, engineered enzymes have emerged as powerful tools for selective transformations, bridging biological and synthetic methodologies.[54,55] These advances collectively reinforce the need for robust chemical methodologies suitable for complex peptide environments.

1.5 Residue-Selective Modification Strategies

Efforts toward controlled peptide and protein functionalization have traditionally focused on the most nucleophilic residues among the 20 proteinogenic amino acids, particularly cysteine and lysine. Cysteine contains thiol side chains capable of undergoing michael additions, disulfide exchange, alkylation and thiol-ene type reactions (Scheme 1.4).

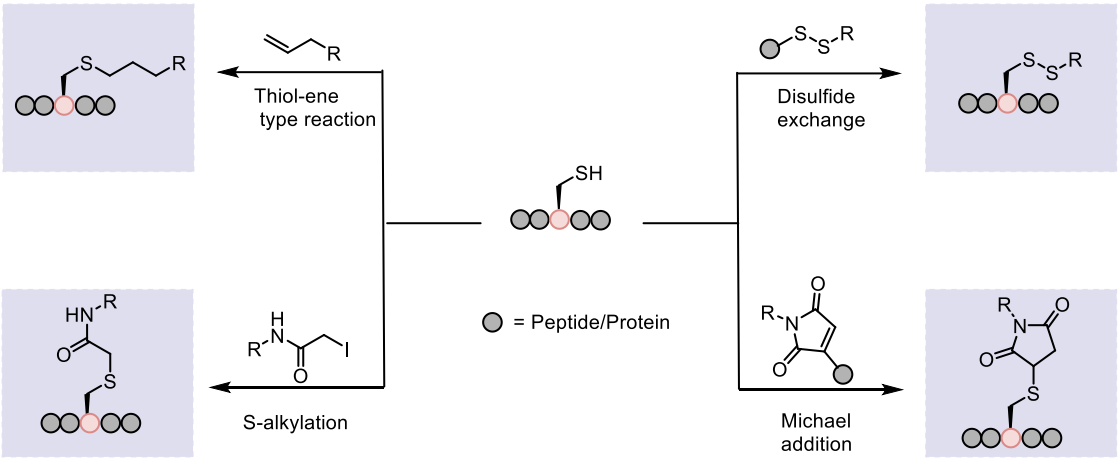

Scheme 1.4: Common cysteine bioconjugation strategies.

Lysine features a primary amine that can participate in acylation, sulfonylation, and other electrophilic reactions (Scheme 1.5).[56–59] While the inherent reactivity of cysteine and lysine allows efficient modification, achieving selectivity challenging. Issues such as overfunctionalization, site selectivity, and undesired cross-reactivity arise, particularly in peptides containing multiple reactive residues.[29,60]

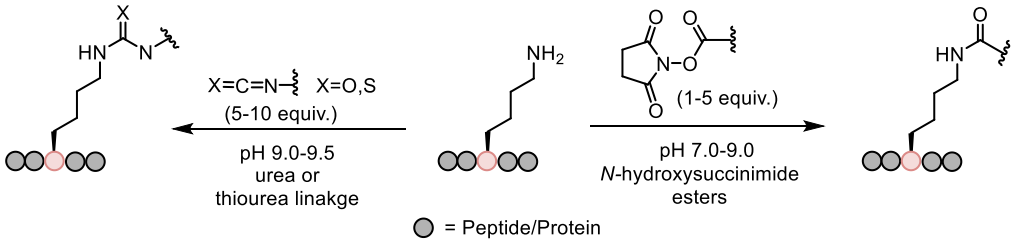

Scheme 1.5: Common lysine bioconjugation strategies.

To address these limitations, attention has increasingly shifted toward alternative amino acid residues, including methionine, histidine, tryptophan, and tyrosine, as platforms for selective modification.

Methionine has been explored as a chemoselective target due to the unique reactivity of its thioether side chain. The nucleophilic character of the thioether enables selective alkylation, as demonstrated by Kramer group in 2012. Its susceptibility to oxidation has more recently been exploited to generate sulfoximines, as reported by the Li group in 2022, further

expanding the scope of methionine functionalization. These oxidative and alkylative strategies illustrate how methionine can serve as a controllable handle for peptide modification under carefully optimized conditions (Scheme 1.6).[61–65]

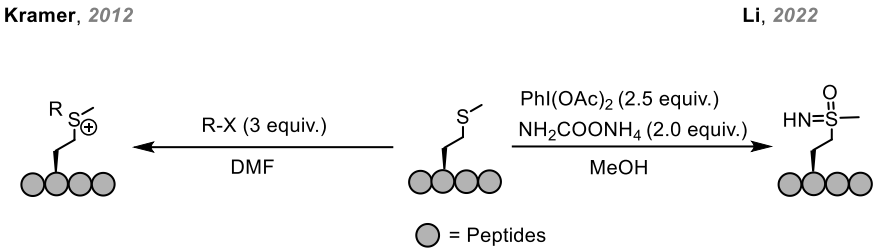

Scheme 1.6: Common methionine modification strategies.

Histidine has likewise attracted interest owing to the pH-dependent reactivity of its imidazole side chain.[66–69] For example, Chang group reported in 2022 the use of thiophosphorodichloridate reagents selective thiophosphorylation under mild conditions. The installed alkyne-functionalized thiophosphoryl group serves as a bioorthogonal handle for subsequent diversification via CuAAC chemistry (Scheme 1.7).[69]

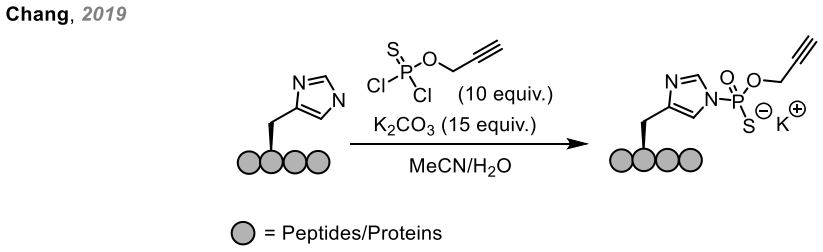

Scheme 1.7: Histidine modification strategies.

Tryptophan, characterized by its electron-rich indole side chain, participates in radical, oxidative, and electrophilic substitution processes. Under oxidative conditions, skeletal editing of the indole framework has been achieved by Morandi group in 2026. Alternatively, the indole nitrogen can engage in an SN_2' reaction with Morita-Baylis-Hillman (MBH) carbonates under nucleophilic substitution conditions, as demonstrated by Sun group 2024 (Scheme 1.8).[70–73]

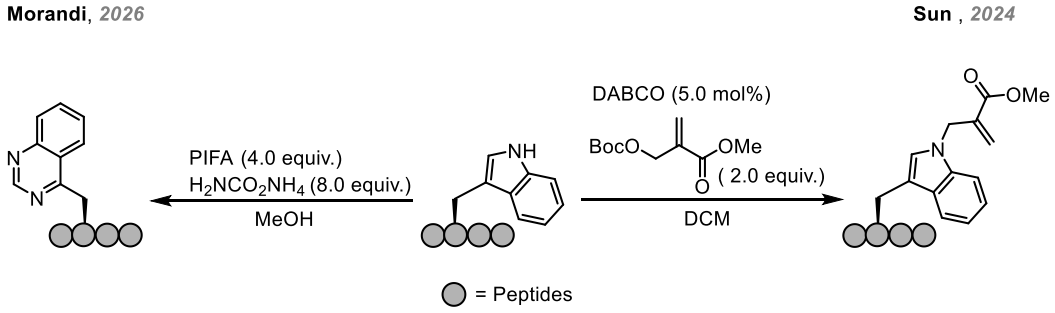

Scheme 1.8: Tryptophan modification strategies.

1.6 Tyrosine as a Strategic Modification Handle

Tyrosine occupies a distinctive position among the proteinogenic amino acids, representing approximately 3.2% of residues in native protein.[74] Its phenolic side chain imparts both polar and hydrophobic character, allowing tyrosine to reside on the protein surface or buried within the hydrophobic core.[75–77] This amphiphilic nature, together with the aromatic core and redox-active properties of the phenolic moiety, renders tyrosine an attractive target for site-selective modification.[78,79]

Tyrosine oxidation plays a central role in a variety of biological processes including the formation of enzymatic cross-links, pigment biosynthesis such as melanin (Figure 1.6 A), and redox signalling pathways.[80,81] Additionally, tyrosine serves as a precursor to various neurotransmitters like dopamine and epinephrine (Figure 1.6 B and C).[82] Collectively, these naturally transformations show the chemical versatility and biological significance of tyrosine, motivating its consideration in chemical modification strategies.

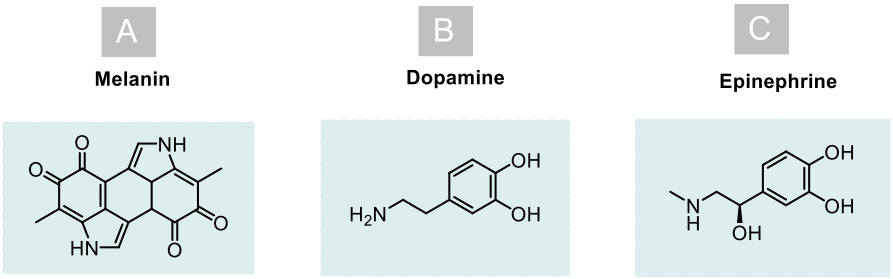

Figure 1.6: Tyrosine as a precursor to : A) melanin biosynthesis and in neurotransmitter B) dopamine and, C) epinephrine

Biosynthetically, tyrosine is widely available across organisms. In plants, bacteria, and fungi tyrosine is produced via the shikimate pathway (Scheme 1.9 A).[83] Whereas, in animals it is produced through the enzymatic hydroxylation of phenylalanine by phenylalanine hydroxylase, which uses the cofactor tetrahydrobiopterin and a non-haem iron for catalysis (Scheme 1.9 B).[84–88] This broad biosynthetic accessibility highlights the fundamental importance of tyrosine across biological domains and its inherent potential for controlled redox chemistry.

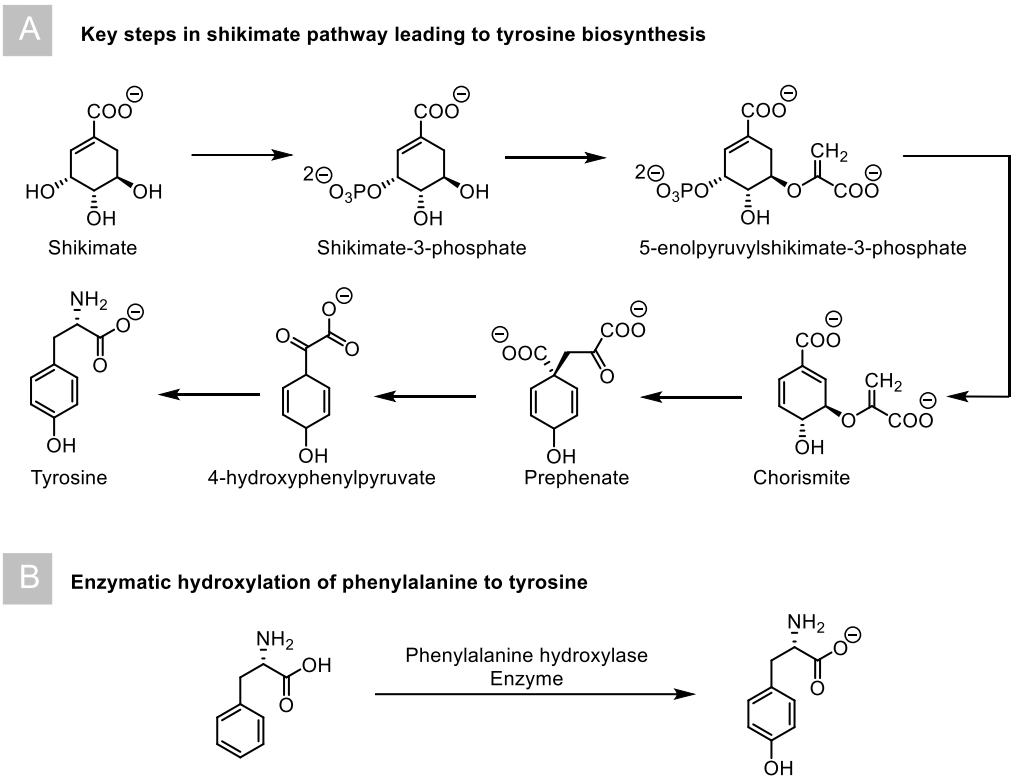

Scheme 1.9: A) Key steps in shikimate pathway leading to tyrosine biosynthesis; B) Enzymatic hydroxylation of phenylalanine to tyrosine.

Despite these attributes, tyrosine has been less explored in peptide modification compared to residues such as cysteine and lysine. While a range of strategies for tyrosine functionalization have been reported,[76] many suffer from limitations such as poor site- or chemoselectivity in the presence of competing residues, undesired side reactions, the reliance on expensive or toxic transition metals, and limited stability of the reagents and resulting bioconjugates. These challenges highlight the continuing need for robust strategies for selective tyrosine modification.

The unique phenolic side chain of tyrosine enables chemoselective targeting that is difficult to achieve with other residues. Modification can occur at multiple sites: the aromatic ring can undergo *ortho*, *meta*, and *para* functionalization (C-modifications), while the phenolic hydroxyl group provides a site for O-modification (Figure 1.7).[89–92] This positional diversity offers multiple entry points for controlled chemical functionalization, providing significant flexibility in the design of site-selective peptide modification strategies. For clarity, modifications at each position are discussed individually in the following sections.

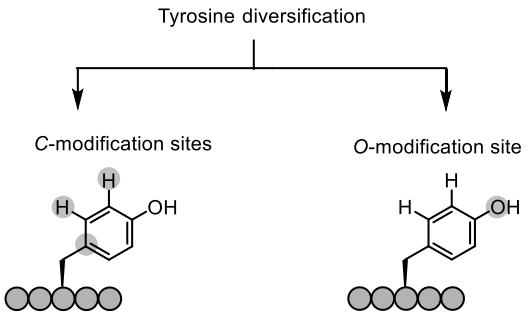

Figure 1.7: Schematic representation of possible chemical modification sites at tyrosine residues.

Among the possible modification sites, the *ortho* position of the tyrosine aromatic ring is discussed first. One example of *ortho*-selective modification is tyrosine nitration. Tyrosine nitration represents an important post-translational modification in vivo and has inspired synthetic approaches for selective tyrosine functionalization. In 2021, Wang and co-workers reported a light-controlled nitration strategy for tyrosine-containing peptides and proteins using dinitro imidazole reagents under biocompatible conditions. Upon irradiation at 390 nm, tyrosine residues were efficiently and selectively converted into 3-nitrotyrosine with rapid kinetics and high chemoselectivity; however, the method was incompatible with cysteine and histidine residues (Scheme 1.10).[93]

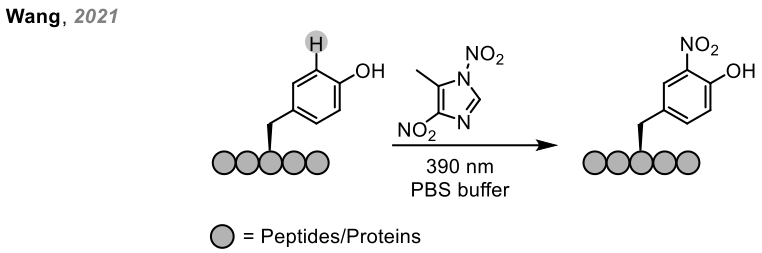

Scheme 1.10: Site-specific nitration of tyrosine residues using dinitroimidazole chemistry.

Another approach for *ortho*-selective functionalization involves Mannich-type bioconjugation. The Francis group developed a three-component Mannich-type tyrosine bioconjugation under mild conditions, involving in situ imine formation from formaldehyde and primary anilines, followed by electrophilic substitution at the tyrosine *ortho* position (Scheme 1.11).[94] While effective, this transformation was limited to electron-rich anilines and did not tolerate cysteine or tryptophan residues. Tanaka and co-workers later reported a cyclic imine strategy with improved selectivity, although cysteine incompatibility remained a key limitation.[95,96]

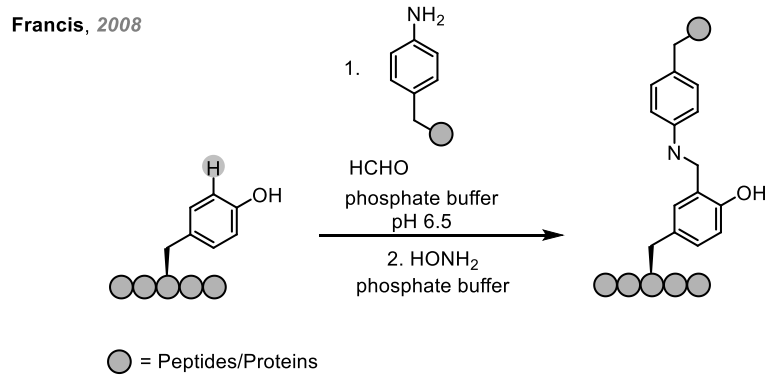

Scheme 1.11: Three-component Mannich type reaction on tyrosine residues.

Azo and diazo coupling reactions have also been widely explored for *ortho*-tyrosine modification. Francis, Barbas, and others demonstrated azo coupling at tyrosine residues for protein functionalization.[97–100] More recently, Yi and co-workers introduced a bench-stable diazo reagent capable of installing alkyne handles selectively at tyrosine residues, enabling subsequent diversification via click chemistry, including fluorescence labeling and PEGylation (Scheme 1.12). Bovine serum albumin (BSA) was employed as a model substrate, and successful fluorescent labeling via FITC conjugation was confirmed by SDS-PAGE analysis.[101] Similarly, Boyle and co-workers reported diazo-coupling-based installation of BODIPY fluorophores onto BSA, further highlighting the utility of *ortho*-selective tyrosine modification strategies.[102]

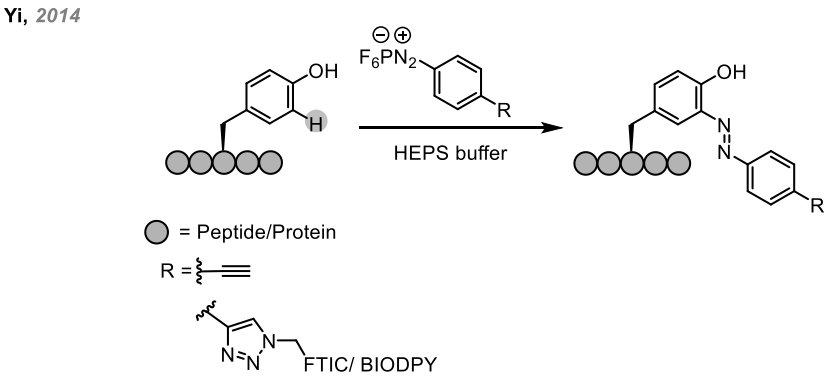

Scheme 1.12: Azo-coupling on tyrosine residues.

Electrochemical approaches provide another route for *ortho*-selective labeling. Recently, Gouin and co-workers reported an electrochemically promoted “Tyr-click” strategy for the selective labeling of tyrosine residues in proteins. In this approach, aromatic-substituted urazoles undergo electrochemical activation to generate reactive intermediates that selectively modify tyrosine side chains. The method was successfully applied to the functionalization of structurally diverse biomolecules, including oxytocin, bovine serum

albumin (BSA), and antibodies, thereby expanding the scope of tyrosine-selective bioconjugation (Scheme 1.13).[103]

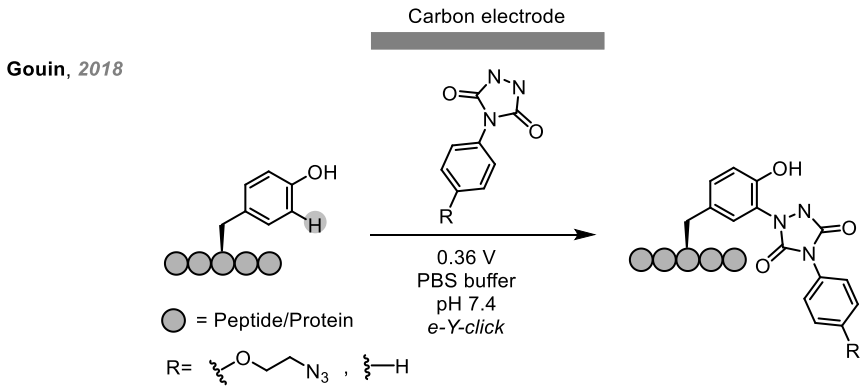

Scheme 1.13: Electrochemically driven tyrosine modification using phenyl-urazole reagents.

Photocatalytic strategies have also been employed for *ortho*-selective modification. MacMillan and co-workers developed a photocatalytic strategy employing 10-hydroxyphenothiazine-3,7-dialdehyde as a multifunctional coupling reagent. Under visible-light irradiation, this aromatic aldehyde undergoes controlled activation and subsequent condensation reactions, enabling the chemoselective modification of tyrosine residues. This approach allows the installation of multifunctional biorthogonal handles and represents a notable advance in selective tyrosine functionalization under mild photocatalytic conditions (Scheme 1.14).[104]

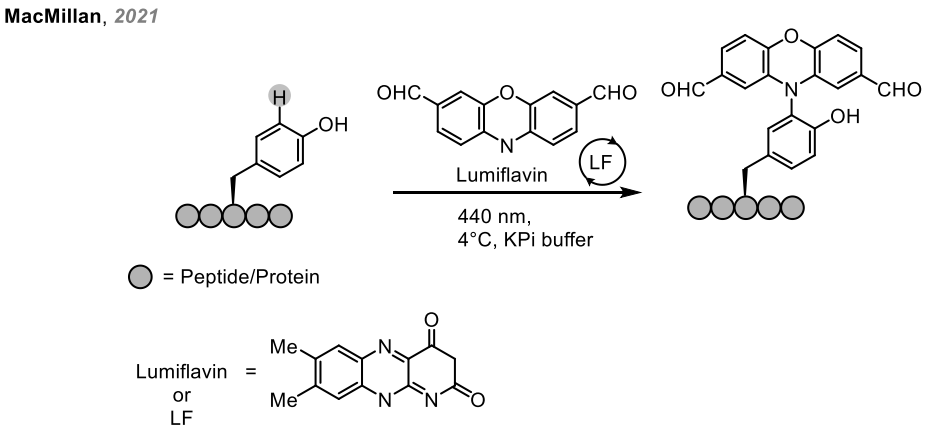

Scheme 1.14: Photocatalytic modification of tyrosine residues using 10-hydroxyphenothiazine-3,7-dialdehyde.

The construction of cyclic peptides as mimics of antimicrobial peptides has also been explored using tyrosine-based crosslinking strategies. In 2007, Rosenberg and co-workers reported the first total synthesis of the antimicrobial peptide aulomycin (aromycin) employing a Suzuki–Miyaura coupling to assemble the macrocyclic core.[105] Although effective, this approach required 14 synthetic steps and delivered the target in an overall yield of only 6.4%. To address

these limitations, Baran and co-workers later reported a significantly streamlined strategy in 2018. Using $[Cu(MeCN)_4][PF_6]$ as the oxidant in combination with Tetramethylethylenediamine (TMEDA) as a bidentate ligand and molecular oxygen as the terminal oxidant, they achieved oxidative C-O bond formation under inert conditions (Scheme 1.15). This method enabled the synthesis of aulomycin analogues in fewer steps, providing the macrocycle in up to 60% isolated yield on a 5 g scale.[106]

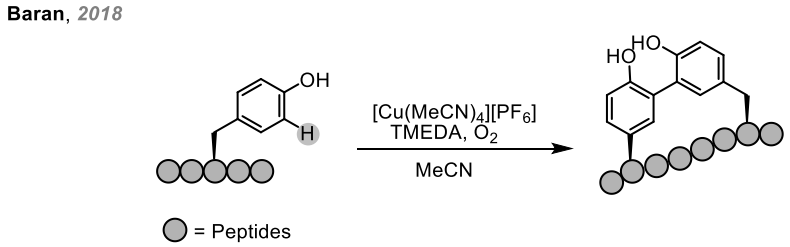

Scheme 1.15: Construction of cyclic peptides via tyrosine residues.

C-H functionalization at the *meta* position of tyrosine remains comparatively underdeveloped and is largely restricted to short peptides or protected tyrosine derivatives. Most reported strategies rely on transition-metal catalysis and require the installation of strong directing groups, high catalyst loadings, and harsh reaction conditions.[89] For example, alkenylation of tyrosine has been achieved following triflation of the phenolic group, using Palladium(II) acetate (10 mol%) as the catalyst and silver acetate as the oxidant in a DCE/DMF solvent system at 130 °C for 72 h, affording the alkenylated product.[107] Ma and co-workers later reported a pyridinamide-directed methylation of tyrosine derivatives, achieving selective functionalization in high yield however, this approach requires preinstalled directing groups and is limited in scope (Scheme 1.16).[108]

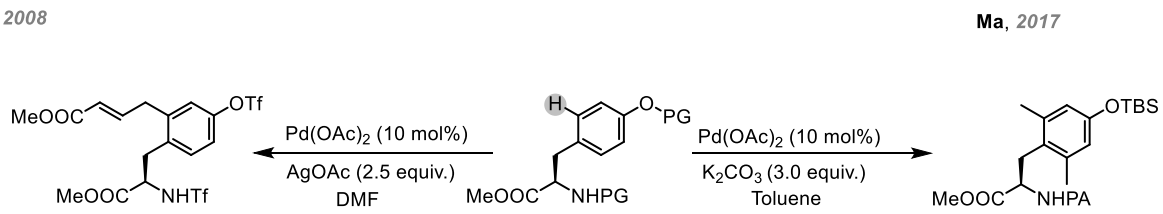

Scheme 1.16: Palladium-catalyzed alkenylation and methylation of tyrosine residues

Additional meta-selective transformations include acetoxylation directed by triflimide, catalyzed by Palladium(II) acetate in the presence of acetic anhydride under elevated temperatures, delivering the desired product in moderate yield (Scheme 1.17).[109]

Vickers, *2010*

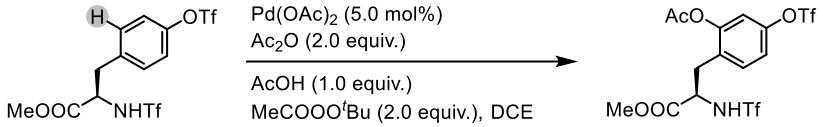

Scheme 1.17: Palladium-catalyzed acetoxylation of tyrosine.

Similarly, Yu and co-workers reported a palladium-catalyzed iodination of tyrosine derivatives using PIDA ((diacetoxyiodo)benzene) and iodine, affording diiodinated products in moderate yield after prolonged reaction times at high temperature (Scheme 1.18).[107] Collectively, these examples shows the reliance of *meta*-C-H functionalization strategies on transition-metal catalysis, directing groups, and forcing conditions, which substantially limit their applicability to complex peptides and proteins.

Yu, *2008*

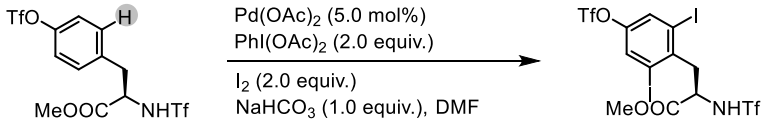

Scheme 1.18: Palladium-catalyzed diiodination of tyrosine residues.

Beyond the *ortho* and *meta* positions, tyrosine can also undergo selective functionalization at the *para* position. In 2021, Kanai and co-workers reported the selective functionalization of tyr-containing peptides and proteins via iminoxyl radicals generated in situ from nitroso precursors using ceric ammonium nitrate (CAN) in citrate buffer (Scheme 1.19). The method exhibited high site-selectivity for the *para* position, and the introduced modification could be subsequently removed through de-click reactions using either penicillamine or photolysis. This approach provides a mild and chemoselective strategy for *para*-functionalization, compatible with complex peptide and protein substrates.[110]

Kanai, *2021*

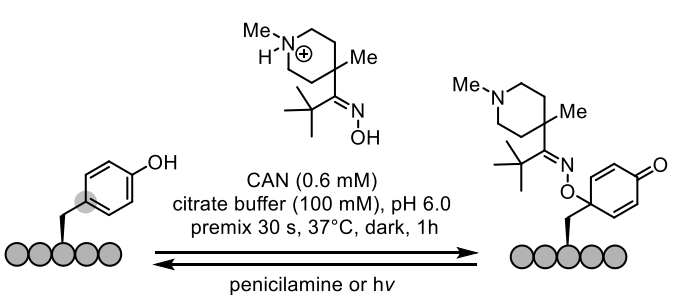

Scheme 1.19: *Para*-selective transformation using iminoxyl radical on tyrosine residues.

Having outlined the C- positions available on tyrosine, this section focuses on O-modification of the phenolic hydroxyl group. In 2011, Francis and co-workers reported direct oxidative modification using cerium(IV) ammonium nitrate as a single-electron oxidant, selectively

introducing PEG onto tyrosine and tryptophan residues (Scheme 1.20). This approach is applicable to both short peptides and proteins.[111]

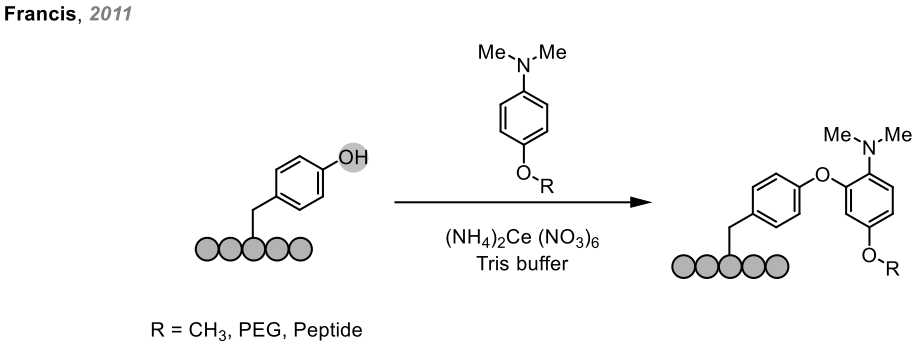

Scheme 1.20: CAN-induced oxidative transformation of tyrosine residues.

Complementary to oxidative approaches, glycosylation offers a biomimetic strategy for O-modification. In 2018, Miller and co-workers reported free *O*-glycosylation of tyrosine-containing peptides using excess calcium hydroxide in water with fluoroglycosyl donors (Scheme 1.21). The reaction selectively yielded β-anomer products from stereodefined α-D-glycosyl donors. Although cysteine residues can compete, this method enables facile synthesis of glycopeptides without extensive protecting group manipulation.[112]

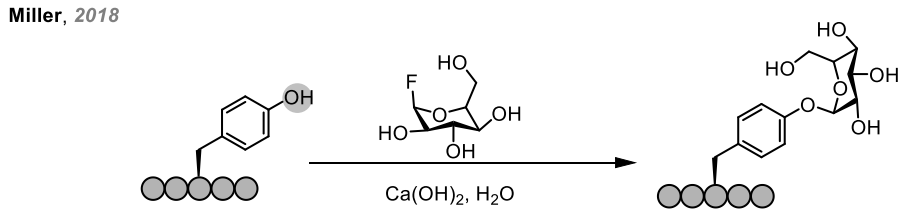

Scheme 1.21: Glycosylation of tyrosine residues using a glycosyl donor.

Recently, Waser and co-workers described a tyrosine bioconjugation approach using EBX reagents in 2022. The method installs hypervalent iodine on tyrosine residues in peptides and proteins, which can be further functionalized via palladium-catalyzed cross-coupling or azide-alkyne cycloaddition (Scheme 1.22).[113]

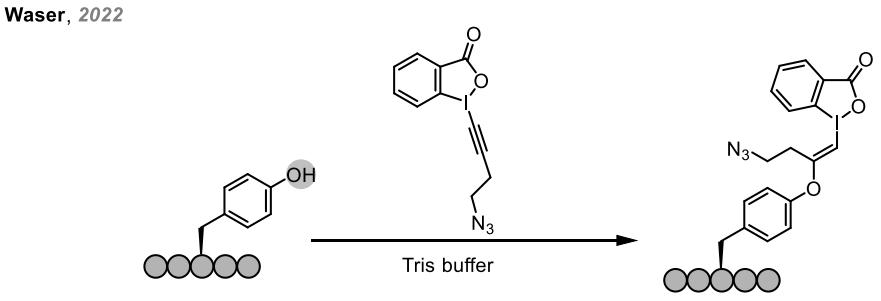

Scheme 1.22: Tyrosine functionalization *via* EBX-mediated chemistry.

In the same year, Li and co-workers introduced 1,3,5-triazine-pyridine (TPC) onto tyr-containing peptides and proteins under neutral conditions at 30 °C (Scheme 1.23). The two alkyne handles on TPC enable further functionalization via click chemistry for molecular imaging applications.[114]

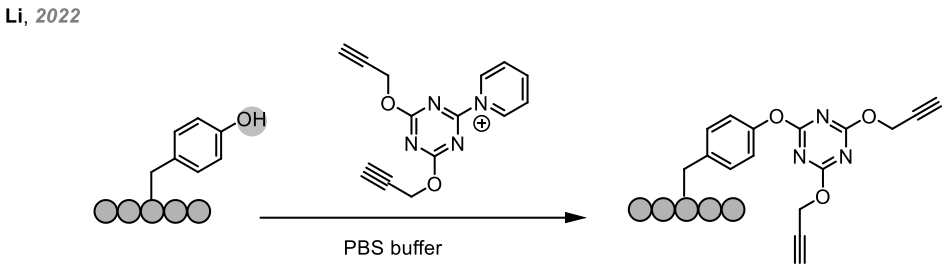

Scheme 1.23: Modification of tyrosine residues using TPC Reagents.

Collectively, these positional modification strategies highlight both the intrinsic chemical richness of tyrosine and the continuing efforts to achieve transformations that are mild, selective, and broadly compatible with complex biomolecular environments.

In parallel with these developments, increasing attention has been directed toward mimicking nature's oxidative strategy, particularly the chemistry of tyrosinase enzyme, which selectively converts phenolic residues into highly reactive *o*-quinones under remarkably gentle conditions (Scheme 1.24). This enzymatic mode of activation enables diversification of tyrosine through controlled quinone formation, extending beyond conventional peripheral modification strategies.

In a synthetic context, hypervalent iodine (HVI) reagents have emerged as versatile tools for tyrosine modification, displaying multiple modes of reactivity depending on their oxidation state and structure. While certain HVI reagents, such as those employed by waser and co-workers, enable direct functionalization of tyrosine residues, other classes operate as oxidants that more closely mimic enzymatic processes.

In particular, hypervalent iodine(V) species are capable of promoting the in situ generation of *o*-quinones from phenolic residues, thereby providing a practical and tunable platform for tyrosine oxidation. This oxidative approach offers broad functional-group tolerance, mild reaction conditions, reduced toxicity compared to many transition metals, and compatibility with aqueous systems. These reagents will be discussed in detail in the following section.

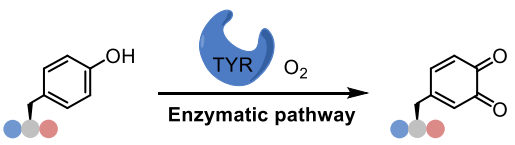

Scheme 1.24: Tyrosine oxidation via tyrosinase enzyme.

1.7 Hypervalent Iodine Reagents(V)

Hypervalent iodine chemistry constitutes a well-established and continuously developing area of modern organic synthesis. These reagents bridge the gap between traditional main-group chemistry and transition-metal-mediated processes, combining strong oxidative capability with operational simplicity.[115–120]

Within this family, iodine(V) compounds-commonly referred to as cyclic λ⁵-iodanes, occupy a distinctive position owing to their characteristic three-center-four-electron bonding arrangement, which governs their high yet tunable oxidizing capacity. These structural features confer well-defined reactivity under comparatively mild conditions, and high functional group tolerance, thereby enabling efficient oxidative transformations. Cyclic iodine(V) reagents are primarily classified into three divisions: (A): 2-iodoxybenzoic acid (IBX), (B) Pseudocyclic iodylarenes, (C) non-cyclic Iodoylarenes (Figure 1.8).

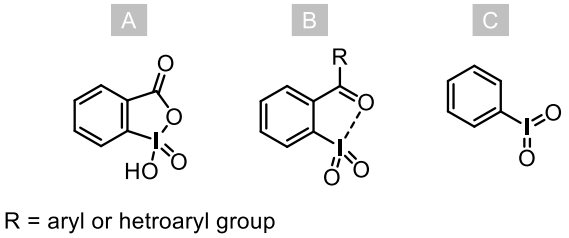

Figure 1.8: Classification of hypervalent iodine(v) compounds.

1.7.1 2-Iodoxybenzoic Acid (IBX): Properties and Preparation

2-Iodoxybenzoic acid (IBX), formally named 1-hydroxy-1-oxo-1λ⁵-benzo[d][1,2]iodaoxol-3(1H)-one, is a widely studied iodine(V) reagent. It was first reported in 1893 by Hartmann and Meyer as the oxidation product of *o*-iodobenzoic acid under alkaline permanganate conditions (Scheme 1.25).[121] Despite this early discovery, its synthetic potential remained largely unexplored for many decades.

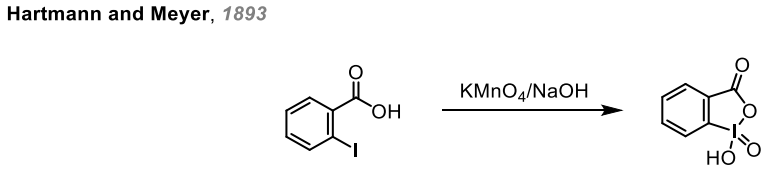

Scheme 1.25: Synthesis of IBX by Hartmann and Meyer.

Earlier synthesis of IBX relied on the oxidation of *o*-iodosobenzoic acid using reagents such as chlorine, aqueous sodium hypochlorite, or sodium periodate. In 1936, Greenbaum

introduced a method employing potassium bromate in aqueous sulfuric acid, which subsequently became a standard route for laboratory-scale synthesis (Scheme 1.26).[122–124]

Greenbaum, *1936*

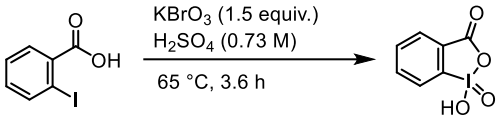

Scheme 1.26: Synthesis of IBX by Greenbaum.

For much of the twentieth century, the practical utility of IBX was constrained by its limited solubility in common organic solvents. Additionally, reports of impact and thermal sensitivity-later traced in part to residual bromate impurities from certain preparation methods-further restricted its widespread adoption.[125]

A turning point came with the work of Santagostino and Frigerio, who developed a safer and scalable synthesis using Oxone® ($2KHSO_5 \cdot KHSO_4 \cdot K_2SO_4$) in water at 70 °C (Scheme 1.27). This protocol provided crystalline IBX in good yield (79–81%) and significantly improved both reproducibility and accessibility.[126] Subsequent investigations also established that IBX exhibits appreciable stability toward hydrolysis, allowing its use under relatively straightforward laboratory conditions without stringent exclusion of moisture or inert atmosphere techniques.[127–131]

Santagostino and Frigerio, *1999*

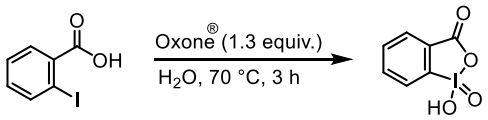

Scheme 1.27: Synthesis of IBX by Santagostino and Frigerio.

Nevertheless, IBX remains a strong oxidizing agent and is classified as an energetic material; accordingly, appropriate precautions regarding impact, friction, and thermal sensitivity must be observed during its handling and storage.[132] Despite these considerations, IBX offers relatively mild and selective oxidative conditions compared with many other oxidants, making it particularly suitable for modifications of sensitive biomolecules such as peptides. This property provides the foundation for the work presented in this thesis, which focuses on using IBX-mediated oxidation for the site-selective modification of tyrosine and other peptide residues under mild conditions.

1.8 Aim of the Thesis

The aim of this thesis is to expand the scope of peptide modification strategies based on hypervalent iodine-mediated *o*-quinone chemistry, with particular emphasis on developing mild, metal-free platforms suitable for late-stage peptide functionalization. By employing oxidative transformations compatible with complex peptide environments, this work seeks to establish versatile and operationally straightforward methods for short peptide diversification.

A central focus of this thesis is the biomimetic oxidation of tyrosine residues to generate reactive *o*-quinone intermediates. Inspired by natural enzymatic processes, these intermediates offer access to highly electrophilic species that can be selectively intercepted by appropriate nucleophiles, enabling controlled chemical modification of peptides (Figure 1.9).

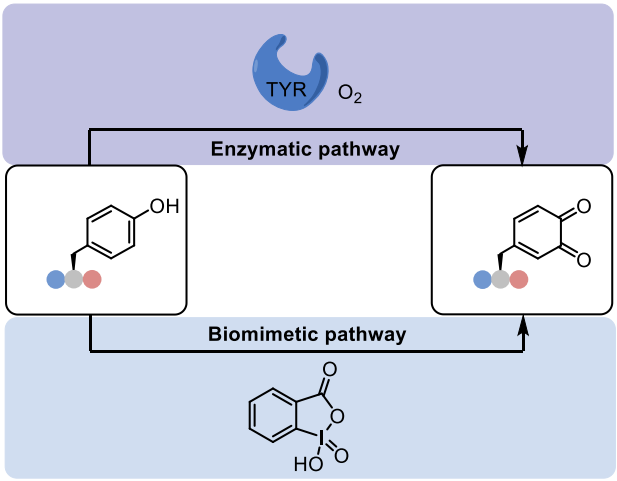

Figure 1.9: Bioinspired strategy for tyrosine modification.

In the chapter 2, the focus is placed on scaffold modification of the phenolic core of tyrosine. Tyrosine is oxidized using IBX to generate the corresponding *o*-quinone, which is subsequently trapped by diamines to form phenazine scaffolds (Scheme 1.28). These products exhibit fluorescence, highlighting their potential utility in molecular imaging and peptide-labelling applications. Amino-acid compatibility screening was carried out to assess functional group tolerance, and the insights gained from these studies were used to design the substrate scope. This chapter establishes tyrosine umpolung as a guiding principle for late-stage peptide diversification and demonstrates the applicability of hypervalent iodine(V) reagents in complex scaffold editing.

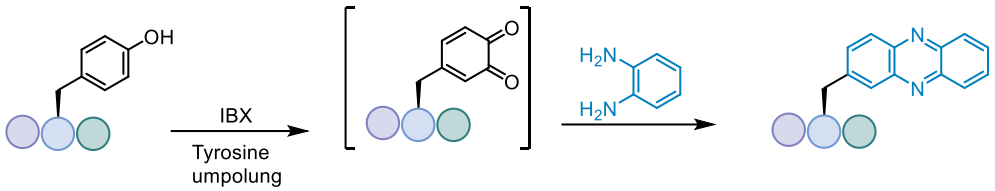

Scheme 1.28: Bioinspired strategy for skeletal tyrosine diversification.

Chapter 3 focuses on peripheral functionalization using the same tyrosine umpolung strategy. In this study, the *o*-quinone generated upon tyrosine oxidation undergoes a thiol-Michael addition with cysteine residues, leading to the formation of stable thiol-catechol adducts (Scheme 1.29). This reactivity enables the development of a site-selective tyrosine-cysteine cross-linking strategy in short peptides.

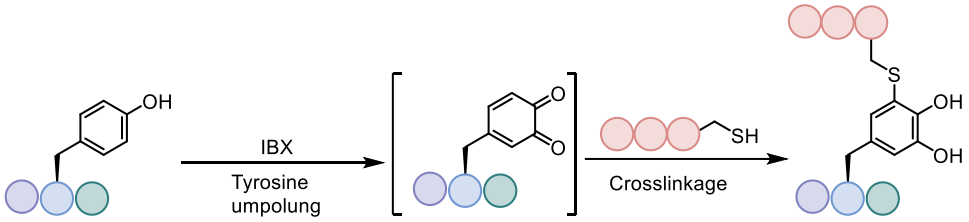

Scheme 1.29: Bioinspired strategy for peripheral tyrosine diversification.

Chapter 4 extends *o*-quinone chemistry toward the development of phenol-derived electrophilic tags for the selective modification of cysteine residues. This chapter presents a complementary cysteine-labelling strategy, with fluorescence as a key design consideration. Two phenolic tagging reagents were introduced. Tag A was chemically synthesized, in which tyramine was coupled to the organic dye dansyl chloride, whereas Tag B was commercially available, consisting of 1-naphthol. In Tag A, a dansyl moiety was incorporated to enhance fluorescence, while Tag B employed a naphthalene-based aromatic core as an alternative fluorescent scaffold. In this approach, cysteine-containing peptides react with phenolic tagging reagents that are oxidized in situ using hypervalent iodine(V) reagents to generate the corresponding *o*-quinones, resulting in the selective modification of cysteine residues and the formation of fluorescently labelled cysteine derivatives (Scheme 1.30).

Collectively, the studies presented in Chapters 2-4 establish mild, metal-free, and versatile methodologies for peptide modification, enhance the understanding of amino-acid-specific reactivity, and provide new tools for late-stage peptide functionalization.

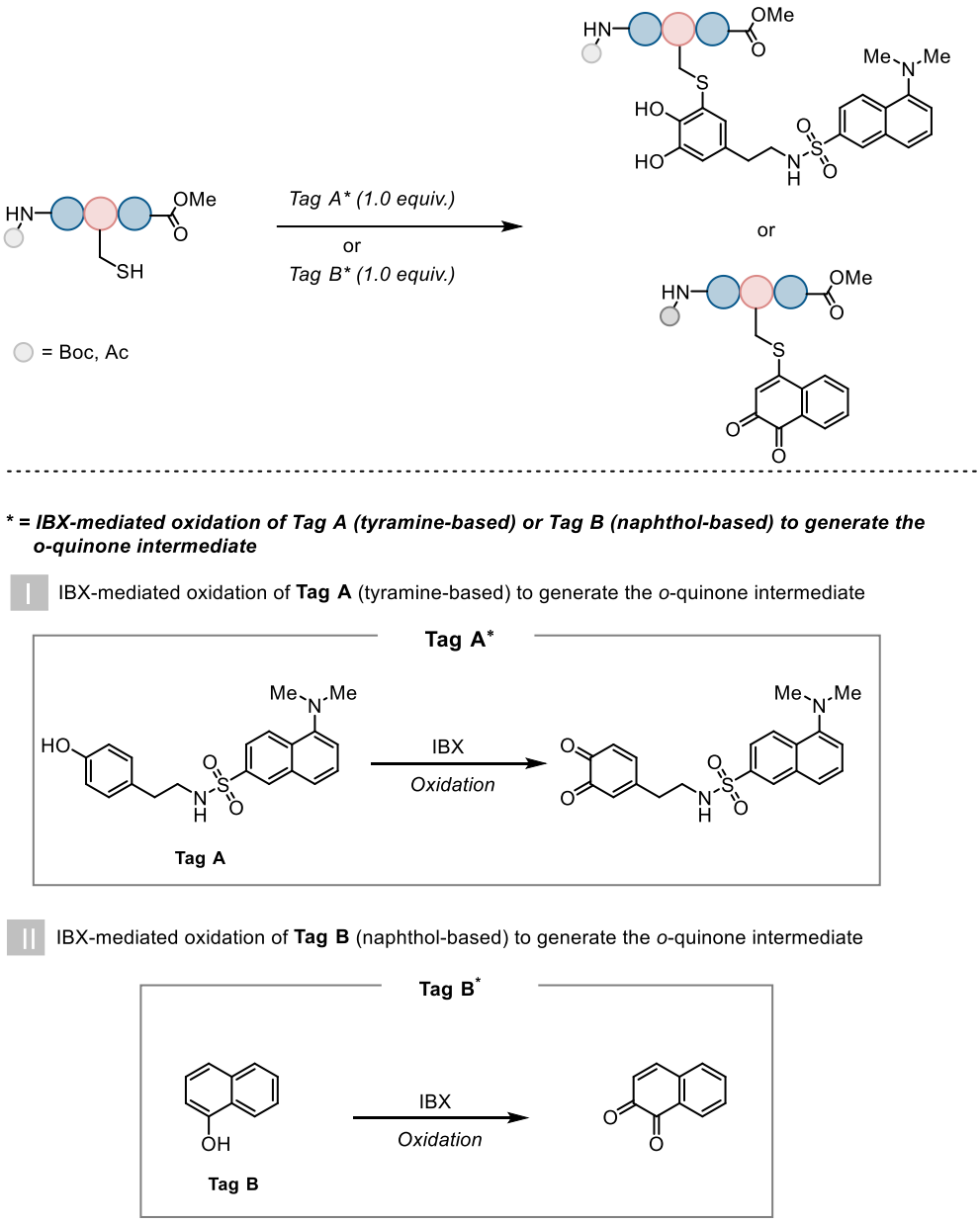

Scheme 1.30: Cysteine labeling with fluorescent Tag A (tyramine attached with dansyl chloride) and Tag B (naphthalene) via in situ *o*-quinone formation.

Chapter 5 reports an independent side project. It aims to implement a strategy for tertiary allylic alcohol rearrangement under continuous-flow conditions (Scheme 1.31). This work builds on previously developed solid-phase-bound hypervalent iodine(V) reagents (**SP-IBS I**), which offer an operationally simpler alternative to conventional batch processes. A key objective of this chapter is the recovery and reuse of the solid-supported catalysts without compromising structural integrity.

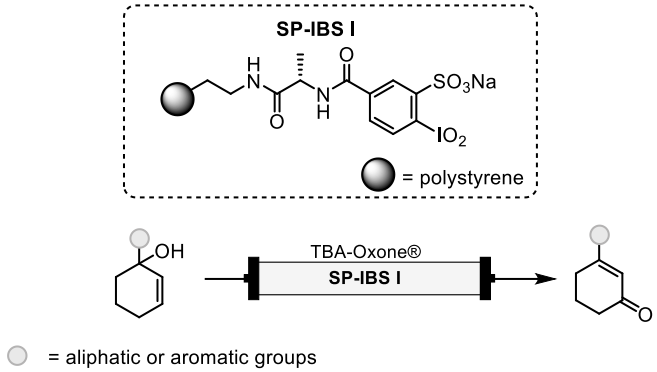

Scheme 1.31: Continuous-flow strategy for *tert.* allylic alcohol rearrangement using **(SP-IBS I)** catalyst, a catalyst reported in earlier studies.

Chapter 2

Bioinspired Tyrosine Diversification using Hypervalent Iodine Reagents

2.1 Introduction

As discussed in the previous section, established chemical strategies for tyrosine modification typically proceed via peripheral functionalization of the side chain, most frequently targeting the *ortho*-positions of the phenolic ring (relative to the hydroxyl group) or at the phenolic oxygen. In contrast, biological modification of tyrosine proceeds through oxidative pathways mediated by tyrosinases and molecular oxygen, resulting in *ortho*-quinone intermediates (Scheme 2.1). Whereas chemical methods typically utilise the intrinsic nucleophilicity of the phenolic side chain, biochemical pathways involve an umpolung of reactivity: oxidation of the phenol to *o*-quinone formally inverts its polarity, converting tyrosine from a nucleophilic residue into an electrophilic conjugated system that can be intercepted by suitable nucleophiles.

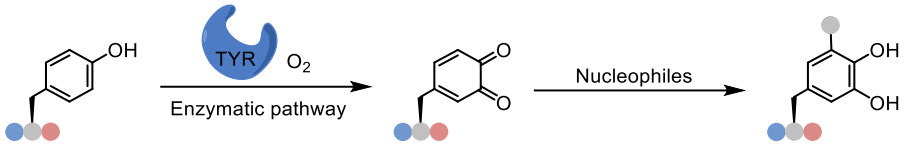

Scheme 2.1: Enzymatic oxidation of tyrosine by tyrosinase generates *ortho*-quinone intermediates that are subsequently intercepted by nucleophiles.

This enzymatic mode of reactivity enables diversification of tyrosine beyond peripheral modification strategies. In a synthetic context, hypervalent iodine reagents have emerged as powerful tools for mimicking this activity through the generation of *o*-quinones. These reagents are valued for their broad functional-group tolerance, mild reaction conditions, low toxicity relative to heavy metals, and compatibility with aqueous environments. This was first demonstrated by Pettus in 2001, who reported the selective oxidation of phenols to *o*-quinones using IBX (1.0 equiv.) at room temperature in DMF or $CDCl_3$ over 6-53 h, depending on the solvent. A variety of examples were reported (Scheme 2.2): *para*-methoxyphenol and *para*-*tert*-butylphenol afforded the corresponding quinones in 99% yield, while 2-Naphthol gave the product in 84% yield. Substrates bearing other substituents, such as ethyl or 2-Methoxy groups, also underwent efficient oxidation to the corresponding *o*-quinones.

For this transformation, a mechanism was proposed in which the phenol initially reacts with IBX, eliminating water to form a hypervalent iodine(V) intermediate. These intermediate delivers oxygen intramolecularly to the most nucleophilic and least sterically hindered *ortho* position of the substrate. During this process, the iodine(V) species is reduced to an iodine(III) intermediate, which subsequently tautomerizes. The oxidation of catechol to *o*-quinone is well documented and is accompanied by the reduction of iodine(III) to iodine(I), ultimately producing the *o*-quinone.[133]

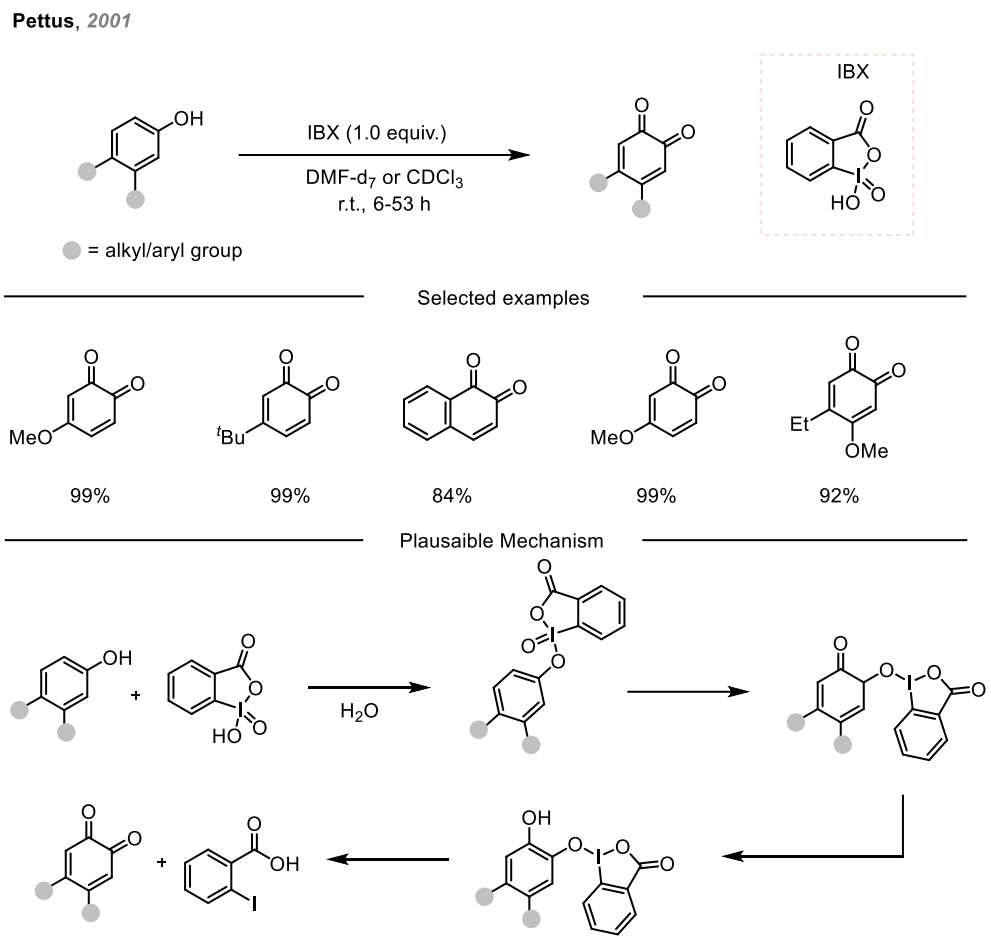

Scheme 2.2: Regioselective oxidation of phenol to *o*-quinone with IBX.

Subsequently, in 2012, a catalytic variant of the stoichiometric IBX oxidation was reported, employing IBS (2-iodoxybenzenesulfonic acid) as a catalytic hypervalent iodine species for quinone formation. In this method, phenolic substrates were oxidized to the corresponding *o*-quinones using a catalytic amount of the sodium salt of 2-iodobenzenesulfonic acid (pre-IBS) and a stoichiometric amount of Oxone® as co-oxidant in the presence of potassium carbonate, tetrabutylammonium hydrogen sulfate, and sodium sulfate. The reaction was carried out in ethyl acetate at 40 °C for 2-24 h, affording the desired *o*-quinones in 50-90% yield (Scheme 2.3).[134]

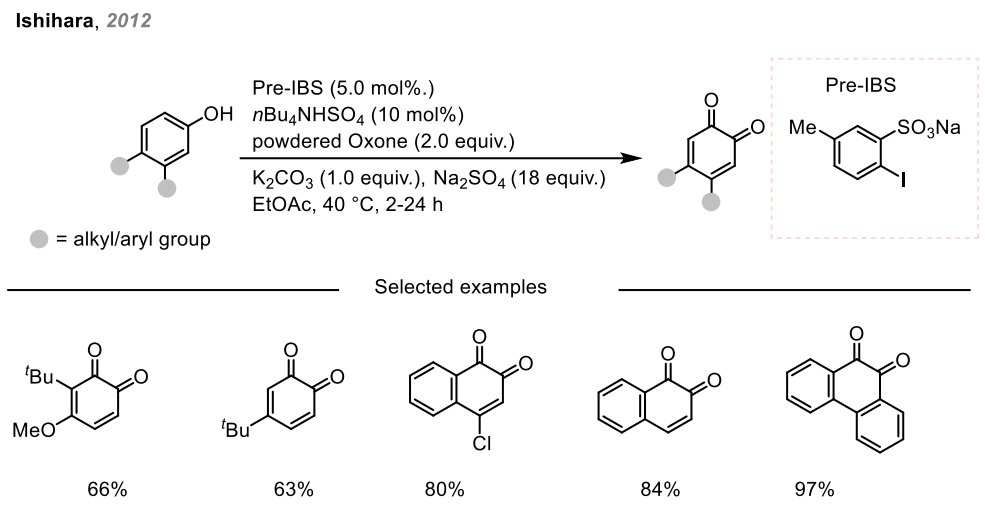

Scheme 2.3: Oxidation of phenol to *o*-quinone with catalytic amount of IBS.

The above methods provided excellent yields; however, both were largely limited to electron-rich phenols, while electron-deficient substrates failed to afford the desired products. This limitation was addressed by Wengryniuk and co-workers in 2019 through the development of a new hypervalent iodine catalyst based on a bidentate nitrogen ligand. Treatment of phenolic substrates with PIDA (1.2 equiv.), TMSOTf (2.4 equiv.), and 4-CO_2Et-bipy (1.2 equiv.) generated the Bi(4-CO_2Et-bipy) hypervalent iodine(V) reagent in situ at room temperature furnished good to excellent yields. Notably, nitrophenol was oxidized to the corresponding *o*-quinone in 99% yield, *p*-cyanophenol gave the desired product in 83% yield, and *p*-methylphenol afforded a 60% yield (Scheme 2.4).

Mechanistically, Bi(N)-HVI-mediated oxidation is proposed to proceed analogously to previously reported I(V)-mediated phenol dearomatization reactions. Initial ligand exchange between the *in situ* generated Bi(N)-HVI and the phenol establishes an equilibrium between monodentate and bidentate complexes. Intramolecular oxygen transfer to the *ortho* position followed by rearomatization affords the I(III)-ligated catechol intermediate. A second oxidation then delivers the *ortho*-quinone, along with fully reduced phenyl iodide and the protonated diamine ligand.[135]

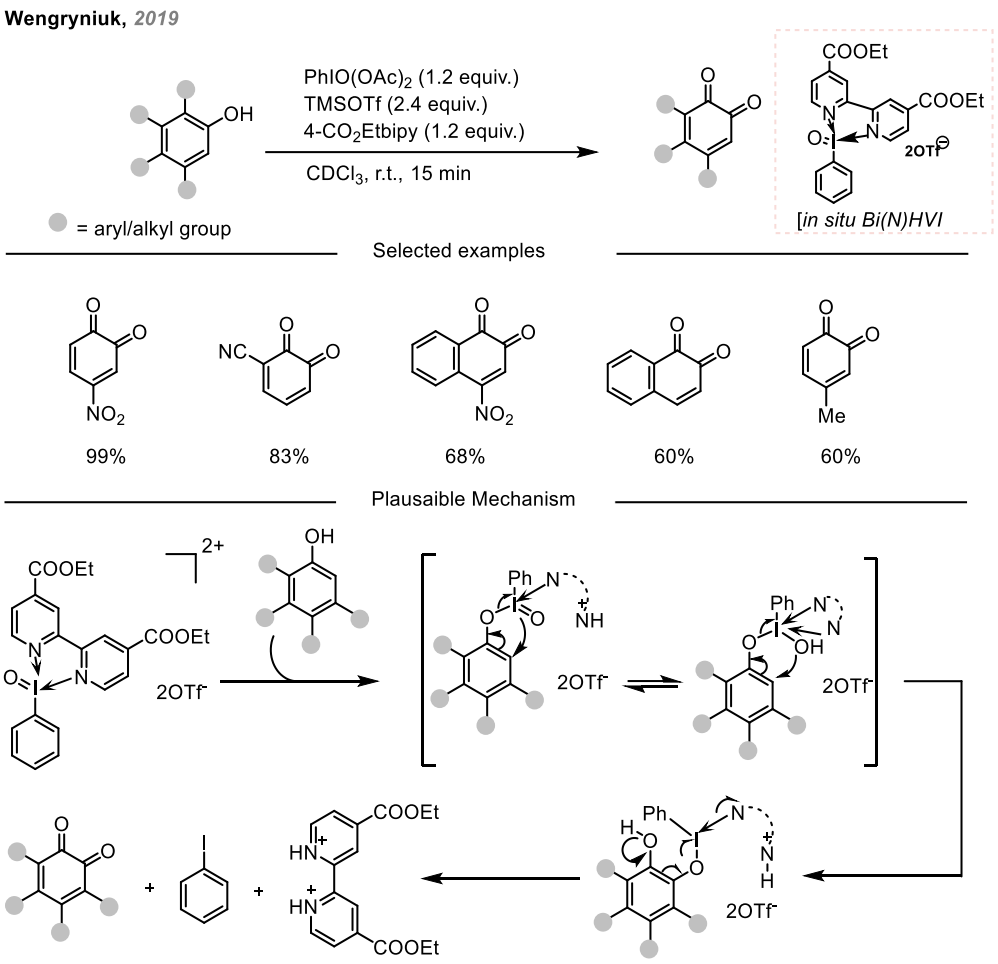

Scheme 2.4: Oxidation of electron deficient phenol to *o*-quinone**.**

Building on the utility of hypervalent iodine reagents for *o*-quinone formation, the Bernini group in 2009 utilised IBX to modify tyrosine-containing di- and tripeptides.[136] In this approach, tyrosine residues were first oxidized to the corresponding *o*-quinones, which were subsequently reduced with sodium dithionite to afford catechols. However, the substrate scope was limited to a small number of examples (Scheme 2.5).

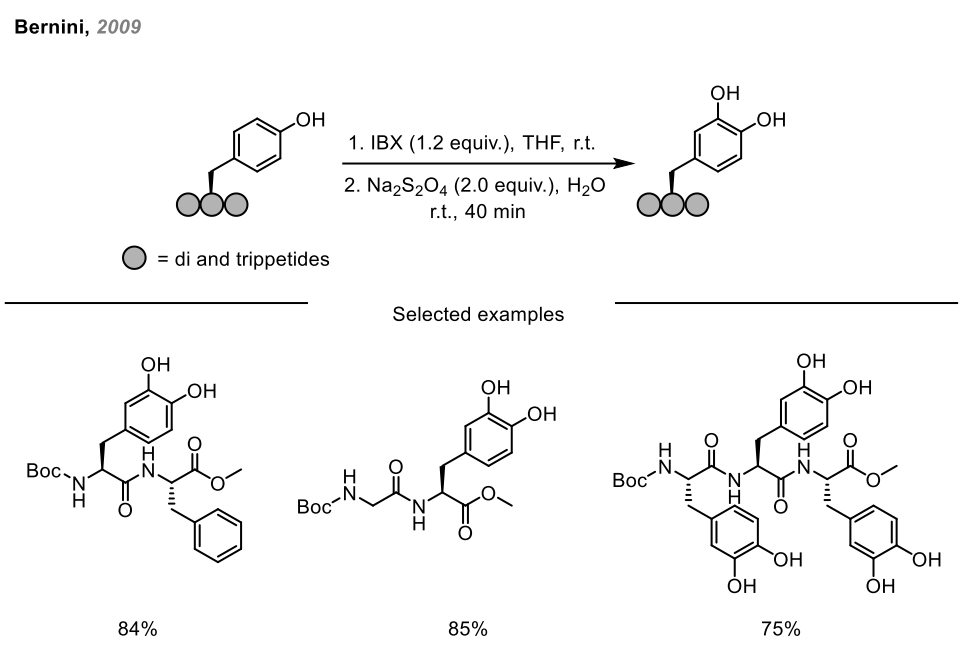

Scheme 2.5: Modification of tyrosine containing peptides using IBX.

Another example of hypervalent iodine-mediated tyrosine oxidative modification was reported in 2024 by the Chandrasekhar group, which developed an amination strategy. Using PIDA (2 equiv.) in methanol, the phenolic side chain of tyrosine was oxidized and trapped by methanol, followed by treatment with trimethyl orthoformate and glycine in methanol at 100 °C for 2 h (Scheme 2.6). This methodology was applicable to tyrosine-containing di- and tripeptides.

Mechanistically, tyrosine is initially oxidized by PIDA and trapped by methanol to form a methoxy intermediate. Subsequent reaction with glycine generates an imine via water elimination. Trimethyl orthoformate then promotes methoxy group elimination, followed by imine hydrolysis to afford the corresponding aniline derivative. Further oxidation with PIDA in methanol furnishes the final aminated product.[137]

Chandrasekhar, *2024*

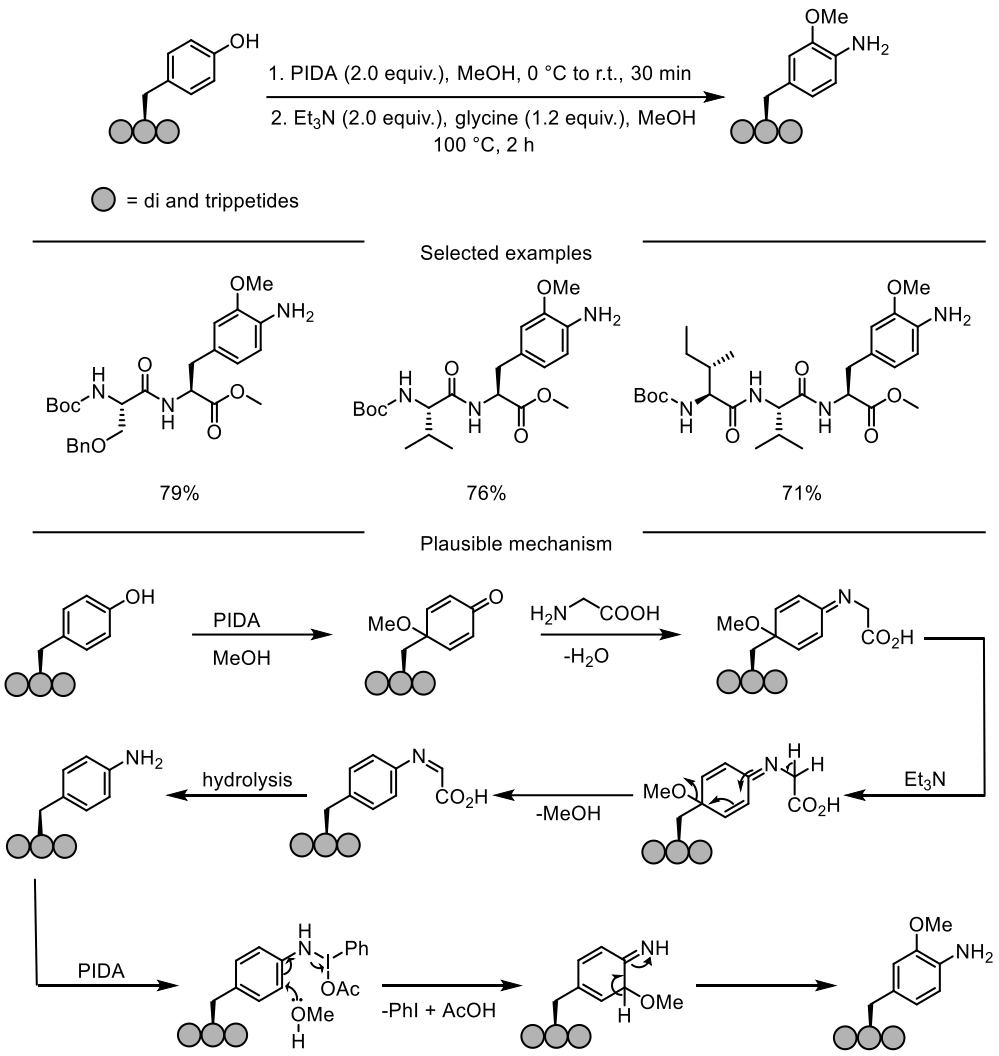

Scheme 2.6: Modification of tyrosine containing peptides to afford aminated products.

Hypervalent iodine reagents, particularly iodine(V) species, have proven to be powerful oxidant. 2-Iodoxybenzoic acid (IBX) is a well-established oxidant for alcohol and phenol oxidation in small-molecule chemistry. Kinetic studies have demonstrated that phenolic substrates are oxidized preferentially over aliphatic alcohols, providing an inherent level of chemoselectivity. This selectivity suggests that IBX and related reagents could selectively target tyrosine residues within peptides.

Despite these advantages, the application of hypervalent iodine reagents to peptide systems-and specifically to biomimetic tyrosine oxidation-has remained largely unexplored. This gap represents a significant opportunity to develop mild, metal-free methods for late-stage peptide functionalization.

2.2 Late-Stage Functionalisation of Peptides

The appeal of Late-stage functionalisation (LSF) lies in its modularity and efficiency. Rather than resynthesizing an entire peptide sequence for each structural variant, a single parent peptide can serve as a common precursor from which multiple analogues are rapidly generated. This capability is particularly valuable in drug discovery, where small structural changes can dramatically influence potency, selectivity, stability, and pharmacokinetic behaviour. From a practical standpoint, late-stage modification offers operational simplicity and synthetic flexibility. Consequently, LSF has become an essential strategy in chemical biology, medicinal chemistry, and peptide-based materials science.

Building on this strategy, LSF can be harnessed to selectively transform tyrosine residues into new functional motifs. Oxidation of tyrosine with IBX generates an *o*-quinone intermediate, which can be intercepted by 1,2-phenylenediamine to afford phenazine scaffolds, representing a true scaffold transformation of the side chain. Beyond structural reprogramming, these phenazine motifs are intrinsically fluorescent, providing a versatile platform for peptide labeling, molecular imaging, and functional studies.

2.3 Project Goals

Methods for the late-stage diversification of peptides remain limited by narrow functional-group tolerance and a reliance on peripheral side-chain reactivity. Chemical strategies for tyrosine modification largely preserve the native nucleophilic character of the phenolic side chain, restricting the range of accessible structural and physicochemical diversity. In contrast, biological systems exploit oxidative activation of tyrosine to transiently invert phenol polarity, enabling bond-forming transformations that are difficult to access synthetically.

The goal of this chapter was to develop a mild, metal-free approach to tyrosine functionalization that translates this enzymatic logic into a practical method for short peptides. Oxidation of tyrosine residues using a hypervalent iodine(V) reagent allows in situ formation of electrophilic *ortho*-quinone intermediates under conditions compatible with diverse amino acid side chains. These *o*-quinones are highly electrophilic species that participate in a broad range of bond-forming reactions with nucleophiles, including amines, thiols, and electron-rich aromatic systems. In biological contexts, such intermediates are generated transiently and consumed rapidly, ensuring precise control over reactivity.

In this chapter, the quinone intermediate was intercepted by phenylenediamines, converting the tyrosine core into phenazine scaffolds (Scheme 2.7). The resulting phenazine motifs are intrinsically fluorescent, providing a built-in functional handle for molecular imaging and labelling applications . Collectively, this work establishes IBX-mediated tyrosine oxidation as a practical and versatile method for late-stage peptide modification, expanding the chemical space accessible from native amino acid residues.

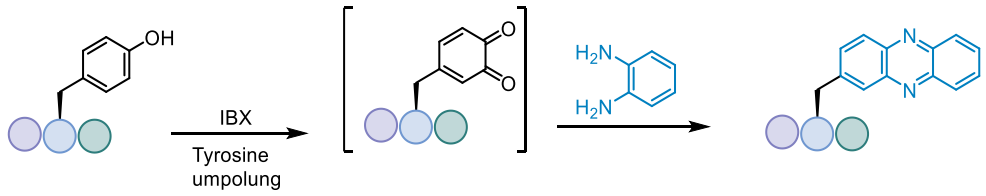

Scheme 2.7: Bioinspired strategy for skeletal tyrosine diversification.

2.4 Optimization Studies

The investigation commenced with the evaluation of a one-pot protocol for the conversion of *N*-Boc-tyrosine methyl ester **2.1** to the corresponding phenazine-derived amino ester **2.2**. Oxidation was carried out using IBX (1.2 equiv.) in THF at room temperature. Upon complete consumption of the starting material, as monitored by TLC, a THF solution of 4-fluorobenzene-1,2-diamine (A, 0.25 M) was introduced, and the reaction mixture was heated at 60 °C for 24 h. Under these initial conditions, compound **2.2** was obtained in 30% yield as an equimolar

mixture of regioisomers (Table 2.1, entry 1) . Subsequent solvent screening (Table 2.1, entries 2–5) demonstrated that the use of methanol, in combination with increased equivalents of A1, led to a substantial improvement in yield, affording **2.2** in 68% yield. In contrast, lowering the temperature during the nucleophilic trapping step resulted in diminished conversion (Table 2.1, entry 6). Replacement of methanol with the less toxic ethanol further enhanced the efficiency, providing the desired phenazine-derived amino ester in 70% yield (Table 2.1, entry 7). Given recent reports concerning the potential explosive hazards associated with IBX, it is noteworthy that the oxidant could be substituted with the safer analogue SIBX[13] with only a marginal decrease in 68% yield (Table 2.1, entry 8).

Table 2.1 Optimization studies for the skeletal modification.

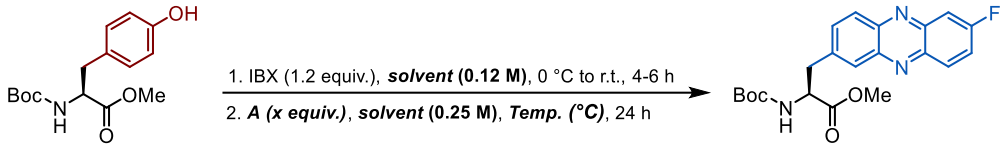

2.1 **2.2**

Entry	A (x equiv.)	Solvent	Temp. (°C)	Yield (%)[a,b]
1	1.2	THF	60	30[a]
2	1.2	Benzene	60	31[a]
3	1.2	MeCN	60	13[a]
4	1.2	Acetone	60	6[a]
5	2.2	MeOH	60	68[a]
6	2.2	MeOH	r.t.	20[a]
7	2.2	EtOH	60	70[a]
8	2.2	EtOH	60	68[b]

[a] Yields determined via ^{19}F NMR using fluorobenzene as internal standard. **2.2** was formed as a 1:1 mixture of regioisomers.[b] SIBX (1.2 equiv.) was used instead of IBX.

To evaluate the broader applicability of this transformation, a tyrosine-containing dipeptide, Boc-Gly-Tyr-OMe **2.3** was selected for optimization. The effect of the equivalents of 1,2-diamine was first investigated (Table 2.2, entries 1-3). Increasing the amount of diamine from 1.2 to 2.2 equivalents resulted in a marked improvement in the yield of the corresponding phenazine-derived product (Table 2.2, entry 2). Further increasing the loading to 5.2 equivalents of diamine, however, did not lead to additional yield enhancement, indicating saturation of the reaction efficiency. In accordance with green chemistry considerations,[138] subsequent studies were therefore conducted using 2.2 equivalents of the 1,2-diamine.

The influence of additives on the reaction outcome was then explored. The addition of triethylamine (TEA) was well tolerated and did not adversely affect the reaction efficiency, whereas the use of N,N-Diisopropylethylamine (DIPEA) led to a modest decrease in 58% yield (Table 2.2, entry 5). Acidic additives were also evaluated: acetic acid had minimal impact on

product formation (Table 2.2, entry 7), while the use of methanesulfonic acid resulted in a pronounced decrease in yield (Table 2.2, entry 6).

Table 2.2 Optimization studies with dipeptide for skeletal modification.

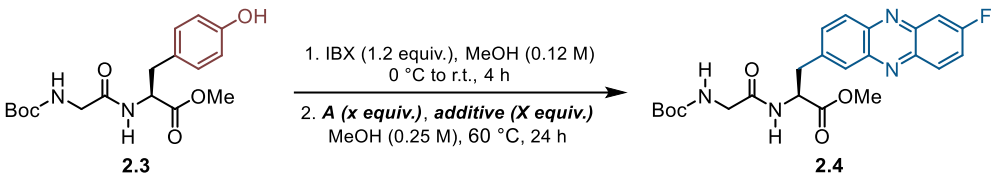

2.3 **2.4**

Entry	A (equiv.)	Additive (equiv.)	Yield (%)[a]
1	1.2	-	57
2	2.2	-	75
3	5.2	-	75
4	2.2	TEA (5.0)	71
5	2.2	DIPEA (5.0)	58
6	2.2	$MeSO_3H$ (5.0)	20
7	2.2	AcOH (5.0)	70

[a] Yields determined via ^{19}F NMR using fluorobenzene as internal standard. **2.4** was formed as a 1.5:1 mixture of regioisomers.

The crude analysis of Table 2.2, entry 2 using ^{19}F NMR and fluorobenzene as an internal standard**. 2.4** was formed as 1.5:1 mixture of regioisomers in 75% yield (Figure 2.1).

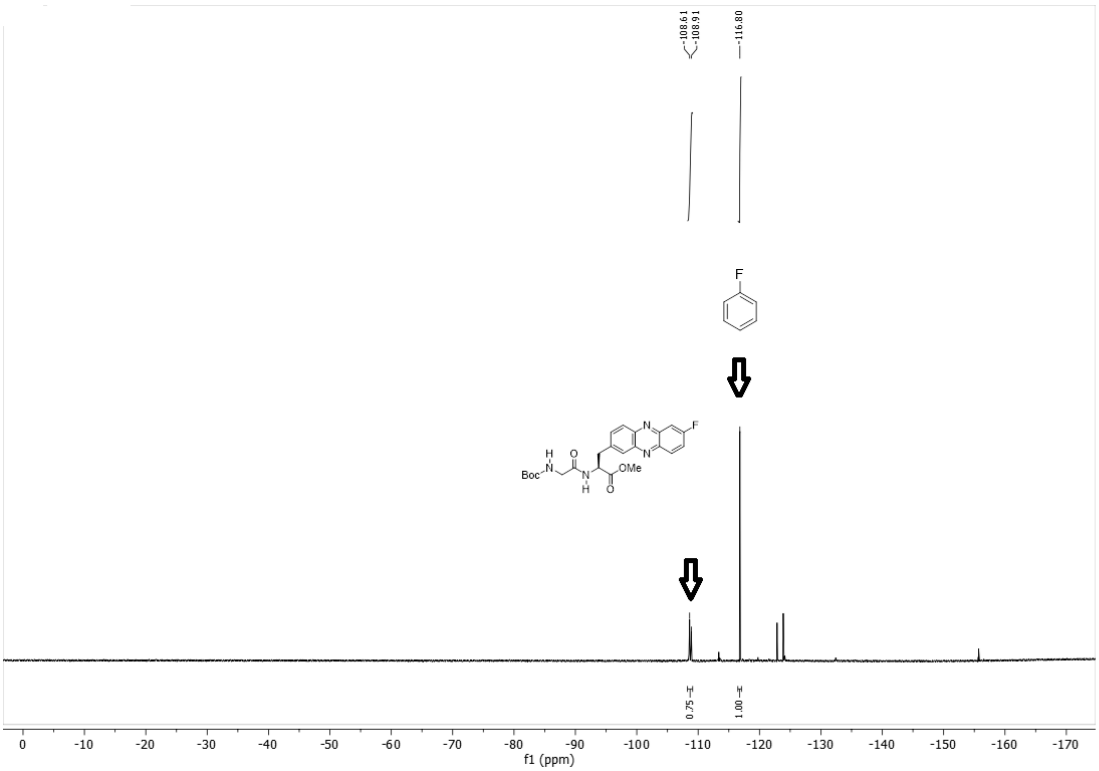

Figure 2.1: Crude analysis of Table 2.2, entry 2 using ^{19}F NMR and fluorobenzene as an internal standard. 2.4 was formed as 1.5:1 mixture of regioisomers in 75% yield. ^{19}F (376 MHz, MeOD) δ -108.6, -108.9, -116.80.

To find biocompatible reaction conditions, water was evaluated as a solvent. Initially, the dipeptide Boc-Gly-Tyr-OMe **2.3** was oxidized in methanol at 0 °C to room temperature. Subsequently, the amount of 4-fluorobenzene-1,2-diamine (A) was increased to 10 equivalents and added as a solution in H_2O/MeCN (19:1), and the reaction mixture was heated to 60 °C, affording the desired product in 26% yield (Table 2.3, entry 1). Further solvent optimization showed that H_2O/MeCN mixtures in ratios of 9:1 and 1:1 improved the yield to 36% and 33%, (Table 2.3, entries 2-3) respectively. Although these yields were modest, the compatibility observed under aqueous conditions highlights the potential for further optimization toward applications in protein modification.

Table 2.3 Optimization studies under aqueous conditions for skeletal modification.

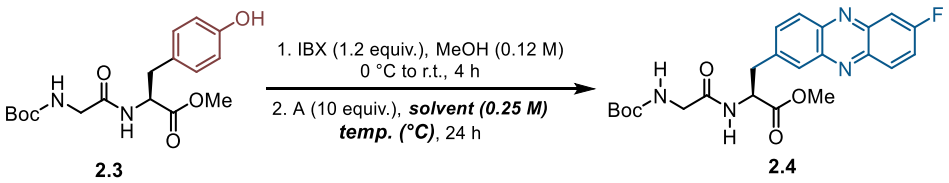

Entry	Solvent	Temp. (°C)	Yield (%)[a]
1	H_2O:MeCN (19:1)	60	26
2	H_2O:CH_3OH (1:1)	r.t.	36
3	H_2O:MeCN (1:1)	r.t.	33

[a] Yields determined via ^{19}F NMR using fluorobenzene as internal standard. **2.4** was formed as a 1.5:1 mixture of regioisomers.

2.5 Amino acid Compatibility Screening

The chemoselectivity of the skeletal modification protocol was evaluated by subjecting *N*-Boc-tyrosine methyl ester **2.1** to the optimized conditions in the presence of 15 canonical amino acids, monitoring both formation of the phenazine-derived amino ester **2.5** and the recovery of the added amino acid (Scheme 2.8).

Aliphatic residues such as valine and isoleucine were well tolerated, with >95% of the additive remaining and compound **2.5** obtained in good yield (66%). Proline exhibited moderate compatibility, with 67% of the additive recovered and **2.5** formed in slightly diminished yield (55%).

Aromatic amino acids, including phenylalanine and tryptophan, displayed excellent tolerance (>90% remaining additive), affording **2.5** in high yields (71-73%). Acidic residues such as aspartic acid had negligible influence on the reaction outcome, with >95% recovery of the additive and a 70% yield of **2.5**. In contrast, basic amino acids, including histidine, arginine, and lysine, markedly suppressed product formation, resulting in low yields (8-18%), likely due to interference with the oxidation step or competing side reactions.

Amidic residues such as asparagine and glutamine were largely inert under the reaction conditions, providing **2.5** in good yields (58-63%). Notably, hydroxy-containing amino acids, including serine and threonine, which are often sensitive to oxidative conditions, were well tolerated (>95% remaining additive), affording moderate yields of **2.5** (58-61%). Sulfur-containing residues showed more varied behavior: methionine and cystine were partially compatible (72–76% additive remaining), delivering **2.5** in moderate to good yields (46–76%), whereas cysteine was completely consumed, and the desired product **2.5** was obtained in only 27% yield.

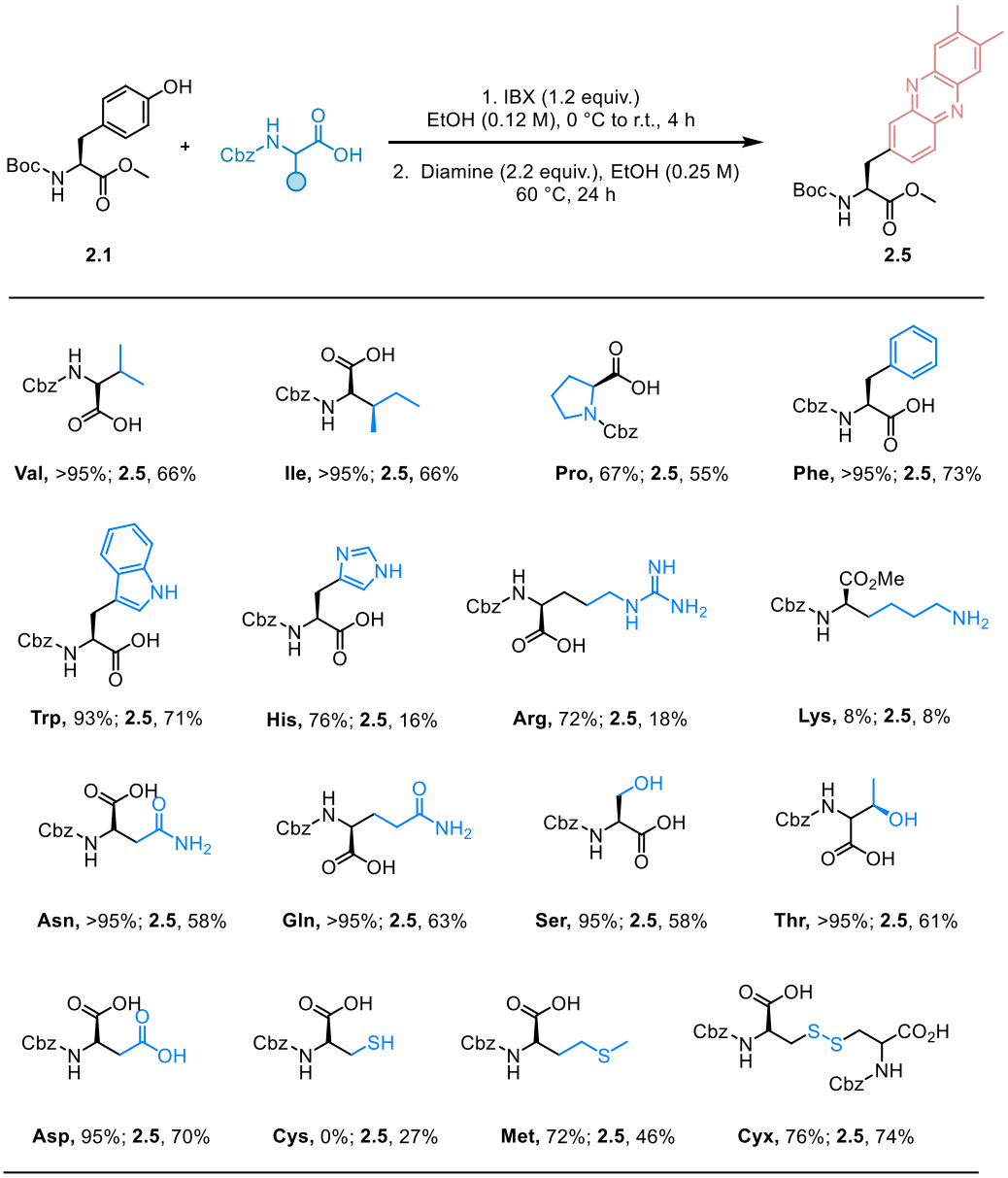

Scheme 2.8: Amino acid compatibility screening with 15 canonical amino acids. Reactions were carried out on 0.05 mmol scale. Yields were determined by HPLC using benzoic acid as internal standard.

Overall, these studies highlight the broad chemoselectivity and functional-group tolerance of the protocol across a diverse set of amino acid side chains, while identifying basic residues and cysteine as the principal limitations (Figure 2.2).

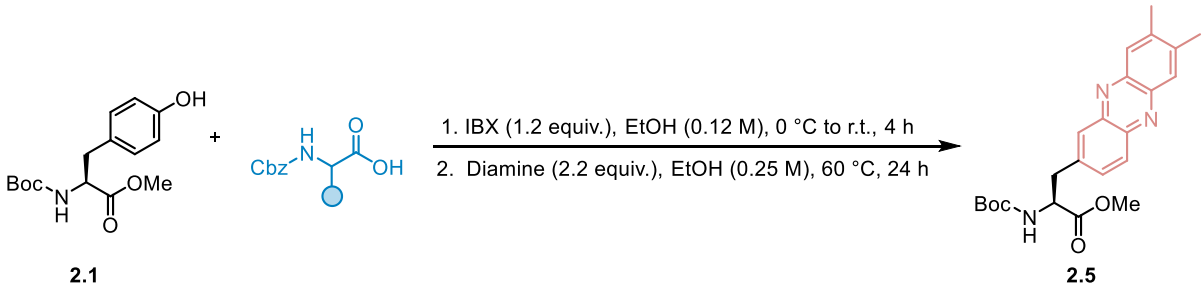

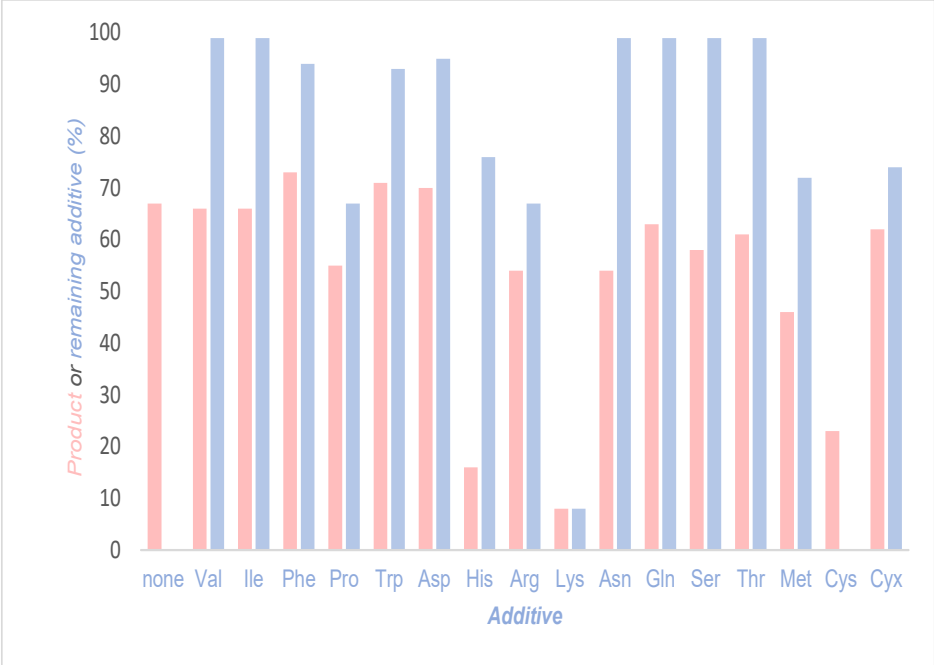

Figure 2.2: Chart illustrating the recovery of intact amino acids and formation of the desired product.

2.6 Scope and Limitations

Having established the chemoselectivity of the transformation, the scope and limitations were subsequently explored (Scheme 2.9). The reactivity of various 1,2-phenylenediamines was first examined using Boc-Gly-Tyr-OMe **2.3** as the model substrate. Unsubstituted *o*-phenylenediamine furnished the corresponding phenazine-derived amino ester **2.6** in excellent yield (80%). Substituents on the phenylenediamine ring, whether electron-withdrawing **2.7-2.8** or electron-donating **2.9-2.11**, showed little effect on the reaction efficiency, providing the desired products in uniformly high yields (72–85%).

In contrast, diamines incorporating extended aromatic systems exhibited substantially reduced reactivity, with compound **2.12** isolated in only 42% yield. Furthermore, less nucleophilic heteroaryl diamines, including pyridine-2,3-diamine and pyrimidine-4,5-diamine, failed to afford detectable amounts of product under the optimized conditions **2.13-2.14**.

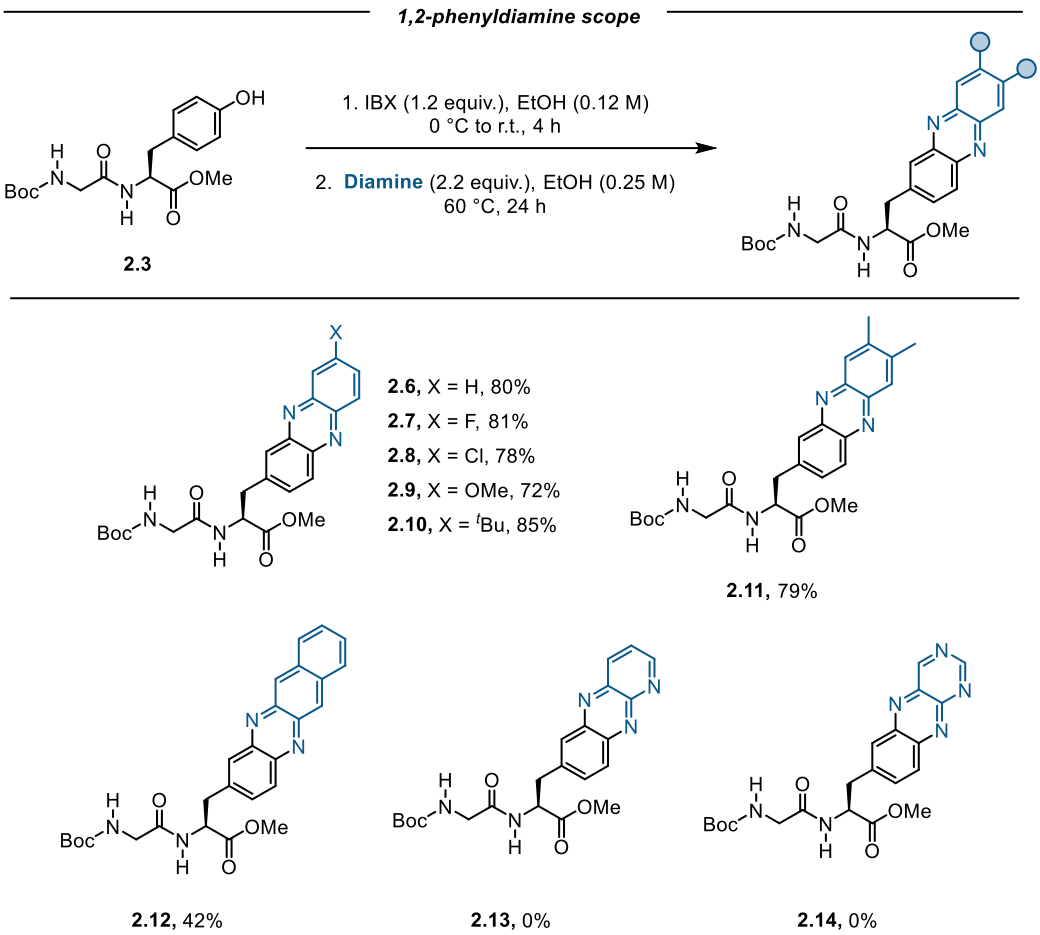

Scheme 2.9: Scope of diversification of tyrosine residue with different diamines. All reactions were carried out on 0.3 mmol scale.

Guided by these observations and the outcomes of the chemoselectivity studies, the transformation was extended to a series of oligopeptides bearing tyrosine residues located either at the C-terminus or within internal positions (Scheme 2.10). Peptides containing aliphatic residues such as valine, glycine, alanine, or leucine in combination with a C-terminal tyrosine were efficiently transformed into the corresponding phenazine-modified peptides **2.15-2.17** in good yields (60–75%). Although proline had previously been identified as a challenging residue, *N*-Boc protection alleviated this limitation, allowing isolation of the tripeptide **2.18** in 73% yield. Aromatic residues, including phenylalanine and tryptophan, as well as polar residues such as glutamic acid methyl ester and glutamine, were well tolerated under the reaction conditions, affording products **2.19-2.22** in yields ranging from 48 to 62%. Notably, peptides containing oxidation-sensitive residues such as serine **2.23**, threonine **2.24**, or methionine **2.25** also proved compatible with the transformation, delivering the desired phenazine-derived peptides in good yields (55–61%).

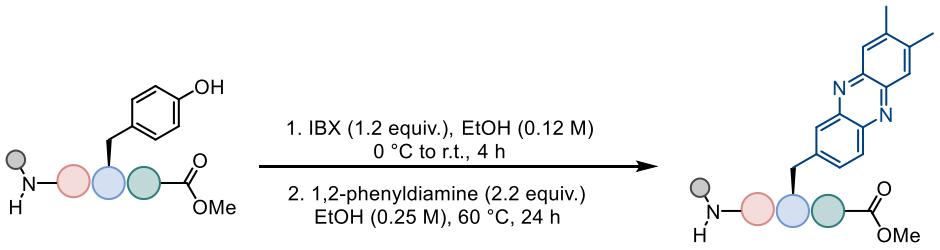

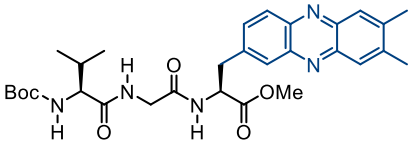

2.15, 71%

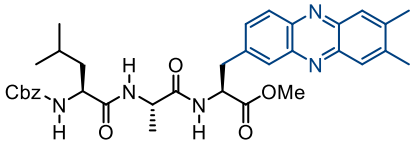

2.16, 60%

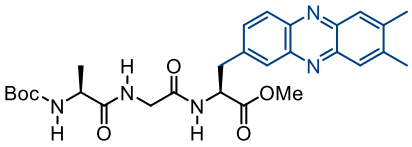

2.17, 75%

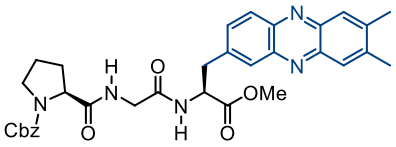

2.18, 73%

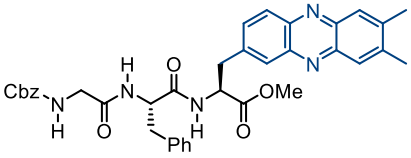

2.19, 62%

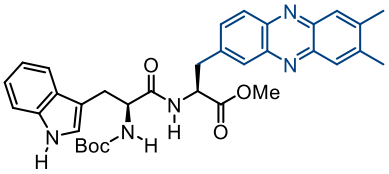

2.20, 55%

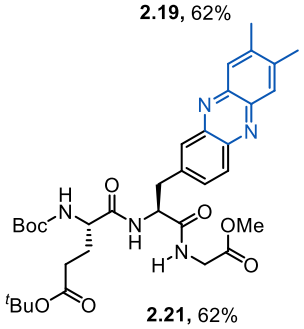

2.21, 62%

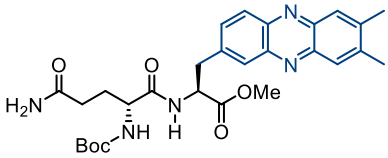

2.22, 48%

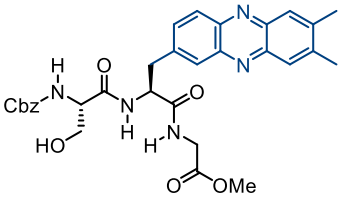

2.23, 55%

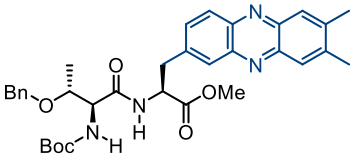

2.24, 61%

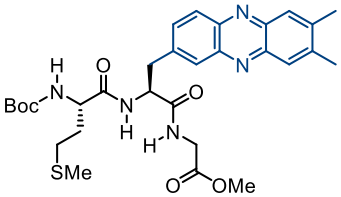

2.25, 62%

Scheme 2.10: Scope of diversification of tyrosine residue in short peptides. All reactions were carried out on 0.25 mmol scale.

2.7 Conclusion

In conclusion, a mild and chemoselective strategy for the late-stage functionalisation of tyrosine residues has been established. IBX-mediated oxidation enables the in situ generation of an *ortho*-quinone intermediate, which undergoes efficient nucleophilic trapping with phenylenediamines. This transformation induces an umpolung of the tyrosine aromatic core and results in the formation of phenazine-modified peptides. The method displays broad functional group tolerance and is compatible with diverse peptide sequences, including those bearing oxidation-sensitive residues. The intrinsic fluorescence of the resulting phenazine motifs further highlights the potential of this approach for peptide labelling and molecular imaging applications.

From a methodological perspective, the transformation exhibits broad functional-group tolerance, operates in densely functionalized oligopeptides, and enables late-stage modification without the need for de novo synthesis or protecting-group-intensive routes. More broadly, this study establishes phenolic umpolung as a transferable design principle for peptide modification and expands the methodological scope of hypervalent iodine(V) chemistry in complex molecular settings.

2.8 Outlook

Based on the amino acid compatibility screenings described in this chapter, basic residues and cysteine were identified as the principal limitations of the transformation. Cysteine, a notable limitation, is addressed in subsequent chapters. Attention was therefore directed toward basic residues. Secondary amines were tested with tyrosine under oxidative conditions. Tyrosine was first oxidized using IBX to generate the corresponding *o*-quinone, which was subsequently treated with the secondary amine like morpholine at room temp. **2.26** affording amine-conjugated catechol product (Scheme 2.11).

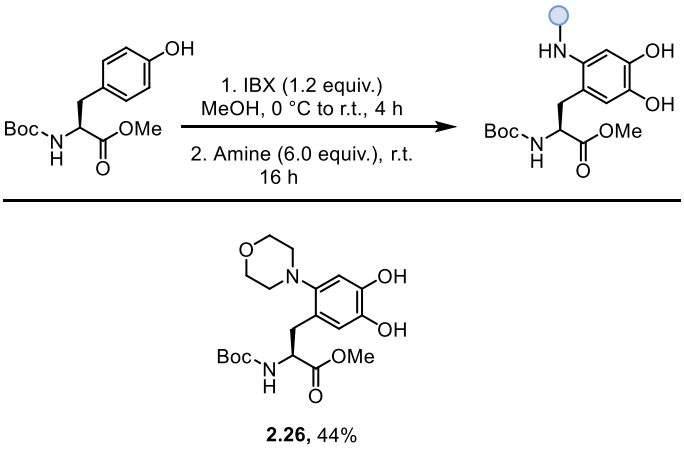

2.26, 44%

Scheme 2.11: Synthesis of tyrosine-amine conjugate.

Related work by the Francis group demonstrated tyrosinase-mediated Proline modification with tyrosinase enzyme (Scheme 2.12).[139] Future work could extend this approach to proline- and lysine-containing peptides, to from tyrosine-proline/lysine cross-linkage with IBX.

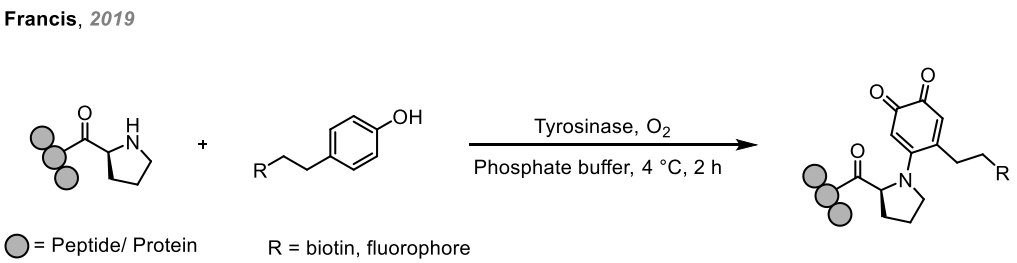

Scheme 2.12: Enzymatic modification of proline residues.

Further expansion involves catechol derived from IBX oxidation of tyrosine, which can be trapped with boronic acids to form boronated ester products.[140,141] Initial studies showed that catechol reacts with boronic acids in the presence of triethylamine to give product **2.28**, and with 2-formylphenylboronic acid/^{t}BuNHOH to afford boron esters **2.29,** (Scheme 2.13), demonstrating new avenues for tyrosine conjugation and highlighting the potential to broaden the chemical versatility of peptides**.**

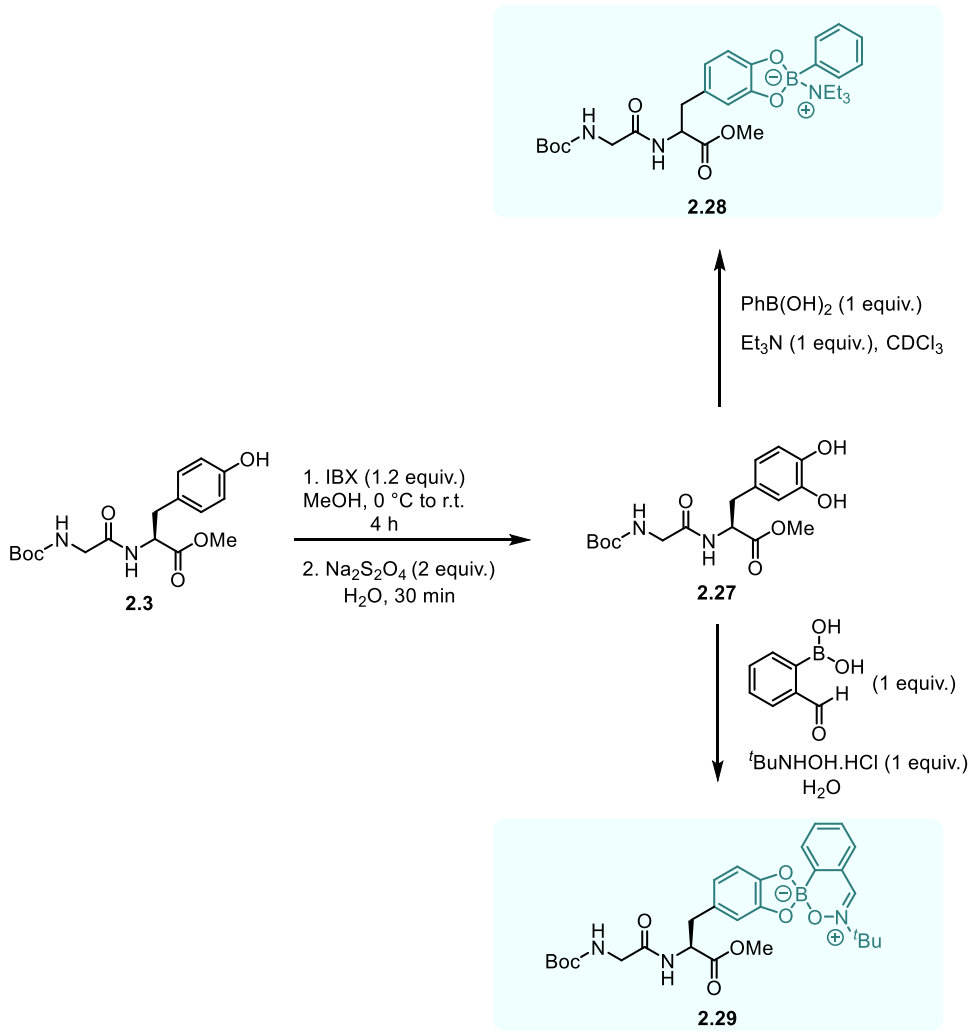

Scheme 2.13: Synthesis of tyrosine-boronate esters from catechol intermediates derived from tyrosine.

In addition, the introduction of 4-azidobenzene-1,2-diamine as a bifunctional coupling partner. The azide functionality would enable subsequent diversification via copper-catalyzed azide-alkyne cycloaddition (CuAAC), thereby expanding the modularity of the IBX-generated tyrosine platform (Scheme 2.14).

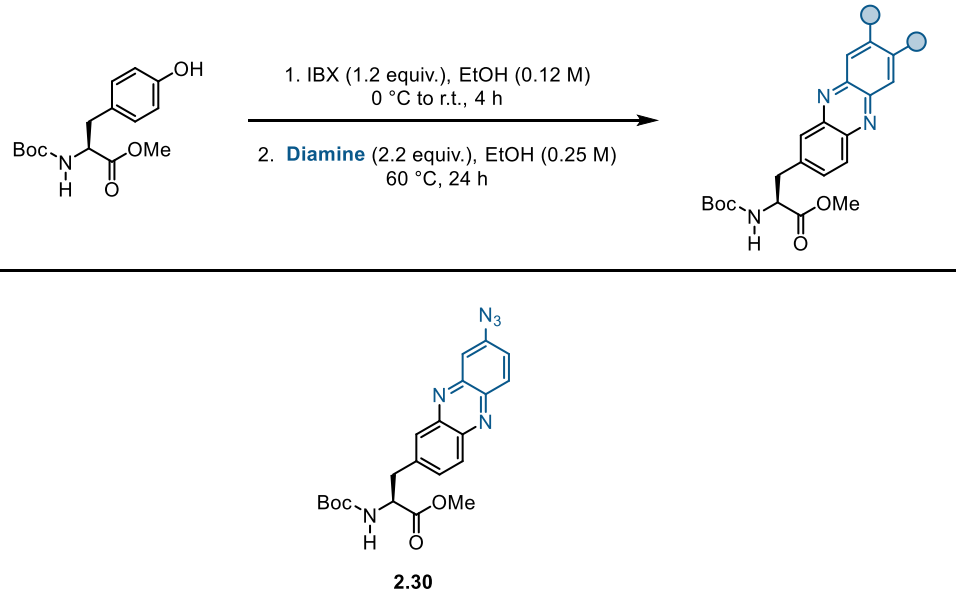

2.30

Scheme 2.14: Functionalization of tyrosine-derived *o*-quinone with 4-azidobenzene-1,2-diamine.

Chapter 3
Tyrosine Modification via Crosslinking Strategies

3.1 Introduction

Covalent Crosslinking in Peptides and Proteins: Biological Significance and Chemical Challenges

The formation of covalent crosslinks between peptides and proteins is a fundamental phenomenon in biological systems, playing important roles in both physiological function and pathological progression. Such crosslinks can arise within a single polypeptide chain (intramolecular or intrachain crosslinks), between two chains of the same protein (interchain crosslinks), or between distinct molecular entities (intermolecular crosslinks).[142] Classic biological examples include interchain and intrachain disulfide bonds in human insulin, enzymatically mediated protein crosslinking in the extracellular matrix, pigment formation and structural reinforcement (Figure 3.1).[143,144]

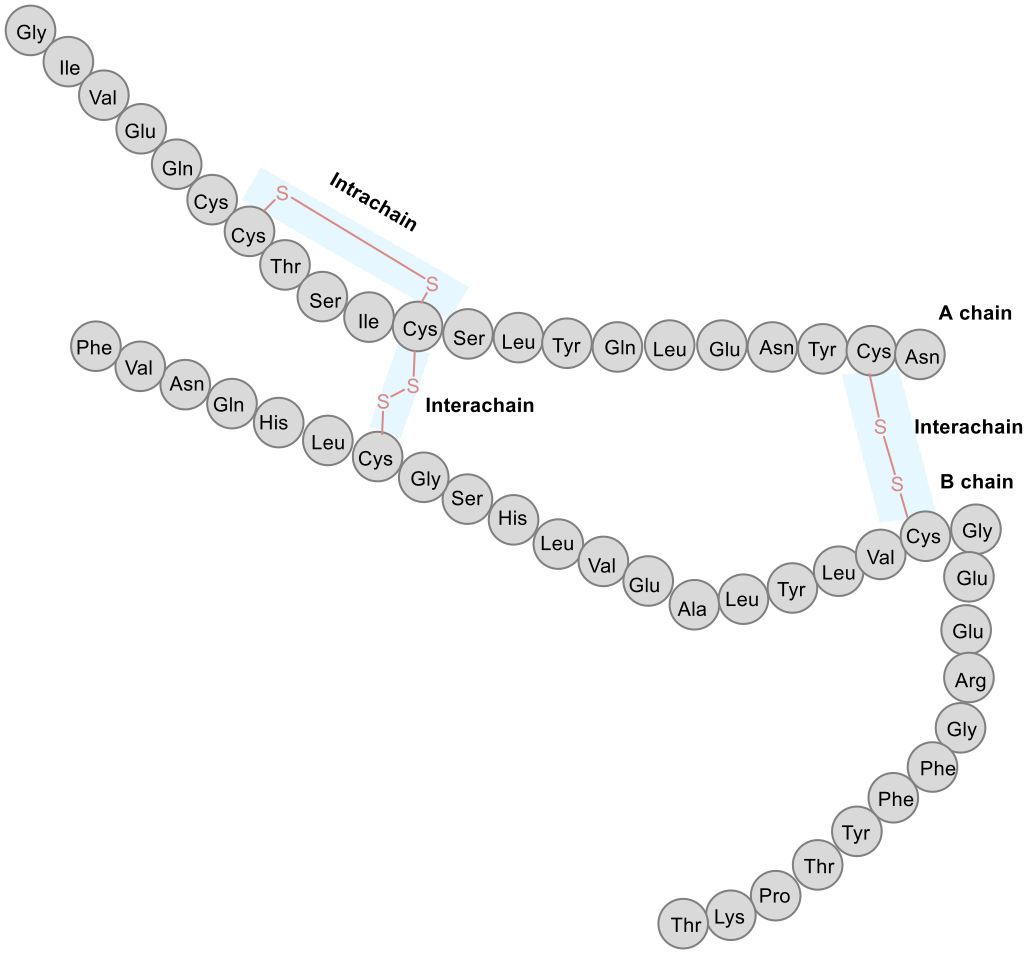

Figure 3.1: Cross linkages in human insulin.

From a structural perspective, covalent crosslinks can stabilize protein structures, regulate conformational dynamics, and enable specific biological activities. In many cases, these linkages are indispensable for proper folding, structural stability, and biological function.[145]

Conversely, uncontrolled or aberrant crosslink formation can be detrimental, leading to altered protein turnover, impaired activity, or aggregation processes associated with aging and disease.[146] Crosslinking therefore constitutes a finely balanced process, acting both as a structural necessity and a potential source of dysfunction.

Despite their biological importance, the selective formation or manipulation of covalent cross-links through purely chemical methods remains a significant challenge. This difficulty arises from the intrinsic complexity of peptides and proteins, which present dense arrays of chemically similar functional groups, making selective residue targeting inherently demanding and often leading to heterogeneous product mixtures. Such limitations are especially problematic in the construction of defined protein-protein and protein-peptide conjugates, which play an increasingly important role in vaccine development, immunotherapy, cellular signaling, and targeted drug delivery.[147] Accordingly, there remains a need for cross-linking strategies capable of selectively targeting native amino acid residues under mild conditions.

3.2 Existing Strategies for Biomolecular Crosslinking and their Limitations

Current chemical approaches to peptide and protein crosslinking largely rely on homobifunctional crosslinking reagents or bioorthogonal coupling reactions. These reagents are broadly classified as homobifunctional or heterobifunctional, depending on the nature of their reactive groups.

Homobifunctional crosslinking agents are bireactive compounds that contain identical functional groups at both termini.[148] Most of these reagents are symmetrically designed, featuring a carbon-chain spacer that connects the two equivalent reactive ends. Such crosslinkers can covalently connect two proteins by reacting with the same type of functional group on each molecule, either intermolecularly to link separate proteins or intramolecularly to stabilize higher-order structure (Figure 3.2).[149] The ability to couple biomolecules possessing distinct binding specificities or catalytic functions significantly expanded the scope for designing multifunctional conjugates. This capability enabled the development of reagent systems widely applied in biochemical assays and molecular targeting applications.

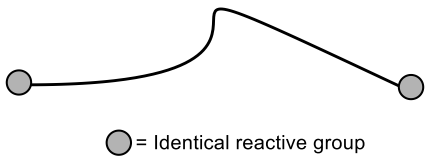

Figure 3.2: General design of homobifunctional crosslinkers showing identical reactive groups connected by a carbon-chain spacer of variable length.

While operationally straightforward, these reagents often provide limited control over site selectivity. During conjugation of two distinct biomolecules, homobifunctional crosslinkers can give rise to undesired side reactions, including self-conjugation, intramolecular crosslinking, and higher-order polymerization. Consequently, the resulting products are frequently heterogeneous and structurally ill-defined.

Despite these well-recognized limitations, homobifunctional reagents remain widely used in a broad range of conjugation applications. In many practical settings, the level of control they afford is sufficient to generate functionally effective bioconjugates. For example, glutaraldehyde-mediated antibody-enzyme conjugates continue to be routinely employed in research and diagnostic platforms, underscoring their enduring utility despite inherent selectivity constraints.

Some common examples of amine-to-amine crosslinkers include dithiobis(succinimidyl propionate) (DSP) which is ideally used for crosslinking intracellular proteins prior to cell lysis, disuccinimidyl suberate (DSS) commonly applied in receptor ligand cross-linking studies, and disuccinimidyl tartrate (DST) which is used when cleavable crosslinks are required while preserving native disulfide bonds (Figure 3.3).[149]

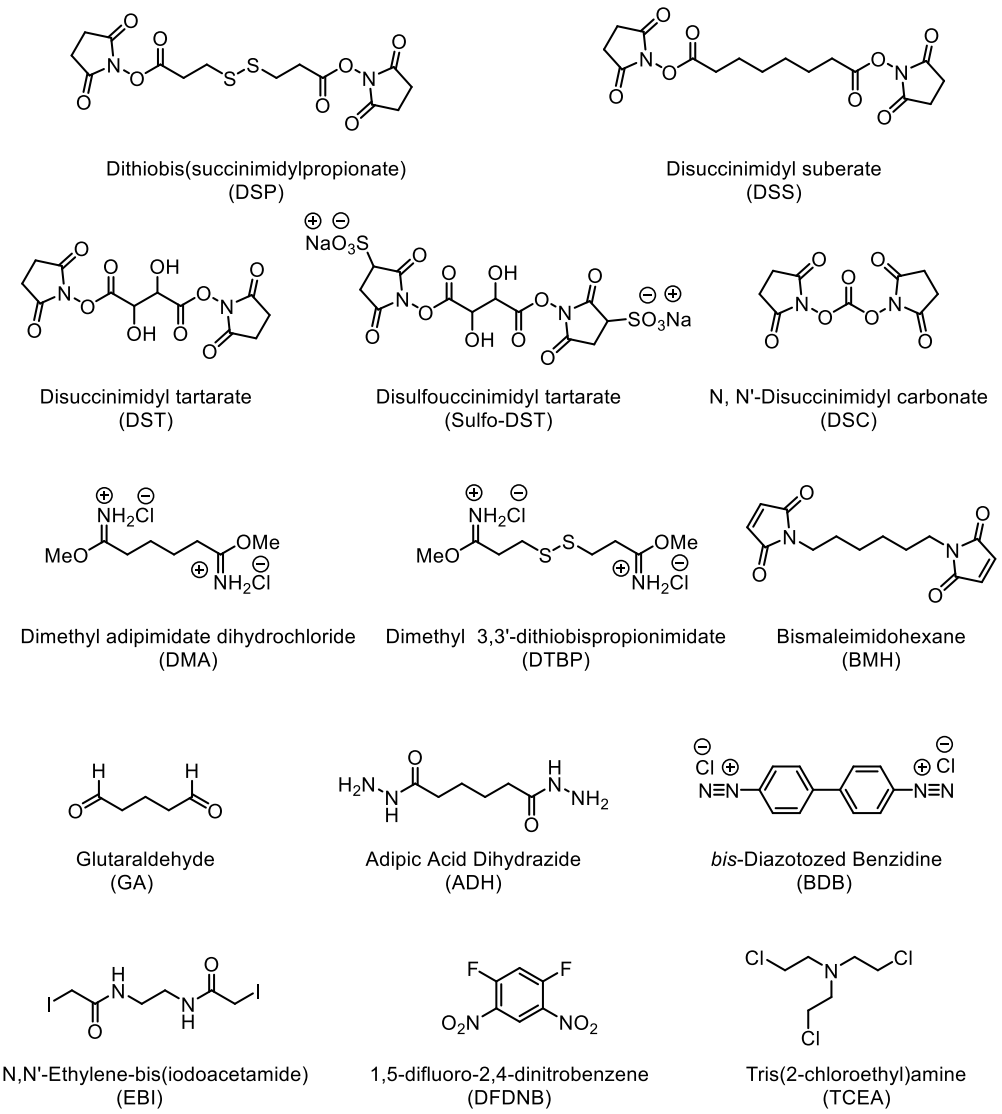

Figure 3.3: Examples of commonly used homobifunctional crosslinking reagents.

At present, the most widely used crosslinkers are homobifunctional *N*-hydroxysuccinimide (NHS) esters that modify lysine ε-amino groups to form amide bonds. For example, dithiobis(succinimidylpropionate) (DSP) reacts with lysine residues at both termini, linking proteins through a central disulfide spacer that can be cleaved under reducing conditions (Scheme 3.1).[150,151]

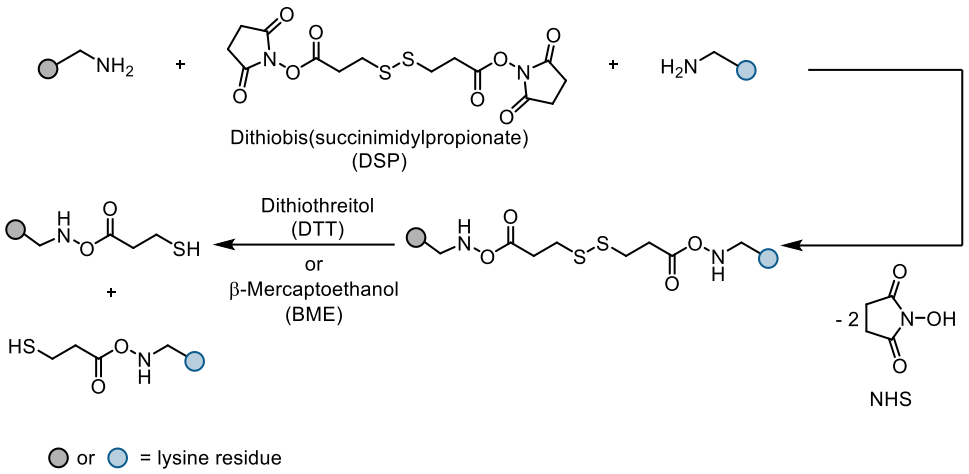

Scheme 3.1: DSP-mediated crosslinking of lysine residues via NHS ester coupling; the resulting disulfide-linked conjugates are cleavable under reducing conditions.

To address the limitations associated with lysine-directed NHS ester chemistry, alternative residue-selective crosslinking strategies have been developed. For example, Huan and Li. reported 4,4′-(disulfanediylbis(ethane-2,1-diyl))bis(1,2,4-triazolidine-3,5-dione) (DBB) as a tyrosine-selective cross-linker. In their approach, DBB was first electrochemically oxidized to generate the reactive species. The activated species reacts with tyrosine residues and forms cross-links upon subsequent electrochemical reduction. Importantly, DBB contains an electrochemically cleavable disulfide bond, enabling controlled and reversible cross-linking. This feature allows the formation of transient crosslinks, which are particularly valuable for probing protein–protein interactions. The resulting conjugates can be efficiently characterized using mass spectrometry following electrochemical cleavage. The reactivity and applicability of DBB were demonstrated using several model peptides and proteins, including angiotensin II, insulin, β-casein, recombinant human growth hormone, and bovine serum albumin (BSA) (Scheme 3.2).[152]

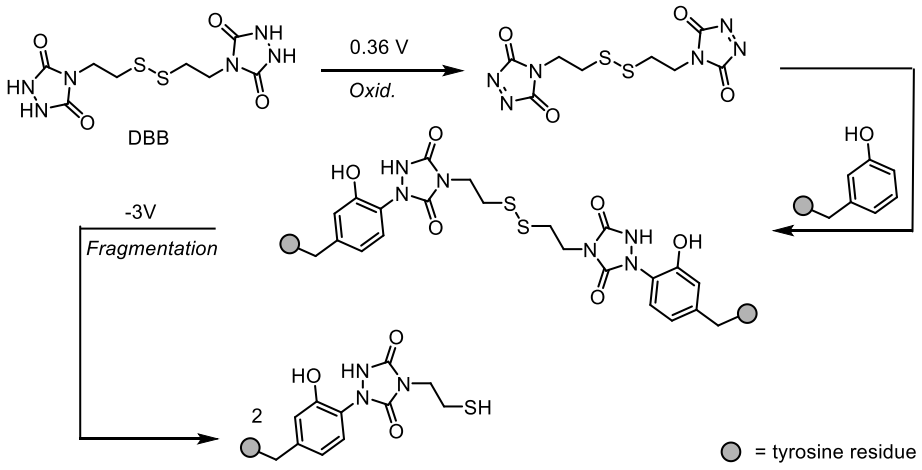

Scheme 3.2: Electrochemically activated DBB-mediated cross-linking of tyrosine residues, followed by reductive cleavage of the disulfide bond.

Crosslinkers targeting glutamic and aspartic residues have also been developed; however, these approaches generally require activation of the carboxylic acid side chains under conditions that can perturb protein structure and compromise biological integrity.[153,154]

Native chemical ligation and enzyme-mediated methods, such as sortase-catalyzed coupling, offer more controlled conjugation strategies but are largely restricted to peptide termini.[155,156] This positional constraint significantly limits molecular design, particularly when internal crosslinks are desired. Genetic fusion of protein domains is another commonly used approach to generate chimeric constructs; however, such strategies often require extensive optimization of linker lengths, may introduce folding or expression challenges, and are typically limited to N- or C-terminal connectivity.[147,157]

In contrast, heterobifunctional crosslinkers contain two different reactive functional groups, enabling sequential (two-step) conjugation strategies that improve selectivity and reduce uncontrolled polymer formation (Figure 3.4). This staged approach allows selective modification of one protein at a specific functional group, followed by reaction with a second biomolecule through a distinct chemical handle. Such reagents are particularly advantageous when direct amine modification is problematic, as lysine residues are often abundant and may be located at enzymatically or structurally critical sites.

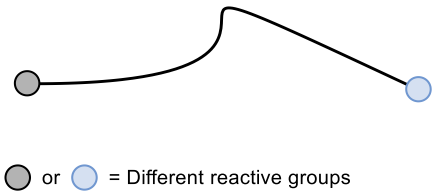

Figure 3.4: General design of heterobifunctional crosslinkers showing different reactive groups connected by a carbon-chain spacer of variable length.

Some common examples of heterobifunctional crosslinkers include m-maleimidobenzoyl-*N*-hydroxysuccinimide ester (MBS), *N*-γ-Maleimidobutyryloxysuccinimide ester (GMBS), *N*-(ε-Maleimidocaproic acid (EMCH) and photoreactive crosslinkers such as *p*-aziobenzoyl hydrazide (ABH) (Figure 3.5).

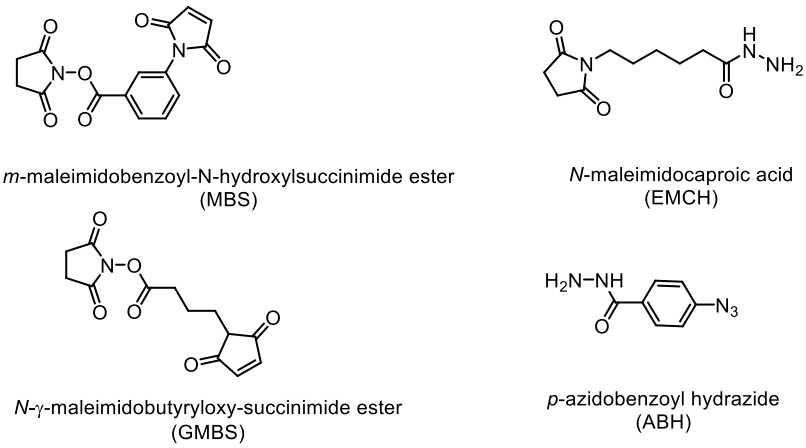

Figure 3.5: Examples of commonly used heterobifunctional crosslinking reagents.

Alternatively, click-type reactions between bioorthogonal functional groups provide high efficiency and selectivity but require prior introduction of non-native handles through artificial amino acid incorporation, metabolic labelling or synthetic steps.[158–160] Collectively, these approaches illustrate the ongoing challenge of achieving residue-selective, structurally defined crosslink formation in native protein systems under mild and biologically compatible conditions.

3.3 Bioinspired Oxidative Crosslinks in Nature

In contrast to many engineered conjugation strategies, nature frequently utilises oxidative chemistry of native amino acid side chains to form covalent crosslinks, providing structural stability and functional diversity. Disulfide bonds are the most well-characterized example and are ubiquitous in extracellular and secreted proteins.[161–163] Nevertheless, ensuring correct disulfide pairing in proteins containing multiple cysteine residues remains a formidable

challenge, highlighting the complexity associated with achieving controlled crosslink formation.[142]

Beyond disulfide bonds, several non-enzymatic cross-links have been identified that arise from oxidative or electrophilic activation of specific amino acid side chains. Cysteine frequently participates in such processes, for example through reaction with dehydroalanine derived from cysteine residues, forming stable C–S thioether linkages, or through formation of sulfenyl amide (S–N) or vinyl ether structures under oxidative conditions.[164–166] Electrophilic intermediates generated from aromatic residues also enable crosslink formation; oxidized tyrosine species can undergo Michael-type addition with nucleophiles such as lysine or cysteine, while cysteine thiols can similarly react with tyrosine-derived quinones to form C–S bonds.[147,167]

Aromatic residues themselves are particularly susceptible to radical-mediated coupling. Tyrosine-tyrosine cross-links arise via phenoxyl radical recombination, forming C–C or C–O linkages, whereas mixed aromatic couplings such as tyrosine–tryptophan and tryptophan-tryptophan crosslinks proceed through C–C, C–N, or C–O bond formation under oxidative conditions (Scheme 3.3).[168–170] In addition, oxidation of tryptophan can generate reactive indolenine intermediates capable of reacting with backbone amides or adjacent residues, contributing further structural diversity.[171] Together, these illustrate the chemical diversity of oxidative and radical-mediated crosslinks found in biological systems.

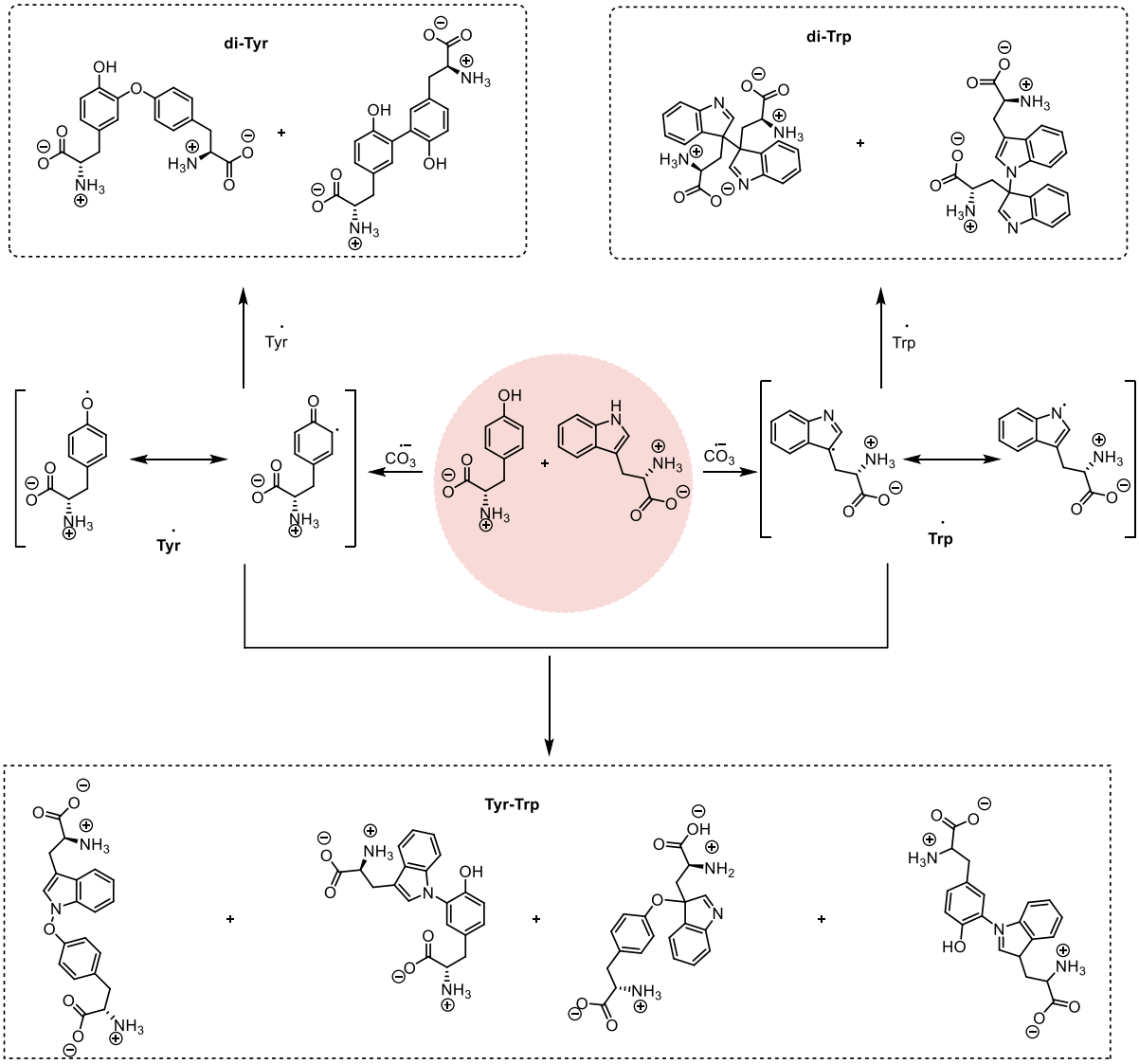

Scheme 3.3: Proposed radical–radical pathways for di-Tyr, di-Trp, and Tyr-Trp crosslink formation. Selected resonance structures of Tyr• and Trp• and possible C–C, C–O, C–N, and O–N linkages are shown.

3.4 Bioinspired Oxidative Crosslinking at the Tyr-Cys Interface

Among proteinogenic amino acids, tyrosine and cysteine occupy a particularly compelling position in oxidative crosslinking chemistry. Both residues are redox-active and participate in biologically relevant oxidative transformations. Tyrosine oxidation is central to enzymatic crosslinking, pigment biosynthesis, and structural reinforcement, while cysteine readily engages in thiol-based redox chemistry (as discussed in chapter 1 and 2).[82,172]

From a chemical perspective, tyrosine-derived *o*-quinones represent highly electrophilic intermediates capable of reacting with nucleophilic side chains, including thiols. Harnessing this intrinsic reactivity may provide a useful strategy for peptide and protein crosslinking that does not rely on pre-installed synthetic handles. However, translating such bioinspired

oxidative transformations into controlled, predictable, and broadly applicable chemical methods remains a significant challenge, particularly in complex peptide environments. Addressing these considerations involve the development of mild, chemoselective, and strategies that emulate natural crosslinking processes while enabling precise molecular control.

Recently, bioinspired tyrosine-cysteine crosslinking was reported using enzymatic oxidation. Francis and co-workers showed that the copper-dependent enzyme tyrosinase can selectively oxidise solvent-exposed tyrosine residues to *o*-quinones, which rapidly undergo conjugate addition with cysteine residues on partner proteins. This transformation proceeds under mild aerobic conditions and enables the direct coupling of full-length proteins within short reaction times. The utility of this approach was demonstrated through the construction of protein–peptide and protein-protein conjugates, including enhanced cellular delivery of CRISPR-Cas9 constructs and site-preserving attachment of reporter proteins to antibody fragments. These results clearly establish tyrosine-derived quinones as competent intermediates for selective tyrosine-cysteine crosslink formation in complex biological settings (Scheme 3.4).[147]

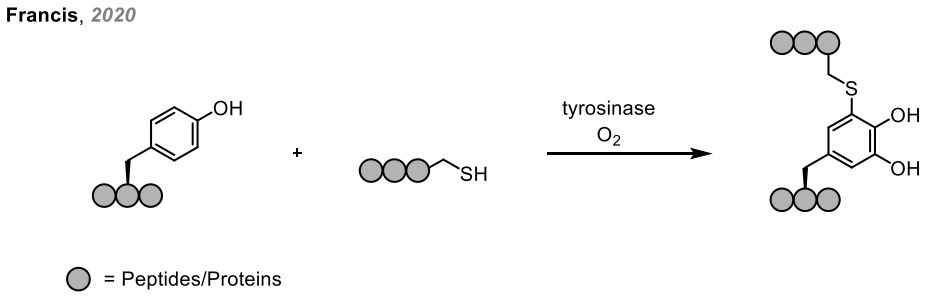

Scheme 3.4: Enzymatic cross-linkage between tyrosine and cysteine residues.

Tyrosine functionalization has previously been achieved through biomimetic enzymatic approaches, wherein tyrosinase-mediated oxidation generates *o*-quinone intermediates. To expand the methods available for tyrosine modification and provide a more operationally accessible alternative, a synthetic strategy was developed to mimic enzymatic tyrosine-cysteine crosslinking. In this approach, tyrosine residues were oxidized using IBX to generate the corresponding *o*-quinone intermediates, consistent with the phenazine-forming reactivity toward 1,2-phenyldiamines described in Chapter 2. In this chapter, these electrophilic quinone species were intercepted by cysteine thiols, affording thiol–catechol adducts via conjugate addition

3.5 Project Goals

This chapter aims to develop a strategy for the direct covalent linkage of native tyrosine and cysteine side chains under controlled oxidative conditions, thereby providing a simple and versatile platform for peripheral tyrosine functionalization. Specifically, it focuses on establishing an oxidative crosslinking methodology for the formation of tyrosine-cysteine linkages in peptides, with the broader objective of expanding the toolbox for native amino acid-based peptide crosslinking (Scheme 3.5).

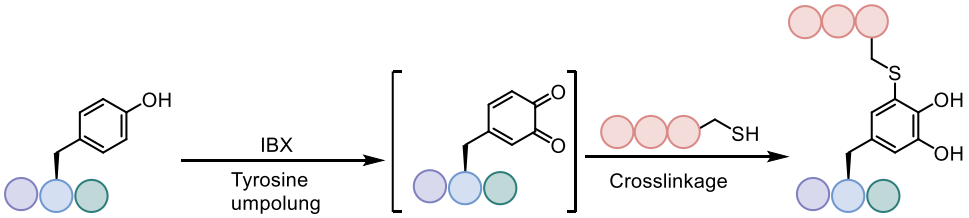

Scheme 3.5: Bioinspired strategy for peripheral tyrosine diversification.

3.6 Optimization Studies

To establish the optimal conditions for tyrosine-cysteine cross-linkage, Boc-Tyr-OMe **2.1** was selected as a model substrate to develop a one-pot protocol for formation of the corresponding thioether-linked product **3.1.** Initial efforts were directed toward optimization of the reaction conditions. Oxidation was performed using 1.2 equiv. of IBX in MeOD, with the temperature raised from 0 °C to room temperature. Upon complete consumption of the starting material, as confirmed by TLC, a MeOD solution of *N*-acetyl-*L*-cysteine methyl ester (1.1 equiv.) was added dropwise at 0 °C under a nitrogen atmosphere. The reaction mixture was then stirred at room temperature for 16 h, affording the desired cross-linked product in 32% yield (Table 3.1, entry 1).

Subsequent solvent screening revealed that replacing MeOD with DMF led to a notable improvement in yield, providing the product in 51% yield (Table 3.1, entry 2). Building on this result, the effect of buffered conditions was examined (Table 3.1, entries 3-5). In entry 3, oxidation of Boc-Tyr-OMe was carried out in DMF (0.125 M), followed by addition of Ac-Cys-OMe (1.1 equiv.) dissolved in a 1:1 mixture of DMF and phosphate buffer (1 M, pH 7.2), which further increased the yield to 55%. Variation of the phosphate buffer pH and concentration did not lead to additional improvement in yield when MeOH was employed as the solvent (Table 3.1, entries 4-5).

Table 3.1 Optimisation studies for tyrosine-cysteine cross linkage

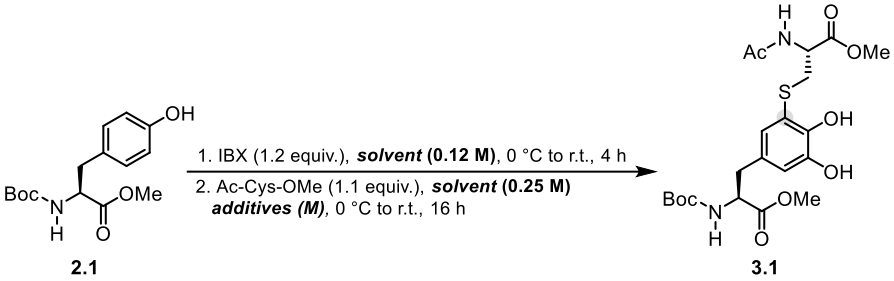

2.1 **3.1**

Entry	Solvent	Additive (M)	Yield (%)
1	MeOD	-	32[a]
2	DMF	-	51[a]
3	DMF	Phosphate buffer (1.0 M), pH 7.2	55[b]
4	MeOH	Phosphate buffer (0.1 M), pH 7.2	48[b]
5	MeOH	Phosphate buffer (1.0 M), pH 7.0	40[b]

[a] Yields determined via ^{1}H NMR using trimethoxybenzene as internal standard.
[b] Isolated yields.

3.7 Scope and Limitations

After optimization, the conditions were extended to peptide-peptide conjugation to assess their generality (Scheme 3.6). Direct coupling of Boc-tyrosine with *N*-acetylcysteine methyl ester afforded the desired cross-linked product **3.1** in 55% yield, whereas reaction of Boc-Trp-Tyr-OMe with *N*-acetyl-*L*-cysteine produced the corresponding conjugate **3.2** in 25% yield. Notably, the methodology was also applicable to the cross-linking of tripeptides containing tyrosine residues positioned either at the C-terminus or within the peptide backbone to cysteine-containing sequences. For instance, conjugation of and Cbz-Pro-Gly-Tyr-OMe and Cbz-Gly-Phe-Tyr-OMe with *N*-acetylcysteine furnished the respective cross-linked peptides **3.3** and **3.4** in 22% and 17% yield. In addition, coupling of Boc-Glu-Tyr-Ala-OMe with Boc-Ala-Gly-Cys-OMe delivered the corresponding hexapeptide **3.5** in 17% yield.

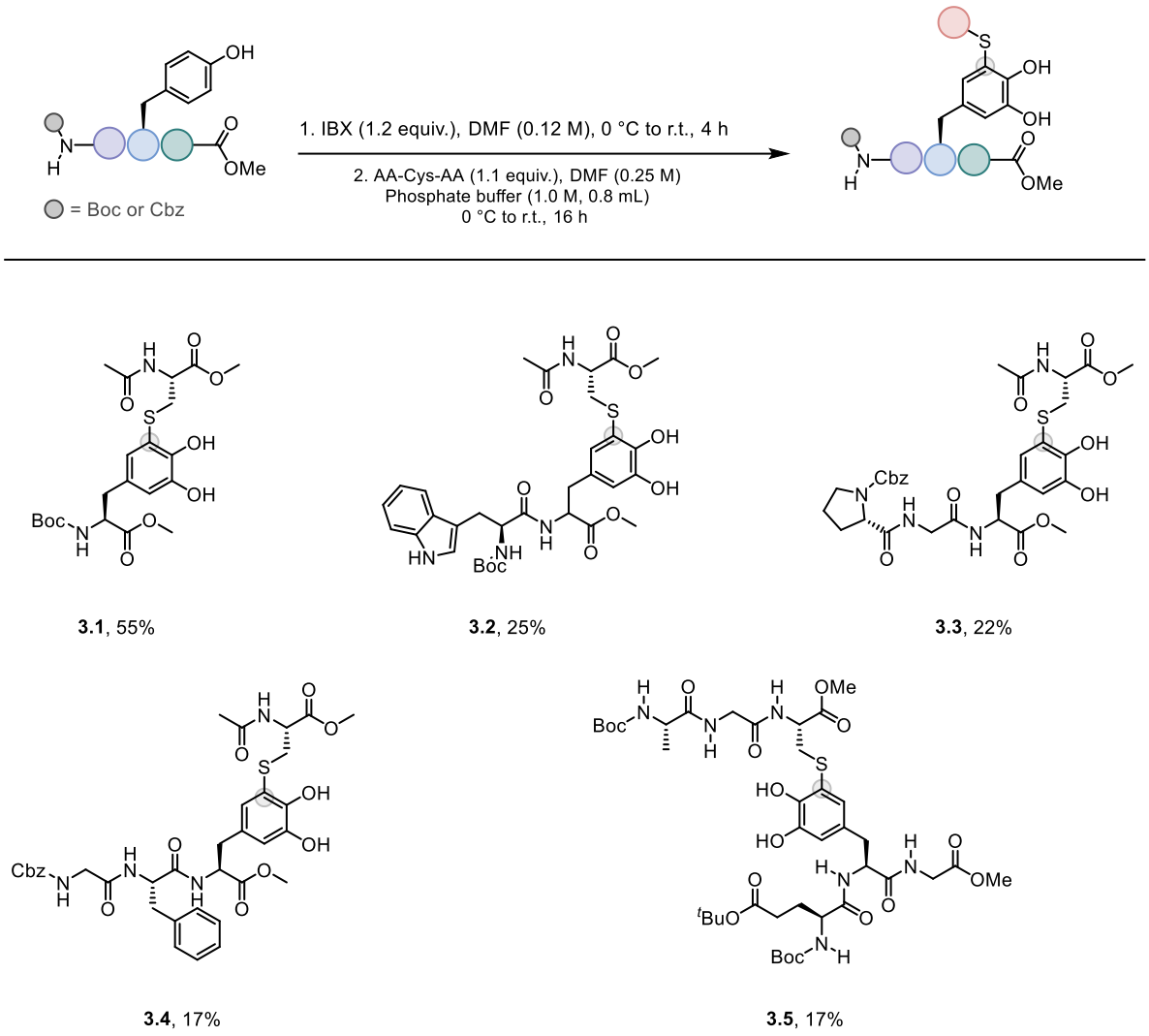

Scheme 3.6: Scope of tyrosine-cysteine cross-linkage. All reactions were carried out on 0.4 mmol scale.

To further explore the scope of this methodology, an attempt was made to conjugate tyrosine-containing peptides with Coenzyme A **3.6** (Scheme 3.7). However, under the optimized conditions, no detectable cross-linked product was observed, indicating that the method may be limited to peptide substrates containing standard amino acid residues.

Collectively, these results demonstrate the potential of this approach for the construction of covalently linked peptide architectures via selective side-chain-to-side-chain conjugation, while also highlighting certain limitations when applied to more complex biomolecules such as Coenzyme A.

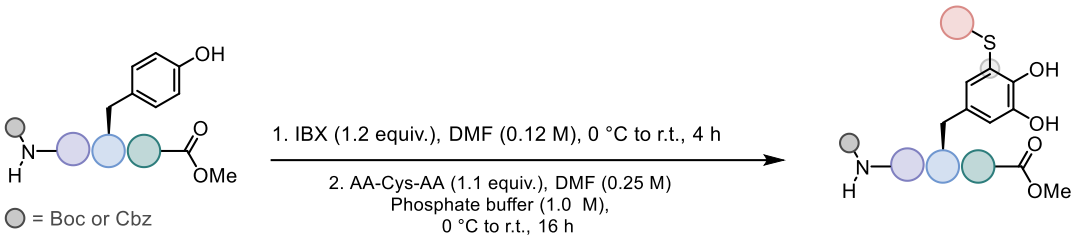

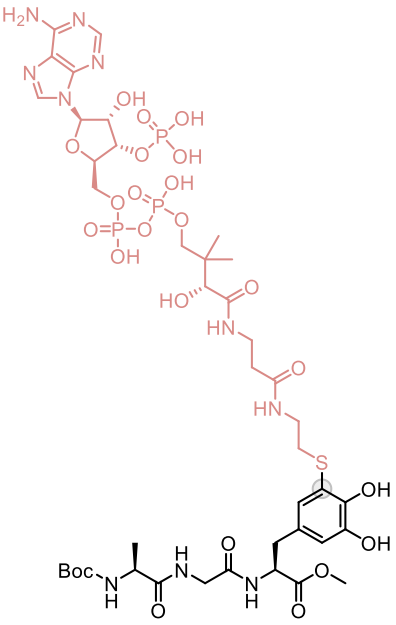

3.6, 0%

Scheme 3.7: Extension to Coenzyme A **3.6** was unsuccessful.

3.8 Conclusion and Outlook

In conclusion, peripheral modification offers a versatile strategy for tyrosine functionalization, with the electrophilic *o*-quinone intermediate serving as an effective platform for peptide cross-linking. Upon oxidation, the o-quinone reacts readily with cysteine thiols to form covalent tyrosine-cysteine linkages under operationally simple conditions by connecting native side chains without preinstalled handles or external cross-linkers. This strategy enables late-stage tyrosine modification in complex peptide environments. By facilitating controlled oxidative cross-linking, *o*-quinones expand the toolkit for constructing stabilized peptides, conjugates, and higher-order assemblies, establishing their utility as central reactive nodes for peptide diversification.

Further expansion of this peripheral modification is possible by trapping the catechol with boronic acids or 1,2-phenyldiamines to install fluorescent handles via site-selective tyrosine–cysteine cross-linkage (Scheme 3.8).

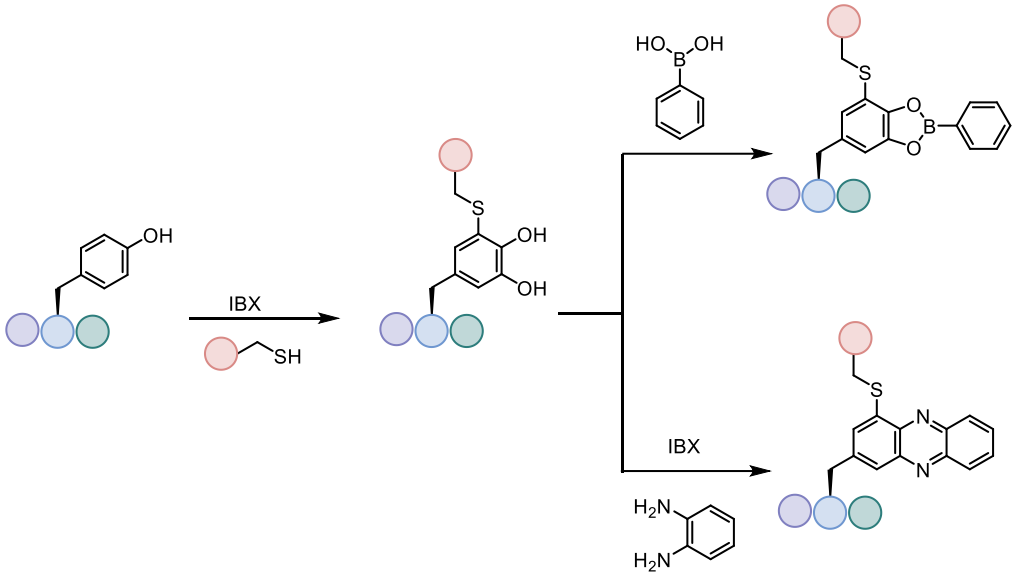

Scheme 3.8: Extension of the tyrosine-cysteine cross-linkage: with boronic acids and 1,2-phenyldiamines.

Chapter 4

Development of Fluorogenic *o*-Quinone Platforms for Selective Cysteine Labeling in Peptides

4.1 Introduction

Site-selective conjugation reactions which enable the modification of proteins with functional tags-such as fluorophores, affinity handles (e.g., biotin), or cytotoxic payloads-have played a central role in advancing biomedical research and therapeutic development.[173,174] Such modifications allow precise investigation of protein function, visualization within complex biological environments, and the construction of targeted bioconjugates.[175,176]

Among the available strategies, peptide tag-based approaches allow the introduction of defined reactive sites into proteins with minimal perturbation of their native structure.[177] These tags are compatible with genetic encoding and chemical synthesis and enable site-selective modification when combined with appropriate chemical handles.[163,178,179] Within this context, choosing an appropriate amino acid residue as the reactive anchor is crucial for achieving high chemoselectivity and controlled labeling.

Cysteine has emerged as one of the most widely used amino acids in peptide tagging strategies, owing to the high reactivity of its thiol side chain. Under mild conditions, the thiol group displays greater intrinsic nucleophilicity than most other proteinogenic side chains, enabling selective modification even in complex peptide or protein environments. Furthermore, cysteine can undergo oxidation of its thiol functionality (Scheme 4.1), highlighting both its chemical versatility and sensitivity under oxidative conditions.[172,180]

Beyond its inherent reactivity, cysteine is relatively rare in proteins, which enhances chemoselectivity, facilitates site-specific incorporation via site-directed mutagenesis, and reduces the likelihood of off-target labeling compared with more abundant residues such as lysine or serine.[181,182] Although numerous cysteine-modification strategies have been developed, its combination of high reactivity and low abundance ensures that cysteine continues to serve as a preferred and reliable target for precise bioconjugation and controlled labeling.

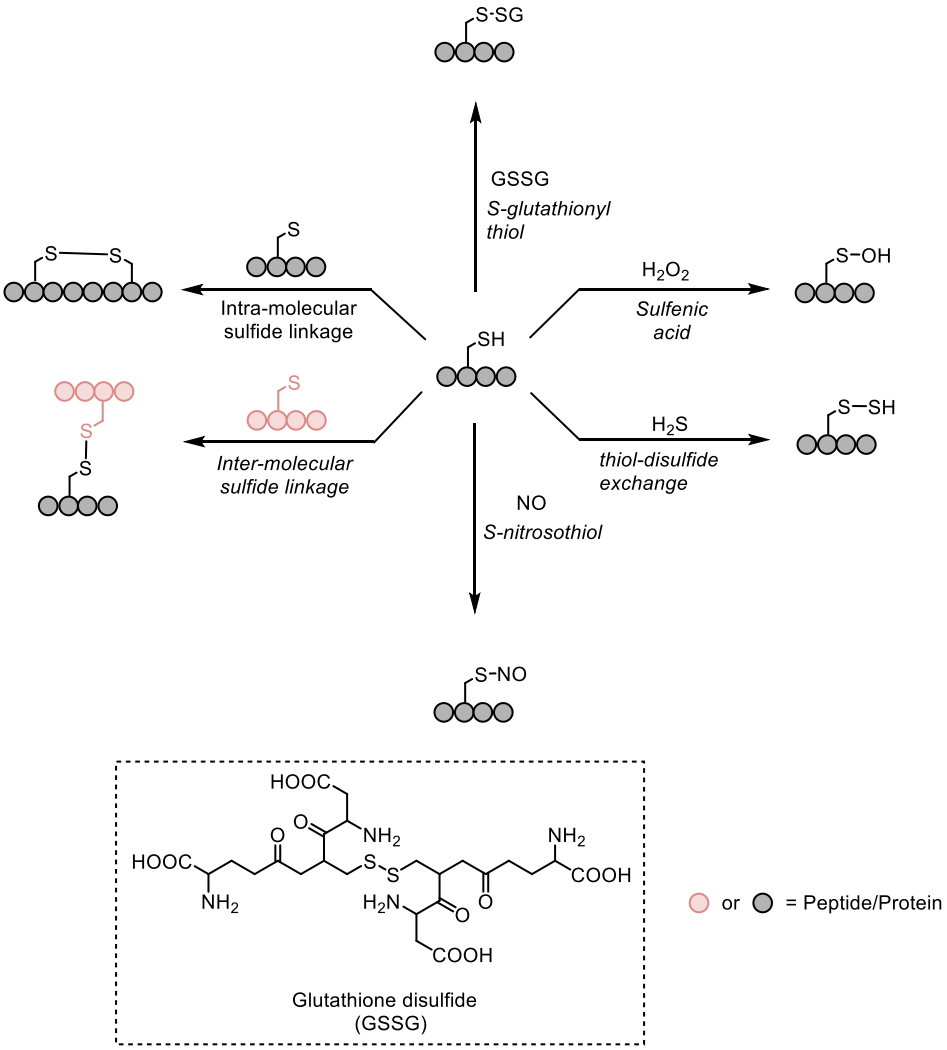

Scheme 4.1: Oxidative Modulation of Cysteine Thiols.

Beyond its chemical reactivity, cysteine plays essential functional roles in biological systems. It is frequently involved in enzymatic catalysis, redox regulation, and the formation of disulfide bonds that govern protein folding and stability as discussed in chapter 3. Consequently, selective cysteine modification enables not only the attachment of functional tags but also serves as a handle for probing protein structure, dynamics, and function.

A wide range of chemical strategies has been developed to target cysteine residues, including reactions with haloacetamides, maleimides, acrylamides, vinyl sulfones, and other activated electrophiles (Scheme 4.2). [183–188]

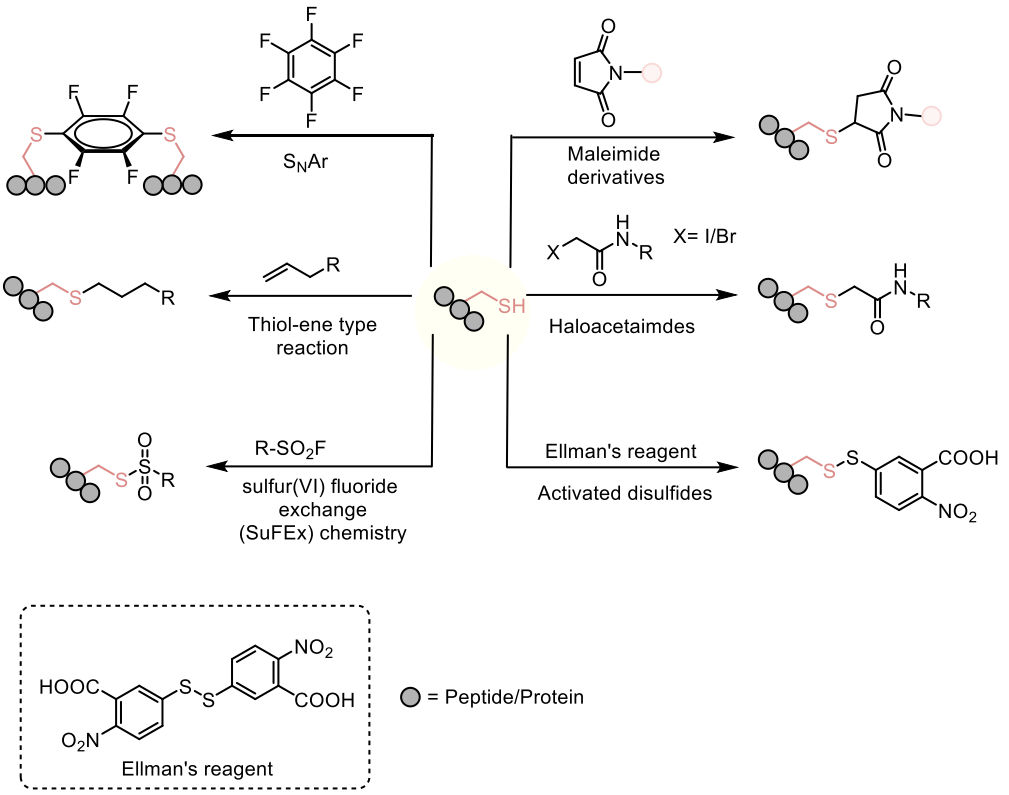

Scheme 4.2: Cysteine tagging strategies.

4.2 Thiol-Michael Addition Reactions

The thiol-Michael addition, first reported in the 1960s by Allen and co-workers, has become a fundamental transformation in organic synthesis and materials chemistry due to the high reactivity of the sulfur–hydrogen bond, which readily forms nucleophilic thiolates under mild conditions.[189]. As a result, the reaction can be performed using diverse precursor systems and gentle catalytic approaches, often under solvent-free or biologically compatible conditions, making it a highly efficient and modular click-type transformation.[190,191]

In chemical biology, thiol-Michael reactions are extensively used for bioconjugation due to their rapid kinetics, chemoselectivity, and compatibility with aqueous and physiological environments. These characteristics align with the principles of click chemistry introduced by Barry Sharpless in 2001 and later awarded the Nobel Prize in Chemistry in 2022.[159] Although the copper-catalyzed azide-alkyne cycloaddition (CuAAC) is widely regarded as the prototypical click reaction, thiol-Michael additions have emerged as powerful alternatives for modifying biomacromolecules.

Originally defined as the addition of an enolate to the β-carbon of an α,β-unsaturated carbonyl compound, the Michael reaction now encompasses a broad range of nucleophiles including thiols, amines, and alcohols and electrophiles such as α,β-unsaturated esters, amides, nitriles,

and nitroalkenes.[192] The key requirement for effective Michael acceptors is an electron-withdrawing group conjugated to an unsaturated bond, which enhances β-carbon electrophilicity and promotes nucleophilic addition.[193]

Despite their widespread use, existing cysteine-modification methods can suffer from limitations such as reversibility, insufficient stability of the conjugate, suboptimal chemoselectivity, or incompatibility with biologically relevant environments. Given these considerations, cysteine modification remains an active and evolving field. Continued development of new cysteine tags is driven by the need for improved stability, tunability, orthogonality, and control over reactivity. Importantly, cysteine tags serve as versatile chemical handles for a broad range of downstream applications, including fluorophore attachment, affinity enrichment, drug conjugation, and structural or mechanistic probing of proteins. These considerations highlight the ongoing opportunities for exploring new chemical scaffolds and reaction paradigms for cysteine-selective bioconjugation.

4.3 Quinone-Based Electrophiles for Cysteine Tagging

Quinones represent a distinct class of Michael acceptors characterized by conjugated, electron-deficient π-systems and redox activity. Upon oxidation of phenolic precursors, quinones can be generated in situ and react readily with cysteine thiolates to form stable C-S bonds. Compared to classical Michael acceptors, quinones offer several unique features, including strong thiol reactivity, redox tunability, and the potential for temporal control over electrophile generation.

Although quinone-based cysteine tagging offers several advantages, it has been less extensively explored due to concerns regarding chemoselectivity and competing reactions. Recent studies, such as the 2024 report by Hang, Wu, and Chu, addressed these challenges using *para*-quinone methides (*p*-QM) for efficient and selective cysteine conjugation (Scheme 4.3).[194] These intermediates enable rapid and chemoselective thiol addition, and have been applied for fluorescent probe attachment. In addition to *p*-QM, *ortho*-quinone methides (*o*-QMs) have also emerged as versatile electrophiles for thiol conjugation, expanding the toolkit for site-selective modification.

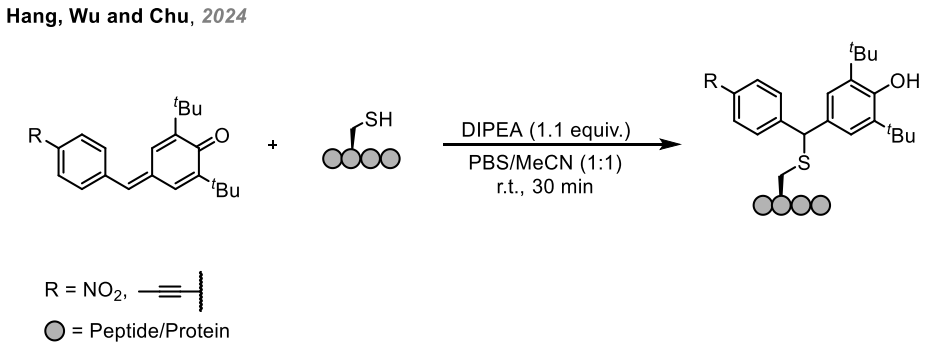

Scheme 4.3: Bioconjugation strategy for cysteine with *p*-QM.

Boons and Popik demonstrated a photochemical approach in which 3-(hydroxymethyl)-2-naphthols were converted into *o*-NQMs upon irradiation, enabling conjugation to cysteine residues in peptides and proteins (Scheme 4.4).[195] This strategy shows the potential of light-mediated generation of reactive intermediates to achieve site-selective thiol modification.

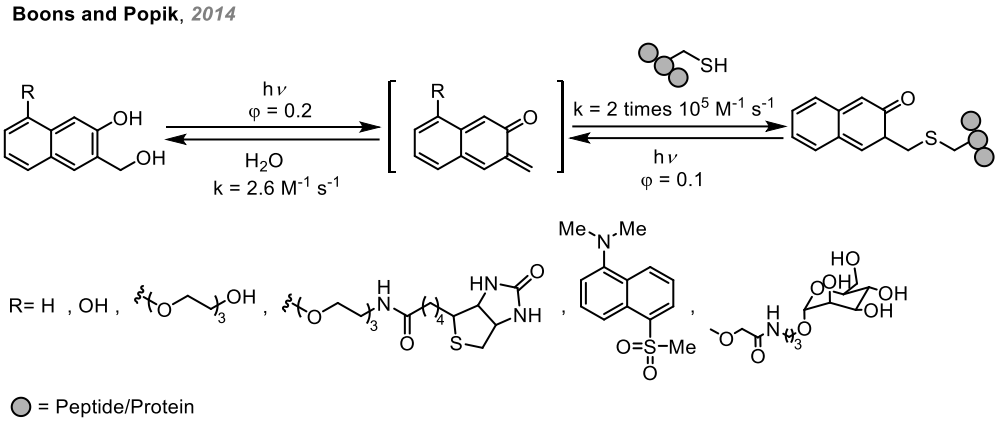

Scheme 4.4: Bioconjugation strategy for cysteine with *o*-NQM.

While quinone-based electrophiles enable selective cysteine modification, their true synthetic value lies in their capacity to introduce functional handles that facilitate downstream detection and analysis. These handles allow further derivatization, visualization, and quantitative characterization of modified biomolecules. Among the various detection strategies, fluorescent tagging is one of the most widely employed approaches due to its sensitivity and versatility.

4.4 Labeling Methods

Numerous techniques are available for tracking biomolecules such as antibodies, proteins, peptides, and amino acids. These include isotope markers, colorimetric biosensors, photochromic compounds, biomaterial-based probes, electrochemical sensors, fluorogenic labels, and fluorescent labels. Among these, fluorescent labeling has emerged as one of the most commonly used methods for biomolecular detection and tracking.

Fluorescent labels offer several advantages. They can detect biomolecules at low concentrations, are often non-destructive to native folding and function, and allow real-time monitoring of molecular processes. These characteristics make them particularly valuable for biochemical analysis, imaging, and mechanistic studies. Selecting an appropriate labeling strategy requires careful consideration of the target system, including the type of biomolecule, accessible amino acid residues, experimental environment, and intended downstream applications.

A variety of fluorescent labeling strategies can be employed depending on the target and context. These include: chemical modification of reactive groups, enzyme-mediated site-specific incorporation, affinity- or covalent-based protein tagging, genetic fusion of fluorescent proteins, and cell imaging with bioorthogonal or membrane-permeable dyes.

Ideally, a fluorescent probe should be small, bright, and photostable, while causing minimal perturbation to the biological system. The label should exhibit high specificity, low background signal, and minimal tendency to oligomerize. Additionally, multiplexing capability allowing simultaneous labeling of multiple targets is often desirable. However, fulfilling all these criteria simultaneously is challenging. In practice, compromises are often necessary, and no universal “perfect” fluorescent label exists. Consequently, the development of improved labeling strategies remains an active area of research. A representative set of commonly used organic dyes that fulfil many of the desired criteria is shown below (Figure 4.1).

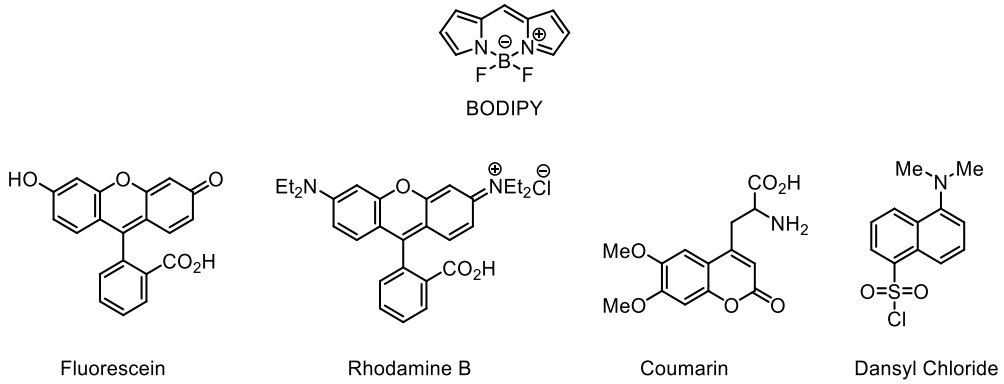

Figure 4.1: Structure of Common dye scaffolds.

Common cysteine-specific commercial probes include maleimide-based dyes such as Cy3, Alexa Fluor 488, and FITC, as well as BODIPY derivatives. These reagents are widely used for covalent cysteine labeling and serve as powerful tools for investigating protein structure and function.[196–200] Among alternative labeling agents, dansyl chloride represents an attractive candidate for covalent modification. Although there are limited reports describing the application of dansyl chloride in structural studies of native proteins or protein complexes, it offers several practical advantages over commonly used commercial probes. Dansyl

derivatives exhibit favourable chromatographic properties and enhanced ionization efficiency in LC–MS analysis. In addition, dansyl chloride displays reactivity across a broad range of pH and temperature conditions. From a cost perspective, it is also significantly more economical on a per-weight basis compared to many fluorescent labeling reagents.[201] Despite these advantages, dansyl chloride has not been systematically explored for selective cysteine labeling, highlighting an opportunity to evaluate its potential as an alternative platform.

In addition to conventional organic dyes, naphthalene-based structures are intrinsically fluorescent due to extended aromaticity. In particular, naphthols represent small, simple aromatic molecules with moderate fluorescence. Their compact size, which makes them minimally perturbing when introduced into peptides, combined with their chemical versatility, makes them suitable candidates for cysteine labeling, providing an alternative platform for introducing fluorescent tags without the steric bulk of conventional dyes.

Furthermore, enzymatic approaches have been employed to generate quinone intermediates under mild conditions. Francis and co-workers reported that tyrosinase, an enzyme capable of oxidizing phenols to *o*-quinones, could be used to attach phenolic cargo to cysteines engineered on antibody surfaces (Scheme 4.5).[202] Using this strategy, site-specific Michael additions between cysteine thiols and enzymatically generated *o*-quinones afforded stable linkages that were more resistant to reversion under physiological conditions than maleimide conjugates. This methodology enabled the construction of antibody-drug conjugates bearing cytotoxic payloads, as well as conjugates incorporating fluorophores and oligonucleotides, demonstrating broad applicability for targeted protein modification.

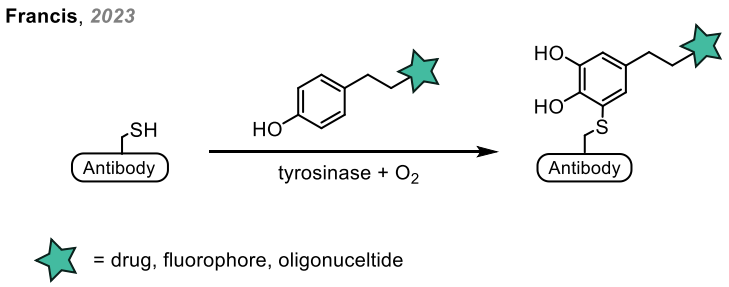

Scheme 4.5: Site-selective modification of a model cysteine-containing protein to add phenol-drug.

Ortho-quinones represent a chemically distinct class of electrophiles for cysteine modification. Formed by oxidation of phenolic precursors, they act as Michael acceptors and undergo thiol-Michael addition with cysteine thiolates. This reactivity, combined with mild oxidative conditions, allows selective cysteine conjugation in both peptide and protein systems, as demonstrated in enzymatic and photochemical approaches.

Phenolic scaffolds with intrinsic photophysical properties, such as tyramine and naphthol, can be converted to *o*-quinones while retaining conjugated aromatic frameworks that exhibit

fluorescence. Incorporating these scaffolds into cysteine-reactive quinone tags enables simultaneous covalent modification and installation of a spectroscopically addressable handle within a single transformation. This approach reduces the need for multistep tag construction and expands the applicability of quinone-mediated cysteine modification in analytical and imaging contexts.

4.5 Project Goals

The objective of this work is to develop a fluorogenic *ortho*-quinone-based platform for selective cysteine labeling through thiol-Michael addition. This study focuses on the design and synthesis of tyramine- and naphthol-derived phenolic tags, which can be oxidized in situ to generate reactive *o*-quinone intermediates (Scheme 4.6).

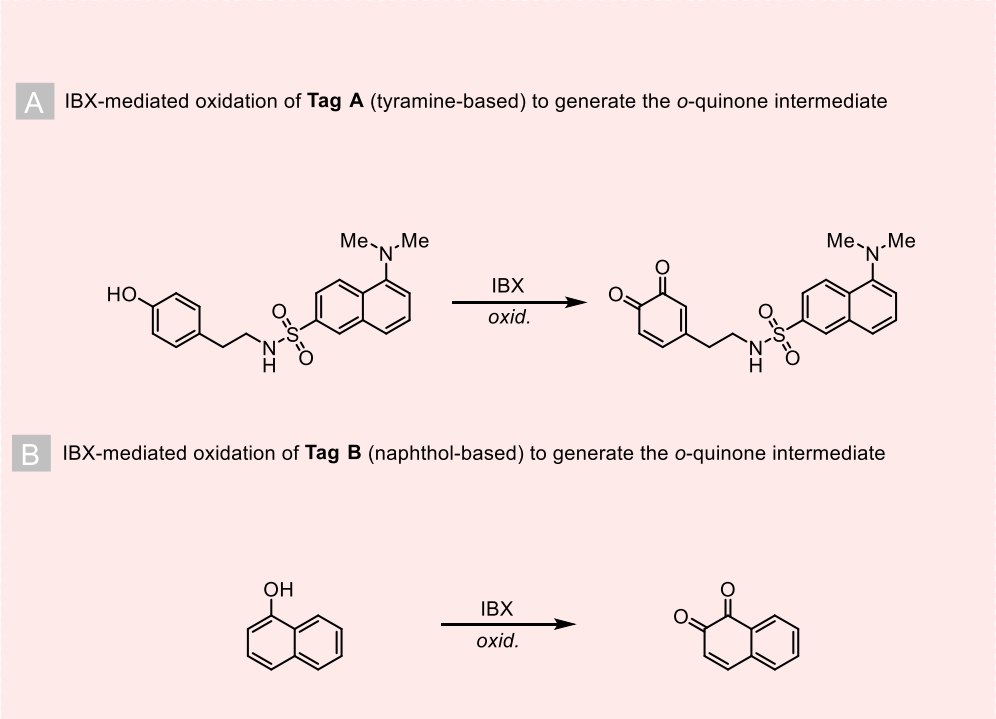

Scheme 4.6: A) IBX-mediated oxidation of Tag A (tyramine-based) to *o*-quinone intermediate Tag A*. B) IBX-mediated oxidation of Tag B (naphthol-based) to *o*-quinone intermediate Tag B*.

These oxidized tags were then employed to label cysteine residues to form thiol-catechol or thiol-quinone adducts (Scheme 4.7), and their efficiency and selectivity toward cysteine were evaluated under biocompatible conditions. In addition, the intrinsic fluorescence of these motifs was leveraged for direct labeling of cysteine residues without additional conjugation steps. Together, these findings provide a simple and versatile strategy for fluorescence-enabled cysteine modification.

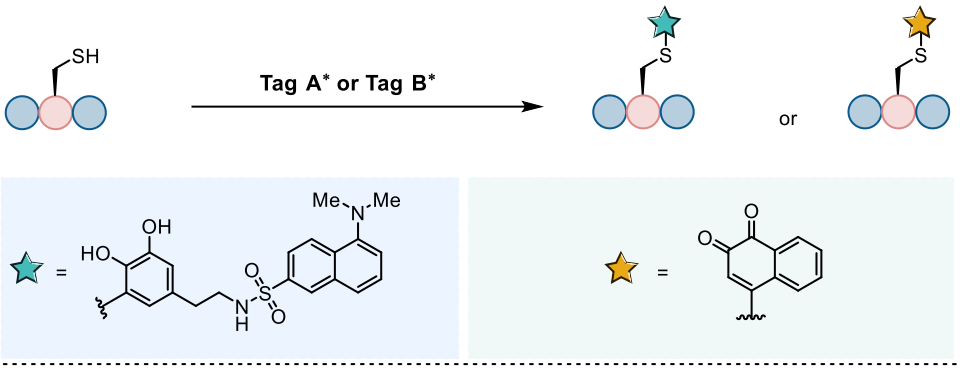

Tag A*: IBX-mediated oxidation of the tyramine-based tag (Tag A) to form the corresponding *o*-quinone intermediate.
Tag B*: IBX-mediated oxidation of the naphthol-based tag (Tag B) to form the corresponding *o*-quinone intermediate.

Scheme 4.7: Cysteine labeling using the oxidized *o*-quinone intermediates (Tag A* and Tag B*) via thiol-Michael addition.

4.6 Results and Discussion

4.6.1 Development and Acquisition of Tags A and B

Based on thiol-Michael reactivity, two fluorescent tags were designed with potential applications in bioimaging for cysteine labeling. **Tag A (4.3)** was prepared by coupling tyramine **4.1** with dansyl chloride **4.2** following by a reported procedure (Scheme 4.8 A).[203] The resulting conjugate **Tag A (4.3)** exhibited strong fluorescence, as illustrated in (Scheme 4.8 B). 1-Naphthol derived **Tag B (4.5)** was selected on the basis of its well-documented fluorescent properties (Scheme 4.6 B). Consistent with literature reports, **Tag B (4.5)** displayed favourable fluorescence characteristics, supporting its suitability for imaging-oriented applications.[204]

A Synthesis of **Tag A**

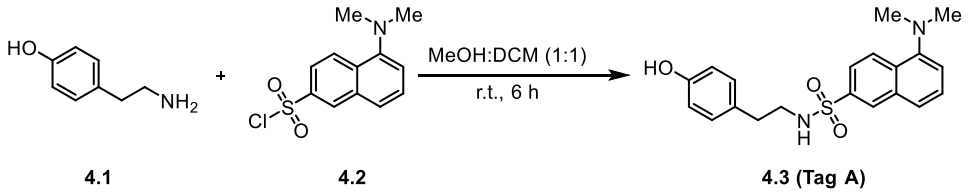

4.1 **4.2** **4.3 (Tag A)**

B Fluorescence emission spectrum of **Tag A**

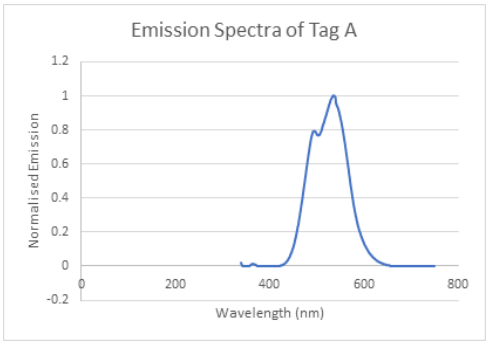

Scheme 4.8: A) Synthesis of **Tag A** and, B). Normalized fluorescence emission spectrum of **Tag A 4.3** in MeOH (5 µM), recorded with excitation at 330 nm.

4.6.2 Oxidation of Tags A and B

To generate the corresponding *o*-quinone intermediates, Tag A and Tag B were oxidized with IBX (1.2 equiv.) in MeOH or DMF (0.12 M) at 0 °C to room temp. (Scheme 4.9 A and B). The reaction progress was monitored by TLC. Upon completion, the resulting *o*-quinone intermediates **4.4** and **4.6** were transferred via cannula into a flask containing the cysteine-bearing substrate.

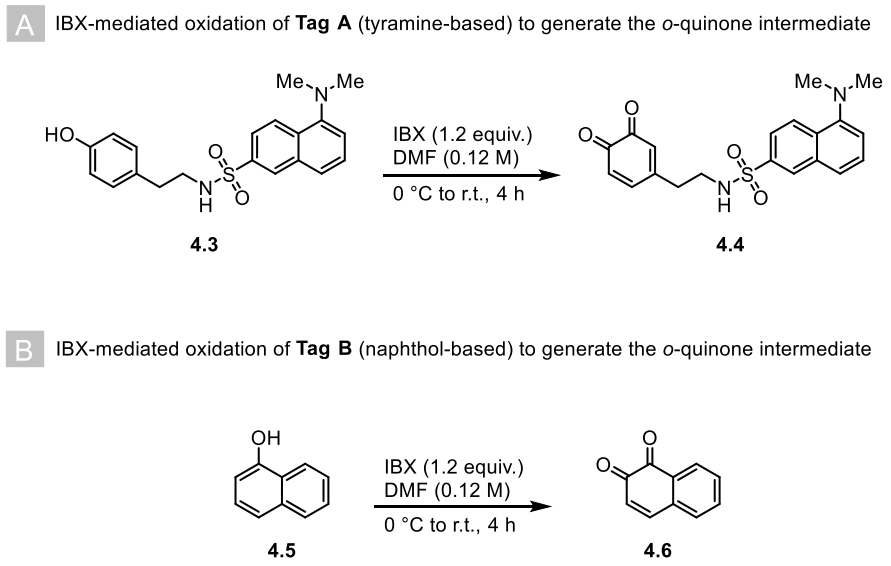

Scheme 4.9: A) Oxidation of Tag A and B)- Oxidation of Tag B with IBX to generate the corresponding *o*-quinone intermediates, Tag A* and Tag B*, respectively.

4.7 Optimization Studies

Following the development of **Tags A and B**, optimization studies were first conducted using **Tag A (4.3)** (Table 4.1). For these experiments, **Tag A (4.3)** was independently oxidized with IBX (1.2 equiv.) in MeOH or DMF (0.12 M) at 0 °C to room temp. to generate the corresponding *o*-quinone intermediate **4.4** (Scheme 4.9 A). The reaction progress was monitored by TLC. Upon completion, the freshly generated *o*-quinone was transferred via cannula into a flask containing *Ac*-Cys-OMe **4.7**, which had been dissolved in MeOD (0.12 M) and cooled to 0 °C. The reaction mixture was then allowed to warm to room temperature and stirred for 19 h, affording the desired thiol-catechol conjugate **4.8** was in 55% yield after 19 h (Table 4.1, entry 1). Shortening the reaction time from 19 h to 2 h resulted in a significant decrease in yield to 38%. (Table 4.1, entry 2). Increasing the equivalents of the quinone (Table 4.1, entries 3-4) proved detrimental, affording the product in reduced yields of 31% and 35%, respectively. Notably, the addition of phosphate buffer to the cysteine solution enhanced the reaction efficiency, delivering the desired product in an improved 60% yield (Table 4.1, entry 6).

Table 4.1 Optimization studies for cysteine labelled strategy using **Tag A (4.3)**

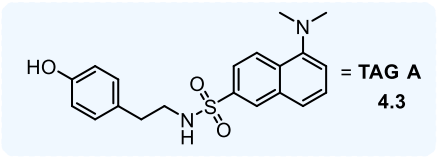

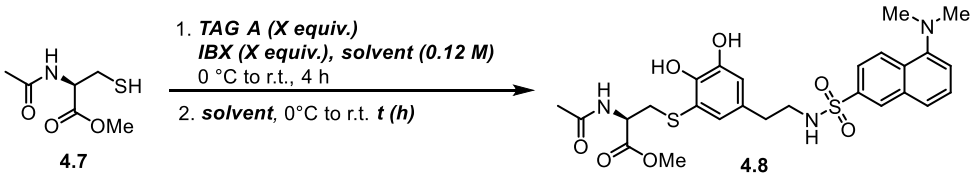

Entry	TAG A (X equiv.)	IBX (X equiv.)	Time (h)	solvent	Yield[a]
1	1.0	1.2	19	MeOD	55
2	1.0	1.2	2	MeOD	38
3	2.0	2.4	19	MeOD	31
4	2.0	2.4	19	DMF	35
5	1.3	1.6	19	MeOD	48
6*	1.0	1.2	19	DMF	60

Independently, **Tag A** was oxidized with IBX (1.2 equiv.) in MeOD (0.12 M) or DMF (0.12 M), depending on the table entry, to generate the corresponding *o*-quinone at 0 °C to r.t. over 4 h. The resulting *o*-quinone was then transferred at 0 °C into a flask containing Ac-Cys-OMe. The solvent was kept consistent with that used for the Ac-Cys-OMe solution.
[a] = Yields were determined by using 1,3,5-trimethoxybenzene as internal standard.* = Phosphate buffer (1.0 M) was used to dissolve Ac-Cys-OMe.

4.8 Scope and Limitations

Following optimization of the reaction conditions, the scope and applicability of the developed labeling strategies were explored. Using **Tag A (4.3)**, the thiol-catechol conjugate methyl *N*-acetyl-S-(5-(2-((5-(dimethylamino)naphthalene)-2-sulfonamido)ethyl)-2,3-dihydroxyphenyl)-*L*-cysteinate **(4.8)** was initially obtained in 60% yield based on crude NMR analysis. However, the isolated yield decreased to 36% after purification by silica gel column chromatography. The reduced yield upon isolation may be attributed to partial oxidation of the thiol-catechol conjugate to the corresponding thiol-quinone conjugate species, potentially promoted by exposure to air, light or silica; however, the extent of this oxidation could not be quantified and remains to be investigated. Similarly, tripeptide **4.9** was isolated in 30% yield (Scheme 4.10)

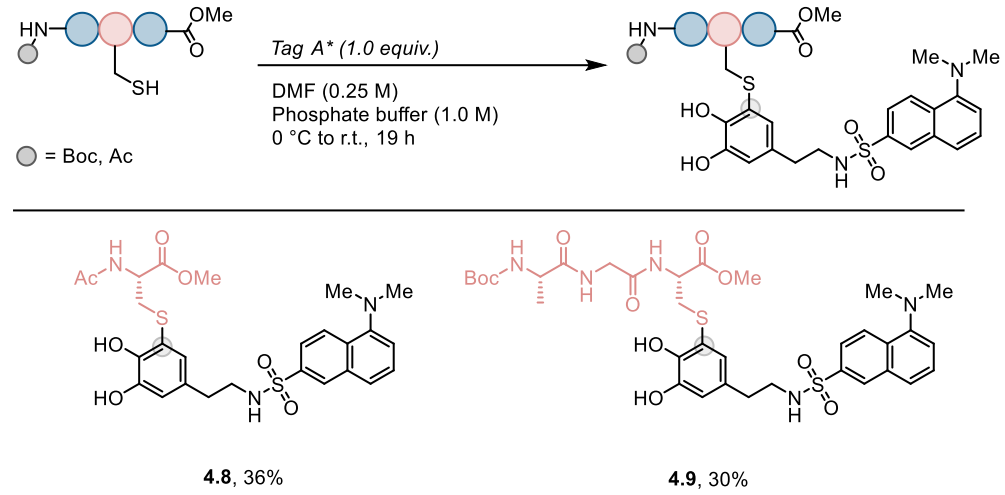

*** = IBX-mediated oxidation of Tag A (tyramine-based) to generate the o-quinone intermediate Tag A***

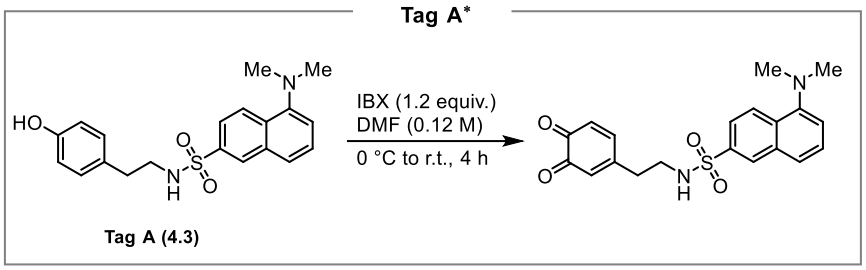

Scheme 4.10: Substrate scope of cysteine-containing peptides labelled with **Tag A (4.3)**.

When **Tag B (4.5)** was subjected to these conditions the product was initially obtained as a mixture with its thiol-catechol **4.10** and oxidised thiol-quinone **4.11** conjugate (Scheme 4.11). The thiol-quinone conjugate **4.11** was isolated in 24% yield after purification by silica gel column chromatography, while the thiol-catechol conjugate **4.10** was observed but could not be isolated in pure form, it was obtained as a mixture of **4.10** and **4.11**.

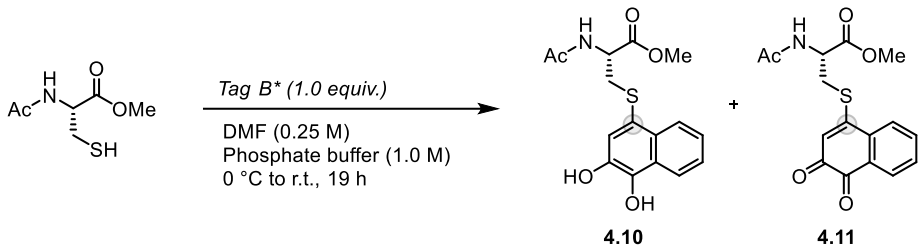

Scheme 4.11: Labeling of Ac-Cys-OMe with **Tag B (4.5).**

The crude LCMS analysis of the above reaction (scheme 4.11) is shown below. A peak at a retention time of 2.915 min corresponds to the thiol-quinone conjugate **4.11**, while the peak at 3.718 min is assigned to the thiol-catechol conjugate **4.10**, as confirmed by mass spectrometric analysis (Figure 4.2).

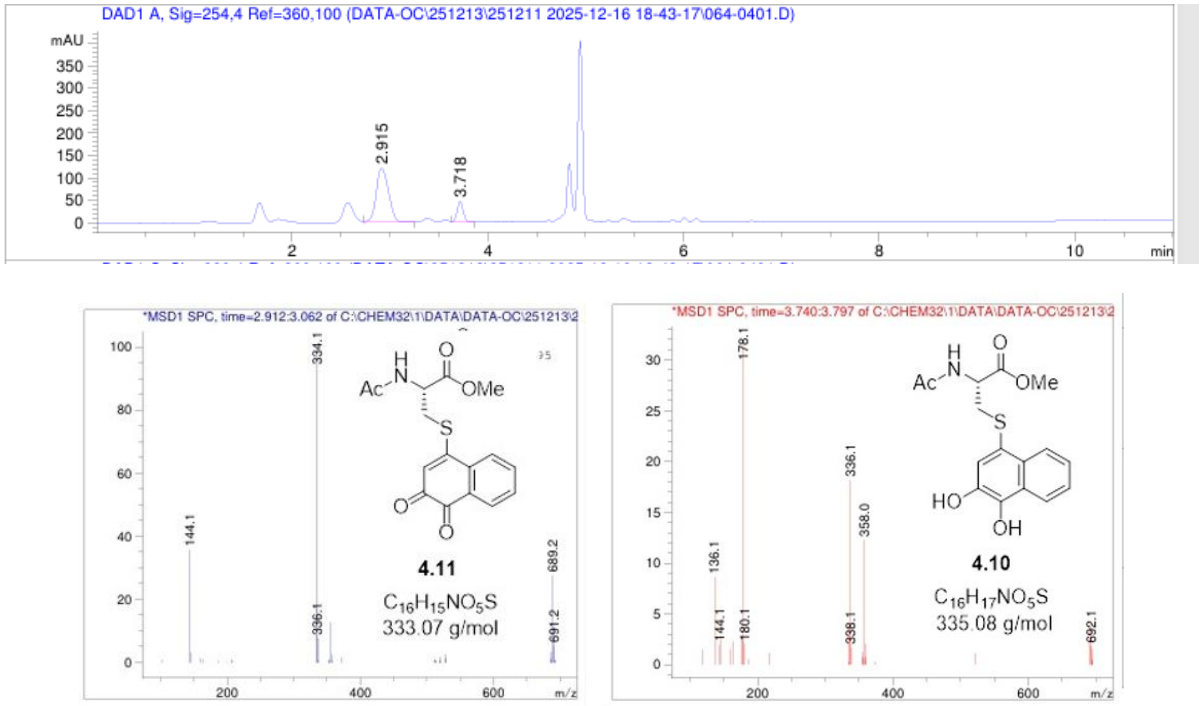

Figure 4.2: LCMS chromatogram of product showing the thiol-catechol **4.10** and thiol-quinone **4.11** conjugates.

From a mechanistic perspective, the reaction of **Tag B (4.5)** with *N*-acetyl-*L*-cysteine methyl ester proceeds via sequential oxidation and thiol conjugate addition steps. Initially, **Tag B (4.5)**

is oxidized by IBX to generate the corresponding 1,2-naphthoquinone intermediate **4.6**, which contains electrophilic carbonyl groups and presents the β-carbon as a Michael acceptor. The thiolate of *N*-acetyl-*L*-cysteine methyl ester, generated at pH 7 in phosphate buffer, undergoes 1,4-conjugate addition at the β-carbon to form a thio-enolate intermediate **4.6a**, which is rapidly protonated by the buffer. Subsequent rearomatization of the naphthalene system, accompanied by proton transfer to the carbonyl oxygens, yields the thiol-catechol conjugate **4.10** as the primary product. Over the extended reaction time 19 h, dissolved molecular oxygen is proposed to oxidize **4.10** via a two-electron, two-proton process, regenerating the quinone system while retaining the thioether linkage to afford the thiol-quinone conjugate **4.11**. This oxidized product is further stabilized by extended conjugation (Scheme 4.12).

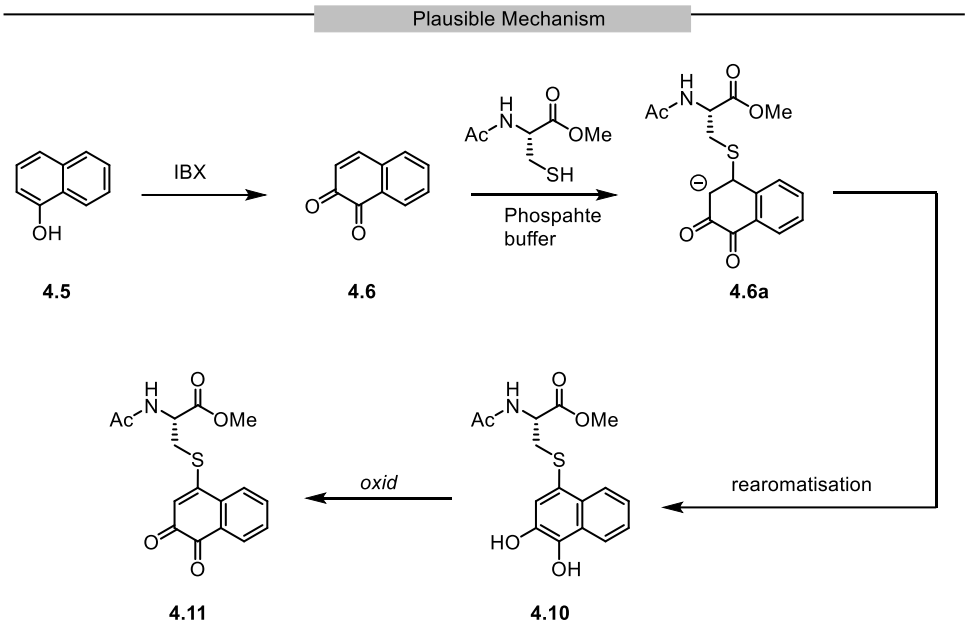

Scheme 4.12: Plausible mechanism of labeling of cysteine with **tag B (4.5).**

Using **Tag B (4.5)** tripeptide **7.15** was isolated as thiol-quinone conjugate **4.12** in 24% yield (Scheme 4.13). while the thiol-catechol conjugate **4.13** was observed but could not be isolated, it was obtained as a mixture of **4.12** and **4.13**.These results highlight the redox sensitivity of the catechol-containing conjugates and shows that either the thiol-catechol or oxidized (thiol-quinone) conjugates can be accessed under the applied conditions.

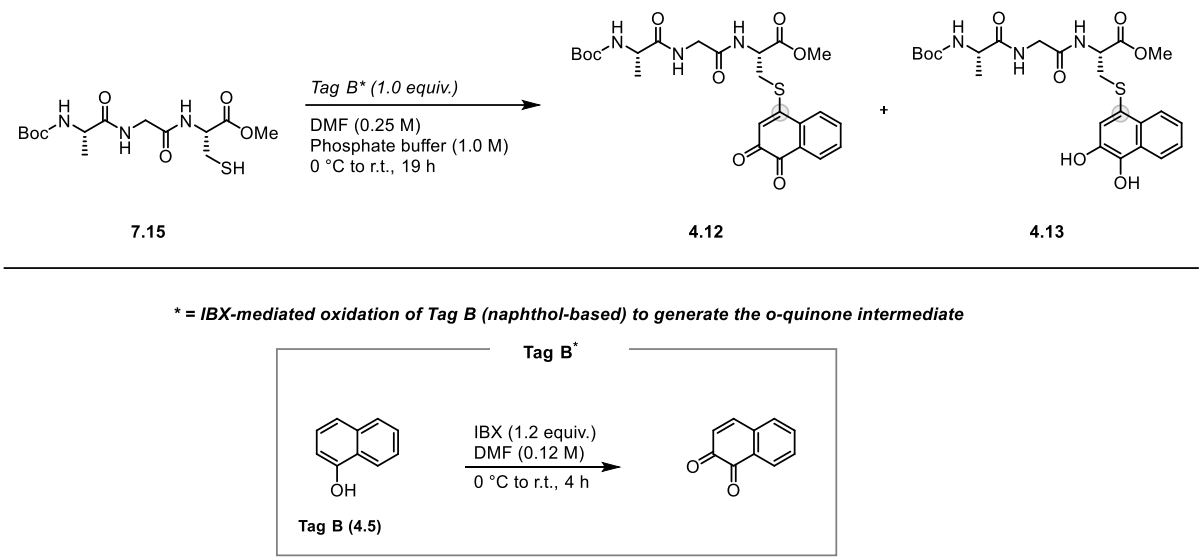

Scheme 4.13: Labeling of a cysteine-containing tripeptide with **tag B (4.5)**.

Labeling with both **Tag A (4.3)** and **Tag B (4.5)** afforded the corresponding cysteine-tagged tripeptides in moderate yields, indicating efficient and selective conjugation at the cysteine residue. Notably, conjugation with **Tag A (4.3)** predominantly yielded the reduced thiol-catechol form, whereas labeling with **Tag B (4.5)** led to isolation of the oxidized thiol-quinone conjugates. Importantly, the quinone form can be readily reduced to the corresponding catechol using sodium dithionite, providing a practical method to control the redox state of the conjugates.

4.9 Conclusion and Outlook

In summary, two cysteine-reactive tagging systems were developed for the modification of cysteine-containing peptides. One tag incorporates an organic fluorophore based on dansyl chloride, enabling fluorescent labeling of peptides, while the second tag is derived from a 1-naphthol scaffold. Both tags were shown to efficiently modify a model cysteine-containing tripeptide, demonstrating their applicability for peptide functionalization.

The ability to introduce fluorogenic and aromatic quinone-based tags onto cysteine residues highlights the potential utility of this approach in areas such as drug development, antibody-drug conjugation, molecular and cellular biology, medical diagnostics, and imaging applications.

In the future, once the optimized conditions are well established, the methodology can be directly translated to solid-phase applications. Cysteine-containing peptides assembled on solid support can be treated with in situ generated *o*-quinone tags to afford the desired conjugated products. Subsequently, the solid support can be cleaved, potentially avoiding further purification and streamlining the overall workflow (Scheme 4.14).

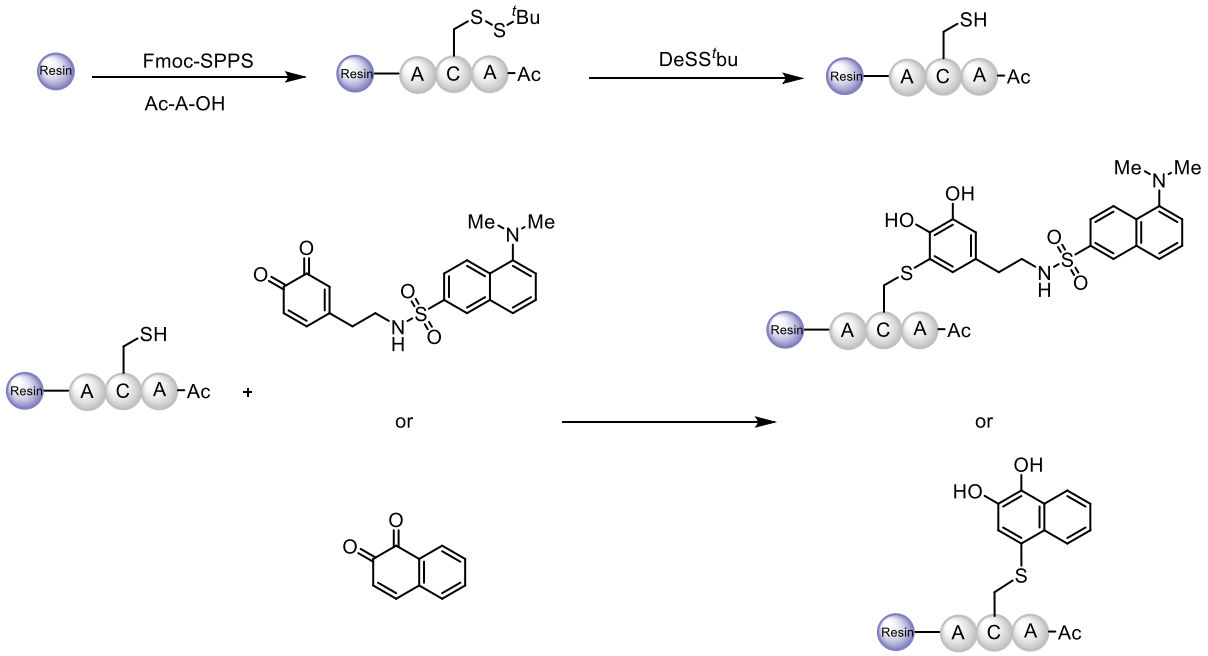

DeSS^{t}bu reagent (DMF: DODT: DIPEA) = (50:5:1)

DODT = 3,6-Dioxa-1,8-octanedithiol

Resin = Rink Amide MBHA resin or 2-CTC resin

Scheme 4.14: Prospective application of the optimized cysteine-tagging methodology to solid-phase peptide systems.

Chapter 5

Oxidative Rearrangement of Tertiary Allylic Alcohols using an Immobilized Hypervalent Iodine Catalyst

5.1 Introduction

Rearrangement reactions, in which a functional group is transposed from one position to another, represent valuable complements to bond-forming processes in the synthesis of complex molecules. Among these, the [1,3]-oxidative rearrangement of tertiary allylic alcohols has emerged as a particularly useful transformation in synthetic organic chemistry.[205] This reaction converts readily accessible tertiary allylic alcohols into α,β-unsaturated carbonyl compounds through allylic transposition accompanied by oxidation. The resulting enone motifs, especially β-substituted and α,β-disubstituted cyclic enones, are commonly found in fragrance compounds and structurally complex natural products, where they function as key intermediates or terminal functional groups (Figure 5.1).[206] The synthetic appeal of this rearrangement lies in its capacity to reorganize the carbon framework while simultaneously installing a conjugated carbonyl system, thereby enhancing molecular complexity in a single step.

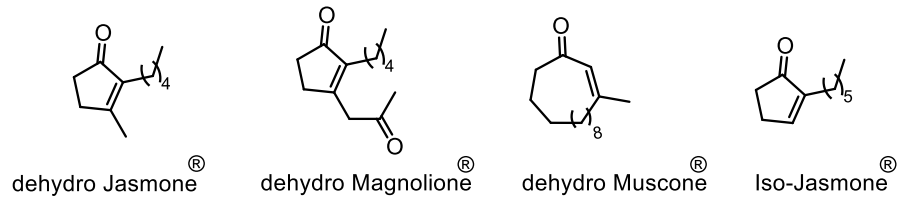

Figure 5.1: Representative examples of fragrance molecules featuring cyclic enone scaffolds.

Within this context, the oxidative rearrangement of tertiary allylic alcohols has emerged as a reliable method for skeletal reorganization, and it has been applied in numerous total syntheses. Since the mid-1970s, chromium(VI)-based oxidants such as pyridinium chlorochromate (PCC), pyridinium dichromate (PDC), and Collin's reagent have been the reagents of choice for promoting allylic transposition of tertiary allylic alcohols.[207,208] In many synthetic sequences, chromium-mediated oxidative rearrangement constitutes a crucial bond-reorganization step (Scheme 5.1).[209]

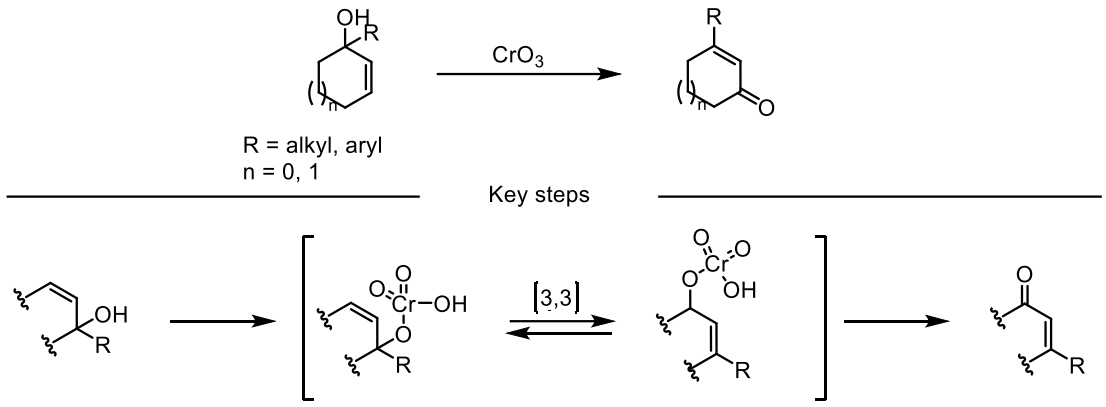

Scheme 5.1: Chromium(VI)-based oxidants (PCC, PDC, and Collin's reagent) employed for the oxidative rearrangement of *tert.* allylic alcohols, highlighting key mechanistic steps involved in the transformation.

Despite their efficiency and reliability, these oxochromium(VI) reagents are associated with significant disadvantages, including toxicity, carcinogenicity, and the generation of environmentally problematic waste. These concerns have strongly motivated the development of alternative, more sustainable oxidation systems.

A significant improvement in this area was achieved with the introduction of organic oxidants. Nitroxyl-based systems such as (2,2,6,6-Tetramethylpiperidin-1-yl)oxyl (TEMPO) and its oxoammonium salt, Bobbitt's salt ($TEMPO^+$ BF^-_4), offered milder and more selective oxidation conditions.[210] However, the most profound impact on oxidative rearrangements has been made by hypervalent iodine reagents. These compounds provide a metal-free alternative that combines mild reaction conditions with high chemoselectivity and operational simplicity. Hypervalent iodine species are capable of mediating a wide range of oxidative transformations, and their versatility has made them indispensable tools in modern synthesis.[211–217]

In this context, Iwabuchi and co-workers first reported the oxidative rearrangement of tertiary allylic alcohols using IBX, achieving conversion to α,β-unsaturated ketones at 55 °C in DMSO. In the same study, a plausible reaction mechanism was proposed involving two competing pathways. In pathway A, solvolysis of the tertiary allylic alcohol generates an allylic cation, which subsequently collapses with IBX at the less substituted terminus to form an isomeric iodic ester that undergoes oxidation. Alternatively, formation of a tertiary iodic ester may precede rearrangement and oxidation, as depicted in pathway B (Scheme 5.2).[218]

Iwabuchi, *2004*

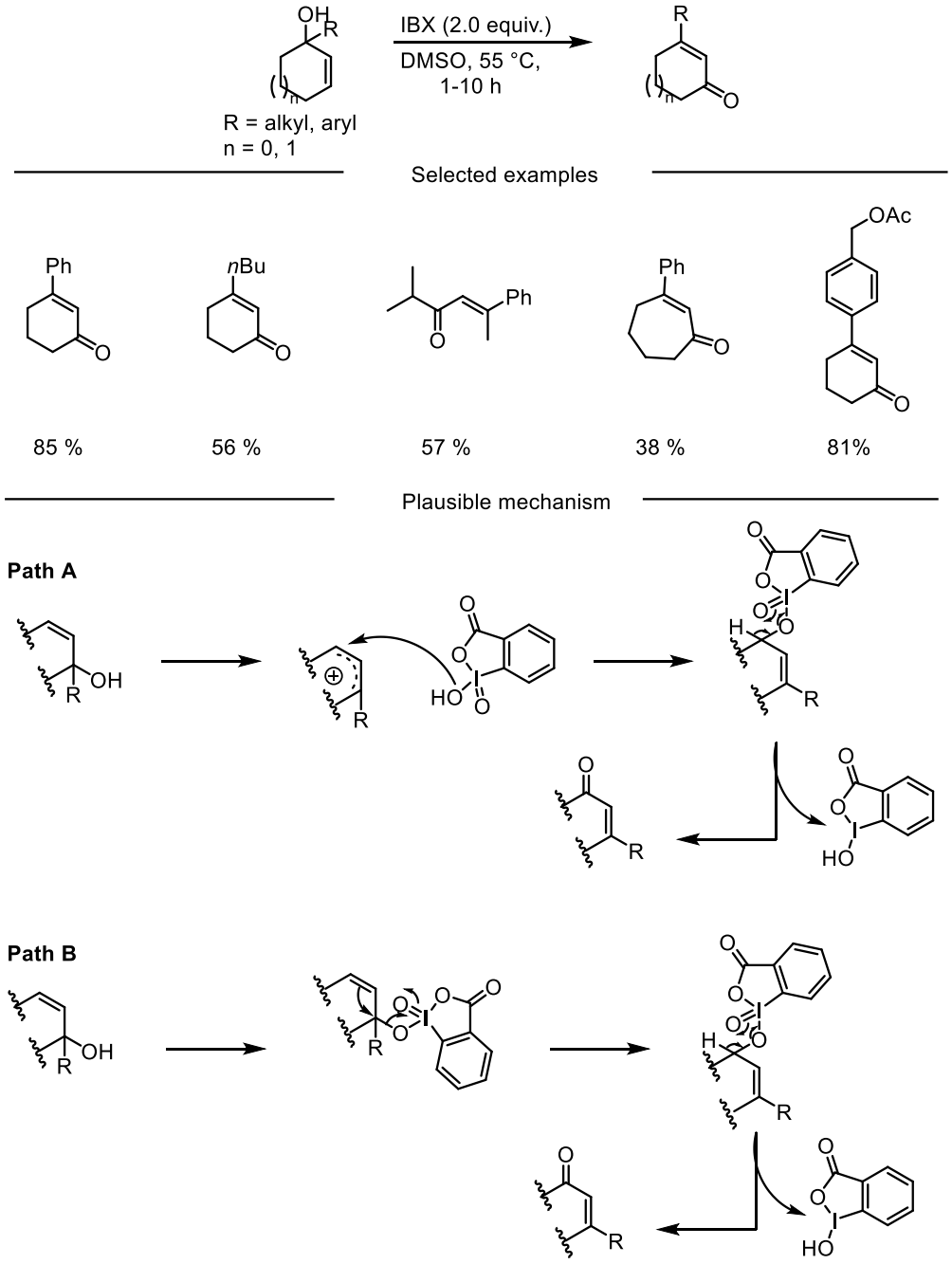

Scheme 5.2: Oxidative rearrangement of *tert.* allylic alcohol using IBX.

While the precise sequence of events remains subject to mechanistic interpretation, both pathways underscore the dual role of IBX as both an activating and oxidizing agent.

Although IBX-mediated rearrangements are synthetically valuable, practical limitations remain. Hypervalent iodine(V) reagents are often required in stoichiometric or excess amounts, which results in significant waste generation. Furthermore, issues related to thermal instability and potential explosion hazards, restrict their broader industrial

implementation.[125,132,219] These challenges prompted efforts to render iodine(V)-mediated oxidations catalytic and recyclable.[220]

An important contribution in this regard was made by, Ishihara and co-workers who developed a catalytic variant of this transformation using IBS in combination with Oxone®. In this system, IBS is generated *in situ* from a pre-IBS catalyst and Oxone®, with the resulting iodine(V) species serving as the active oxidant responsible for the oxidative rearrangement (Scheme 5.3).[221] This work demonstrated that oxidative rearrangements of tertiary allylic alcohols could be achieved under catalytic iodine(V) conditions, thereby significantly reducing reagent consumption and improving the sustainability profile of the transformation.

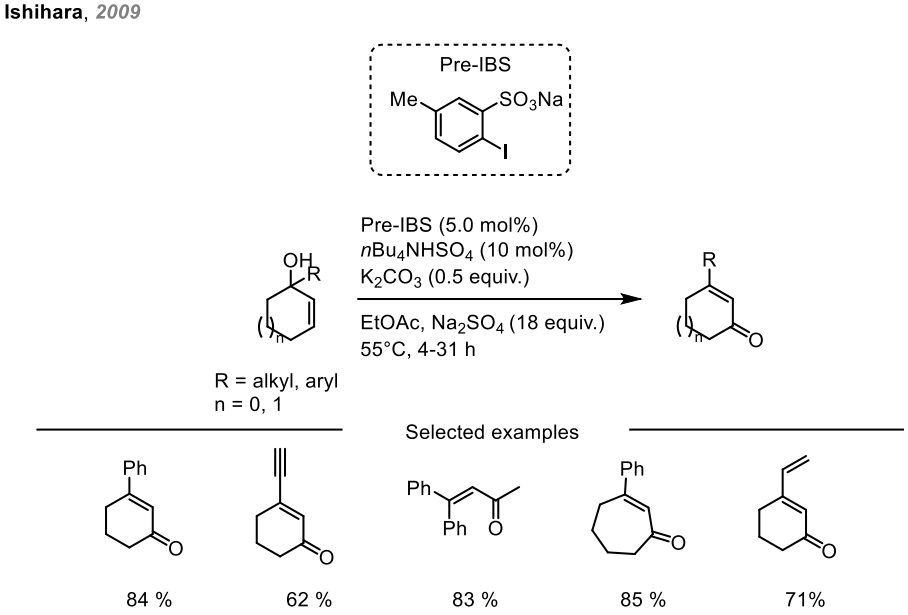

Scheme 5.3: Oxidative rearrangement of *tert.* allylic alcohol using catalytic amount of IBS.

5.2 Solid-Supported Hypervalent Iodine Reagents

Parallel to the development of catalytic systems, strategies aimed at improving reagent recyclability were explored. In 2001, Giannis and Rademann independently addressed this challenge by developing polymer-supported versions of IBX.[222] Immobilization of the hypervalent iodine unit on a solid support enhanced thermal stability and reduced impact sensitivity, while also simplifying product isolation through straightforward filtration. Importantly, the resin-bound iodosobenzoic acid intermediate could be reoxidized to regenerate the active iodine(V) species, thereby enabling reagent recycling.

In subsequent years, multiple research groups reported additional solid-supported hypervalent iodine derivatives employing related design strategies (Figure 5.2).[223–227] In parallel, soluble yet readily re-isolable iodine(V) reagents were also developed, allowing recovery and reuse of the oxidant and thereby reducing organic waste generation.[228–232] Collectively, these

advances highlighted the significant hypervalent iodine systems as more sustainable alternatives to conventional stoichiometric oxidants.[233–235]

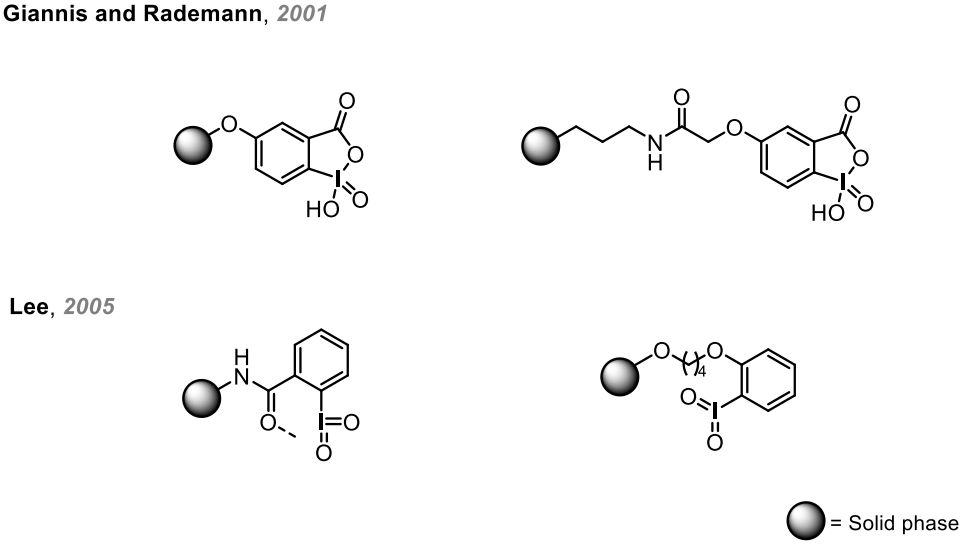

Figure 5.2 Selected examples of immobilized iodine(V) compounds.

While these developments improved safety and sustainability, the methods were mostly confined to batch reactions, and scale-up or implementation in continuous-flow systems remained unexplored.

5.3 Continuous-Flow

Continuous-flow chemistry offers an attractive platform to further enhance the safety, efficiency, and scalability of oxidative transformations. In contrast to conventional batch processes, continuous-flow systems allow reagents to be introduced into a reactor in a controlled and continuous manner. Precise regulation of parameters such as temperature, residence time, pressure, and concentration can be achieved, often resulting in improved selectivity and reproducibility. The high surface-area-to-volume ratios characteristic of flow reactors facilitate efficient heat and mass transfer, which is particularly advantageous for exothermic or potentially hazardous oxidations.[236–238] Furthermore, immobilized catalysts can be incorporated into fixed-bed reactors, minimizing catalyst leaching and simplifying downstream processing.[239,240] Despite higher initial setup costs and the need for specialized expertise, continuous-flow technology has emerged as a powerful and increasingly sustainable tool in modern synthesis.[241,242]

Building upon these concepts, Kirsch and co-workers in 2019 reported a recyclable IBX- and IBS-based hypervalent iodine catalyst (**SP-IBX I** and **SP-IBS I**) in which a peptide linker was employed to connect the hypervalent iodine unit to the solid support. The **SP-IBS I** catalyst was applied in combination with nBu$_4$NHSO$_5$ as terminal co-oxidant under phase-transfer

conditions, enabling the selective oxidation of primary and secondary alcohols to the corresponding carbonyl compounds. The resulting material demonstrated excellent recyclability, retaining its catalytic activity over multiple oxidation cycles without significant loss of performance (Scheme 5.4).[243] Subsequent developments further expanded this approach through immobilization of the IBS catalyst on alternative supports (**SP-IBS II**), such as silica (SiO_2) (Scheme 5.6).[244]

Kirsch, *2019*

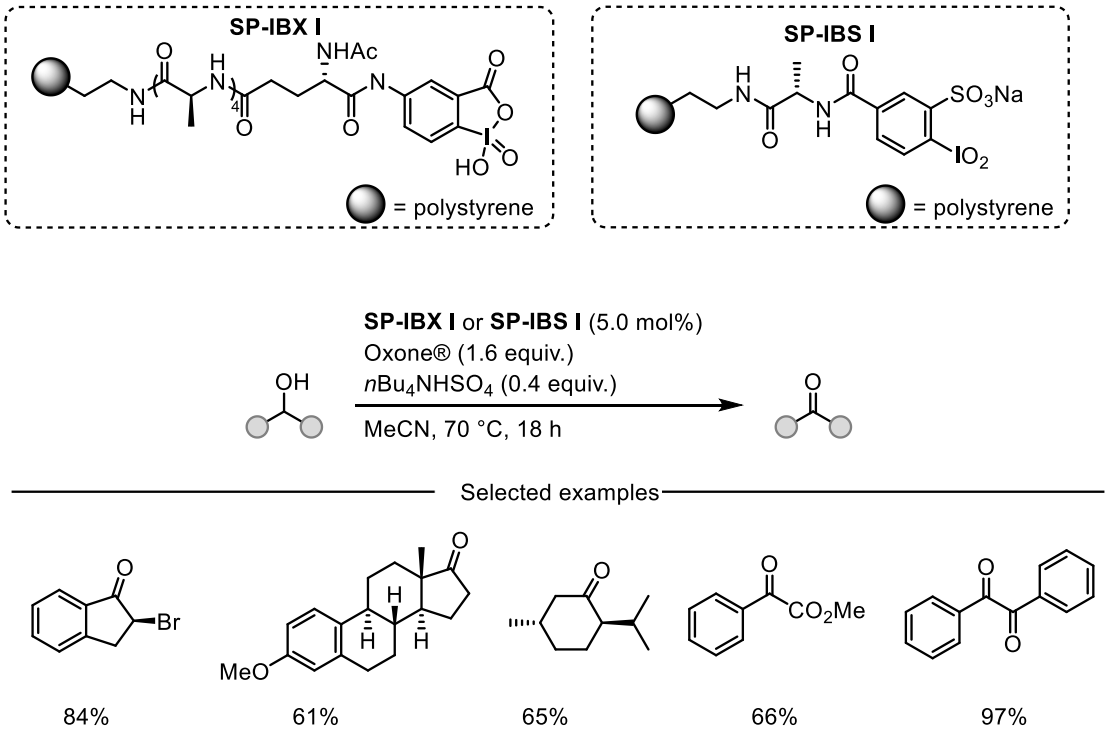

Scheme 5.4: Oxidation of primary and secondary alcohols to carbonyl compounds using solid-supported hypervalent iodine catalysts.

These solid-supported IBS catalysts were successfully integrated into continuous-flow setups. Under flow conditions, the immobilized iodine(V) catalyst, used in conjunction with a suitable terminal oxidant, enabled efficient and selective oxidation reactions with minimal catalyst leaching and sustained activity over numerous cycles. These studies clearly demonstrate that the combination of hypervalent iodine catalysis with continuous-flow processing represents a viable strategy for achieving safer and more sustainable oxidative transformations at scale (Scheme 5.5).[245]

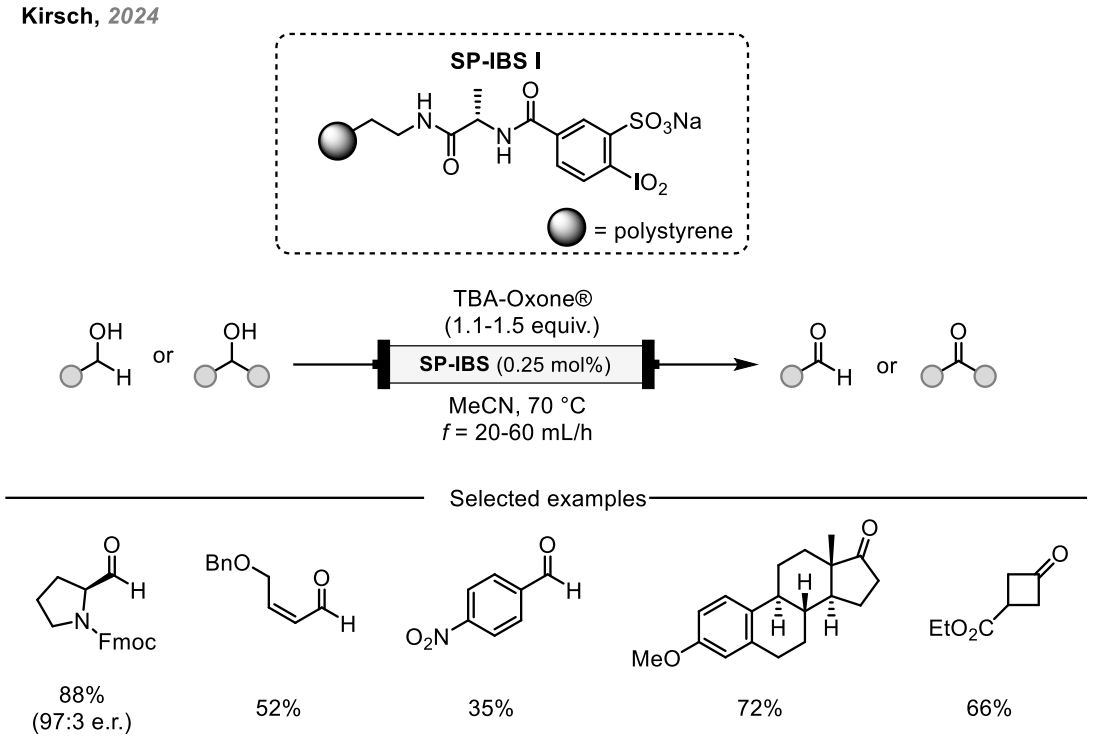

Scheme 5.5: Application of a solid-supported IBS catalyst for continuous-flow oxidation of alcohols.

In 2026, the approach was further extended to scalable oxidative cleavage of β-substituted primary alcohols under continuous-flow conditions using a silica-supported iodine(V) catalyst (**SP-IBS II**) in combination with TBA-Oxone® as the terminal oxidant. This approach provided rapid and selective access to γ-lactones and γ-lactams under mild conditions, demonstrating broad substrate scope and high functional group tolerance. Notably, the catalyst remained reusable for more than 15 cycles, and the process was readily scalable, further highlighting the potential of solid-supported hypervalent iodine catalysts for flow-based oxidative transformations (Scheme 5.6).[244]

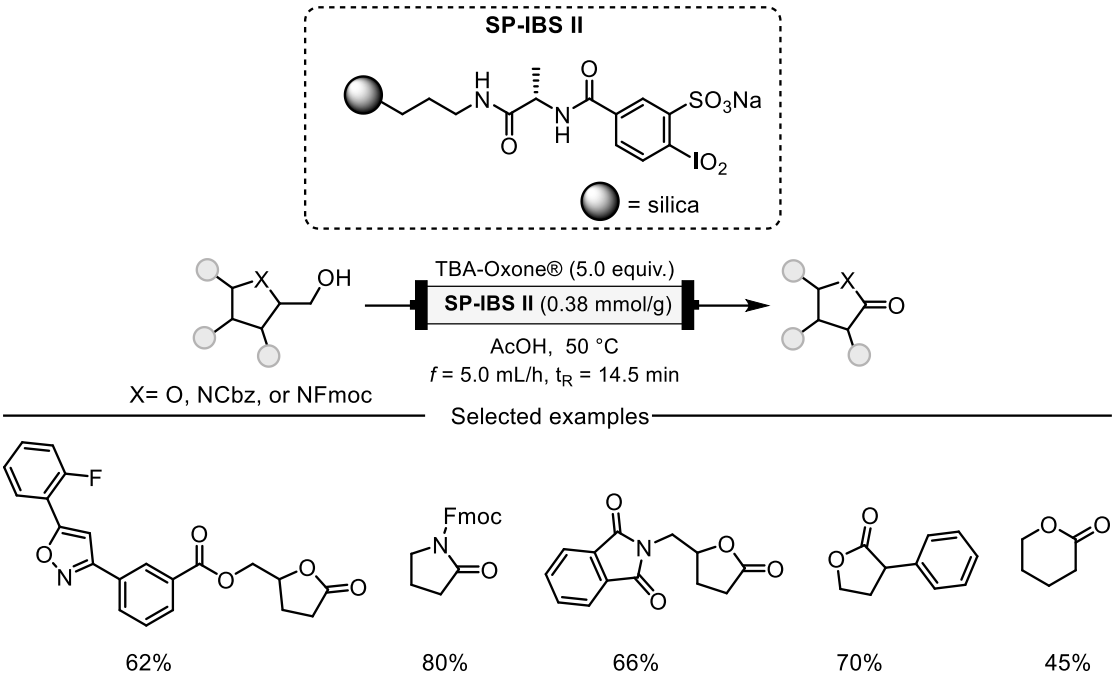

Scheme 5.6: Solid-supported IBS catalyst for continuous-flow oxidative cleavage of β-substituted primary alcohols.

Despite these advances, the application of solid-supported iodine(V) catalysts to the oxidative rearrangement of tertiary allylic alcohols under continuous-flow conditions remains underexplored. Given the synthetic importance of α,β-unsaturated carbonyl compounds and the limitations associated with existing IBX- and IBS-based methods, the development of a recyclable, metal-free, flow-compatible, and scalable rearrangement protocol is highly desirable.

5.4 Project Goals

The objective of this chapter was to explore the use of the solid-supported IBS catalyst (**SP-IBS I**) for the oxidative rearrangement of tertiary allylic alcohols under batch and continuous-flow conditions (Scheme 5.7). The study focuses on developing a robust, metal-free, and mild method with reusable catalyst, while identifying key factors influencing catalyst regeneration to enable a scalable and efficient process.

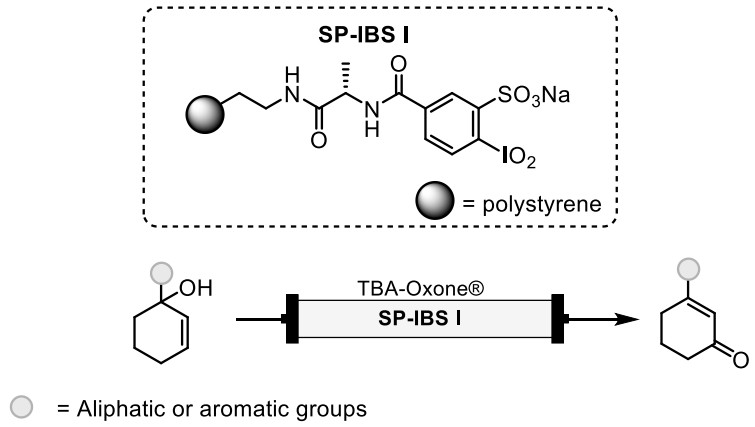

Scheme 5.7: Continuous-flow strategy for *tert.* allylic alcohol rearrangement using **(SP-IBS I)** catalyst, a catalyst reported in earlier studies.

5.5 Results and Discussion

To start with, the development of a robust solid-supported hypervalent iodine(V) catalyst involved the synthesis of a polystyrene-supported iodine(V) system, following the procedure reported by Kirsch and co-workers. The IBS precursor was prepared from 2-amino-5-methylbenzenesulfonic acid, which underwent a Sandmeyer-type reaction to introduce the iodine substituent, affording compound 5.1 in 50% yield. Subsequent oxidation of the benzylic methyl group using potassium permanganate furnished the corresponding carboxylic acid **5.2** in 90% yield. This compound served as the key precursor for the subsequent solid-phase synthesis (Scheme 5.8).

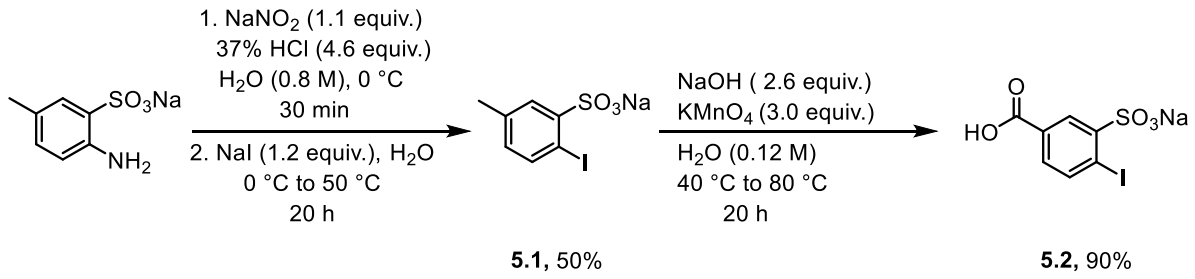

Scheme 5.8: Synthesis of IBS building block for the solid-phase-peptide synthesis.

Using precursor **5.2**, the solid-phase synthesis was carried out via standard Fmoc-based peptide coupling on a polystyrene-Et-NH_2 resin. Alanine was first coupled to the resin, followed by attachment of 5.2 using *O*-(7-azabenzotriazol-1-yl)-N,N,N',N'-tetramethyluronium hexafluorophosphate (HATU) and DIPEA in DMSO. After acetylation, the resin-bound precursor was oxidized with TBA-Oxone® in the presence of methanesulfonic acid in DCM at room temperature to generate the active hypervalent iodine(V) catalyst **SP-IBS I** (Scheme 5.9).

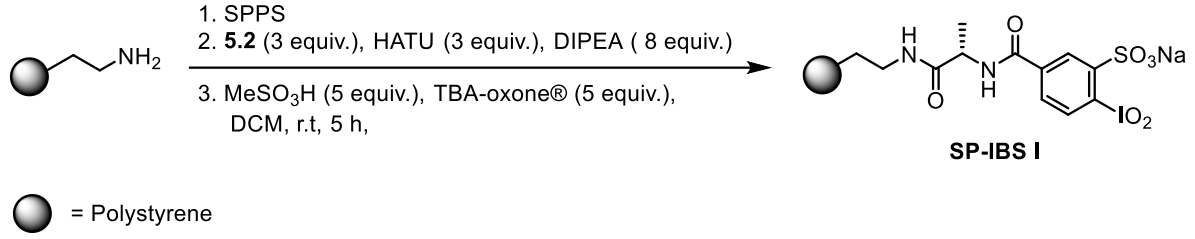

Scheme 5.9: Synthesis of solid-bound IBS catalyst (**SP-IBS I**).

The amount of active iodine(V) immobilized on the resin was evaluated both theoretically and experimentally. The theoretical loading was calculated as 0.75 mmol/g (equation 1, experimental Section). Experimentally, 30 mol% of SP-IBS I was reacted with L-(–)-borneol as a probe substrate, and GC-FID analysis indicated 21% conversion, corresponding to approximately 70% of the theoretical maximum. From this, the effective loading of the immobilized catalyst was determined to be 0.53 mmol/g (Scheme 5.10). This measurement provides an activity-based assessment of the accessible hypervalent iodine(V) sites on the polymer support.

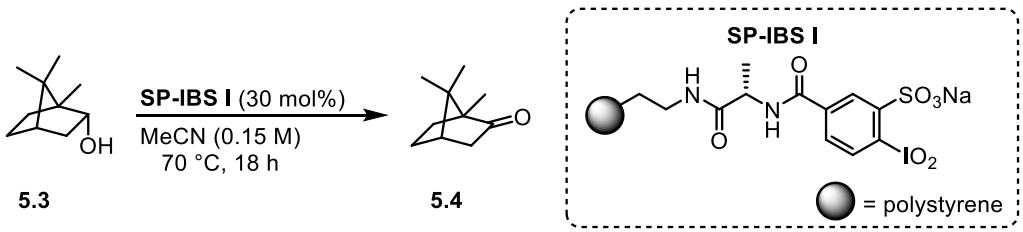

Scheme 5.10: Determination of the loading of the resin (conversion determined by GC-FID).

5.5.1 Stoichiometric Batch Reaction

The reactivity of **SP-IBS I** was first evaluated using 1-phenylcyclohex-2-en-1-ol **5.5** under stoichiometric conditions. Treatment with 1.5 equivalents of the immobilized catalyst in ethyl acetate at 60 °C for 4 hours afforded the desired α,β-unsaturated ketone 5.6 in 87% yield, along with 11% of the corresponding diene **5.7** (Scheme 5.11). Complete conversion was observed, confirming that the solid-supported catalyst is capable of promoting the oxidative rearrangement efficiently under batch conditions.

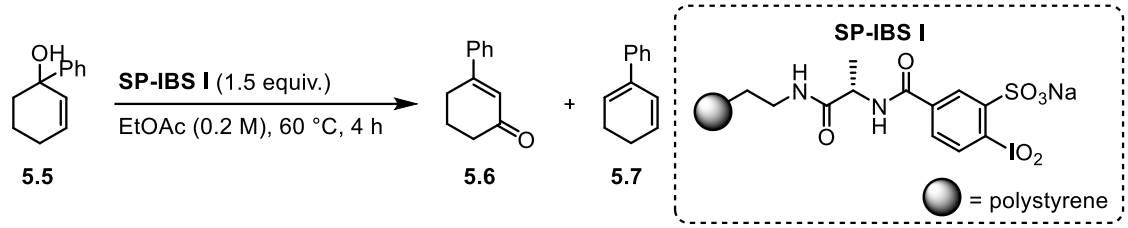

Scheme 5.11: Oxidative rearrangement of *tert.* allylic alcohol using a stoichiometric amount of solid-supported IBS (**SP-IBS I**).

5.6 Optimization studies in batch

Encouraged by the stoichiometric results, 1-phenylcyclohex-2-en-1-ol **5.5** was chosen as a model for optimization studies. Each reaction parameter was systematically varied while maintaining the others constant to identify the optimal conditions. The optimization focused on catalyst loading, solvent selection, reaction temperature, and the choice of co-oxidants and bases. In addition, conditions were evaluated to maximize catalyst reusability. The screening results, summarized in Tables 5.1–5.5, provided insight into the most efficient reaction setup.

5.6.1 Determination of Optimal Catalyst Loading

To identify suitable conditions for the oxidative rearrangement of tertiary allylic alcohols, the optimization initially focused on determining the appropriate catalyst loading. Substrate **5.5** was selected as the model compound, and the catalyst loading was varied between 5 and 15 mol% (Table 5.1, entries 1-3). All reactions were performed using Oxone® (1.0 equiv., finely ground prior to use) in the presence of a phase-transfer catalyst (10 mol%), sodium sulfate, and potassium carbonate as the base in ethyl acetate at 60 °C for 4 h. Under these conditions, a catalyst loading of 10 mol% proved optimal, affording the desired product **5.6** in 30% yield.

Table 5.1 Optimization of catalyst's amount

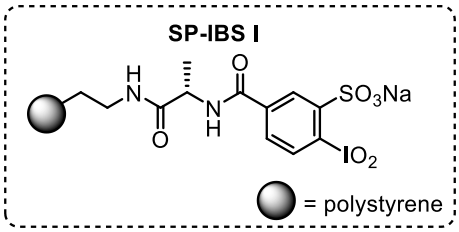

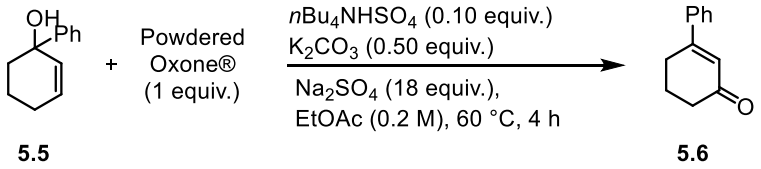

5.5 **5.6**

Entry	SP-IBS I (X equiv.)	Yields[a]%
1	0.05	20
2	0.10	30
3	0.15	30

[a] = Isolated yields.

5.6.2 Selection of Co-Oxidant

To further identify optimal conditions for the oxidative rearrangement of tertiary allylic alcohols, the study summarized in Table 5.2 began with an evaluation of different co-oxidants. The amount of Oxone® was systematically varied from 0.25 to 1.0 equivalent under standard conditions. An increase in the amount of Oxone from 0.25 to 1.0 equivalent resulted in a gradual improvement in yield of desired product **5.6** (Table 5.2, entries 1-4). Complete conversion under the standard conditions required a stoichiometric amount of Oxone (1.0 equiv.) (Table 5.2, entry 4).

However, increasing the amount further to 2.0 equiv. resulted in a reduced yield of 25%, accompanied by the formation of additional side products despite full conversion (Table 5.2, entry 5). In addition, alternative oxidants such as peracetic acid, *meta*-chloroperoxybenzoic acid (*m*CPBA), cumyl hydroperoxide, and urea-hydrogen peroxide were examined in HFIP (Table 5.2, entries 6-8). In all cases, only trace amounts of the desired product were detected. Based on these results, 1.0 equivalent of Oxone was selected as the standard condition for subsequent studies (Table 5.2, entry 4).

Table 5.2 The examination of co-oxidant

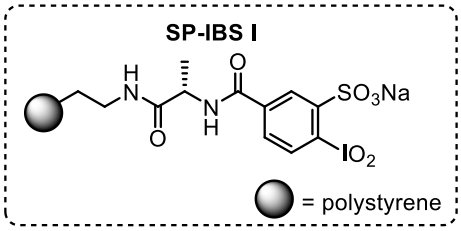

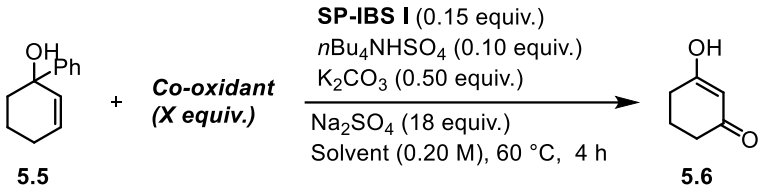

5.5 **5.6**

Entry	Co-oxidant (X equiv.)	Solvent	Yields%
1	Oxone®, (0.25)	EtOAc	15[a]
2	Oxone®, (0.50)	EtOAc	18[a]
3	Oxone®, (0.75)	EtOAc	23[a]
4	Oxone®, (1.0)	EtOAc	30[a]
5	Oxone®, (2.0)	EtOAc	25[a]
6	CH_3CO_3H, (1.0)	HFIP	-[b]
7	*m*CPBA, (1.0)	HFIP	-[b]
8	$C_6H_5C(CH_3)_2OOH$, (1.0)	HFIP	-[b]
9	urea-H_2O_2, (1.0)	HFIP	-[b]

[a]= isolated yields, [b]= Yields were determined using dimethyl sulfone as an internal standard with ^1H NMR.

5.6.3 Optimization of Base Amount

To further optimize the reaction conditions, the amount of potassium carbonate was systematically varied from 0.25 to 1.0 equivalent under standard conditions (Table 5.3, entries 1-4). Variations in base loading noticeably affected the reaction outcome, with higher amounts sometimes leading to increased substrate decomposition and lower yields of the desired product. Substituting potassium carbonate with cesium carbonate did not provide a significant improvement in reaction performance (Table 5.3, entry 5). Overall, the standard base loading of 0.5 equivalent afforded the most consistent results and was therefore adopted for subsequent optimization studies (Table 5.3, entry 2).

Table 5.3 Determination of base

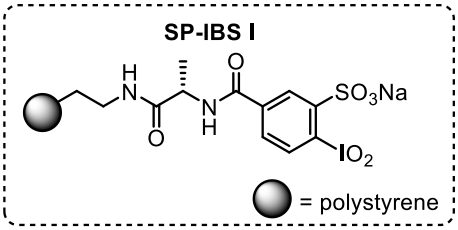

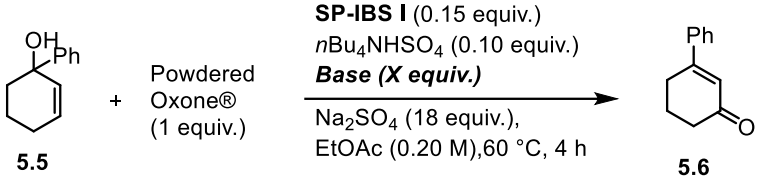

5.5 5.6

Entry	Base (X equiv.)	Yields[a]%
1	K_2CO_3, (0.25)	11
2	K_2CO_3, (0.50)	30
3	K_2CO_3, (0.75)	21
4	K_2CO_3, (1.0)	10
5	Cs_2CO_3, (0.50)	30

[a] = Isolated yields.

5.6.4 Effect of Reaction Temperature

The effect of temperature on the reaction was investigated over a range of 40-70 °C under the standard conditions (Table 5.4, entries 1-4). The screening results indicated that a minimum temperature of 60 °C was required to achieve full conversion. At lower temperatures (Table 5.4, entries 1-2), incomplete conversion was observed even after 18 h. Increasing the temperature further to 70 °C did not provide any significant improvement. Therefore, a reaction temperature of 60 °C (Table 5.4, entry 3) was selected for subsequent studies.

Table 5.4 Variation of temperature

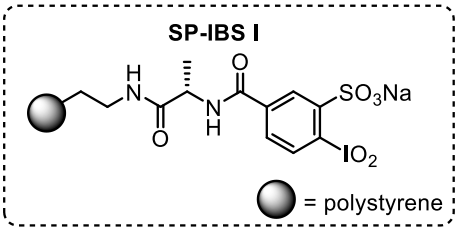

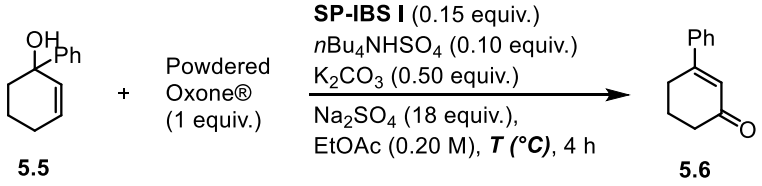

5.5 **5.6**

Entry	T (°C)	Yields [a]%
1	40	-
2	50	-
3	60	30
4	70	27

[a] = Isolated yields.

5.6.5 Solvent Screening

For further optimization, various solvents were screened under the standard reaction conditions. Ethyl acetate, HFIP, and 1,4-dioxane (Table 5.5, entries 1-3) all afforded comparable yields of the desired product. In contrast, the use of acetonitrile led to a complex reaction mixture, as indicated by a poorly resolved TLC profile (Table 5.5, entry 4). Based on these results, ethyl acetate was selected as the solvent for subsequent reactions (Table 5.5, entry 1).

Table 5.5 Screening of solvents

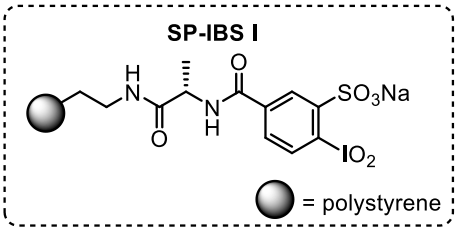

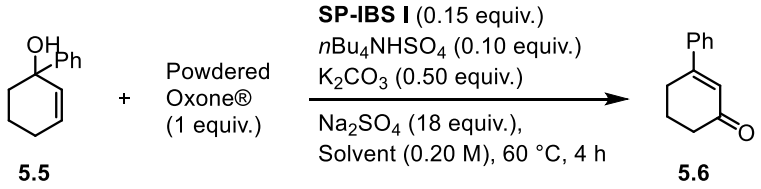

5.5 **5.6**

Entry	Solvent	Yields [a]%
1	EtOAc	30
2	HFIP	28
3	1,4-dioxane	30
4	MeCN	10

[a] = Isolated yields.

Despite moderate catalytic yields in batch (~30%), complete substrate conversion was achieved, providing valuable insights for process optimization. These preliminary results indicated that continuous-flow, with its precise control over residence time, mixing, and oxidant exposure, could offer a more efficient and selective platform for the oxidative rearrangement of tertiary allylic alcohols. This observation provided the rationale for translating the optimized batch conditions into a flow system.

5.7 Scope and Limitations

Nevertheless, the established conditions were applied to a range of tertiary allylic alcohols using the solid-supported IBS catalyst to evaluate the generality and scope of the oxidative rearrangement. For these studies, the catalyst loading was increased to 15 mol%, Oxone® (1.0 equiv., finely ground) was used as the co-oxidant, and potassium carbonate (0.5 equiv.) with sodium sulfate (18 equiv.) served as the base system in ethyl acetate. Reaction times were varied between 4 and 12 hours to ensure adequate conversion for different substrates. Substrates bearing various substituents, including phenyl, butyl, and hexyl groups, afforded the corresponding α,β-unsaturated carbonyl products **5.6-5.8** in 28–40% yield (Scheme 5.11). In all cases, the reactions reached complete conversion, with the corresponding dienes as the major side products. These findings suggest that, although the batch system enables

productive rearrangement, further improvements in selectivity and yield can be achieved through continuous-flow implementation.

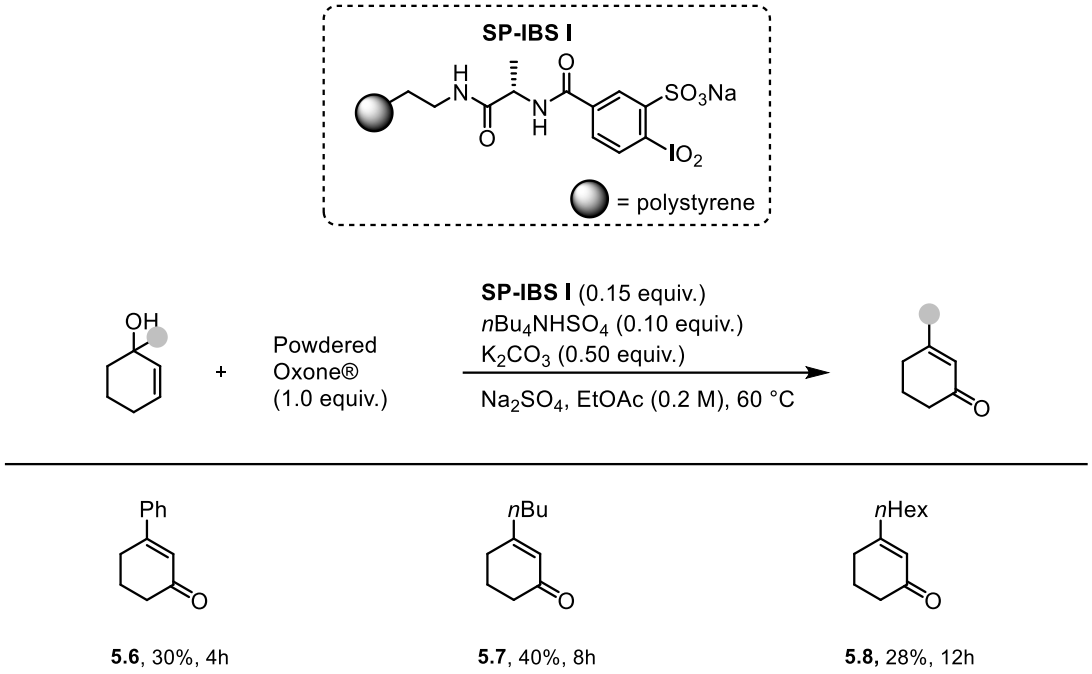

Scheme 5.12: Substrate scope of oxidative rearrangement of tert. allylic alcohol.

5.8 Continuous-Flow Approach

To overcome the limitations observed under batch conditions, particularly the predominant formation of diene byproducts despite complete conversion, the study was directed toward continuous-flow operation. Since reactivity was not the primary concern, but rather selectivity, a flow-based approach was considered advantageous due to its precise control over residence time, mixing, and oxidant exposure-parameters that are critical in hypervalent iodine-mediated oxidations. It was anticipated that improved control of these factors could suppress competing side reactions and enhance formation of the desired α,β-unsaturated carbonyl products.

Accordingly, the oxidative rearrangement was carried out using a fixed-bed reactor packed with the immobilized SP-IBS I catalyst. Separate solutions of TBA-Oxone® and the tertiary allylic alcohol substrate were delivered at defined flow rates using a two-channel syringe pump and combined through a T-mixer before entering the heated packed-bed reactor. The reaction mixture passed through the catalyst bed under controlled flow conditions, and the resulting solution was collected for subsequent analysis. This setup follows a procedure similar to that reported by Kirsch and co-workers in earlier studies (Figure 5.2).

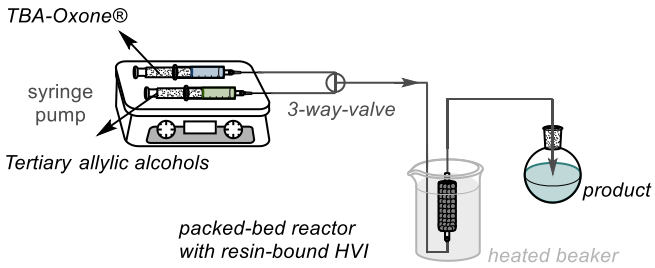

Figure 5.3 : Continuous-flow setup for the oxidative rearrangement of *tert.* allylic alcohols using solid-support HVI.

5.9 Optimization in Continuous-Flow

Initial experiments were performed under continuous-flow conditions at 60 °C using two separate streams: one containing the tertiary allylic alcohol substrate **5.5** and the other TBA-Oxone® as the co-terminal oxidant. The streams were combined via a T-mixer and passed through the SP-IBS-packed bed reactor with a residence time of 14 min. Under these conditions, the desired rearranged product **5.6** was obtained in 31% yield, accompanied by 47% of a side product (Table 5.6, entry 1). To evaluate the intrinsic reactivity of the immobilized catalyst in the absence of the external oxidant, the substrate solution was subsequently passed directly through the **SP-IBS I** packed reactor at 60 °C without TBA-Oxone®. Increasing the residence time to 17 min led to an improved yield of 52% of the desired product (Table 5.6, entry 2). This result suggested that the presence of TBA-Oxone® under the initial conditions may contribute to side reactions or non-productive pathways. Further optimization focused on solvent effects. Replacing the initial solvent with ethyl acetate and extending the total residence time to 61 min resulted in a significant increase in product yield to 74% (Table 5.6, entry 3).

Table 5.6: Continuous-flow optimization of the oxidative rearrangement of *tert.* allylic alcohols.

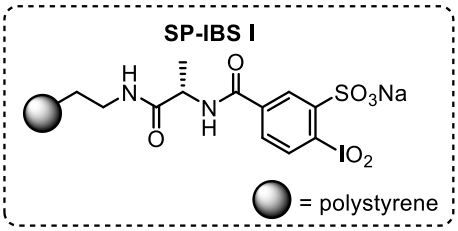

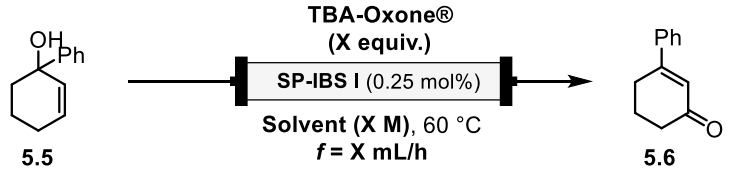

5.5 5.6

Entry	Solvent (X M)	TBA-Oxone® (X equiv.)	*f* (X mL/h)	t_R (min)	Yield[a]%
1.	MeCN (0.2)	1	14.4	14	31
2	MeCN (0.03)	-	12	17	52
3	EtOAc (0.03)	-	3	61	74

[a]= Yields were determined using dimethyl sulfone as an internal standard with ^{1}H NMR.

These results demonstrate the pronounced influence of residence time and solvent choice on reaction efficiency in flow, highlighting continuous-flow as the more effective platform for controlling selectivity and improving product yield. While catalytic turnover with TBA-Oxone® remains a challenge, these preliminary studies provide a clear pathway toward fully catalytic and scalable implementation.

5.10 Conclusion and Outlook

In conclusion, the oxidative rearrangement of tertiary allylic alcohols proceeds in excellent yield under batch conditions when stoichiometric amounts of **SP-IBS I** are employed, highlighting the high intrinsic reactivity of the iodine(V) species. Under continuous-flow conditions, the immobilized **SP-IBS I** catalyst also facilitated productive conversion in the absence of a terminal co-oxidant, providing good yields that were further enhanced through adjustment of residence time and solvent parameters.

However, when catalytic quantities of **SP-IBS I** were used in combination with TBA-Oxone® as a terminal oxidant under flow conditions, only low conversions were observed. These results indicate that efficient in situ regeneration of the active iodine(V) species remains a critical challenge for achieving fully catalytic turnover in continuous flow.

Future investigations will therefore focus on identifying alternative co-oxidants capable of selectively and efficiently reoxidizing the iodine species under flow conditions. The establishment of a compatible and robust oxidation system would enable sustained catalyst turnover, thereby improving the practicality, efficiency, and scalability of the continuous-flow oxidative rearrangement of tertiary allylic alcohols.

Chapter 6
Conclusion

Conclusion

Methods for the late-stage diversification of peptides remain limited by narrow functional-group tolerance and a reliance on peripheral side-chain reactivity. Chemical strategies for tyrosine modification largely preserve the native nucleophilic character of the phenolic side chain, thereby restricting the range of accessible structural and physicochemical diversity. In contrast, biological systems exploit oxidative activation of tyrosine to transiently invert phenol polarity, enabling bond-forming transformations that are difficult to access synthetically.

In this thesis, Chapters 2 and 3 describe a metal-free methodological platform that translates this enzymatic logic into a practical synthetic strategy for short peptides. Mild oxidation of tyrosine residues using a hypervalent iodine(V) reagent enables the controlled in situ generation of electrophilic *o*-quinone intermediates under conditions compatible with a broad range of amino acid side chains. Selective interception of this common intermediate allows two orthogonal modification modes within a unified framework: (i) transformation of tyrosine core into phenazine scaffolds and (ii) peripheral modification through site-selective tyrosine-cysteine cross-linking.

Chapter 2 focuses primarily on skeletal modification of the tyrosine residue to access phenazine derivatives. An initial amino acid compatibility study was conducted to evaluate the tolerance of diverse side chains under the oxidative conditions. Subsequently, a range of diamines was explored, several of which afforded products exhibiting intrinsic fluorescence. Tyrosine-containing oligopeptides bearing Boc or Cbz protecting groups were successfully diversified using 1,2-phenylenediamine, furnishing more than ten phenazine-modified examples (Scheme 6.1). Notably, the resulting phenazine scaffolds displayed fluorescent properties, highlighting their potential utility in molecular imaging applications.

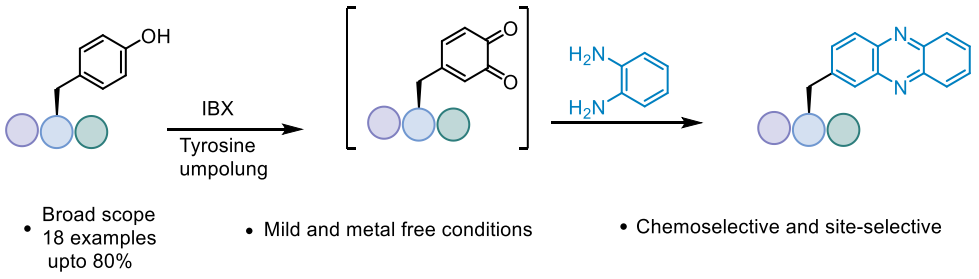

Scheme 6.1 : Bioinspired strategy for skeletal Tyrosine diversification (chapter 2 summary).

In Chapter 3, the focus shifted to peripheral modification through side-chain cross-linking. The in situ generated *o*-quinone intermediate was selectively intercepted by cysteine-containing peptides, enabling tyrosine–cysteine conjugation. tyrosine-containing dipeptides and

tripeptides were successfully coupled with cysteine and cysteine-containing dipeptides, and five representative examples were demonstrated (Scheme 6.2).

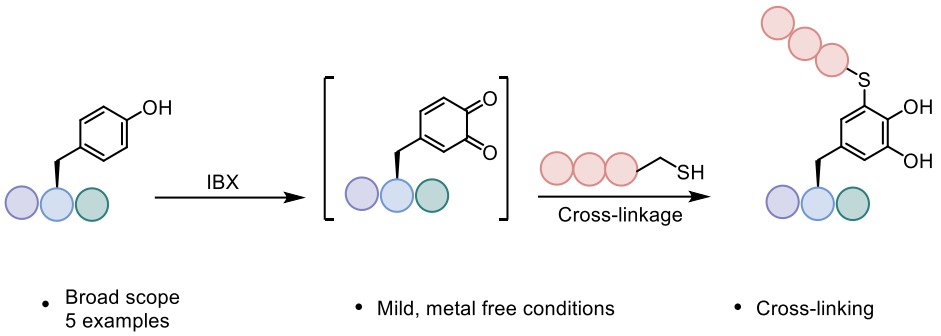

Scheme 6.2 : Bioinspired strategy for peripheral Tyrosine diversification (chapter 3 summary).

Collectively, chapter 2 and 3 establish a transformation that exhibits broad functional-group tolerance, operates in densely functionalized oligopeptides, and enables late-stage modification without the need for *de novo* synthesis or protecting-group-intensive routes. More broadly, this work introduces phenolic umpolung as a transferable design principle for peptide modification and expands the methodological scope of hypervalent iodine(V) chemistry in complex molecular settings.

Chapter 4 extends *o*-quinone chemistry toward phenol-derived electrophilic tags for selective cysteine modification. Two fluorescent tagging systems- a synthetically prepared dansyl-tyramine conjugate (Tag A) and a commercially available 1-naphthol scaffold (Tag B)-were developed and shown to efficiently label a model cysteine-containing peptide via in situ oxidation to the corresponding *o*-quinones. These results establish a complementary cysteine-labelling strategy in which fluorescence is an integral design feature, highlighting the potential of this approach for peptide functionalization and future applications in chemical biology, diagnostics, and therapeutic development (Scheme 6.3).

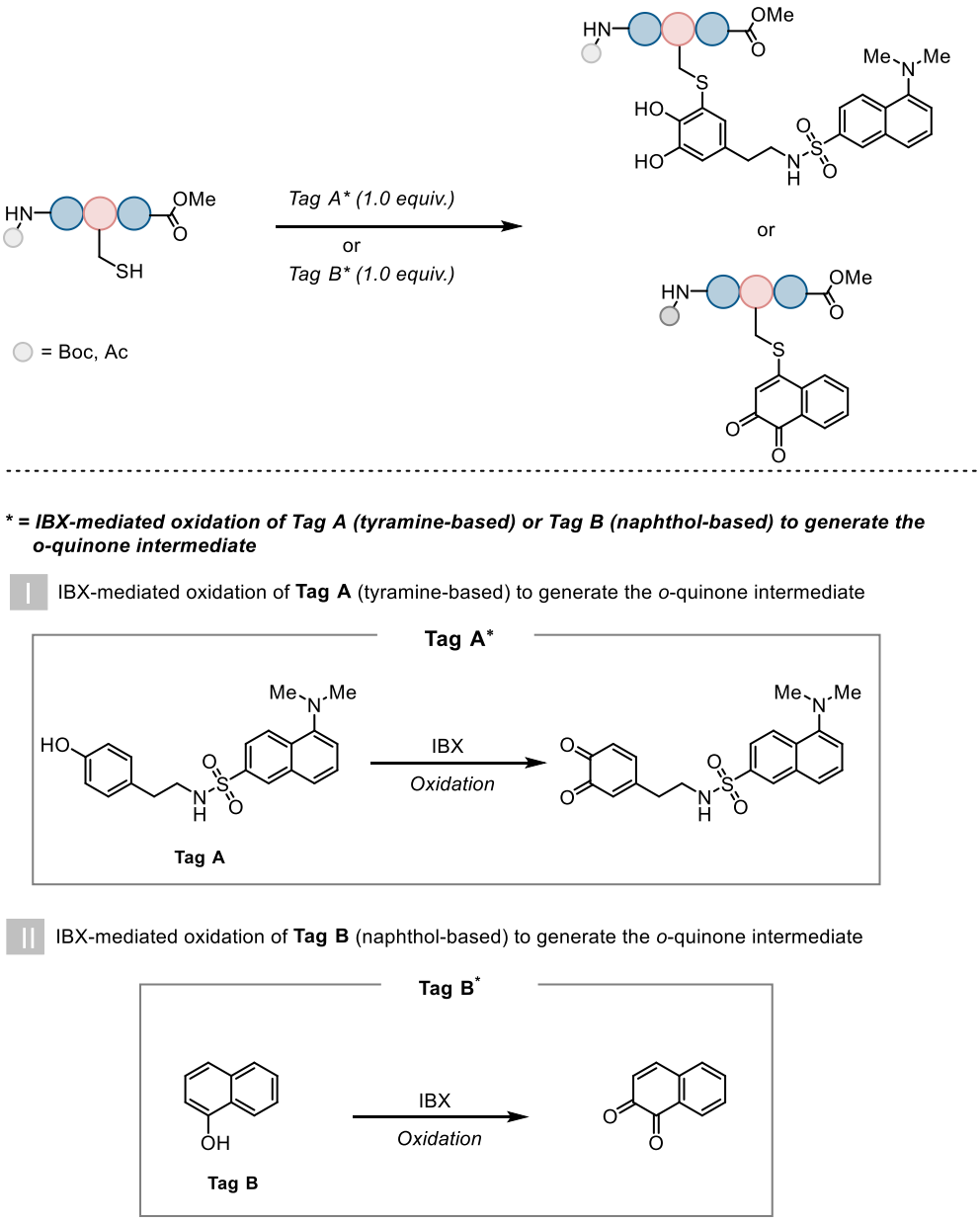

Scheme 6.3: Cysteine labeling with fluorescent Tag A (tyramine attached with dansyl chloride) and Tag B (naphthalene) via in situ *o*-quinone formation (chapter 4 summary).

Chapter 5 describes an independent side project focusing on the development of a solid-supported hypervalent iodine(V) system for oxidative rearrangement chemistry. The solid-phase batch studies demonstrated promising reactivity and high yields, validating the viability of the supported system. However, further investigation under continuous-flow conditions is necessary to fully realize its potential in terms of productivity, scalability, and catalyst recyclability.

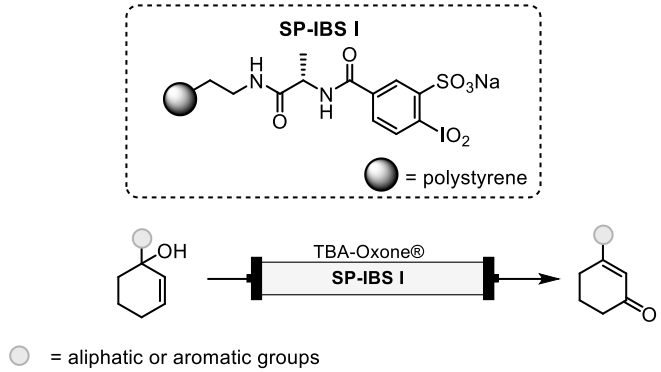

Scheme 6.4: Continuous-flow strategy for *tert.* allylic alcohol rearrangement using established catalyst (chapter 5 summary).

Overall, this dissertation presents synthetic strategies for peptide diversification based on quinone intermediates generated by hypervalent iodine reagents. It demonstrates methods for the selective modification of tyrosine residues, as well as the labeling of cysteine-containing peptides, thereby expanding the synthetic toolbox for site-selective peptide functionalization.

Chapter 7
Experimental Section

7.1 General information

All reactions were performed in oven-dried glassware under argon, unless otherwise stated. Reaction mixtures were heated in a paraffin oil bath, with the temperature regulated using a contact thermometer. Cooling was accomplished using appropriate cooling baths prepared in plastic or Dewar vessels, or by means of a Julabo FT902 cryostat (Julabo GmbH). Ice-water and ice-sodium chloride baths were employed to maintain temperatures between 0 °C and −15 °C, while an acetone-dry ice bath was used to reach temperatures down to -78 °C. Reaction temperatures were continuously monitored and controlled with a calibrated thermometer.

7.2 Solvents & Reagents

Before use, anhydrous solvents such as DCM, MeCN, THF, and Et_2O were purified using an MB-SPS 800 solvent purification system (MBraun GmbH). The purified solvents were then stored over activated molecular sieves and handled under an inert nitrogen atmosphere. Other dry solvents were purchased from commercial suppliers and used directly without further treatment. Cyclohexane and ethyl acetate used for flash column chromatography were distilled prior to use. All commercially available reagents were employed as received without additional purification. Compounds prepared in-house were assessed for purity before being utilized in subsequent reactions.

7.3 Analytics

Thin-layer chromatography (TLC) was conducted on precoated plates (silica gel 60 F254 or ALUGRAM® ALOX N / UV254). Spots were visualized under UV light (254 nm) or by staining with basic potassium permanganate ($KMnO_4$), ninhydrin, cerium ammonium molybdate (CAM), or *p*-anisaldehyde solutions, followed by heating for development.

Flash column chromatography was carried out using silica gel (40-60 µm) or neutral alumina (Brockmann Grade I, 58 Å) as the stationary phase. For certain reactions, silica gel was pretreated with a 1-5% (v/v) solution of triethylamine in cyclohexane to deactivate it, and excess triethylamine was subsequently removed by washing with pure cyclohexane. Unless otherwise noted, cyclohexane/ethyl acetate mixtures were used as eluents.

7.4 Instruments

Nuclear magnetic resonance (NMR) spectra were recorded on Bruker Avance III 400 and 600 instruments. ^{1}H NMR spectra were obtained at 400 or 600 MHz, ^{13}C NMR at 101 or 151 MHz, ^{19}F NMR at 376 MHz, and ^{11}B NMR at 128 MHz. Chemical shifts (δ) are reported in ppm relative to residual solvent peaks, and coupling constants (*J*) are expressed in Hz. Signal multiplicities follow conventional abbreviations. All measurements were performed at 300 K

unless stated otherwise. High-resolution mass spectrometry (HRMS) was performed on a Bruker micrOTOF instrument equipped with ESI or APCI ionisation. Infrared (IR) spectra were recorded on a Bruker ALPHA spectrometer using attenuated total reflection (ATR). Spectra were analyzed with OPUS 7.5 software, and absorption bands were categorized by intensity as weak (w), medium (m), or strong (s). UV/Vis absorption spectrometry was conducted using a Mettler Toledo UV5. Fluorescence spectra were recorded on JASCO, FP-8350 spectrofluorometer. The Amino acid compatibility screening was conducted on an Agilent 1260 HPLC.

7.5 Safety Statement

IBX is a highly energetic and impact-sensitive oxidizing agent that poses a risk of explosive decomposition. It must be handled strictly in small quantities and stored at low temperature, away from heat and ignition sources. Mechanical shock, friction, and direct heating should be carefully avoided.[132] When feasible, reactions should be performed using dilute solutions, and safer alternatives such as SIBX are recommended.

7.6 Chapter 2: Bioinspired Tyrosine Diversification using Hypervalent Iodine Reagents

7.6.1 Synthesis and Characterisation of Starting Materials.

General Procedure for the synthesis of tyrosine-containing peptides (GP1):

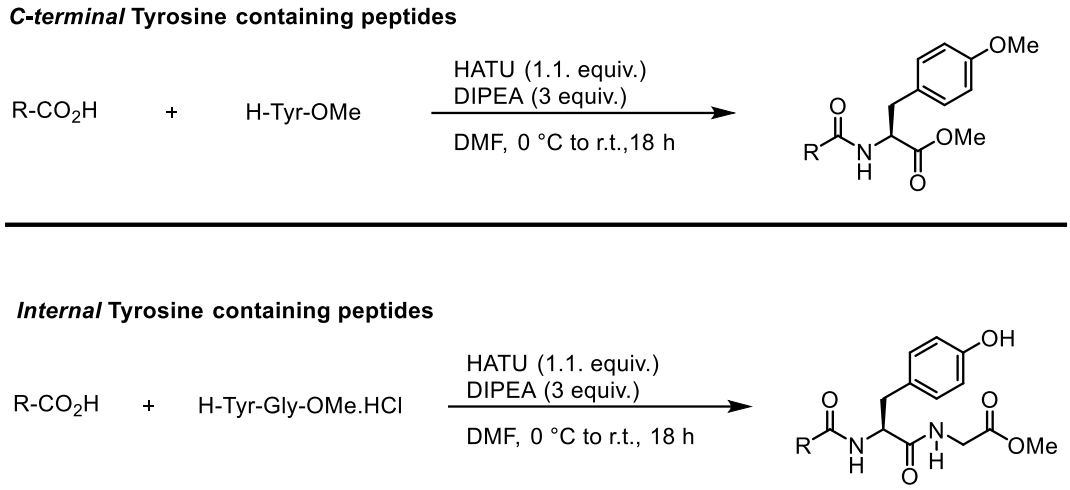

Scheme 7.1: General Procedure to synthesize tyrosine-containing peptides.

The corresponding free C-terminus amino acid (1.0 equiv.) was dissolved in DMF (0.10 M) under nitrogen and cooled to 0 °C. To the stirred solution, HATU (1.1 equiv.) and DIPEA (3.0 equiv.) were added, and the mixture was stirred for 10 minutes. A solution of Tyr-OMe or Tyr-Gly-OMe•HCl (1.1 equiv.) in DMF was subsequently added. The reaction was allowed to warm to room temperature and stirred overnight. Upon completion, the reaction mixture was diluted with ethyl acetate and washed successively with water, 1 M HCl, saturated sodium bicarbonate, and brine. The organic layer was dried over Na_2SO_4, filtered, and concentrated under reduced pressure. The crude product was purified by flash column chromatography to afford the desired product.

Boc-Val-Gly-Tyr-OMe (7.1)

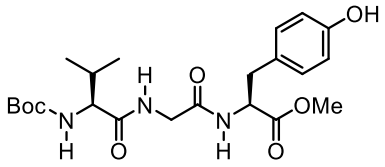

$C_{22}H_{33}N_3O_7$
451.23 g/mol

Boc-Val-Gly-Tyr-OMe was synthesized following GP1 with Boc-Val-Gly-OH (500 mg, 1.80 mmol, 1.1 equiv.) HATU (832 mg, 2.20 mmol, 1.1 equiv.), DIPEA (979 µL, 5.50 mmol, 3.0 equiv.) and H-Tyr-OMe (391 mg, 2.01 mmol, 1.1 equiv.) DMF (10 mL). The crude product was purified by column chromatography on silica gel eluting with CyHex/EtOAc (1:1) gave **7.1** as a white solid in 52% yield (428 mg, 947 µmol).

^{1}H NMR (400 MHz, $CDCl_3$) δ 7.65 (br,1H), 7.15 (d, *J* = 4.7 Hz, 1H), 7.12 (d, *J* = 9.1 Hz, 1H), 6.91 (d, *J* = 8.5 Hz, 2H), 6.70 (d, *J* = 8.5 Hz, 2H), 5.38 (d, *J* = 8.6 Hz, 1H), 4.80 (dd, *J* = 8.1, 5.3 Hz, 1H), 4.03- 3.86 (m, 2H), 3.83 (m, 1H), 3.70 (s, 3H), 3.05 (dd, *J* = 14.0, 5.3 Hz, 1H), 2.93 (dd, *J* = 14.0, 6.8 Hz, 1H), 2.08 (m, 1H), 1.42 (s, 9H), 0.92 (d, 6.7 Hz, 3H), 0.86 (d, J=6.8 H, 3H) ppm.

^{13}C NMR (151 MHz, $CDCl_3$) δ 172.7, 172.1, 168.9, 156.3, 155.8, 130.4, 127.0, 115.8, 80.4, 60.1, 53.7, 52.6, 42.9, 37.1, 31.0, 28.4, 19.4, 17.7 ppm.

IR (ATR): $\tilde{\nu}$ [cm^{-1}] = 3337, 2970, 2932, 2884, 1666, 1466, 1408, 1379, 1341, 1304, 1160, 950, 816.

HRMS (APCI) m/z calcd. for $C_{22}H_{34}N_3O_7$ ($[M+H]^+$): 452.2393, found 452.2391.

R_f (CyHex/EtOAc, 3:7) = 0.26 [$KMnO_4$].

Cbz-Leu-Ala-Tyr-OMe (7.2)

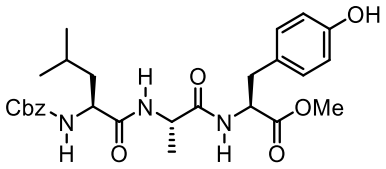

$C_{27}H_{35}N_3O_7$
513.25 g/mol

Cbz-Leu-Ala-Tyr-OMe was synthesized following GP1 with Cbz-Leu-Ala-OH (400 mg, 1.20 mmol, 1.0 equiv.) HATU (497 mg, 1.30 mmol, 1.1 equiv.), DIPEA (623 µL, 3.60 mmol, 3.0 equiv.) and H-Tyr-OMe (255 mg, 1.30 mmol, 1.1 equiv.) in DMF (15 mL). The crude product was purified by column chromatography on silica gel eluting with CyHex/EtOAc (1:1) gave **7.2** as a white solid in 69% yield (426 mg, 829 µmol).

^{1}H NMR (400 MHz, DMSO-d_6) δ 9.20 (s, 1H), 8.15 (d, *J* = 7.4 Hz, 1H), 7.91 (d, *J* = 7.5 Hz, 1H), 7.40 (d, *J* = 8.4 Hz, 1H), 7.34 (s, 4H), 7.30 (d, 1H), 6.98 (d, *J* = 7.9 Hz, 2H), 6.66 (d, *J* = 7.5 Hz, 2H), 5.02 (s, 2H), 4.37 (q, *J* = 7.2 Hz, 1H), 4.31 (p, *J* = 7.1 Hz, 1H), 4.05 (td, *J* = 9.3, 5.1 Hz, 1H), 3.56 (s, 3H), 2.86 (m, 2H), 1.61 (dt, *J* = 13.6, 7.2 Hz, 1H), 1.42 (ddt, *J* = 17.4, 13.7, 6.9 Hz, 2H), 1.19 (d, *J* = 7.0 Hz, 3H), 0.87-0.84 (m, 6H) ppm.

^{13}C NMR (151 MHz, DMSO-d_6) δ 172.2, 171.9, 171.8, 156.0, 155.9, 137.1, 129.9, 128.3, 127.7, 127.6, 126.9, 115.1, 65.3, 54.0, 53.0, 51.7, 47.7, 40.6, 35.9, 24.2, 23.1, 21.3, 18.2 ppm.

IR (ATR): $\tilde{\nu}$ [cm^{-1}] = 3328, 2969, 1656, 1517, 1455, 1379, 1242, 1160, 1128, 1106, 950, 816, 735, 697.

HRMS (ESI) m/z calcd. for $C_{27}H_{35}N_3NaO_7$ ([M+Na]$^+$): 536.2360, found 536.2367.

R_f (CyHex/EtOAc, 1:9) = 0.70 [$KMnO_4$].

Boc-Ala-Gly-Tyr-OMe (7.3)

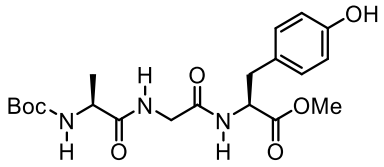

$C_{20}H_{29}N_3O_7$
423.20 g/mol

Boc-Ala-Gly-Tyr-OMe was synthesized following GP1 with Boc-Ala-Gly-OH (400 mg, 1.62 mmol, 1.0 equiv.) HATU (680 mg, 1.79 mmol, 1.1 equiv., DIPEA (860 µL, 4.87 mmol, 3.0 equiv.) and H-Tyr-OMe (349 mg, 1.79 mmol, 1.1 equiv.) in DMF (20 mL). The crude product was purified by column chromatography on silica gel eluting with CyHex/EtOAc (1:9) gave **7.3** as a white solid in 80% yield (551 mg, 1.30 mmol).

^{1}H NMR (600 MHz, $CDCl_3$) δ 7.32 (s, 1H), 7.17 (d, *J* = 8.0 Hz, 1H), 6.90 (d, *J* = 8.4 Hz, 2H), 6.69 (d, *J* = 8.4 Hz, 2H), 5.52 (s, 1H), 4.76 (td, *J* = 7.4, 5.6 Hz, 1H), 4.16 (s, 1H), 3.89 (d, *J* = 16.2 Hz, 1H), 3.78 (dd, *J* = 16.8, 5.2 Hz, 1H), 3.66 (s, 3H), 3.02 (dd, *J* = 14.0, 5.3 Hz, 1H), 2.92 (dd, *J* = 14.1, 7.0 Hz, 1H), 2.79 (s, 1H), 1.40 (s, 9H), 1.29 (d, *J* = 7.0 Hz, 3H) ppm.

^{13}C NMR (101 MHz, $CDCl_3$)) δ 173.9, 172.2, 169.2, 169.1, 155.8, 130.4, 126.9, 115.8, 80.5, 53.7, 53.5, 52.5, 50.4, 42.9, 38.8, 37.0, 28.4, 18.5 ppm.

IR (ATR): $\tilde{\nu}$ [cm^{-1}] =3296, 2978, 1737, 1651, 1615, 1596, 1514, 1445, 1366, 1220, 1160, 1120, 1067, 1043, 1025, 829, 784, 757.

HRMS (ESI) m/z calcd. for $C_{20}H_{29}N_3NaO_7$ ($[M+Na]^+$): 446.1899, found 446.1898.

R_f (CyHex/EtOAc, 1:9) = 0.24 [$KMnO_4$].

Cbz-Pro-Gly-Tyr-OMe (7.4)

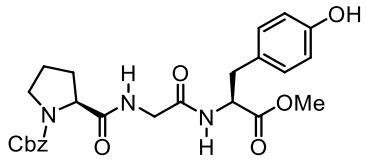

$C_{25}H_{29}N_3O_7$
483.20 g/mol

Cbz-Pro-Gly-Tyr-OMe was synthesized following GP1 with Cbz-Pro-Gly-OH (1.00 g, 3.26 mmol, 1.0 equiv.) HATU (1.36 g, 3.59 mmol, 1.1 equiv.), DIPEA (1.75 mL, 9.79 mmol, 3.0 equiv.) and H-Tyr-OMe (701 mg, 3.59 mmol, 1.1 equiv.) in DMF (35 mL). The crude product was purified by column chromatography on silica gel eluting with CyHex/EtOAc (1:9) gave **7.4** as a white solid in 70% yield (1.11 g, 2.29 mmol).

^{1}H NMR (400 MHz, $CDCl_3$) δ 7.32 (s, 5H), 7.19 (s, 1H), 6.93 (d, *J* = 8.1 Hz, 2H), 6.70 (d, *J* = 8.5 Hz, 2H), 5.17 (d, *J* = 12.5 Hz, 1H), 5.05 (d, *J* = 12.5 Hz, 1H), 4.77 (q, *J* = 6.8 Hz, 1H), 4.35 – 4.21 (m, 1H), 3.97 (d, *J* = 17.9 Hz, 1H), 3.73 (s, 1H), 3.69 (s, 3H), 3.61- 342 (m, 2H), 3.07 (m, 1H), 2.94 (dd, *J* = 14.0, 7.0 Hz, 1H), 2.20 – 1.77 (m, 4 H) ppm.

^{13}C NMR (101 MHz, $CDCl_3$) δ 173.1, 172.2, 169.3, 156.0, 155.8, 136.3, 130.4, 128.6, 128.2, 127.9, 127.2, 115.7, 67.5, 61.0, 54.0, 52.5, 47.2, 42.9, 37.0, 29.6, 24.7 ppm.

IR (ATR): $\tilde{\nu}$ [cm^{-1}] = 3288, 3063, 2951, 1740, 1651, 1614, 1595, 1514, 1416, 1356, 1211, 1172, 1120, 1020, 984, 919, 828, 801, 768, 735, 697.

HRMS (APCI) m/z calcd. for $C_{25}H_{30}N_3O_7$ ($[M+H]^+$): 484.2078, found 484.2078.

R_f (EtOAc) = 0.31 [$KMnO_4$].

Cbz-Gly-Phe-Tyr-OMe (7.5)

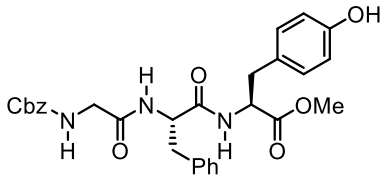

$C_{29}H_{31}N_3O_7$
533.22 g/mol

Cbz-Gly-Phe-Tyr-OMe was synthesized following GP1 with Cbz-Gly-Phe-OH (900 mg, 2.53 mmol, 1.0 equiv.) HATU (1.05 g, 2.78 mmol, 1.1 equiv.), DIPEA (1.30 mL, 7.60 mmol, 3.0 equiv.) and H-Tyr-OMe (542 mg, 2.78 mmol, 1.1 equiv.) in DMF (30 mL). The crude product was purified by column chromatography on silica gel eluting with CyHex/EtOAc (3:7) gave **7.5** as a white solid in 79% yield (1.07 g, 2.00 mmol).

^{1}H NMR (400 MHz, DMSO-d_6) δ 9.24 (s, 1H), 8.48 (d, *J* = 7.5 Hz, 1H), 7.99 (d, *J* = 8.4 Hz, 1H), 7.39 – 7.29 (m, 6H), 7.26 – 7.15 (m, 5H), 6.99 (d, *J* = 8.5 Hz, 2H), 6.67 (d, *J* = 8.5 Hz, 2H), 5.02 (s, 2H), 4.56 (td, *J* = 8.9, 4.6 Hz, 1H), 4.39 (td, *J* = 7.9, 6.5 Hz, 1H), 3.57 (s, 3H), 3.35 (s, 1H), 2.96 (dd, *J* = 13.8, 4.5 Hz, 1H), 2.92 – 2.80 (m, 2H), 2.73 (dd, *J* = 13.8, 9.3 Hz, 1H) ppm.

^{13}C NMR (101 MHz, DMSO-d_6) δ 171.8, 171.1, 168.7, 156.4, 156.0, 137.5, 137.0, 130.0, 129.2, 128.3, 128.0, 127.8, 127.7, 126.9, 126.3, 115.1, 65.5, 54.0, 53.4, 51.8, 43.3, 37.7, 36.0 ppm.

IR (ATR): $\tilde{\nu}$ [cm^{-1}] = 3400, 3283, 3086, 2954, 1739, 1704, 1659, 1638, 1614, 1598, 1556, 1515, 1497, 1443, 1418, 1392, 1372, 1323, 1271, 1239, 1190, 1164, 1112, 1101, 1080, 994, 933, 912, 897, 802, 785, 698.

HRMS (ESI) m/z calcd. for $C_{29}H_{31}N_3NaO_7$ ([M+Na]$^+$): 556.2053, found 556.2054.

R_f (CyHex/EtOAc, 3:7) = 0.12 [$KMnO_4$].

Boc-Gln-Tyr-OMe (7.6)

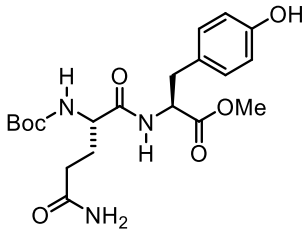

$C_{20}H_{29}N_3O_7$
423.20 g/mol

Boc-Gln-Tyr-OMe was synthesized following GP1 with Boc-Gln-OH (500 mg, 2.03 mmol, 1.0 equiv.) HATU (926 mg, 2.44 mmol, 1.2 equiv.), DIPEA (719 µL, 4.06 mmol, 3.0 equiv.) and H-Tyr-OMe (404 mg, 2.07 mmol, 1.1 equiv.) in DMF (20 mL). The crude product was purified by column chromatography on silica gel eluting with DCM/MeOH (47:3) gave **7.6** as a white solid in 48% yield. (413 mg, 975 µmol).

^{1}H NMR (400 MHz, DMSO-d_6) δ 9.21 (s, 1H), 8.08 (d, J = 7.6 Hz, 1H), 7.21 (s, 1H), 6.93 (d, *J* = 8.4 Hz, 2H), 6.80 (d, *J* = 8.2 Hz, 1H), 6.72 (s, 1H), 6.61 (d, *J* = 8.4 Hz, 2H), 4.41 – 4.25 (m, 1H), 3.87 (td, *J* = 8.6, 5.1 Hz, 1H), 3.52 (s, 3H), 2.96 – 2.73 (m, 2H), 2.13 – 1.92 (m, 2H), 1.77 (tt, *J* = 12.0, 5.7 Hz, 1H), 1.60 (dtd, *J* = 15.3, 9.5, 6.4 Hz, 1H), 1.33 (s, 9H) ppm.

^{13}C NMR (101 MHz, DMSO-d_6) δ 173.8, 171.9, 156.0, 155.1, 129.9, 126.9, 115.1, 78.1, 53.8, 51.7, 36.0, 31.4, 28.2, 27.8 ppm.

IR (ATR): $\tilde{\nu}$ [cm^{-1}] = 3306, 2979, 1737, 1662, 1615, 1516, 1447, 1392, 1367, 1247, 1168, 1116, 1050, 1025, 829.

HRMS (ESI) m/z calcd. for $C_{20}H_{29}N_3NaO_7$ ([M+Na]$^+$): 446.1895, found 446.1898.

R_f (DCM/MeOH, 9:1) = 0.37.

Boc-Trp-Tyr-OMe (7.7)

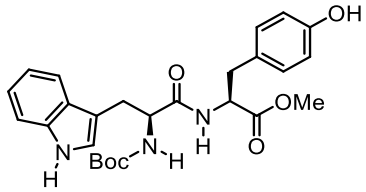

$C_{26}H_{31}N_3O_6$
481.22 g/mol

Boc-Trp-Tyr-OMe was synthesized following a modified GP1 with Boc-Trp-OH (2.00 g, 6.57 mmol, 1.0 equiv.) DCC (1.64 g, 7.89 mmol,1.2 equiv.), HOBT (1.21 g, 7.89 mmol, 1.2 equiv.) NMM (2.16 mL, 19.7 mmol, 3.0 equiv.) and H-Tyr-OMe (1.28 g, 6.57 mmol, 1.0 equiv.) in DCM (20 mL). The crude product was purified by column chromatography on silica gel eluting with CyHex/EtOAc (3:2) gave **7.7** as a white solid in 63% yield (2.00 g, 4.15 mmol). Characterization data were in accordance with literature.[246]

^{1}H NMR (400 MHz, $CDCl_3$) δ 8.32 (s, 1H), 7.61 (d, *J* = 7.8 Hz, 1H), 7.32 (d, *J* = 8.0 Hz, 1H), 7.17 (t, *J* = 7.5 Hz, 1H), 7.09 (t, *J* = 7.4 Hz, 1H), 6.85 (s, 1H), 6.62 (t, *J* = 10.9 Hz, 5H), 6.34 (d, *J* = 7.6 Hz, 1H), 5.20 (s, 1H), 4.71 (d, *J* = 7.1 Hz, 1H), 4.43 (s, 1H), 3.61 (s, 3H), 3.25 (br, 1H), 3.11 (dd, *J* = 14.6, 6.9 Hz, 1H), 2.85 (tt, *J* = 14.1, 8.6 Hz, 2H), 1.42 (s, 9H) ppm.

^{13}C NMR (101 MHz, $CDCl_3$) δ 171.6, 171.5, 155.6, 155.3, 142.5, 136.2, 130.2, 127.4, 126.8, 123.4, 122.1, 119.6, 118.7, 115.5, 111.3, 80.5, 55.4, 53.4, 52.3, 37.0, 28.2, 28.1 ppm.

IR (ATR): $\tilde{\nu}$ [cm^{-1}] = 3339, 2974, 2931, 1734, 1663, 1615, 1596, 1515, 1457, 1439, 1392, 1367, 1232, 1165, 1123, 744.

HRMS (ESI+) m/z calcd. for $C_{26}H_{31}NaN_3O_6$ ($[M+Na]^+$): 504.2103, found 504.2105.

R_f (CyHex/EtOAc, 3:7) = 0.53 [$KMnO_4$].

Boc-Thr(Bn)-Tyr-OMe (7.8)

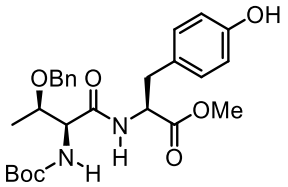

$C_{26}H_{34}N_2O_7$
486.24 g/mol

Boc-Thr(Bn)-Tyr-OMe was synthesized following a modified GP1 with Boc-Thr(Bn)-OH (1.00 g, 3.23 mmol, 1.0 equiv.) DCC (808 mg, 3.88 mmol, 1.2 equiv.) HOBT (594 mg, 3.88 mol, 1.2 equiv.) TEA (450 µL, 3.23 mmol, 1.0 equiv.) and H-Tyr-OMe (631 mg, 3.23 mmol, 1.0 equiv.) in DCM (15 ml). The crude product was purified by column chromatography on silica gel eluting with CyHex/EtOAc (4:1) gave **7.8** as a white solid in 85% yield (1.34 g, 2.75 mmol).

^{1}H NMR (400 MHz, $CDCl_3$) δ 7.78 (s, 1 H), 7.37 – 7.15 (m, 6 H), 6.82 (d, *J* = 8.0 Hz, 2H), 6.68 (d, *J* = 8.3 Hz, 2H), 5.59 (d, *J* = 7.3 Hz, 1H), 4.75 (q, *J* = 6.4 Hz, 1H), 4.57 (d, *J* = 11.4 Hz, 1H), 4.47 (d, *J* = 11.4 Hz, 1H), 4.31 (dd, *J* = 7.6, 3.1 Hz, 1H), 4.13 (dd, *J* = 6.5, 3.2 Hz, 1H), 3.61 (s, 3 H), 3.02 – 2.84 (m, 2 H), 1.44 (s, 9H), 1.19 (d, *J* = 6.3 Hz, 3H) ppm.

^{13}C NMR (101 MHz, $CDCl_3$) δ 171.5, 169.9, 155.8, 155.7, 137.6, 130.0, 128.3, 127.7, 127.7, 126.4, 115.5, 80.3, 74.5, 71.2, 57.5, 53.7, 52.1, 37.0, 28.1, 14.9 ppm.

IR (ATR): $\tilde{\nu}$ [cm^{-1}] = 3417, 3316, 2978, 2931, 2875, 1719, 1689, 1654, 1615, 1597, 1529, 1514, 1448, 1385, 1364, 1349, 1327, 1302, 1285, 1220, 1163, 1118, 11104, 1090, 1058, 1022, 980, 925, 890, 862, 844,827, 808, 781, 732, 695.

HRMS (ESI) m/z calcd. for $C_{26}H_{34}N_2NaO_7$ ([M+Na]$^+$): 509.2263, found 509.2258.

R_f (CyHex/EtOAc, 1:1) = 0.61 [$KMnO_4$].

Boc-Tyr-Gly-OMe (7.9a)

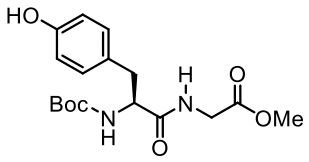

$C_{17}H_{24}N_2O_6$
352.16 g/mol

Step I: Boc-Tyr-Gly-OMe was synthesized following GP1 with Boc-Tyr-OH (7.03 g, 25.0 mmol, 1.0 equiv.) HATU (10.5 g, 2.75 mmol, 1.1 equiv.), DIPEA (7.00 ml, 50.0 mmol, 2.0 equiv.) and Gly-OMe (3.15 g, 25.1 mmol, 1.0 equiv.) in DMF (0.2 L). The crude product was purified by column chromatography on silica gel eluting with cyclohexane-EtOAc (1:1) gave **7.9a** as a white solid in 80% yield (7.04 g, 20.0 mmol). Characterization data were in accordance with literature.[247]

^{1}H NMR (600 MHz, DMSO-d_6) δ 8.68 (s, 1H), 7.85 (t, *J* = 5.7 Hz, 1H), 7.04 – 7.00 (m, 2H), 6.68 (d, *J* = 8.5 Hz, 2H), 6.14 (s, 1H), 4.19 (td, *J* = 8.7, 5.1 Hz, 1H), 3.94 – 3.81 (m, 2H), 3.66 (s, 3H), 3.05 – 2.91 (m, 1H), 2.73 (dd, *J* = 14.1, 8.8 Hz, 1H), 1.35 (s, 9H).

^{13}C NMR (151 MHz, DMSO-d_6) δ 171.4, 169.3, 155.3, 154.3, 129.4, 127.5, 114.6, 77.8, 55.5, 50.8, 40.3, 36.6, 27.6 ppm.

IR (ATR): $\tilde{\nu}$ [cm^{-1}] = 3306, 2978, 1737, 1662, 1614, 1516, 1447, 1392, 1367, 1247, 1168, 1116, 1050, 1025, 829.

HRMS (ESI+) m/z calcd. for $C_{17}H_{24}N_2NaO_6$ ([M+Na]$^+$): 375.152, found 375.1527.

R_f (CyHex/EtOAc,1:4) = 0.66.

Tyr-Gly-OMe.HCl (7.9b)

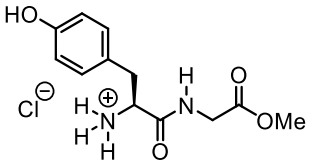

$C_{12}H_{17}ClN_2O_4$
288.09 g/mol

Step II: Following a modified reported procedure,[106] to a flame-dried, N_2-purged flask containing 7.9a (1.88 g, 5.34 mmol 1.0 equiv.) was added dry MeOH (50 mL) at 0 °C. Acetyl chloride (1.80 mL, 28.6 mmol, 5.0 equiv.) was added dropwise, and the mixture was allowed to warm to room temperature and stirred for 18 h. Solvent was removed under reduced pressure to afford compound **7.9b** as a light yellow foamy solid (quantitative yield).

^{1}H NMR (600 MHz**,** DMSO-d_6**)** δ 9.56 – 9.30 (m, 1H), 9.14 (d, *J* = 5.5 Hz, 1H), 8.28 (s, 3H), 7.08 (d, *J* = 7.6 Hz, 2H), 6.71 (d, *J* = 7.6 Hz, 2H), 4.00 (s, 1H), 3.96 – 3.81 (m, 2H), 3.63 (s, 3H), 3.04 (t, *J* = 7.1 Hz, 1H), 2.92 (dd, *J* = 14.1, 6.7 Hz, 1H).

^{13}C NMR (151 MHz**,** DMSO-d_6**)** δ 169.5, 168.5, 156.4, 130.4, 124.5, 115.1, 53.4, 51.8, 40.5, 35.8 ppm.

IR (ATR): $\tilde{\nu}$ [cm^{-1}] = 3339, 2970, 2932, 2884, 1745, 1683, 1616, 1518, 1465, 1406, 1378, 1341, 1303, 1223, 1160, 1127, 1106, 949, 816.

HRMS (ESI) m/z calcd. For $C_{12}H_{17}N_2O_4$ ($[M+H]^+$): 253.1183, found 253.1183.

R_f (DCM/MeOH, 9:1) = 0.30.

Boc-Glu(O^{t}bu)-Tyr-Gly-OMe (7.10)

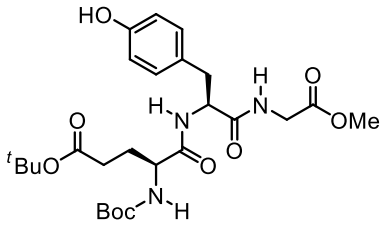

$C_{26}H_{39}N_3O_9$
537.27 g/mol

Boc-Glu(O^{t}bu)-Tyr-Gly-OMe was synthesized following GP1 with Boc-Glu(O^{t}bu)-OH (400 mg, 1.32 mmol, 1.0 equiv.), HATU (552 g, 1.45 mmol, 1.1 equiv.), DIPEA (700 µL, 3.96 mmol, 3.0 equiv.) and **7.9b** (419 mg, 3.63 mmol, 1.1 equiv.) in DMF (15 mL). The crude product was purified by column chromatography on silica gel eluting with DCM/MeOH (49:1) gave **7.10** as a white solid in 74% yield (53 mg, 985 µmol).

^{1}H NMR (400 MHz, MeOD) δ 7.05 (d, *J* = 8.4 Hz, 2H), 6.70 (d, *J* = 8.5 Hz, 1H), 4.61 (dd, *J* = 8.3, 5.6 Hz, 1H), 3.98 (dd, *J* = 8.7, 5.5 Hz, 1H), 3.92 (s, 2H), 3.71 (s, 3H), 3.09 (dd, *J* = 14.1, 5.7 Hz, 1H), 2.89 (dd, *J* = 14.0, 8.3 Hz, 1H), 2.20 (t, *J* = 7.5 Hz, 2H), 1.98 – 1.83 (m, 1H), 1.75 (ddd, *J* = 14.1, 6.9, 1.5 Hz, 1H), 1.44 (d, *J* = 7.6 Hz, 18H) ppm.

^{13}C NMR (101 MHz, MeOD) δ 174.2, 174.0, 173.9, 171.4, 158.1, 157.3, 131.4, 128.7, 116.3, 81.8, 81.0, 55.7, 55.7, 52.6, 41.9, 37.8, 32.5, 28.7, 28.3 ppm.

IR (ATR): $\tilde{\nu}$ [cm^{-1}] = 3318, 2978, 1759, 1726, 1679, 1653, 1638, 1653, 1638, 1596, 1515, 1449, 1391, 1367, 1335, 1290, 1228, 1209, 1151, 1115, 1078, 1037, 1011, 861, 830, 780, 744.

HRMS (APCI) m/z calcd. for $C_{26}H_{40}N_3O_9$ ([M+H]$^+$): 538.2754, found 538.2759.

R_f (DCM/MeOH,19:1) = 0.31.

Cbz-Ser-Tyr-Gly-OMe (7.11)

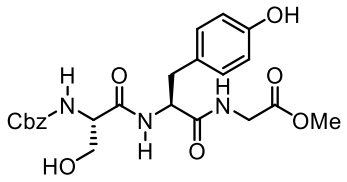

$C_{23}H_{27}N_3O_8$
473.18 g/mol

Cbz-Ser-Tyr-Gly-OMe was synthesized following GP1 with Cbz-Ser-OH (660 mg, 2.76 mmol, 1.0 equiv.) HATU (1.15 g, 3.03 mmol, 1.1 equiv., DIPEA (1.46 mL, 8.28 mmol, 3.0 equiv.) and **7.9b** (796 mg, 2.76 mmol, 1.1 equiv.) in chloroform (30 mL). The crude product was purified by column chromatography on silica gel eluting with DCM/MeOH (19:1) gave **7.11** as a white solid in 76% yield (995 mg, 2.10 mmol).

^{1}H NMR (400 MHz, DMSO-d_6) δ 9.28 (br, 1H), 8.52 (t, *J* = 5.9 Hz, 1H), 8.01 (d, *J* = 8.3 Hz, 1H), 7.43 – 7.21 (m, 5H), 6.77 – 6.56 (m, 2H), 5.09 – 4.85 (m, 2H), 4.45 (td, *J* = 8.6, 4.5 Hz, 1H), 4.13 – 3.96 (m, 1H), 3.84 (dd, *J* = 5.9, 1.7 Hz, 2H), 3.62 (s, 3H), 3.49 (d, *J* = 6.1 Hz, 2H), 2.93 (dd, *J* = 13.9, 4.6 Hz, 1H), 2.72 (dd, *J* = 13.9, 8.9 Hz, 1H) ppm.

^{13}C NMR (101 MHz, DMSO-d_6) δ 171.6, 170.1, 170.0, 155.9, 155.9, 136.9, 130.1, 128.4, 127.8, 127.7, 127.5, 114.9, 65.5, 61.8, 57.2, 54.1, 51.7, 40.6, 36.7 ppm.

IR (ATR): $\tilde{\nu}$ [cm^{-1}] = 3491, 3389, 3293, 3089, 3032, 2948, 1737, 1638, 1593, 1558, 1515, 1454, 1439, 1402, 1360, 1294, 1265, 1227, 1174, 1099, 1081, 1068, 1044, 1025, 977, 924, 909, 845, 814, 787, 743.

HRMS (APCI) m/z calcd. for $C_{23}H_{28}N_3O_8$ ([M+Na]$^+$): 474.1872, found 474.1871.

R_f (DCM/MeOH,19:1) = 0.10.

Boc-Met-Tyr-Gly-OMe (7.12)

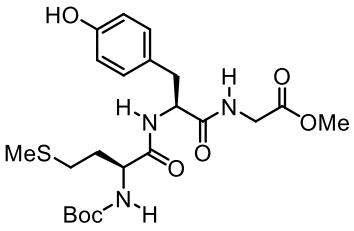

$C_{22}H_{33}N_3O_7S$
483.20 g/mol

Boc-Met-Tyr-Gly-OMe was synthesized following GP1 with Boc-Met-OH (500 mg, 2.01 mmol, 1.0 equiv.) HATU (839 mg, 2.21 mmol, 1.0 equiv., DIPEA (1.06 ml, 6.02 mmol, 3.0 equiv.) and **7.9b** (637 mg, 2.21 mmol, 1.1 equiv.) in DMF (20 mL). The crude product was purified by column chromatography on silica gel eluting with DCM/MeOH (49:1) gave **7.12** as a white solid in 70% yield (682 mg, 1.41 mmol).

^{1}H NMR (400 MHz, DMSO-d_6) δ 9.12 (s, 1H), 8.42 (t, *J* = 5.9 Hz, 1H), 7.73 (d, *J* = 8.3 Hz, 1H), 7.14 - 6.92 (m, 3H), 6.59 (d, *J* = 8.5 Hz, 2H), 4.45 (td, *J* = 8.5, 4.7 Hz, 1H), 3.91 (td, *J* = 8.3, 5.3 Hz, 1H), 3.81 (t, *J* = 5.4 Hz, 2H), 3.59 (s, 3H), 2.86 (dd, *J* = 13.9, 4.7 Hz, 1H), 2.67 (dd, *J* = 13.9, 8.9 Hz, 1H), 2.30 (ddd, *J* = 9.0, 6.9, 2.4 Hz, 2H), 1.97 (s, 3H), 1.81 -1.60 (m, 2H), 1.34 (s, 9H) ppm.

^{13}C NMR (101 MHz, DMSO-d_6) δ 171.6, 171.2, 170.1, 155.8, 155.3, 130.2, 127.5, 114.8, 78.3, 53.8, 53.6, 51.7, 40.6, 37.0, 31.8, 29.6, 28.2, 14.6 ppm.

IR (ATR): $\tilde{\nu}$ [cm^{-1}] = 3312, 2980, 2952, 2921, 1753, 1679, 1654, 1638, 1595, 1516, 1433, 1390, 1371, 1326, 1311, 1229, 1109, 1050, 1007, 990, 962, 890, 856, 830, 805, 779, 743, 712, 689.

HRMS (APCI) m/z calcd. for $C_{22}H_{34}N_3O_7S$ ([M+H]$^+$): 484.2114, found 484.2112.

R_f (DCM/MeOH, 19:1) = 0.25.

1-Hydroxy-1λ⁵-benzo[d][1,2]iodaoxol-3-(1H)-one (7.13)

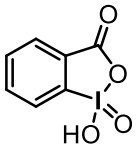

$C_7H_5IO_4$
279.92 g/mol

Following a reported procedure, in a 500 mL round bottom flask, 2-iodobenzoic acid (10.0 g,40.3 mmol, 1.0 equiv.) and oxone (37.2 g, 121.0 mmol, 3.0 equiv.) was dissolved in 350 mL water and stirred at room temperature for 30 minutes. The reaction mixture was then stirred at 70 °C for 3 h and then cooled to 5 °C. and left at this temperature for 2 h. The resulting solid was filtered and washed several times with ice cold water and ice-cold acetone. After drying under high vacuum, **7.13** was obtained as a solid in 88% yield (9.93 g, 35.48 mmol). Data were in accordance with literature.[248]

^{1}H NMR (600 MHz, DMSO) δ 8.15 (d, *J* = 8.0 Hz, 1H), 8.03 (dd, *J* = 7.5, 1.4 Hz, 1H), 8.00 (td, *J* = 8.0, 7.3, 1.4 Hz, 1H), 7.84 (td, *J* = 7.4, 1.1 Hz, 1H) ppm.

^{13}C NMR (151 MHz, DMSO) δ 167.44, 146.56, 133.33, 132.91, 131.43, 130.05, 124.97 ppm.

IR (ATR): $\tilde{\nu}$ [cm-1] = 3071, 1633, 1582, 1564, 1434, 1330, 1294, 1245, 1159, 1138, 830, 773, 760, 748, 692, 569.

HRMS (ESI+) m/z calcd. for $[M-H]^-$ $[C_7H_4IO_4]^-$ 278.9233, found 278.9160.

Boc-Gly-Tyr-OMe (2.3)

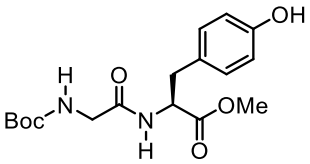

$C_{17}H_{24}N_2O_6$
352.16 g/mol

Boc-Gly-Tyr-OMe was synthesized following a modified GP1 with Boc-Gly-OH (5.00 g, 28.5 mmol, 1.0 equiv.) HOBT (4.24 g, 31.4 mmol, 1.1 equiv.) TEA (11.8 mL, 85.6 mmol, 3.0 equiv.) and H-Tyr-OMe (5.60 g, 28.5 mmol, 1.0 equiv.) in DCM (75 mL). The crude product was purified by column chromatography on silica gel eluting with CyHex/EtOAc, (3:2) gave **2.3** as a white solid in 75% yield (7.54 g, 21.4 mmol). Characterization data were in accordance with the literature.[249]

^{1}H NMR (600 MHz, DMSO-d_6) δ 9.21 (s, 1H), 8.07 (d, *J* = 7.8 Hz, 1H), 6.97 (d, *J* = 8.1 Hz, 2H), 6.89 (t, *J* = 6.3 Hz, 1H), 6.65 (d, *J* = 8.4 Hz, 2H), 4.40 (q, *J* = 7.4 Hz, 1H), 3.58 (s, 3H), 3.57 – 3.45 (m, 2H), 2.87 (m, 1H), 2.80 (m,1H), 1.37 (s, 9H).

^{13}C NMR (151 MHz, DMSO-d_6) δ 171.9, 169.3, 156.0, 155.7, 130.0, 126.9, 115.0, 78.0, 53.7, 51.7, 42.8, 36.1, 28.1 ppm.

IR (ATR): $\tilde{\nu}$ [cm^{-1}] = 3315, 2978, 1656, 1615, 1595, 1514, 1443, 1391, 1366, 1215, 1158, 1050, 1027, 985, 941, 844, 829, 782.

HRMS (ESI) m/z calcd. for $C_{17}H_{24}N_2NaO_6$ ([M+Na]$^+$): 375.1530, found 375.1527.

R_f (CyHex/EtOAc, 3:7) = 0.51 [$KMnO_4$].

Amino Acid Compatibility Screening

The Amino acid compatibility screening was conducted on an Agilent 1260 HPLC.

All calibrations were performed using HPLC, whose method is as follows:

Column

Luna 3u C8(2) 100A, 100 * 4.6 mm.

Method

ACN +0.05% FA/H2O + 0.05% FA, 5-95% ACN, 0.75 mL/min, 220 nm.

Calibration Curve for Amino Acids

The retention times of amino acids were determined through individual analysis using HPLC. Three calibration solutions were prepared with three different amounts (0.03 mmol, 0.05 mmol, 0.07 mmol of each amino acids) along with 0.07 mmol of benzoic acid as an internal standard in 20 mL of ethanol. Later, standard HPLC 3-point calibration lines were plotted for each compound separately using area relative to the benzoic acid.

Calibration Curve for the Starting Material and Product

The retention times of starting material and products were determined through individual analysis using standard HPLC. Five calibration solutions were prepared with five different amounts of both products, i.e. 0.01, 0.03, 0.05, 0.07, 0.09 mmol of compounds in 20 ml of ethanol, along with 0.09 mmol of benzoic acid as the internal standard. Later, HPLC 5-Point calibration lines were plotted for starting materials, product using area relative to the benzoic acid as internal standard (Figure 7.1 A and B).

A **Calibration curve of starting material (Boc-Tyr-OMe) with benzoic acid as IS.**

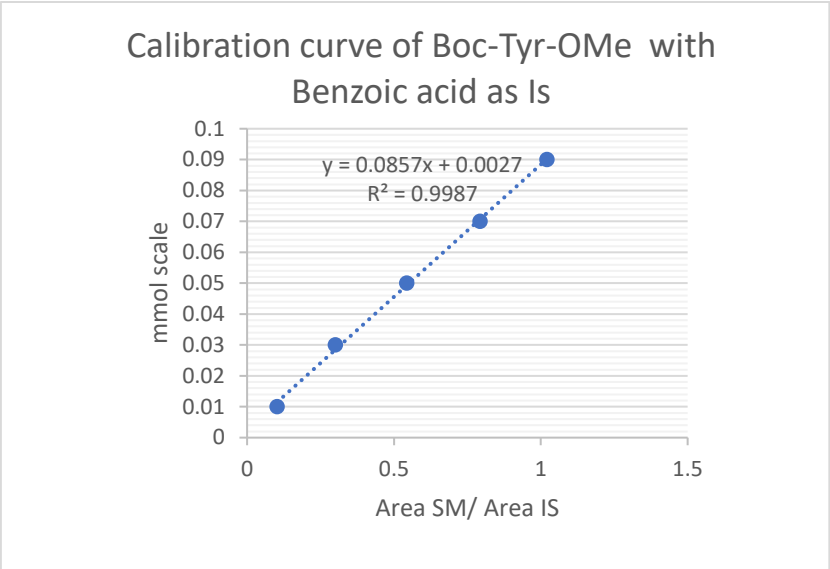

B **Calibration curve of Product 2.5 with benzoic acid as IS.**

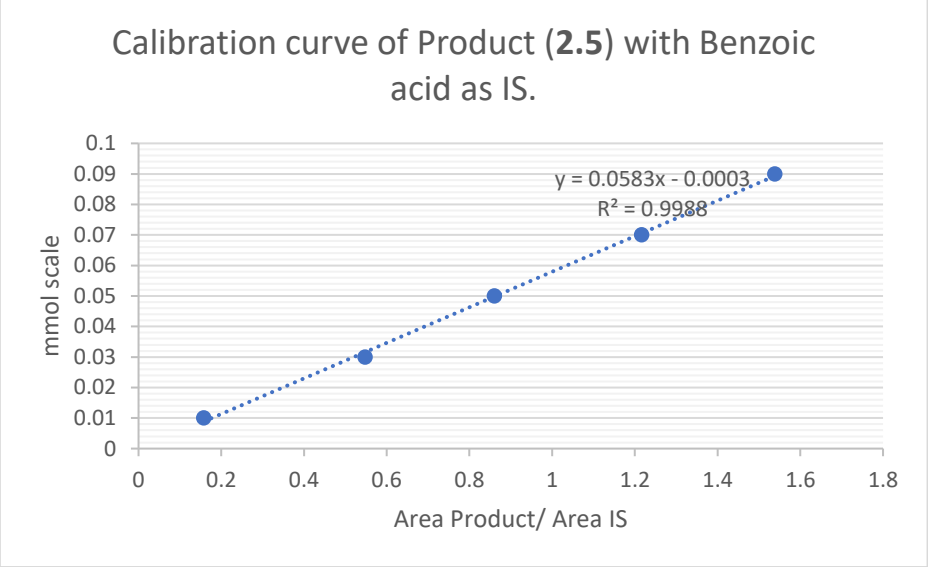

Figure 7.1: A): Calibration Curve of Boc-Tyr-OMe (starting material), B) Calibration Curve of Product. **(2.5)**

Control reaction without amino acids additive

A 4 mL screw-cap vial equipped with a magnetic stir bar was charged with 1 (14.7 mg, 50.0 µmol, 1.0 equiv.) and IBX (16.8 mg, 60.0 µmol, 1.2 equiv.) in EtOH (0.4 mL, 0.125 M) at 0 °C. The reaction mixture was allowed to warm to r.t. and stirred for 4 h. A solution of 4,5-dimethylbenzene-1,2-diamine (14.9 mg, 110 µmol, 2.2 equiv.) in EtOH (0.2 mL, 0.250 M) was then added dropwise under a nitrogen atmosphere. The vial was sealed, and the mixture was stirred at 60 °C for 24 h. After this period, benzoic acid (6.10 mg, 50.0 µmol, 1.0 equiv.) was added, and the reaction mixture was diluted with EtOH to a total volume of 20 mL. An aliquot (1 mL) was taken out from the reaction mixture in a 1.5 mL glass vial and analyzed by HPLC. For control reaction, the yield was 67%.

General protocol for screening (GP2)

In a 4 mL glass vial equipped with a magnetic stirring bar, an amino acid (50.0 µmol, 1.0 equiv.) was added along with **1** (14.7 mg, 50.0 µmol, 1.0 equiv.), and IBX (16.8 mg, 60.0 µmol 1.2 equiv.) in EtOH (0.125 M) at 0 °C. and the reaction was warmed to r.t. and stirred for 4 h. A solution of 4,5-dimethylbenzene-1,2-diamine (14.9 mg, 110 µmol, 2.2 equiv.) in EtOH (0.2 mL, 0.250 M) was then added dropwise under a nitrogen atmosphere. The vial was sealed, and the mixture was stirred at 60 °C for 24 h. After this period, benzoic acid (6.10 mg, 50.0 µmol, 1.0 equiv.) was added, and the reaction mixture was diluted with ethanol to a total volume of 20 mL. An aliquot (1.0 mL) was taken out from the reaction mixture in a 1.5 mL glass vial and analyzed by HPLC.

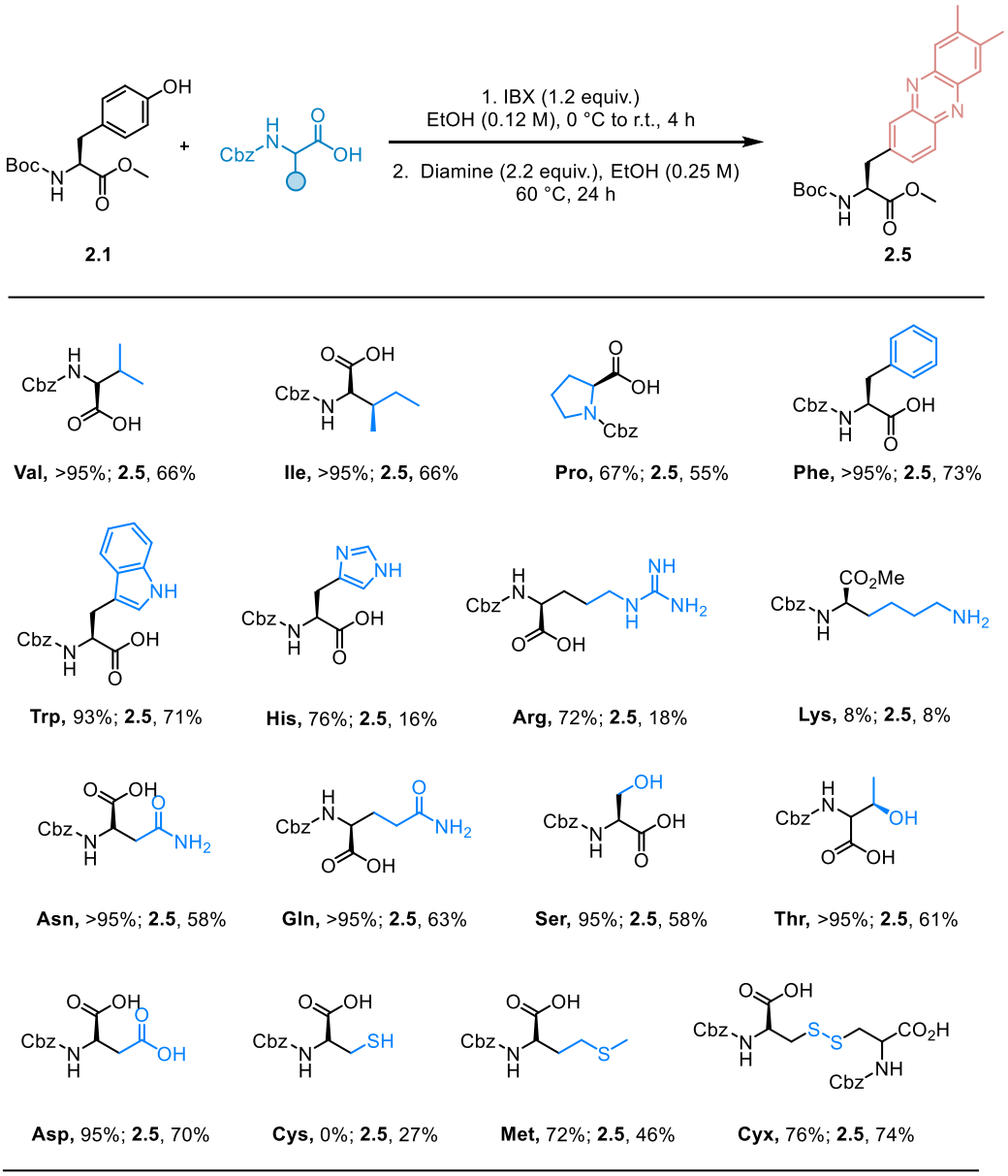

Scheme 7.2: Amino acid compatibility screening with 15 canonical amino acids. Reactions were carried out on 0.05 mmol scale. Yields were determined by HPLC using benzoic acid as internal standard.

7.6.2 Chapter 2: Synthesis and Characterisation of Products

General Procedure (GP3)

To an oven-dried 25 mL round-bottom flask equipped with a magnetic stir bar were added the corresponding tyrosine-containing starting material (0.25 mmol, 1.0 equiv.) and IBX (1.2 equiv.) in EtOH (0.125 M) at 0 °C. The reaction mixture was allowed to warm to r.t. and stirred for 4 h. A solution of the corresponding 4,5-dimethylbenzene-1,2-diamine (2.2 equiv.) in EtOH (1.2 mL, 0.25 M) was added dropwise. The mixture was heated at 60 °C for 24 h. The solvent was removed under reduced pressure, and the residue was diluted with EtOAc (20 mL) and washed with saturated $NaHCO_3$ (3 × 10 mL) and brine (10 mL). The organic phase was dried with Na_2SO_4, filtered, and concentrated under reduced pressure. The crude residue was purified by flash silica gel column chromatography to afford the desired product.

Methyl (S)-2-((*tert*-butoxycarbonyl)amino)-3-(7/8-fluorophenazin-2-yl)propanoate (mixture of regioisomers) (2.2)

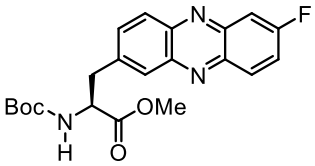

$C_{21}H_{22}FN_3O_4$
399.16 g/mol

The compound **2.2** was synthesized according to GP3 using **2.1** (148 mg, 500 µmol, 1.0 equiv.) and IBX (168 mg, 600 mmol, 1.2 equiv.) in 4 mL of EtOH. 4-fluorobenzene-1,2-diamine (139 mg, 1.10 mmol, 2.2 equiv.) in 2 mL of EtOH was then added. The reaction was purified by flash column chromatography on silica gel eluting with CyHex/EtOAc (3:2) to produce **2.2** as a 1.5:1 mixture of regioisomers, isolated as yellow solid in 60% yield (121 mg, 302 µmol).

^{1}H NMR (400 MHz, $CDCl_3$) δ 8.02 (dt, *J* = 10.3, 5.3 Hz, 1H), 7.94 (dd, *J* = 8.9, 6.0 Hz, 1H), 7.80 (d, *J* = 5.4 Hz, 1H), 7.61 (ddd, *J* = 9.2, 5.8, 2.7 Hz, 1H), 7.48 (dddd, *J* = 23.7, 10.6, 8.2, 2.5 Hz, 2H), 5.42 (d, *J* = 8.1 Hz, 1H), 4.68 (q, *J* = 6.9 Hz, 1H), 3.67 (s, 3H), 3.33 (dd, *J* = 13.9, 5.5 Hz, 1H), 3.19 (dd, *J* = 14.1, 7.0 Hz, 1H), 1.27 (s, 9H) ppm.

^{13}C NMR (151 MHz, $CDCl_3$) δ 172.0, 163.7, 163.6, 162.1, 161.9, 155.1, 143.8, 143.7, 143.6, 143.5, 143.3, 142.7, 142.5, 142.5, 141.9, 141.9, 140.9, 140.6, 140.1, 139.2, 132.9, 132.1, 131.9, 131.9, 131.8, 131.8, 129.6, 129.3, 129.1, 128.8, 122.4, 122.2, 122.0, 111.6, 111.5, 111.5, 111.4, 80.0, 54.2, 52.4, 38.8, 38.7, 28.2 ppm.

^{19}F NMR (376 MHz, $CDCl_3$) δ -105.7, -106.0 ppm.

IR (ATR): $\tilde{\nu}$ [cm^{-1}] = 3328, 2966, 1737, 1684, 1637, 1613, 1526, 1491, 1469, 1441, 1389, 1357, 1327, 1301, 1287, 1275, 1250, 1222, 1200, 1161, 1105, 1029, 994, 977, 954, 927, 901, 881, 852, 835, 821, 798, 778, 737, 675, 632, 600.

HRMS (ESI) m/z calcd. for $C_{21}H_{22}FN_3NaO_4$ ($[M+Na]^+$): 422.1480, found 422.1487.

R_f (CyHex/EtOAc, 3:2) = 0.36.

Methyl (S)-2-((*tert*-butoxycarbonyl)amino)-3-(7,8-dimethylphenazin-2-yl)propanoate (2.5)

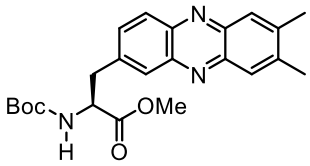

$C_{23}H_{27}N_3O_4$
409.20 g/mol

The compound **2.5** was synthesized according to GP3 using **2.1** (148 mg, 500 µmol, 1.0 equiv.) and IBX (168 mg, 600 µmol, 1.2 equiv.) in 4 mL of EtOH. 4,5-dimethylbenzene-1,2-diamine (150 mg, 1.10 mmol, 2.2 equiv.) in 2 mL of EtOH was then added. The reaction was purified by flash column chromatography on silica gel eluting with CyHex/EtOAc (3:2) to produce **2.5** as a yellow solid in 65% yield (134 mg, 327 µmol).

^{1}H NMR (400 MHz, $CDCl_3$) δ 8.10 (d, *J* = 8.9 Hz, 1H), 7.92 (td, *J* = 3.1, 1.5 Hz, 3H), 7.57 (dd, *J* = 8.9, 2.0 Hz, 1H), 5.16 (d, *J* = 8.2 Hz, 1H), 4.74 (q, *J* = 6.7 Hz, 1H), 3.73 (s, 3H), 3.39 (dd, *J* = 13.9, 5.6 Hz, 1H), 3.28 (dd, *J* = 13.9, 6.6 Hz, 1H), 2.52 (s, 6H), 1.37 (s, 9H) ppm.

^{13}C NMR (101 MHz, $CDCl_3$) δ 172.2, 155.2, 143.1, 142.9, 142.3, 142.1, 141.8, 138.5, 131.7, 129.7, 129.3, 128.0, 127.9, 80.2, 54.3, 52.6, 38.9, 28.4, 20.8, 20.8 ppm.

IR (ATR): $\tilde{\nu}$ [cm^{-1}] = 3300, 2954, 2923, 1738, 1695, 1637, 1529, 1468, 1447, 1396, 1364, 1341, 1326, 1285, 1259, 1266, 1174, 1149, 1118, 1038, 1001, 977, 964, 944, 891, 872, 856, 838, 788, 776, 744, 715, 696, 655, 627.

HRMS (ESI) m/z calcd. For $C_{23}H_{26}N_4NaO_5$ ([M+Na]$^+$): 432.1893, found 432.1894.

R_f (CyHex/EtOAc, 1:2) = 0.33.

Methyl (S)-2-(2-((*tert*-butoxycarbonyl)amino)acetamido)-3-(phenazin-2-yl)propanoate (2.6)

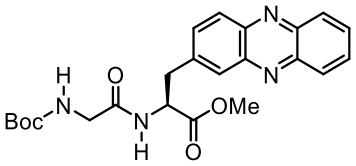

$C_{23}H_{26}N_4O_5$
438.19 g/mol

The compound **2.6** was synthesized according to GP3 using **2.3** (106 mg, 300 µmmol, 1.0 equiv.) and IBX (101 mg, 360 µmol, 1.2 equiv.) in 2.4 mL of EtOH. Benzene-1,2-diamine (71.4 mg, 660 µmol, 2.2 equiv.) in 1.2 mL of EtOH was then added. The reaction was purified by flash column chromatography on silica gel eluting with CyHex/EtOAc (3:2) to produce **2.6** as a yellow solid in 80% yield (106 mg, 241µmol).

^{1}H NMR (600 MHz, $CDCl_3$) δ 8.27 – 8.24 (m, 2H), 8.20 (d, *J* = 8.9 Hz, 1H), 8.04 – 7.99 (m, 1H), 7.92 – 7.79 (m, 2H), 7.66 (dd, *J* = 8.9, 1.9 Hz, 1H), 6.8 (s, 1H), 5.14 (s, 1H), 5.05 (q, *J* = 6.4 Hz, 1H), 3.81 (t, *J* = 6.8 Hz, 2H), 3.75 (s, 3H), 3.49 (dd, *J* = 14.0, 5.8 Hz, 1H), 3.38 (dd, *J* = 14.0, 6.2 Hz, 1H) 1.37 (s, 9H) ppm.

^{13}C NMR (151 MHz, $CDCl_3$) δ 171.5, 169.5, 156.2, 143.6, 143.3, 143.3, 142.9, 139.5, 132.6, 131.0, 130.7, 130.0, 129.8, 129.4, 129.1, 80.6, 53.0, 52.8, 44.6, 38.6, 28.4 ppm.

IR (ATR): $\tilde{\nu}$ [cm^{-1}] = 3306, 2979, 2929, 1742, 1677, 1511, 1438, 1391, 1366, 1249, 1218, 1166, 1118, 1050, 1028, 862, 759, 735, 701.

HRMS (ESI) m/z calcd. for $C_{23}H_{26}N_4NaO_5$ ($[M+Na]^+$): 461.1794, found 461.1795.

R_f (CyHex/EtOAc, 1:2) = 0.27.

Methyl (S)-2-(2-((*tert*-butoxycarbonyl)amino)acetamido)-3-(7/8-fluorophenazin-2-yl)propanoate (mixture of regioisomers) (2.7)

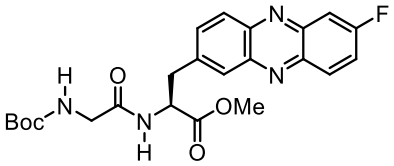

$C_{23}H_{25}FN_4O_5$
456.18 g/mol

The compound **2.7** was synthesized according to GP3 using **2.3** (106 mg, 300 µmol, 1.0 equiv.) and IBX (101 mg, 360 µmol, 1.2 equiv.) in 2.4 mL of EtOH. 4-fluorobenzene-1,2-diamine (83.3 mg, 660 µmol, 2.2 equiv.) in 1.2 mL of EtOH was then added. The reaction was purified by flash column chromatography on silica gel eluting with CyHex/EtOAc (3:2) to produce **2.7** as 1.5:1 mixture of regioisomers, isolated as orange solid in 81% yield (112 mg, 245 µmol).

^{1}H NMR (600 MHz, DMSO-d_6) δ 8.33 (m, 2H), 8.17 – 8.11 (m, 1H), 8.04 (d, *J* = 13.5 Hz, 1H), 7.99 – 7.95 (m, 1H), 7.93 – 7.83 (m, 2H), 6.82 (t, *J* = 6.3 Hz, 1H), 4.76 (q, *J* = 7.8 Hz, 1H), 3.65 (s,1H), 3.50 (m, 2H), 3.41 – 3.36 (m, 1H), 3.25 (ddd, *J* = 14.0, 9.4, 2.0 Hz, 1H), 1.29 (s, 9H).

^{13}C NMR (151 MHz, DMSO-d_6) δ 171.6, 169.5, 163.4, 163.2, 161.7, 161.5, 155.6, 143.3, 143.2, 142.9, 142.2, 142.2, 142.2, 141.5, 141.4, 140.5, 140.5, 140.2, 133.7, 132.9, 132.2, 132.1, 132.1, 129.1, 128.6, 128.5, 128.0, 122.7, 122.5, 122.3, 111.4, 111.3, 111.2, 111.2, 77.9, 52.6, 52.0, 42.8, 36.9, 36.8, 28.0 ppm.

^{19}F NMR (376 MHz, DMSO-d_6) δ -105.6, -105.7.

IR (ATR): $\tilde{\nu}$ [cm^{-1}] = 3310, 3063, 2976, 2928, 1743, 1681, 1615, 1516, 1446, 1391, 1366, 1286, 1250, 1214, 1170, 1111, 1050, 1029, 976, 943, 861, 832, 779, 736, 634.

HRMS (ESI) m/z calcd. for $C_{23}H_{25}FN_4NaO_5$ ($[M+Na]^+$): 479.1702, found 479.1701.

R_f (CyHex/EtOAc, 1:2) = 0.35.

Methyl (S)-2-(2-((*tert*-butoxycarbonyl)amino)acetamido)-3-(7/8-chlorophenazin-2-yl)propanoate (mixture of regioisomers) (2.8)

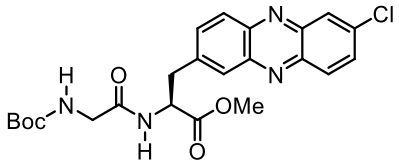

$C_{23}H_{25}ClN_4O_5$
472.15 g/mol

The compound **2.8** was synthesized according to GP3 using **2.3** (106 mg, 300 µmol, 1.0 equiv.) and IBX (101 mg, 360 µmol, 1.2 equiv.) in 2.4 mL of EtOH. 4-chlorobenzene-1,2-diamine (94.1 mg, 660 µmol, 2.2 equiv.) in 1.2 mL of EtOH was then added. The reaction was purified by flash column chromatography on silica gel using CyHex/EtOAc (3:2) to produce **2.8** as 2.5:1 mixture of regioisomers, isolated as yellow solid in 78% yield (111 mg, 234 µmol).

^{1}H NMR (600 MHz, $CDCl_3$) δ 8.20 (dd, *J* = 8.6, 2.2 Hz, 1H), 8.16 – 8.12 (m, 2H), 7.95 – 7.94 (m, 1H), 7.74 (dt, *J* = 9.2, 2.5 Hz, 1H), 7.65 (ddd, *J* = 8.9, 3.5, 1.9 Hz, 1H), 6.84 (s, 1H), 5.18 (s, 1H), 5.04 (q, *J* = 6.8 Hz, 1H), 3.89 – 3.76 (m, 2H), 3.75 (s, 3H), 3.50 – 3.43 (m, 1H), 3.35 (ddd, *J* = 14.0, 6.3, 2.1 Hz, 1H), 1.37 (d, *J* = 2.9 Hz, 9H) ppm.

^{13}C NMR (151 MHz, $CDCl_3$) δ 171.5, 169.6, 169.6, 156.2, 143.4, 143.4, 143.1, 142.8, 142.0, 142.0, 140.1, 139.6, 136.9, 136.6, 133.2, 132.8, 132.2, 132.0, 131.1, 130.9, 130.0, 129.9, 129.4, 129.2, 128.2, 127.9, 80.5, 53.0, 52.8, 44.6, 38.6, 38.5, 28.3 ppm.

IR (ATR): $\tilde{\nu}$ [cm^{-1}] = 3306, 2976, 2929, 1742, 1676, 1511, 1438, 1391, 1365, 1249,1218, 1166, 1118, 1050, 1028, 862, 759, 735, 701, 650.

HRMS (ESI) m/z calcd. for $C_{23}H_{25}ClN_4NaO_5$ ($[M+Na]^+$): 495.1403, found 495.1406.

R_f (CyHex/EtOAc, 1:2) = 0.19.

Methyl (S)-2-(2-((*tert*-butoxycarbonyl)amino)acetamido)-3-(7-methoxyphenazin-2-yl)propanoate (mixture of regioisomers) (2.9)

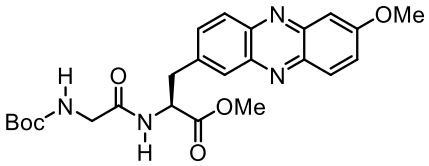

$C_{24}H_{28}N_4O_6$
468.20 g/mol

The compound **2.9** was synthesized according to GP3 using **2.3** (106 mg, 300 µmol, 1.0 equiv.) and IBX (101 mg, 361 µmol, 1.2 equiv.) in 2.4 mL of EtOH. 4-methoxybenzene-1,2-diamine (91.2 mg, 660 µmol, 2.2 equiv.) in 1.2 mL of EtOH was then added. The reaction was purified by flash column chromatography on silica gel eluting with CyHex/EtOAc (1:1) to produce **2.9** as 1.5:1 mixture of regioisomers, isolated as yellow solid in 72% yield (102 mg, 217 µmol).

^{1}H NMR (400 MHz, $CDCl_3$) δ 8.12 – 8.00 (m, 2H), 7.89 (dd, *J* = 8.4, 1.9 Hz, 1H), 7.56 (ddd, *J* = 17.2, 8.9, 2.0 Hz, 1H), 7.48 (dd, *J* = 9.5, 2.8 Hz, 1H), 7.37 (t, *J* = 3.1 Hz, 1H), 6.84 (d, *J* = 7.6 Hz, 1H), 5.26 – 5.18 (m, 1H), 5.02 (dq, *J* = 8.3, 4.2 Hz, 1H), 4.01 (s, 3H), 3.80 (m, 2H), 3.73 (s, 3H), 3.43 (dt, *J* = 13.9, 5.1 Hz, 1H), 3.33 (ddd, *J* = 13.9, 6.2, 3.8 Hz, 1H), 1.36 (s, 9H) ppm.

^{13}C NMR (101 MHz, $CDCl_3$) δ 171.6, 171.5, 169.5, 161.7, 161.4, 156.1, 145.1, 142.8, 142.5, 141.7, 141.2, 140.9, 140.8, 139.2, 137.4, 132.3, 131.0, 130.8, 130.7, 130.0, 129.5, 129.1, 128.5, 126.6, 126.5, 104.6, 104.3, 80.4, 56.1, 56.1, 53.1, 52.8, 44.5, 38.5, 38.3, 28.3 ppm.

IR (ATR): $\tilde{\nu}$ [cm^{-1}] = 3314, 2975, 2934, 1742, 1680, 1637, 1611, 1516, 1493, 1457, 1431, 1391, 1365, 1292, 1221, 1168, 1118, 1050, 856, 827, 782, 636.

HRMS (ESI) m/z calcd. for $C_{24}H_{28}N_4NaO_6$ ($[M+Na]^+$): 491.1898, found 491.1901.

R_f (CyHex/EtOAc, 1:2) = 0.16.

Methyl (S)-2-(2-((*tert*-butoxycarbonyl)amino)acetamido)-3-(7-(*tert*-butyl)phenazin-2-yl)propanoate (mixture of regioisomers) (2.10)

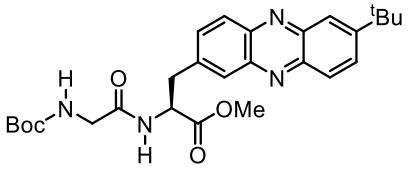

$C_{27}H_{34}N_4O_5$
494.25 g/mol

The compound **2.10** was synthesized according to GP3 using **2.3** (106 mg, 300 µmol, 1.0 equiv.) and IBX (101 mg, 361 µmol, 1.2 equiv.) in 2.4 mL of EtOH. 4-(*tert*-butyl)benzene-1,2-diamine (108 mg, 660 µmol, 2.2 equiv.) in 1.2 mL of EtOH was then added. The reaction was purified by flash column chromatography on silica gel eluting with CyHex/EtOAc (1:1) to produce **2.10** as 1.1:1 mixture of regioisomers, isolated as yellow solid in 85% yield (127 mg, 256 µmol).

^{1}H NMR (400 MHz, $CDCl_3$) δ 8.14 – 8.06 (m, 3H), 7.92 – 7.88 (m, 2H), 7.68 – 7.57 (m, 1H), 6.94 (s, 1H), 5.27 (t, *J* = 6.0 Hz, 1H), 5.01 (q, *J* = 6.5 Hz, 1H), 3.82 – 3.77 (m, 2H), 3.71 (s, 3H), 3.46 – 3.39 (m, 1H), 3.32 (dt, *J* = 14.0, 6.1 Hz, 1H), 1.45 (s, 9H), 1.34 (d, *J* = 1.0 Hz, 9H) ppm.

^{13}C NMR (101 MHz, $CDCl_3$) δ 171.6, 171.5, 169.6, 169.5, 156.1, 154.2, 153.9, 143.7, 143.6, 143.2, 142.9, 142.7, 142.4, 142.3, 138.8, 138.5, 132.1, 131.8, 130.6, 130.4, 129.8, 129.7, 129.3, 129.1, 129.0, 128.8, 80.4, 65.9, 53.0, 52.7, 44.4, 38.4, 35.6, 30.8, 28.3 ppm.

IR (ATR): $\tilde{\nu}$ [cm^{-1}] = 3307, 2966, 1744, 1679, 1509, 1445, 1392, 1366, 1277, 1249, 1217, 1169, 1050, 1026, 864, 832, 736, 654.

HRMS (ESI) m/z calcd. for $C_{27}H_{34}N_4NaO_5$ ($[M+Na]^+$): 517.2424, found 517.2424.

R_f (CyHex/EtOAc, 1:2) = 0.29.

Methyl (S)-2-(2-((*tert*-butoxycarbonyl)amino)acetamido)-3-(7,8-dimethylphenazin-2-yl)propanoate (2.11)

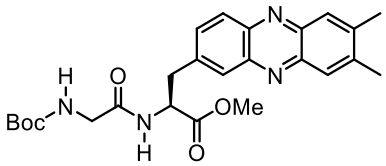

$C_{25}H_{30}N_4O_5$
466.22 g/mol

The compound **2.11** was synthesized according to GP3 using **2.3** (106 mg, 300 µmol, 1.0 equiv.) and IBX (101 mg, 361µmol, 1.2 equiv.) in 2.4 mL of EtOH. 4,5-dimethylbenzene-1,2-diamine (90.0 mg, 660 mmol, 2.2 equiv.) in 1.2 mL of EtOH was then added. The reaction was purified by flash column chromatography on silica gel using CyHex/EtOAc (1:1) to produce **2.11** as a yellow solid in 79% yield (111 mg, 237 µmol).

^{1}H NMR (400 MHz, $CDCl_3$) δ 8.05 (d, *J* = 8.9 Hz, 1H), 7.93 – 7.78 (m, 3H), 7.52 (dd, *J* = 8.9, 1.9 Hz, 1H), 7.01 (d, *J* = 7.1 Hz, 1H), 5.37 (d, *J* = 5.9 Hz, 1H), 5.00 (q, *J* = 6.5 Hz, 1H), 3.82 – 3.77 (m, 2H), 3.72 (s, 3H), 3.39 (dd, *J* = 13.9, 5.7 Hz, 1H), 3.28 (dd, *J* = 13.9, 6.5 Hz, 1H), 2.49 (dd, *J* = 3.5, 1.1 Hz, 6H), 1.34 (s, 9H) ppm.

^{13}C NMR (101 MHz, $CDCl_3$) δ 171.6, 169.6, 156.2, 143.0, 142.8, 142.8, 142.2, 142.0, 141.8, 138.2, 131.5, 129.7, 129.2, 127.9, 127.8, 80.3, 53.1, 52.7, 44.4, 38.3, 28.3, 20.7 ppm.

IR (ATR): $\tilde{\nu}$ [cm^{-1}] = 3314, 2980, 2931, 1741, 1718, 1679, 1508, 1448, 1367, 1252, 1218, 1169, 1028.

HRMS (ESI) m/z calcd. for $C_{25}H_{30}N_4NaO_5$ ($[M+Na]^+$): 489.2104, found 489.2108.

R_f (CyHex/EtOAc, 1:2) = 0.16.

Methyl (S)-3-(benzo[b]phenazin-2-yl)-2-(2-((*tert*-butoxycarbonyl)amino) acetamido)propanoate (2.12)

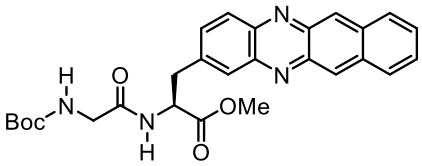

$C_{27}H_{28}N_4O_5$
488.21 g/mol

The compound **2.12** was synthesized according to GP3 using **2.3** (106 mg, 300 µmol, 1.0 equiv.) and IBX (101 mg, 361 µmol, 1.2 equiv.) in 2.4 mL of EtOH. Naphthalene-2,3-diamine (104 mg, 660 µmol, 2.2 equiv.) in 1.2 mL of EtOH was then added. The reaction was purified by flash column chromatography on silica gel using CyHex/EtOAc (7:3) to produce **2.12** as an orange solid in 42% yield (62.0 mg, 127 µmol).

^{1}H NMR (400 MHz, $CDCl_3$) δ 8.71 (dt, *J* = 12.3, 2.9 Hz, 2H), 8.06 – 7.96 (m, 3H), 7.83 (d, *J* = 1.9 Hz, 1H), 7.53 (dd, *J* = 9.1, 2.0 Hz, 1H), 7.46 – 7.41 (m, 2H), 7.12 (s, 1H), 5.43 (t, *J* = 5.8 Hz, 1H), 5.04 (q, *J* = 6.6 Hz, 1H), 3.83 (d, *J* = 5.8 Hz, 2H), 3.74 (s, 3H), 3.40 (dd, *J* = 14.2, 5.8 Hz, 1H), 3.27 (dd, 1H), 1.34 (s, 9H) ppm.

^{13}C NMR (101 MHz, $CDCl_3$) δ 171.6, 169.8, 156.2, 144.1, 143.7, 140.0, 139.9, 139.4, 134.6, 134.4, 132.6, 130.1, 129.3, 128.6, 128.5, 127.6, 127.4, 126.9, 126.9, 80.4, 52.9, 52.8, 44.4, 38.5, 28.3 ppm.

IR (ATR): $\tilde{\nu}$ [cm^{-1}] = 3532, 3337, 3059, 2980, 2971, 2925, 2855, 1740, 1685, 1502, 1460, 1367, 1332, 1250, 1166, 1051, 1027, 965, 955, 861, 763, 731, 689, 675, 649, 636.

HRMS (ESI) m/z calcd. for $C_{27}H_{28}N_4NaO_5$ ($[M+Na]^+$): 511.1957, found 511.1952.

R_f (CyHex/EtOAc, 1:2) = 0.19.

Methyl (6S,12S)-12-((7,8-dimethylphenazin-2-yl)methyl)-6-isopropyl-2,2-dimethyl-4,7,10-trioxo-3-oxa-5,8,11-triazatridecan-13-oate (2.15)

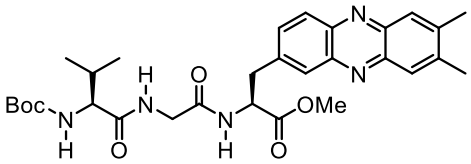

$C_{30}H_{39}N_5O_6$
565.29 g/mol

The compound **2.15** was synthesized according to GP3 using **7.1** (113 mg, 250 µmol, 1.0 equiv.) and IBX (84.1 mg, 300 µmol, 1.2 equiv.) in 2 mL of EtOH. 4,5-dimethylbenzene-1,2-diamine (76.5 mg, 550 µmol, 2.2 equiv.) in 1 mL of EtOH was then added. The reaction was purified by flash column chromatography on silica gel eluting with CyHex/EtOAc (1:1) to produce **2.15** as yellow solid in 71% yield (101 mg, 178 µmol).

^{1}H NMR (400 MHz, $CDCl_3$) δ 8.11 (d, *J* = 8.9 Hz, 1H), 7.96 – 7.91 (m, 3H), 7.57 (dd, *J* = 8.9, 1.9 Hz, 1H), 7.05 (d, *J* = 7.7 Hz, 1H), 6.95 (t, *J* = 5.5 Hz, 1H), 5.30 (dd, *J* = 19.6, 8.6 Hz, 1H), 4.99 (q, 1H), 4.06 – 3.88 (m, 3H), 3.72 (s, 3H), 3.42 (dd, *J* = 14.1, 5.9 Hz, 1H), 3.31 (dd, *J* = 13.9, 6.6 Hz, 1H), 2.54 (s, 6H), 2.09 – 1.99 (m, 1H), 1.37 (s, 9H), 0.82 (dd, *J* = 14.9, 6.8 Hz, 6H) ppm.

^{13}C NMR (101 MHz, $CDCl_3$) δ 172.5, 171.5, 168.8, 156.1, 143.0, 142.6, 142.5, 142.4, 142.0, 138.7, 131.8, 129.8, 128.9, 128.1, 127.6, 80.1, 60.2, 53.2, 52.7, 43.2, 38.4, 30.8, 28.4, 20.8, 20.8, 19.4, 17.8 ppm.

IR (ATR): $\tilde{\nu}$ [cm^{-1}] = 3310, 2958, 1735, 1688, 1635, 1517, 1446, 1390, 1365, 1349, 1292, 1245, 1220, 1168, 1134, 1044, 1018, 1044, 1018, 1004, 983, 968, 866, 836, 784, 703, 659.

HRMS (ESI) m/z calcd. for $C_{30}H_{39}N_5NaO_6$ ($[M+Na]^+$): 588.2790, found 588.2793.

R_f (CyHex/EtOAc, 1:4) = 0.12.

Methyl (5S,8S,11S)-11-((7,8-dimethylphenazin-2-yl)methyl)-5-isobutyl-8-methyl-3,6,9-trioxo-1-phenyl-2-oxa-4,7,10-triazadodecan-12-oate (2.16)

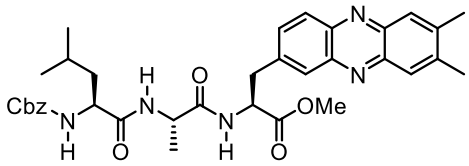

$C_{35}H_{41}N_5O_6$
627.31 g/mol

The compound **2.16** was synthesized according to GP3 using **7.2** (128 mg, 250 µmol, 1.0 equiv.) and IBX (84.1 mg, 300 µmol, 1.2 equiv.) in 2 mL of EtOH. 4,5-dimethylbenzene-1,2-diamine (75.0 mg, 550 µmol, 2.2 equiv.) in 1 mL of EtOH was then added. The reaction was purified by flash column chromatography on silica gel eluting with CyHex/EtOAc (2:3) to produce **2.16** as yellow solid in 60% yield (94.2 mg, 150 µmol).

^{1}H NMR (600 MHz, DMSO-d_6) δ 8.18 (d, *J* = 7.7 Hz, 1H), 8.09 (d, *J* = 8.9 Hz, 1H), 7.98 (dt, *J* = 19.8, 1.6 Hz, 3H), 7.75 (dd, *J* = 8.9, 2.0 Hz, 1H), 7.68 (d, *J* = 7.5 Hz, 1H), 7.37 – 7.25 (m, 5H), 7.08 (br, 1H), 5.01 (d, *J* = 2.9 Hz, 2H), 4.79 – 4.71 (m, 1H), 4.31 (p, *J* = 7.1 Hz, 1H), 4.01 (q, *J* = 7.7 Hz, 1H), 3.63 (s, 3H), 3.38 (dd, *J* = 14.2, 5.7 Hz, 1H), 3.27 (dd, *J* = 14.1, 8.6 Hz, 1H), 2.54 (s, 6H), 1.57 (dt, *J* = 13.4, 6.7 Hz, 1H), 1.39 (t, *J* = 7.2 Hz, 2H), 1.17 (d, *J* = 7.0 Hz, 3H), 0.79 (dd, *J* = 6.6, 3.6 Hz, 6H) ppm.

^{13}C NMR (151 MHz, DMSO-d_6) δ 171.9, 171.4, 171.0, 155.4, 142.1, 141.8, 141.5, 141.4, 141.3, 139.3, 136.7, 131.7, 128.5, 128.1, 127.9, 127.3, 127.1, 127.1, 127.1, 65.1, 53.0, 52.7, 51.5, 47.7, 40.4, 36.6, 22.4, 21.1, 19.6, 19.6, 17.8 ppm.

IR (ATR): $\tilde{\nu}$ [cm^{-1}] = 3385, 3271, 3061, 3030, 2950, 1731, 1710, 1672, 1650, 1539, 1504, 1496, 1465, 1439, 1367, 1343, 1285, 1268, 1234, 1167, 1136, 1076, 1046, 1027, 1001, 977, 935, 867, 834, 778, 750, 695, 623, 603.

HRMS (ESI) m/z calcd. for $C_{35}H_{41}N_5NaO_6$ ([M+Na]$^+$): 650.2948, found 650.2949.

R_f (CyHex/EtOAc, 3:7) = 0.40.

Benzyl (S)-2-((2-(((S)-3-(7,8-dimethylphenazin-2-yl)-1-methoxy-1-oxopropan-2-yl)amino)-2-oxoethyl)carbamoyl)pyrrolidine-1-carboxylate (2.17)

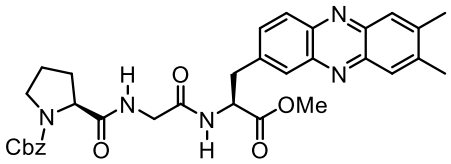

$C_{33}H_{35}N_5O_6$
597.26 g/mol

The compound **2.17** was synthesized according to GP3 using **7.4** (121 mg, 250 µmol, 1.0 equiv.) and IBX (84.1 mg, 300 µmol, 1.2 equiv.) in 2 mL of EtOH. 4,5-dimethylbenzene-1,2-diamine (75.0 mg, 550 µmol, 2.2 equiv.) in 1 mL of EtOH was then added. The reaction was purified by flash column chromatography on silica gel eluting with CyHex/EtOAc (1:9) to produce **2.17** as yellow solid in 73% yield (110 mg, 184 µmol).

^{1}H NMR (400 MHz, $CDCl_3$) δ 8.17 (d, *J* = 8.9 Hz, 1H), 7.54 (s, 1H), 7.26 – 7.10 (m, 5H), 5.08 (d, *J* = 12.5 Hz, 1H), 4.94 (dd, *J* = 23.2, 9.4 Hz, 2H), 4.30 (dd, *J* = 8.4, 4.2 Hz, 1H), 3.96 (s, 2H), 3.72 (s, 3H), 3.50 – 3.39 (m, 2H), 3.34 (dd, *J* = 13.8, 8.0 Hz, 1H), 2.56 (s, 6H), 2.17 (t, *J* = 5.9 Hz, 1H), 2.12 – 2.00 (m, 1H), 2.03 – 1.92 (m, 1H), 1.88 – 1.77 (m, 1H).

^{13}C NMR (101 MHz, $CDCl_3$) δ 172.7, 171.4, 169.4, 156.2, 143.1, 142.9, 142.6, 141.5, 136.4, 132.7, 129.8, 128.5, 128.1, 128.0, 127.7, 67.3, 61.2, 53.1, 52.8, 47.3, 43.1, 38.2, 29.5, 20.9 ppm.

IR (ATR): $\tilde{\nu}$ [cm^{-1}] = 3316, 2951, 2881, 1734, 1696, 1666, 1642, 1525, 1444, 1418, 1353, 1275, 1212, 1168, 1124, 1090, 1025, 1002, 914, 869, 836, 820, 766, 731, 716, 695, 658, 620, 601.

HRMS (ESI) m/z calcd. for $C_{33}H_{35}N_5NaO_6$ ($[M+Na]^+$): 620.2483, found 620.2483.

R_f (DCM:MeOH, 95:5) = 0.19.

Methyl (8S,11S)-8-benzyl-11-((7,8-dimethylphenazin-2-yl)methyl)-3,6,9-trioxo-1-phenyl-2-oxa-4,7,10-triazadodecan-12-oate (2.18)

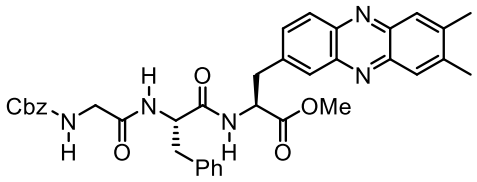

$C_{37}H_{37}N_5O_6$
647.27 g/mol

The compound **2.18** was synthesized according to GP3 using **7.5** (134 mg, 250 µmol, 1.0 equiv.) and IBX (84.1 mg, 300 µmol, 1.2 equiv.) in 2 mL of EtOH. 4,5-dimethylbenzene-1,2-diamine (75.0 mg, 550 mmol, 2.2 equiv.) in 1 mL of EtOH was then added. The reaction was purified by flash column chromatography on silica gel eluting with CyHex/EtOAc (1:4) to produce **2.18** as yellow solid in 62% yield (101 mg, 155 µmol).

^{1}H NMR (600 MHz, DMSO-d_6) δ 8.63 (d, *J* = 7.7 Hz, 1H), 8.11 (d, *J* = 8.9 Hz, 1H), 8.03 – 7.92 (m, 4H), 7.78 (dd, *J* = 8.8, 1.9 Hz, 1H), 7.39 – 7.10 (m, 11H), 5.00 (s, 2H), 4.80 – 4.68 (m, 1H), 4.56 (td, *J* = 8.6, 4.8 Hz, 1H), 3.61 (s, 3H), 3.58 (d, *J* = 6.0 Hz, 1H), 3.50 (dd, *J* = 16.9, 6.0 Hz, 1H), 3.37 (dd, *J* = 14.0, 5.8 Hz, 1H), 3.27 (dd, *J* = 14.1, 9.0 Hz, 1H), 2.94 (dd, *J* = 13.8, 4.9 Hz, 1H), 2.73 (dd, *J* = 13.8, 9.0 Hz, 1H), 2.52 (s, 6H) ppm.

^{13}C NMR (151 MHz, DMSO-d_6) δ 171.4, 171.4, 171.1, 171.0, 168.7, 168.6, 156.3, 142.3, 142.2, 142.0, 142.0, 141.8, 141.6, 139.6, 137.4, 137.0, 132.1, 129.1, 128.9, 128.3, 128.3, 127.9, 127.7, 127.6, 127.4, 127.3, 126.2, 65.4, 53.4, 53.0, 52.9, 51.9, 43.3, 40.1, 37.6, 36.7, 20.1, 20.0 ppm.

IR (ATR): $\tilde{\nu}$ [cm^{-1}] = 3293, 2954, 1729, 1653, 1531, 1531, 1466, 1445, 1409, 1367, 1314, 1279, 1227, 1156, 1112, 1080, 1042, 1001, 985, 926, 900, 870, 838, 823, 790, 745, 718, 696, 640, 606.

HRMS (ESI) m/z calcd. for $C_{37}H_{37}N_5NaO_6$ ([M+Na]$^+$): 670.2636 found 670.2636.

R_f (CyHex/EtOAc, 1:4) = 0.25.

Methyl (S)-2-((S)-2-((*tert*-butoxycarbonyl)amino)-3-(1*H*-indol-3-yl)propanamido)-3-(7,8-dimethylphenazin-2-yl)propanoate (2.19)

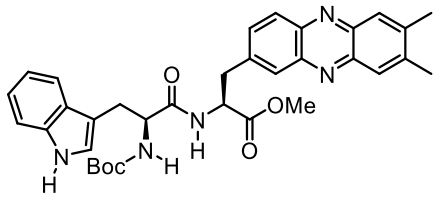

$C_{34}H_{37}N_5O_5$
595.28 g/mol

The compound **2.19** was synthesized according to GP3 using **7.7** (121 mg, 250 µmol, 1.0 equiv.) and IBX (84.1 mg, 300 µmol, 1.2 equiv.) in 2 mL of EtOH. 4,5-dimethylbenzene-1,2-diamine (75.0 mg, 550 µmol, 2.2 equiv.) in 1 mL of EtOH was then added. The reaction was purified by flash column chromatography on silica gel eluting with CyHex/EtOAc (2:3) to produce **2.19** as yellow solid in 55% yield (83.0 mg, 139 µmol).

^{1}H NMR (400 MHz, $CDCl_3$) δ 8.53 (s, 1H), 8.02 (s, 1H), 7.99 (d, *J* = 5.4 Hz, 2H), 7.77 (s, 1H), 7.62 (d, *J* = 7.5 Hz, 1H), 7.33 – 7.26 (m, 2H), 7.10 (pd, *J* = 7.0, 1.3 Hz, 2H), 7.00 (d, *J* = 2.3 Hz, 1H), 6.50 (d, *J* = 7.4 Hz, 1H), 5.13 (s, 1H), 4.89 (d, *J* = 6.8 Hz, 1H), 4.47 (s, 1H), 3.66 (s, 3H), 3.38–3.10 (m, 4H), 2.57 (s, 6H), 1.37 (s, 9H) ppm.

^{13}C NMR (151 MHz, $CDCl_3$) δ 171.8, 171.3, 155.6, 143.0, 142.8, 142.5, 142.3, 142.1, 138.9, 136.6, 131.9, 129.6, 128.9, 128.2, 127.8, 127.8, 123.4, 122.5, 120.0, 119.0, 111.4, 110.9, 80.4, 55.8, 53.4, 52.5, 38.7, 28.4, 28.2, 20.7, 20.7 ppm.

IR (ATR): $\tilde{\nu}$ [cm^{-1}] = 3325, 3058, 3014, 2983, 2945, 2926, 1734, 1683, 1650, 1524, 1437, 1390, 1367, 1340, 1306, 1291, 1279, 1243, 1227, 1199, 1169, 1139, 1126, 1098, 1062, 1046, 1013, 999, 976, 889, 866, 835, 820, 799, 755, 731, 718, 686, 651, 628, 604.

HRMS (ESI) m/z calcd. for $C_{34}H_{37}N_5NaO_5$ ($[M+Na]^+$): 618.2686, found 618.2687.

R_f (CyHex/EtOAc, 1:2) = 0.38.

Methyl (6S,9S)-6-(3-(*tert*-butoxy)-3-oxopropyl)-9-((7,8-dimethylphenazin-2-yl)methyl)-2,2-dimethyl-4,7,10-trioxo-3-oxa-5,8,11-triazatridecan-13-oate (2.20)

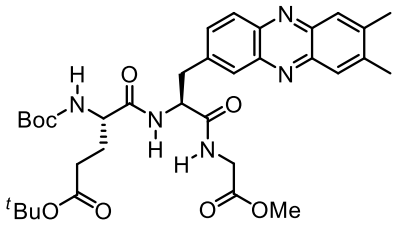

$C_{34}H_{45}N_5O_8$
651.33 g/mol

The compound **2.20** was synthesized according to GP3 using **7.10** (134 mg, 250 µmol, 1.0 equiv.) and IBX (84.1 mg, 300 µmol, 1.2 equiv.) in 2 mL of EtOH. 4,5-dimethylbenzene-1,2-diamine (75.0 mg, 550 µmol, 2.2 equiv.) in 1 mL of EtOH was then added. The reaction was purified by flash column chromatography on silica gel eluting with DCM/MeOH (97:3) to produce **2.20** as yellow solid in 62% yield (102 mg, 156 µmol).

^{1}H NMR (400 MHz, DMSO-d_6) δ 8.60 (t, *J* = 5.9 Hz, 1H), 8.07 – 7.96 (m, 3H), 7.91 (s, 2H), 7.77 (dd, *J* = 8.8, 1.9 Hz, 1H), 6.83 (d, *J* = 8.3 Hz, 1H), 4.81 (dd, *J* = 9.2, 4.6 Hz, 1H), 3.88 (t, *J* = 6.5 Hz, 2H), 3.81 (tdd, *J* = 8.3, 5.5, 2.8 Hz, 2H), 3.60 (s, 1H), 3.07 (dd, *J* = 13.9, 9.8 Hz, 1H), 2.47 (s, 6H), 1.94 (t, *J* = 7.7 Hz, 2H), 1.64 – 1.43 (m, 2H), 1.24 (s, 9H) ppm.

^{13}C NMR (101 MHz, DMSO-d_6**)** δ 171.5, 171.3, 170.1, 155.2, 142.3, 142.3, 142.0, 141.8, 141.6, 140.1, 132.4, 128.5, 128.5, 127.4, 127.4, 79.5, 78.2, 53.8, 52.8, 51.7, 40.7, 38.2, 31.2, 28.0, 27.6, 27.3, 20.1, 20.1 ppm.

IR (ATR): $\tilde{\nu}$ [cm^{-1}] = 3300, 3258, 2978, 2933, 1727, 1686, 1665, 1644, 1548, 1525, 1466, 1444, 1392, 1366, 1340, 1293, 1246, 1226, 1157, 1098, 1068, 1046, 1027, 1002, 887, 868, 849, 840, 827, 812, 777, 756, 720, 645, 614.

HRMS (ESI) m/z calcd. for $C_{31}H_{39}N_5NaO_8$ ([M+Na]$^+$): 674.3154, found 674.3154.

R_f (DCM/MeOH, 95:5) = 0.54.

Methyl (5S,11S)-5-(3-amino-3-oxopropyl)-11-((7,8-dimethylphenazin-2-yl)methyl)-3,6,9-trioxo-1-phenyl-2-oxa-4,7,10-triazadodecan-12-oate (2.21)

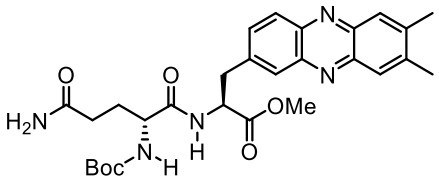

$C_{28}H_{35}N_5O_6$
537.26 g/mol

The compound **2.21** was synthesized according to GP3 using **7.6** (106 mg, 250 µmol, 1.0 equiv.) and IBX (84.1 mg, 300 µmol, 1.2 equiv.) in 2 mL of EtOH. 4,5-dimethylbenzene-1,2-diamine (75.0 mg, 0.550 mmol, 2.2 equiv.) in 1 mL of EtOH was then added. The reaction was purified by flash column chromatography on silica gel eluting with DCM/MeOH, (95:5) to produce **2.21** as yellow solid in 48% yield (64.6 mg, 120 µmol).

^{1}H NMR (400 MHz, DMSO-d_6) δ 8.34 (d, *J* = 7.6 Hz, 1H), 8.07 (d, *J* = 8.8 Hz, 1H), 7.99 (s, 1H), 7.94 (s, 2H), 7.83 – 7.73 (m, 1H), 7.19 (s, 1H), 6.78 – 6.65 (m, 2H), 4.75 (td, *J* = 8.4, 5.4 Hz, 1H), 3.97 – 3.83 (m, 1H), 3.63 (s, 1H), 3.27 (d, J = 9.0 Hz, 1H), 2.51 (s, 6H), 2.11 – 1.91 (m, 2H), 1.80 (td, *J* = 11.4, 4.9 Hz, 1H), 1.67 (dd, *J* = 15.3, 8.0 Hz, 1H), 1.26 (s, 9H) ppm.

^{13}C NMR (101 MHz, DMSO-d_6) δ 173.7, 172.1, 171.7, 155.0, 142.3, 142.3, 142.0, 141.9, 141.7, 141.6, 139.6, 132.1, 128.8, 128.4, 127.3, 127.3, 78.0, 53.8, 52.8, 52.0, 36.8, 31.4, 28.0, 27.7, 20.1, 20.0 ppm.

IR (ATR): $\tilde{\nu}$ [cm^{-1}] =3314, 2924, 2854, 1742, 1662, 1525, 1450, 1392, 1367, 1316, 1250, 1222, 1168, 1054, 1025, 1004, 866, 716, 640.

HRMS (ESI) m/z calcd. for $C_{28}H_{35}N_5NaO_6$ ([M+Na]$^+$): 560.2480, found 560.2480.

R_f (DCM/MeOH, 95:5) = 0.12.

Methyl ((S)-2-((S)-2-(((benzyloxy)carbonyl)amino)-3-hydroxypropanamido)-3-(7,8-dimethylphenazin-2-yl)propanoyl)glycinate (2.22)

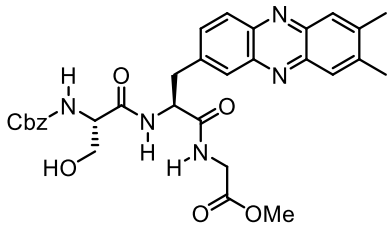

$C_{31}H_{33}N_5O_7$
587.24 g/mol

The compound **2.22** was synthesized according to GP3 using **7.11** (118 mg, 250 µmol, 1.0 equiv.) and IBX (84.1 mg, 300 µmol, 1.2 equiv.) in 2 ml of EtOH. 4,5-dimethylbenzene-1,2-diamine (75.0 mg, 550 µmol, 2.2 equiv.) in 1 mL of EtOH was then added. The reaction was purified by flash column chromatography on silica gel eluting with DCM/MeOH (95:5) to produce **2.22** as red solid in 55% yield (82.0 mg,139 µmol).

^{1}H NMR (600 MHz, DMSO-d_6) δ 8.57 (t, *J* = 5.8 Hz, 1H), 8.17 (d, *J* = 8.4 Hz, 1H), 8.06 (d, *J* = 8.9 Hz, 1H), 8.01 (d, *J* = 1.9 Hz, 1H), 7.95 (s, 2H), 7.81 (dd, *J* = 8.8, 1.9 Hz, 1H), 7.38 – 7.19 (m, 5H), 7.14 (d, *J* = 8.1 Hz, 1H), 4.97 – 4.87 (m, 3H), 4.81 (td, *J* = 8.8, 4.5 Hz, 1H), 4.07 – 3.99 (m, 1H), 3.91 (t, *J* = 5.4 Hz, 2H), 3.63 (s, 3H), 3.43 (t, *J* = 6.0 Hz, 2H), 3.40 – 3.34 (m, 1H), 3.12 (dd, *J* = 13.9, 9.4 Hz, 1H), 2.51 (s, 6H) ppm.

^{13}C NMR (101 MHz, DMSO-d_6) δ 171.2, 170.1, 170.1, 155.8, 142.4, 142.3, 142.0, 141.9, 141.7, 141.6, 140.2, 136.8, 132.6, 128.5, 128.5, 128.3, 127.8, 127.7, 127.4, 65.5, 61.8, 57.2, 53.2, 51.8, 40.7, 38.0, 20.1 ppm.

IR (ATR): $\tilde{\nu}$ [cm^{-1}] = 3270, 2951, 2920, 1744, 1724, 1692, 1638, 1540, 1465, 1447, 1397, 1367, 1297, 1268, 1237, 1210, 1174, 1143, 1104, 1061, 1012, 961, 911, 867, 840, 825, 784, 756, 714, 694, 671, 643, 613.

HRMS (ESI) m/z calcd. for $C_{28}H_{35}N_5NaO_7$ ([M+Na]$^+$): 610.2271, found 610.2272.

R_f (DCM:MeOH, 95:5) = 0.19.

Methyl (S)-2-((2S,3R)-3-(benzyloxy)-2-((*tert*-butoxycarbonyl)amino)butanamido)-3-(7,8-dimethylphenazin-2-yl)propanoate (2.23)

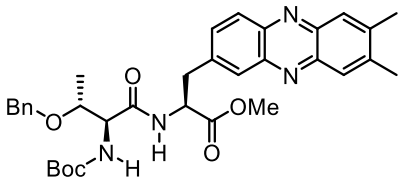

$C_{33}H_{38}N_4O_6$
586.28 g/mol

The compound **2.23** was synthesized according to GP3 using **7.8** (122 mg, 250 µmol, 1.0 equiv.) and IBX (84.1 mg, 300 µmol, 1.2 equiv.) in 2 mL of EtOH. 4,5-dimethylbenzene-1,2-diamine (75.0 mg, 550 µmol, 2.2 equiv.) in 1 mL of EtOH was then added. The reaction was purified by flash column chromatography on silica gel eluting with CyHex/EtOAc (7:3) to produce **2.23** as yellow solid in 61% yield (92.0 mg,153 µmol).

^{1}H NMR (400 MHz, $CDCl_3$) δ 8.04 (d, *J* = 8.9 Hz, 1H), 8.01 – 7.93 (m, 3H), 7.49 (dd, *J* = 8.9, 1.9 Hz, 1H), 7.37 – 7.28 (m, 1H), 7.23 – 7.07 (m, 5H), 5.47 (d, *J* = 6.8 Hz, 1H), 5.01 (q, *J* = 6.4 Hz, 1H), 4.62 – 4.45 (m, 2H), 4.32 – 4.28 (m, 1H), 4.17 (d, *J* = 3.6 Hz, 1H), 3.70 (s, 3H), 3.36 (dd, *J* = 13.9, 5.8 Hz, 1H), 3.29 (dd, *J* = 13.9, 6.2 Hz, 1H), 2.57 (s, 6H), 1.40 (s, 9H), 1.18 (d, *J* = 6.4 Hz, 3H) ppm.

^{13}C NMR (101 MHz, $CDCl_3$) δ 171.3, 170.1, 155.9, 142.7, 142.7, 142.5, 142.5, 142.2, 142.0, 138.8, 137.9, 131.9, 131.0, 129.5, 129.0, 128.8, 128.4, 127.9, 127.8, 127.7, 80.3, 74.8, 71.5, 57.7, 53.3, 52.6, 38.6, 28.4, 20.8, 15.1 ppm.

IR (ATR): $\tilde{\nu}$ [cm^{-1}] = 3321, 2970, 2924, 1739, 1677, 1660, 1660, 1524, 1446, 1366, 1305, 1275, 1244, 1215, 1164, 1118, 1055, 1028, 1013, 931, 866, 833, 798, 781, 735, 717, 694, 660, 602.

HRMS (ESI) m/z calcd. for $C_{34}H_{40}N_4NaO_6$] ([M+Na]$^+$): 623.2841, found 623.2840.

R_f (CyHex/EtOAc, 3:2) = 0.16.

Methyl ((S)-2-((S)-2-(((benzyloxy)carbonyl)amino)-4-(methylthio)butanamido)-3-(7,8-dimethylphenazin-2-yl)propanoyl)glycinate (2.24)

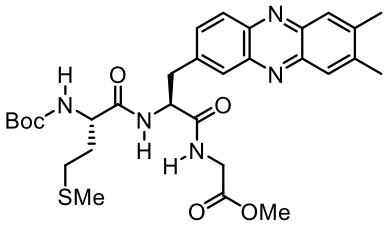

$C_{30}H_{39}N_5O_6S$
597.26 g/mol

The compound **2.24** was synthesized according to GP3 using **7.12** (121 mg, 250 µmol, 1.0 equiv.) and IBX (84.1 mg, 300 µmol, 1.2 equiv.) in 2 mL of EtOH. 4,5-dimethylbenzene-1,2-diamine (75.0 mg, 550 µmol, 2.2 equiv.) in 1 mL of EtOH was then added. The reaction was purified by flash column chromatography on silica gel eluting with DCM/MeOH (49:1) to produce **2.24** as yellow solid in 62% yield (92.7 mg,155 µmol).

^{1}H NMR (400 MHz, DMSO-d_6) δ 8.74 (s, 1H), 8.04 (t, 3H), 7.95 (s, 2H), 7.84 (d, *J* = 9.0 Hz, 1H), 6.92 (d, *J* = 8.1 Hz, 1H), 4.83 (q, *J* = 8.5 Hz, 1H), 3.98 – 3.87 (m, 2H), 3.87 – 3.80 (m, 1H), 3.63 (s, 3H), 3.12 (dd, *J* = 13.8, 9.8 Hz, 1H), 2.52 (s, 6H), 2.26 – 2.06 (m, 2H), 1.79 (s, 3H), 1.59 (q, *J* = 7.7 Hz, 2H), 1.27 (s, 9H), 1.02 (dd, *J* = 9.9, 6.2 Hz, 1H) ppm.

^{13}C NMR (101 MHz, DMSO-d_6) δ 171.3, 171.3, 170.0, 155.2, 142.3, 142.2, 141.9, 141.8, 141.6, 140.1, 132.5, 128.6, 128.5, 127.4, 78.2, 53.9, 52.8, 51.7, 40.6, 38.1, 31.8, 29.5, 28.0, 20.1, 20.1, 14.4 ppm.

IR (ATR): $\tilde{\nu}$ [cm^{-1}] =3425, 2252, 2126, 1664, 1295, 1153, 1050, 1023, 1002, 821.5, 759.4, 613.59.

HRMS (ESI+) m/z calcd. for $C_{30}H_{39}N_5NaO_6S$ ([M+Na]$^+$): 620.2513, found 620.2513.

R_f (DCM/MeOH, 95:5) = 0.3.

Emission Spectra of Compounds 2.6-2.12

Stock solutions of compounds **2.6-2.12** were prepared in 50 mL of DCM to give a 10 µM concentration, and 4 mL aliquots were taken for measurement. The UV-Vis absorption spectra were recorded to determine the maximum absorption wavelengths (λ_{max}) for each compound. Using these λ_{max} values, the fluorescence emission spectra were measured by exciting each solution at its maximum absorption wavelength in DCM. The resulting normalized emission spectra are presented in Figure 7.2. The wavelengths of maximum absorptions are shown here in nm.

compound	**2.6**	**2.7**	**2.8**	**2.9**	**2.10**	**2.11**	**2.12**
λ_{abs} (nm)	280	250	280	258	257	258	280

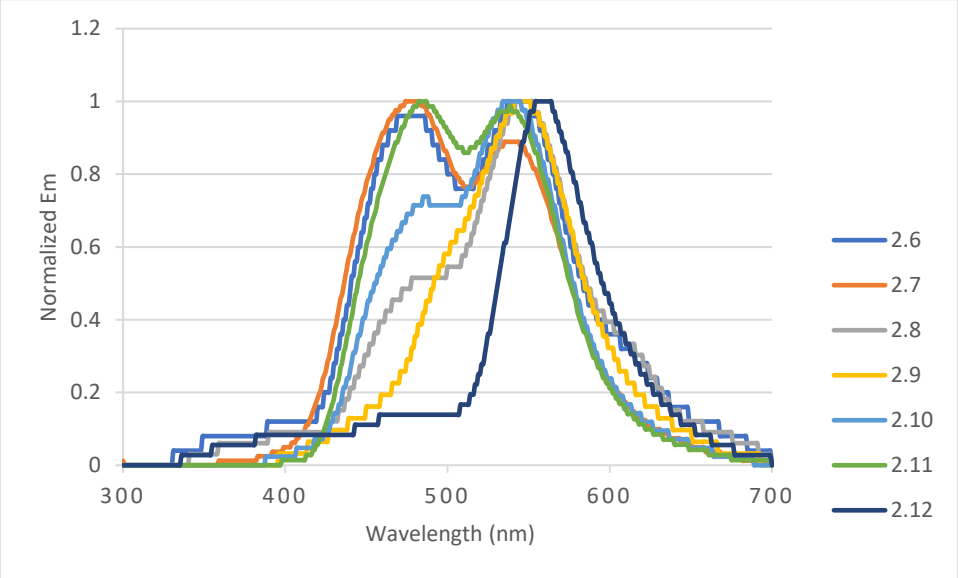

Figure 7.2: Normalized Fluorescence spectra of compound **2.6–2.12** in DCM (10 µM).

Methyl (S)-2-((tert-butoxycarbonyl)amino)-3-(4,5-dihydroxy-2-morpholinophenyl)propanoate (2.26)

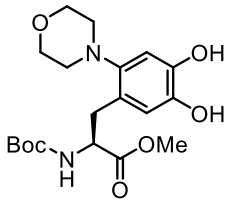

$C_{19}H_{28}N_2O_7$
396.19 g/mol

The compound **2.26** was synthesized using **2.1** (148 mg, 500 µmol, 1.0 equiv.) and IBX (168 mg, 600 µmol, 1.2 equiv.) in 4 mL of EtOH. The reaction mixture was stirred at 0 °C and allowed to warm to room temp. over 4 h. Subsequently, morpholine (259 µL, 3.01 mmol, 6.0 equiv.) was added at room temp., and the reaction was stirred for an additional 16 h. The reaction mixture was washed with saturated sodium bicarbonate solution and brine, then dried over anhydrous sodium sulfate. After filtration and concentration under reduced pressure, the crude product was purified by flash column chromatography on silica gel using DCM/MeOH (49:1) to produce **2.26** as yellow solid in 44% yield (87.4 mg, 220 µmol).

^{1}H NMR (400 MHz, $CDCl_3$) δ 7.33 (d, *J* = 5.6 Hz, 1H), 6.72 (s, 1H), 6.63 (s, 1H), 4.20 (q, *J* = 4.7 Hz, 1H), 3.87 (d, *J* = 5.4 Hz, 4H), 3.68 (s, 3H), 2.88 (td, *J* = 15.0, 6.6 Hz, 4H), 2.80 -2.65 (m, 2H), 1.36 (s, 9H).

^{13}C NMR (101 MHz, $CDCl_3$) δ 173.2, 156.2, 144.3, 143.8, 141.7, 124.3, 117.7, 108.7, 80.3, 67.3, 56.7, 53.6, 52.3, 32.9, 28.4.

HRMS (ESI+) m/z calcd. for $C_{19}H_{28}N_2NaO_7$ ($[M+Na]^+$): 419.1788, found 419.1789.

R_f (CyHex/EtOAc, 1:1) = 0.41.

Methyl (S)-2-(2-((*tert*-Butoxycarbonyl)amino)acetamido)-3-(3,4-dihydroxyphenyl)propanoate (2.27)

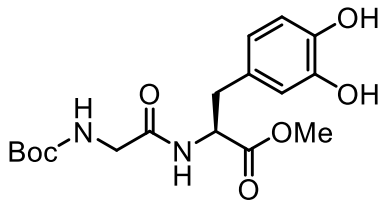

$C_{17}H_{24}N_2O_7$
368.16 g/mol

Following a modified procedure, compound **2.27** was synthesized using **2.3** (500 mg, 1.42 mmol, 1.0 equiv.) and IBX (477 mg, 1.70 mmol, 1.2 equiv.) in MeOH (12 mL). The reaction was stirred from 0 °C to room temperature for 4 h. Afterwards, in situ reduction was carried out with sodium dithionite (494 mg, 2.84 mmol, 2.0 equiv.) in water (12 mL) for 40 min. The reaction mixture was purified by flash column chromatography on silica gel eluting with CyHex/EtOAc (7:3) to afford **2.27** as a white solid in 68% yield (355 mg, 0.96 mmol).

^{1}H NMR (600 MHz, $CDCl_3$) δ 6.82 (d, *J* = 8.0 Hz, 1H), 6.72 (d, *J* = 8.0 Hz, 1H), 6.59 (d, *J* = 2.1 Hz, 1H), 6.45 (dd, *J* = 8.1, 2.1 Hz, 1H), 5.50 (s, 1H), 4.78 (s, 1H), 3.76 (s, 2H), 3.71-3.77 (s, 3H), 3.09-2.88 (m, 2H), 1.44 (s, 9H).

^{13}C NMR (151 MHz, $CDCl_3$) δ 172.1, 169.9, 156.7, 143.9, 121.4, 116.9, 115.4, 81.1, 53.6, 52.7, 44.2, 36.9, 28.4 ppm.

HRMS (ESI) m/z calcd. for $C_{17}H_{24}N_2O_7$ ($[M+Na]^+$): 391.1469, found 391.1476.

R_f (CyHex/EtOAc, 3:2) = 0.33.

7.7 Chapter 3: Tyrosine Modification via Crosslinking strategies.

7.7.1 Synthesis and Characterisation of Starting Materials

(Boc-Ala-Gly-Cys-OMe)$_2$ (7.14)

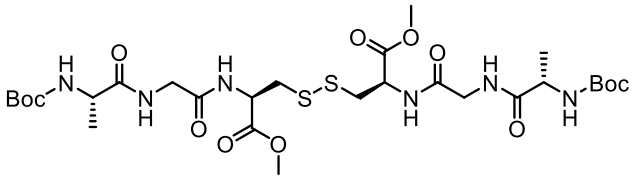

$C_{28}H_{48}N_6O_{12}S_2$
724.28 g/mol

Following a modified reported procedure, Boc-Ala-Gly-OH (1.00 g, 4.06 mmol, 1.0 equiv.) was dissolved in anhydrous DCM (40 mL) in a 100 mL oven-dried round-bottom flask. EDCI (0.93 g, 4.87 mmol, 1.2 equiv.) and N-hydroxy-2,5-pyrrolidinedione (HOSu, 0.56 g, 4.89 mmol, 1.2 equiv.) were added sequentially, and the mixture was stirred at room temp. for 30 min. To the activated solution was added (H-Cys-OMe)$_2$ (0.83 g, 2.44 mmol, 0.60 equiv), followed by DIPEA (0.86 mL, 4.88 mmol, 1.2 equiv.). The reaction mixture was stirred at r.t. for 6 h. The mixture was washed with 1 M HCl (2 ×), saturated $NaHCO_3$ (2 ×), and brine, dried over anhydrous Na_2SO_4, filtered, and concentrated under reduced pressure. The crude residue was purified by silica gel column chromatography in CyHex/EtoAc (1:4) to afford 7.14 compound as a white solid in 70% yield (1.04 g, 1.44 mmol).

^{1}H NMR (400 MHz, $CDCl_3$) δ 7.56 (d, *J* = 8.0 Hz, 2H), 7.50 (s, 2H), 5.60 (s, 2H), 4.81 (td, *J* = 7.9, 4.7 Hz, 2H), 4.26 (s, 2H), 4.04 (dd, *J* = 9.9, 5.8 Hz, 4H), 3.72 (s, 6H), 3.16 (dd, *J* = 14.3, 4.7 Hz, 2H), 3.01 (dd, *J* = 14.3, 8.0 Hz, 2H), 1.40 (s, 18H), 1.37 (d, *J* = 7.1 Hz, 6H) ppm.

^{13}C NMR (101 MHz, $CDCl_3$) δ 174.1, 170.7, 169.5, 155.8, 80.2, 52.9, 52.4, 50.4, 43.2, 40.7, 28.5, 18.7ppm.

IR (ATR): $\tilde{\nu}$ [cm-1] = 3330, 2971, 2939, 2830, 1665, 1466, 1409, 1379, 1341, 1305, 1161, 1128, 1028, 951, 817, 637.

HRMS (ESI+) m/z calcd. for $[M+H]^+$ $[C_{28}H_{49}N_6O_{12}S_2]^+$ 725.2772, found 725.2844.

R_f (EtOAc) = 0.2.

Boc-Ala-Gly-Cys-OMe (7.15)

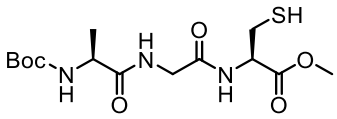

$C_{14}H_{25}N_3O_6S$
363.15 g/mol

Following a modified reported procedure,[250] in a 100 mL oven-dried round-bottom **7.14** (Boc-Ala-Gly-Cys-OMe)$_2$ (1.00 g, 1.38 mmol, 1.0 equiv.) was dissolved in DCM (30 mL). followed by *n*Bu$_3$P (1.35 mL, 5.52 mmol, 4.0 equiv.) and H_2O (0.14 mL). The reaction mixture was stirred at r.t. for 3 h. After completion of reaction, the crude residue was washed with brine. The organic layer was dried over Na_2SO_4, filtered, and concentrated under reduced pressure. The crude was purified by silica gel column chromatography in CyHex/EtOAc (1:1) to afford the reduced product **7.15** as colorless oil in 80% yield (401 mg, 1.10 mmol).

^{1}H NMR (400 MHz, DMSO-d_6) δ 8.46 – 7.78 (m, 2H), 6.93 (d, *J* = 7.3 Hz, 1H), 4.71 – 4.46 (m, 1H), 3.97 (q, *J* = 7.3 Hz, 1H), 3.87 – 3.70 (m, 2H), 3.65 (s, 3H), 2.90 – 2.70 (m, 2H), 2.46 (t, *J* = 8.6 Hz, 1H), 1.37 (s, 9H), 1.18 (d, *J* = 7.1 Hz, 3H) ppm.

^{13}C NMR (101 MHz, DMSO-d_6) δ 173.1, 170.5, 168.9, 155.2, 78.2, 54.4, 52.1, 49.7, 41.9, 28.2, 25.4, 18.0 ppm.

IR (ATR): $\tilde{\nu}$ [cm^{-1}] = 3436, 2971, 2251, 2125, 1744, 1672, 1530, 1453, 1366, 1249, 1169, 1052, 1023, 1004, 821, 758, 622.

HRMS (ESI) m/z calcd. for $C_{14}H_{25}N_3NaO_6S$ ([M+Na]$^+$): 386.1355, found 386.1356.

R_f (CyHex/EtOAc, 3:7) = 0.10 [$KMnO_4$].

7.7.2 Synthesis and Characterisation of Tyrosine-Cysteine Cross-linkage Products

General Procedure for tyrosine cross-linking (GP4)

An oven-dried 25 mL round-bottom flask equipped with a magnetic stir bar was charged with the tyrosine-containing starting material (400 µmol, 1.0 equiv.) and IBX (1.2 equiv.) in DMF (3.2 mL, 0.125 M) at 0 °C. The mixture was allowed to warm to rt and stirred for 4 h. A solution of N-acetyl-*L*-cysteine methyl ester (1.1 equiv.) in DMF/MeOH (0.8 mL, 0.25 M) and phosphate buffer (pH 7.2, 1 M, 0.8 mL) was added dropwise under N_2 at 0 °C, and the reaction was stirred for 16 h. The solvent was removed under reduced pressure, and the residue was diluted with EtOAc. The organic phase was washed sequentially with saturated $NaHCO_3$ solution, brine and dried over Na_2SO_4, filtered, and concentrated under reduced pressure. The crude residue was purified by flash column chromatography on silica gel to afford the desired product.

Methyl N-acetyl-S-(5-((S)-2-((tert-butoxycarbonyl)amino)-3-methoxy-3-oxopropyl)-2,3-dihydroxyphenyl)-*L*-cysteinate (3.1)

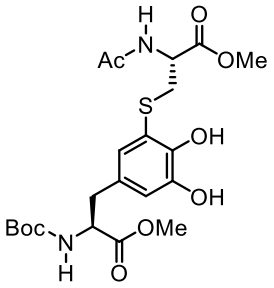

$C_{21}H_{30}N_2O_9S$
486.17 g/mol

Compound **3.1** was synthesized according to GP4 using **2.1** (118 mg, 400 µmol, 1.0 equiv.) and IBX (134 mg, 480 µmol, 1.2 equiv.) in DMF (3.2 mL). N-acetyl-*L*-cysteine methyl ester (77.9 mg, 440 µmol, 1.1 equiv.) in DMF (0.8 mL) and phosphate buffer (pH 7.2, 1 M, 0.8 mL) was then added. The crude reaction mixture was purified by flash column chromatography on silica gel eluting with CyHex/EtOAc (1:1) to afford **3.1** as a yellow solid in 55% (107 mg, 220 µmol).

^{1}H NMR (600 MHz, MeOD) δ 6.82 (d, *J* = 2.2 Hz, 1H), 6.72 (d, *J* = 2.1 Hz, 1H), 4.64 (dd, *J* = 7.3, 4.9 Hz, 1H), 4.40 (dd, *J* = 8.4, 5.7 Hz, 1H), 3.79 (s, 3H), 3.69 (s, 3H), 3.36 (dd, *J* = 14.0, 5.0 Hz, 1H), 3.28 (dd, *J* = 14.1, 7.4 Hz, 1H), 3.02 (dd, *J* = 13.9, 5.7 Hz, 1H), 2.86 (dd, *J* = 13.9, 8.5 Hz, 1H), 2.05 (s, 3H), 1.48 (s, 9H) ppm.

^{13}C NMR (151 MHz, MeOD) δ 174.2, 173.1, 172.4, 157.7, 146.5, 145.9, 129.7, 126.7, 120.4, 117.4, 80.7, 56.5, 53.7, 52.8, 52.6, 37.9, 36.5, 28.7, 22.4 ppm.

IR (ATR): $\tilde{\nu}$ [cm^{-1}] = 3351, 2980, 2487, 2219, 2135, 2071, 1737, 1685, 1653, 1586, 1479, 1424, 1367, 1280, 1222, 1166, 1119, 1062, 1017, 973, 834, 779.

HRMS (APCI) m/z calcd. for $C_{21}H_{29}N_2O_9S$ ([M-H]$^-$): 485.1598, found 485.1599.

R_f (CyHex/EtOAc, 95:5) = 0.42.

Methyl N-acetyl-S-(5-(2-((S)-2-((*tert*-butoxycarbonyl)amino)-3-(1*H*-indol-3-yl)propanamido)-3-methoxy-3-oxopropyl)-2,3-dihydroxyphenyl)-*L*-cysteinate (3.2)

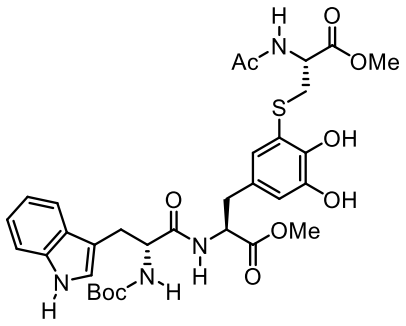

$C_{32}H_{40}N_4O_{10}S$
672.25 g/mol

Compound **3.2** was synthesized according to GP4 using **7.7** (199 mg, 400 µmol, 1.0 equiv.) and IBX (134 mg, 480 µmol, 1.2 equiv.) in DMF (3.2 mL). N-acetyl-*L*-cysteine ester (77.9 mg, 440 µmol, 1.1 equiv.) in DMF (0.8 mL) and phosphate buffer (pH 7.2, 1 M, 0.8 mL) was then added. The crude reaction mixture was purified by flash column chromatography on silica gel eluting with CyHex/EtOAc (1:1) to afford **3.2** as a yellow solid in 25% (67.6 mg, 100 µmol).

^{1}H NMR (400 MHz, MeOD) δ 7.65 (d, *J* = 7.8 Hz, 1H), 7.40 (d, *J* = 8.0 Hz, 1H), 7.20 – 7.10 (m, 2H), 7.08 (t, *J* = 7.5 Hz, 1H), 6.74 (s, 1H), 6.65 (s, 1H), 4.71 (t, *J* = 6.5 Hz, 2H), 4.60 (m, 2H), 4.45 (q, *J* = 9.6 Hz, 1H), 3.73 (s, 3H), 3.63 (s, 3H), 3.38 – 3.18 (m, 3H), 2.92 (d, *J* = 7.1 Hz, 2H), 2.01 (s, 3H), 1.43 (s, 9H) ppm.

^{13}C NMR (101 MHz, MeOD) δ 174.6, 173.2, 173.1, 172.5, 157.5, 146.6, 146.1, 138.1, 129.2, 128.9, 126.9, 124.6, 122.4, 120.4, 119.8, 117.5, 116.6, 112.3, 110.9, 80.8, 56.9, 55.0, 53.8, 52.9, 37.8, 36.5, 29.3, 28.6, 22.4 ppm.

IR (ATR): $\tilde{\nu}$ [cm^{-1}] =3364, 2977, 2953, 2493, 1737, 1655, 1593, 1454, 1434, 1367, 1279, 1223,1169, 1051, 1011, 744.

HRMS (ESI) m/z calcd. for $C_{32}H_{40}N_4NaO_{10}S$ ([M+Na]$^+$): 695.2358, found 695.2357.

R_f (DCM/MeOH, 95:5) = 0.28.

Benzyl (S)-2-((2-(((S)-3-(3-(((R)-2-acetamido-3-methoxy-3-oxopropyl)thio)-4,5-dihydroxyphenyl)-1-methoxy-1-oxopropan-2-yl)amino)-2-oxoethyl)carbamoyl)pyrrolidine-1-carboxylate (3.3)

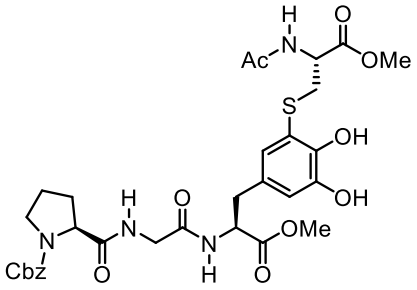

$C_{31}H_{38}N_4O_{11}S$
674.23 g/mol

Compound **3.3** was synthesized according to GP4 using **7.4** (193 mg, 400 µmol, 1.0 equiv.) and IBX (134 mg, 480 µmol, 1.2 equiv.) in DMF (3.2 mL). N-acetyl-*L*-cysteine ester (77.9 mg, 440 µmol, 1.1 equiv.) in DMF (0.8 mL) and phosphate buffer (pH 7.2, 1 M, 0.8 mL) was then added. The crude reaction mixture was purified by RP-HPLC (H_2O:MeCN 7:4 in 40 min.) Fractions containing the desired product were lyophilized to afford **3.3** as white solid in 17% (46.0 mg, 68.1 µmol).

^{1}H NMR (400 MHz, $CDCl_3$) δ 7.56 (s,1H), 7.31 (s, 5H), 6.80 (s, 1H), 6.71 (d, *J* = 5.6 Hz, 2H), 6.62 – 6.58 (m, 1H), 5.12 (s, 1H), 5.00 (d, *J* = 12.6 Hz, 1H), 4.82 – 4.70 (m, 2H), 4.31 (t, *J* = 6.2 Hz, 1H), 4.01 (d, *J* = 17.4 Hz, 1H), 3.87 (dd, *J* = 16.8, 5.5 Hz, 1H), 3.71 (s, 3H), 3.61 (s, 3H), 3.56 (dt, *J* = 7.4, 3.3 Hz, 1H), 3.49 (q, *J* = 5.9 Hz, 1H), 3.32 (dd, *J* = 14.2, 4.6 Hz, 1H), 3.21 (dd, *J* = 14.2, 6.0 Hz, 1H), 3.07 – 2.98 (m, 1H), 2.89 (dd, *J* = 14.6, 7.2 Hz, 1H), 2.15 – 2.07 (m, 2H), 1.90 (s, 3H), 1.84 (dd, *J* = 12.5, 6.6 Hz, 1H) ppm.

^{13}C NMR (101 MHz, $CDCl_3$) δ 173.2, 171.8, 171.1, 170.8, 169.1, 156.1, 144.6, 136.3, 128.6, 128.3, 127.9, 126.9, 118.6, 117.7, 61.1, 53.5, 52.9, 52.8, 52.6, 47.3, 43.1, 36.9, 36.6, 29.7, 24.7, 22.8 ppm.

IR (ATR): $\tilde{\nu}$ [cm^{-1}] =3305, 2954, 2471, 2069, 1739, 1649, 1589, 1536,1427, 1356, 1276, 1214, 1179, 1121, 1026, 981, 919, 871, 771, 741, 699, 612.

HRMS (ESI) m/z calcd. for $C_{31}H_{37}N_4O_{11}S$ ([M-H]$^-$): 673.2182, found 673.2185.

R_f (DCM/MeOH, 95:5) = 0.24.

Methyl N-acetyl-S-(5-((S)-2-((S)-2-(2-(((benzyloxy)carbonyl)amino)acetamido)-3-phenylpropanamido)-3-methoxy-3-oxopropyl)-2,3-dihydroxyphenyl)-*L*-cysteinate (3.4)

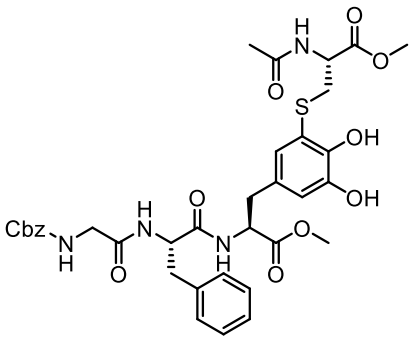

$C_{35}H_{40}N_4O_{11}S$
724.24 g/mol

Compound **3.4** was synthesized according to GP4 using **7.5** (213 mg, 400 µmol, 1.0 equiv.) and IBX (134 mg, 480 mmol, 1.2 equiv.) in DMF (3.2 mL). N-acetyl-*L*-cysteine methyl ester (77.9 mg, 440 µmol, 1.1 equiv.) in DMF (0.8 mL) and phosphate buffer (pH 7.2, 1 M, 0.8 mL) was then added. The crude reaction mixture was purified by flash column chromatography on silica gel eluting with DCM/MeOH (95:5) to afford **3.4** as a pink solid in 22% (63.8 mg, 88.0 µmol).

^{1}H NMR (400 MHz, $CDCl_3$) δ 7.33 – 7.27 (m, 6H), 7.20 – 7.06 (m, 7H), 6.81 (d, *J* = 7.6 Hz, 1H), 6.68 (s, 1H), 6.56 (d, *J* = 2.0 Hz, 1H), 5.92 (s, 1H), 5.07 (s, 2H), 4.88 – 4.65 (m, 3H), 3.90 – 3.73 (m, 2H), 3.68 (s, 3H), 3.60 (s, 3H), 3.33 – 2.77 (m, 6H), 1.88 (s, 3H).ppm.

^{13}C NMR (101 MHz, $CDCl_3$) δ 171.6, 171.2, 171.1, 171.0, 170.0, 157.0, 144.5, 144.4, 136.4, 136.2, 129.4, 128.6, 128.6, 128.3, 128.1, 127.0, 126.8, 118.7, 117.8, 67.4, 54.4, 53.5, 52.9, 52.8, 52.6, 44.4, 38.1, 36.9, 36.8, 22.8.ppm.

IR (ATR): $\tilde{\nu}$ [cm^{-1}] =3305, 3066, 2953, 2252, 1734, 1653, 1518, 1437, 1373, 1346, 1216, 1177, 1128, 1047, 904, 725, 648.

HRMS (ESI) m/z calcd. for $C_{35}H_{39}N_4O_{11}S$ ($[M-H]^-$): 723.2343, found 723.2342.

R_f (DCM/MeOH, 95:5) = 0.24.

Methyl (6S,12R)-12-(((5-((S)-2-((S)-5-(tert-butoxy)-2-((tertbutoxycarbonyl)amino)-5-oxopentanamido)-3-((2-methoxy-2-oxoethyl)amino)-3-oxopropyl)-2,3-dihydroxyphenyl)thio)methyl)-2,2,6-trimethyl-4,7,10-trioxo-3-oxa-5,8,11-triazatridecan-13-oate (3.5)

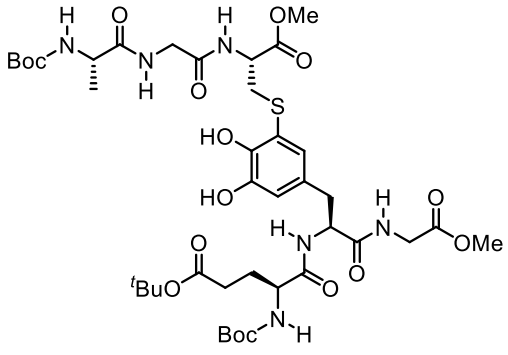

$C_{40}H_{62}N_6O_{16}S$
914.39 g/mol

Compound **3.5** was synthesized according to GP4 using **7.15** (108 mg, 200 µmol, 1.0 equiv.) and IBX (67.2 mg, 240 µmol, 1.2 equiv.) in DMF (1.6 mL). S14 (80.0 mg, 220 µmol, 1.1 equiv.) in DMF (0.4 mL) and phosphate buffer (pH 7.2, 1 M, 0.4 mL) was then added. The crude reaction mixture was purified by RP-HPLC (H_2O: MeCN 7:3 in 40 min.) Fractions containing the desired product were lyophilized to afford **3.5** as white solid in 17% (31.3 mg, 34.2 µmol).

^{1}H NMR (400 MHz, MeOD) δ 6.95 – 6.78 (m, 1H), 6.76 – 6.67 (m, 1H), 4.72 (dd, *J* = 7.7, 6.1 Hz, 1H), 4.64 – 4.55 (m, 1H), 4.23 – 4.17 (m, 1H), 4.11 (d, *J* = 6.4 Hz, 1H), 4.04 – 4.00 (m, 2H), 3.99 (s, 1H), 3.80 (s, 3H), 3.67 (s, 3H), 3.31 (dd, *J* = 14.0, 7.5 Hz, 1H), 3.09 (dd, *J* = 14.0, 6.1 Hz, 1H), 2.95 (dd, *J* = 13.8, 7.8 Hz, 1H), 2.34 (t, *J* = 7.6 Hz, 2H), 2.03 (dtd, *J* = 13.1, 7.7, 5.4 Hz, 1H), 1.88 (ddd, *J* = 13.9, 8.7, 6.9 Hz, 2H), 1.54 – 1.50 (m, 27H), 1.44 (dd, *J* = 7.2, 3.1 Hz, 4H), 1.39 – 1.34 (m, 1H) ppm.

^{13}C NMR (101 MHz, MeOD) δ 176.3, 174.3, 174.1, 174.1, 173.7, 172.3, 171.5, 158.0, 157.9, 146.5, 146.0, 129.7, 126.9, 120.1, 117.8, 81.8, 81.0, 80.8, 55.5, 53.6, 52.9, 52.7, 51.8, 43.4, 42.0, 38.0, 36.3, 32.7, 28.8, 28.7, 28.4, 18.3 ppm.

IR (ATR): $\tilde{\nu}$ [cm^{-1}] =3323, 2978, 2934, 2477, 1653, 1524, 1437, 1394, 1367, 1249, 1220, 1161, 1048, 1028, 847, 781.

HRMS (APCI) m/z calcd. for $C_{40}H_{63}N_6O_{16}S$ ([M+H]$^+$): 915.4013, found 915.4016.

R_f (DCM/MeOH, 95:5) = 0.22.

7.8 Chapter 4: Development of Fluorogenic *o*-Quinone Platforms for Selective Cysteine Labeling in Peptides

7.8.1 Synthesis and Characterisation of Starting Materials and Products

General Procedure for Products (GP5)

An oven-dried flask equipped with a magnetic stir bar was charged with **Tag A or Tag B** (1.0 equiv.) in DMF (0.125 M) at 0 °C. The tag was oxidized with IBX (1.2 equiv.) at 0 °C, and the reaction mixture was allowed to warm to room temperature and stirred for 4 h to ensure complete oxidation.

In another oven-dried 25 mL round-bottom flask, the cysteine-containing starting material (400 µmol, 1.0 equiv.) was dissolved in DMF (1.6 mL, 0.25 M) at 0 °C under N_2. Phosphate buffer (pH 7.2, 1.0 M, 1.6 mL) was then added.

The freshly prepared oxidized tag solution was transferred via cannula from one flask to the cysteine-containing flask at 0 °C, and the resulting reaction mixture was stirred for 16 h under N_2.The solvent was removed under reduced pressure, and the residue was diluted with EtOAc. The organic phase was washed sequentially with saturated $NaHCO_3$ solution, brine, dried over Na_2SO_4, filtered, and concentrated under reduced pressure. The crude residue was purified by flash column chromatography on silica gel to afford the desired product.

5-(Dimethylamino)-*N*-(4-hydroxyphenethyl)naphthalene-2-sulfonamide (4.3)

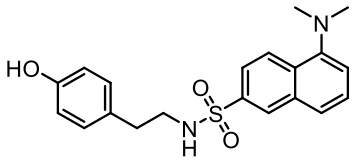

$C_{20}H_{22}N_2O_3S$
370.14 g/mol

Following a reported procedure, a flame-dried, N_2-purged flask containing a solution of tyramine (1.10 g, 8.02 mmol) in absolute MeOH (22 mL) was treated dropwise with a solution of dansyl chloride (2.59 g, 9.62 mmol) in DCM (22 mL) while stirring vigorously at room temperature. The highly fluorescent solution was stirred for an additional 16 h at room temperature and protected from UV light during this time. After completion of the reaction (monitored by TLC), the reaction mixture was washed with brine, saturated $NaHCO_3$ solution, and brine. The organic phase was collected, dried over Na_2SO_4, and the solvent was removed under reduced pressure. The crude product was purified by flash column chromatography on silica gel (DCM/MeOH 95:5) to afford **4.3** as a yellow-green solid (1.00 g, 2.70 mmol, 34%). Characterization data were in accordance with literature.[203]

^{1}H NMR (600 MHz, $CDCl_3$) δ 8.54 (d, *J* = 8.5 Hz, 1H), 8.22 (dd, *J* = 7.3, 1.1 Hz, 1H), 8.16 (d, *J* = 8.7 Hz, 1H), 7.57 – 7.41 (m, 2H), 7.18 (d, *J* = 7.6 Hz, 1H), 6.74 (d, *J* = 7.9 Hz, 2H), 6.60 (d, *J* = 8.0 Hz, 2H), 5.52 (s, 1H), 4.72 (td, *J* = 6.2, 1.9 Hz, 1H), 3.13 (q, *J* = 6.6 Hz, 2H), 2.90 (s, 6H), 2.56 (t, *J* = 6.9 Hz, 2H) ppm.

^{13}C NMR (151 MHz, $CDCl_3$) δ 154.6, 134.7, 130.5, 129.8, 129.7, 129.7, 129.4, 128.5, 123.4, 118.9, 115.6, 115.4, 45.6, 44.6, 34.8 ppm.

IR (ATR): $\tilde{\nu}$ [cm^{-1}] = 3054, 2898, 2807, 1995, 1602, 1581, 1540, 1491, 1421, 1377, 1342, 1264, 961, 926, 859, 729, 702.

HRMS (APCI) m/z calcd. for $C_{20}H_{23}N_2O_3S$ ($[M+H]^+$): 371.1422, found 371.1424.

R_f (DCM/MeOH, 95:5) = 0.47.

A stock solution of compound **4.3** was prepared in methanol (MeOH) to obtain a final concentration of 5 µM. From this stock, 4 mL aliquots were transferred into quartz cuvettes (1 cm path length) for spectroscopic measurements. The UV-Vis absorption spectrum of the solution was first recorded to determine the maximum absorption wavelength (λ_max). Based on the absorption data, fluorescence emission measurements were performed. For compound **4.3**, fluorescence emission was recorded in MeOH using an excitation wavelength of 330 nm. The emission maximum was observed at 536 nm. The emission spectra were normalized for comparison purposes. The normalized emission spectra are shown in Figure 7.3, and the corresponding maximum absorption wavelengths are summarized in nanometers (nm).

All measurements were carried out at room temperature.

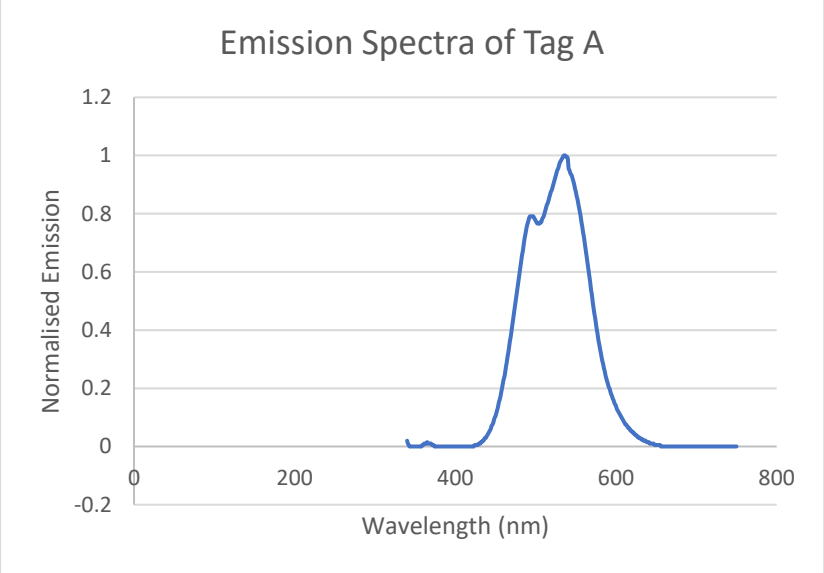

Figure 7.3: Normalized fluorescence emission spectrum of compound **4.3** in MeOH (5 µM), recorded with excitation at 330 nm.

N-(3,4-dihydroxyphenethyl)-5-(dimethylamino)naphthalene-2-sulfonamide (7.16)

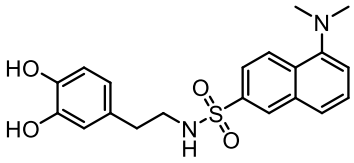

$C_{20}H_{22}N_2O_4S$
386.13 g/mol

Compound **7.16** was obtained as a side product during the synthesis of compound **4.8** according to GP5. In an oven-dried flask equipped with a magnetic stir bar, **Tag A (**370 mg, 1.00 mmol, 1.0 equiv.) was dissolved in DMF (8 mL) and oxidized with IBX (336 mg, 1.20 mmol, 1.2 equiv.) at 0 °C. The reaction mixture was stirred and allowed to warm to room temperature over 4 h to ensure complete oxidation. In another oven-dried flask, *N*-acetyl-*L*-cysteine methyl ester (177 mg, 1.00 mmol, 1.0 equiv.) was dissolved in DMF (2 mL), and phosphate buffer (pH 7.2, 1 M, 2 mL) at 0 °C.

The freshly prepared oxidized tag solution was added dropwise to the cysteine-containing solution at 0 °C, and the reaction mixture was stirred for 16 h under N_2. After completion, the crude mixture was purified by flash column chromatography on silica gel (DCM/MeOH, 95:5), affording compound **7.16** as a yellow solid in 30% yield (116 mg, 300 µmol).

^{1}H NMR (600 MHz, MeOD) δ 8.57 (dt, *J* = 8.5, 1.1 Hz, 1H), 8.36 (dt, *J* = 8.7, 1.0 Hz, 1H), 8.21 (dd, *J* = 7.3, 1.3 Hz, 1H), 7.58 (dt, *J* = 8.6, 7.3 Hz, 2H), 7.28 (dd, *J* = 7.6, 0.9 Hz, 1H), 6.60 (d, *J* = 8.0 Hz, 1H), 6.52 (d, *J* = 2.1 Hz, 1H), 6.31 (dd, *J* = 8.0, 2.1 Hz, 1H), 3.11 – 3.03 (m, 2H), 2.89 (s, 6H), 2.52 (dd, *J* = 8.5, 6.7 Hz, 2H) ppm.

^{13}C NMR (151 MHz, MeOD) δ 153.1, 146.1, 144.7, 137.0, 131.3, 131.2, 131.1, 130.9, 130.0, 129.0, 124.2, 120.9, 120.5, 116.7, 116.4, 116.3, 45.8, 36.5 ppm.

R_f (DCM/MeOH, 95:5) = 0.55

Methyl *N*-acetyl-S-(5-(2-((5-(dimethylamino)naphthalene)-2-sulfonamido)ethyl)-2,3-dihydroxyphenyl)-*L*-cysteinate (4.8)

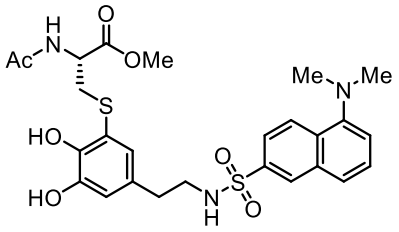

$C_{26}H_{31}N_3O_7S_2$
561.16 g/mol

Compound **4.8** was synthesized according to GP5. In an oven-dried flask, **Tag A** (370 mg, 1.00 mmol, 1.0 equiv.) was dissolved in DMF (8 mL) and oxidized with IBX (336 mg, 1.20 mmol, 1.2 equiv.) at 0 °C. The reaction mixture was stirred and allowed to warm to room temperature over 4 h to ensure complete oxidation.

In another oven-dried flask, N-acetyl-*L*-cysteine methyl ester (177 mg, 1.00 mmol, 1.0 equiv.) was dissolved in DMF (2 mL) and phosphate buffer (pH 7.2, 1 M, 2 mL) at 0 °C.

The freshly prepared oxidized Tag A solution was then added to the cysteine-containing reaction mixture at 0 °C. After completion, the crude reaction mixture was purified by flash column chromatography on silica gel (DCM/MeOH, 95:5), affording compound **4.8** as a yellow solid in 36% yield (202 mg, 360 µmol).

^{1}H NMR (600 MHz, MeOD) δ 8.66 – 8.53 (m, 1H), 8.37 (d, *J* = 8.7 Hz, 1H), 8.23 (dd, *J* = 7.3, 1.3 Hz, 1H), 7.61 (ddd, *J* = 8.7, 7.4, 5.1 Hz, 2H), 7.32 (d, *J* = 7.5 Hz, 1H), 6.59 (d, *J* = 2.1 Hz, 1H), 6.52 (d, *J* = 2.1 Hz, 1H), 4.57 (dd, *J* = 7.5, 5.0 Hz, 1H), 3.66 (m,1H) 3.62 (s, 3H), 3.28 (dd, *J* = 14.0, 4.9 Hz, 1H), 3.18 (dd, *J* = 14.0, 7.6 Hz, 1H), 3.11 (t, *J* = 7.2 Hz, 2H), 2.94 (s, 6H), 2.85 (d, *J* = 0.8 Hz, 1H), 2.54 (t, *J* = 7.3 Hz, 1H), 1.99 (s, 3H) ppm.

^{13}C NMR (151 MHz, MeOD) δ 173.16, 172.43, 146.40, 145.41, 137.07, 131.43, 131.06, 130.98, 130.88, 130.05, 129.02, 126.09, 124.31, 120.73, 120.15, 53.66, 52.78, 36.37, 36.33, 22.35 ppm.

HRMS (ESI) m/z calcd. for $C_{26}H_{31}N_3NaO_7S_2$ ($[M+Na]^+$): 584.1492, found 584.1496.

R_f (DCM/MeOH, 97:3) = 0.4.

Methyl *N*-(*tert*-butoxycarbonyl)-*L*-alanylglycyl-S-(5-(2-((5-(dimethylamino)naphthalene)-1-sulfonamido)ethyl)-2,3-dihydroxyphenyl)-*L*-cysteinate (4.9)

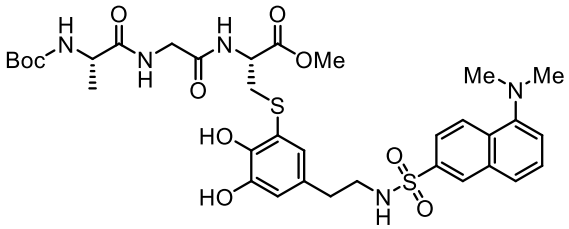

$C_{34}H_{45}N_5O_{10}S_2$
747.26 g/mol

Compound **4.9** was synthesized according to GP5. In an oven-dried flask equipped with a magnetic stir bar, **Tag A** (370 mg, 1.00 mmol, 1.0 equiv.) was dissolved in DMF (8 mL) and oxidized with IBX (336 mg, 1.20 mmol, 1.2 equiv.) at 0 °C. The reaction mixture was stirred and allowed to warm to room temperature to ensure complete oxidation.

In another oven-dried flask, compound **7.15** (364 mg, 1.00 mmol, 1.0 equiv.) was dissolved in DMF (2 mL), and phosphate buffer (pH 7.2, 1 M, 2 mL) was added at 0 °C.

The freshly prepared oxidized **Tag A** solution was then added to the **7.15** reaction mixture at 0 °C. After completion, the crude reaction mixture was purified by flash column chromatography on silica gel (DCM/MeOH, 95:5), affording compound **4.9** as a yellow solid in 30% yield (224 mg, 300 µmol).

^{1}H NMR (600 MHz, $CDCl_3$) δ 8.48 (d, *J* = 8.4 Hz, 1H), 8.24 (d, *J* = 8.6 Hz, 1H), 8.17 (d, *J* = 7.0 Hz, 1H) 7.67 – 7.32 (m, 5H), 7.26 (s, 2H), 7.11 (d, *J* = 7.5 Hz, 1H), 6.65 (s, 1H), 6.54 (s, 1H), 6.00 (s, 1H), 5.62 (s, 1H), 4.63 (d, *J* = 6.8 Hz, 1H), 4.23 (s, 1H), 4.06 – 3.81 (m, 2H), 3.50 (s, 3H), 3.22 (s, 2H), 3.08 (s, 2H), 2.83 (s, 6H), 2.50 (s, 2H), 1.35 (s, 12H) ppm.

^{13}C NMR (151 MHz, $CDCl_3$) δ 174.3, 170.6, 169.6, 155.8, 151.8, 144.6, 144.0, 135.1, 130.7, 130.3, 129.8, 129.5, 129.2, 126.4, 123.1, 119.0, 118.3, 117.0, 115.2, 80.3, 52.7, 52.4, 50.5, 45.4, 44.1, 43.0, 36.9, 35.2, 28.3, 18.4 ppm.

R_f (DCM/MeOH, 95:5) = 0.36.

Methyl *N*-acetyl-S-(3,4-dioxo-3,4-dihydronaphthalen-1-yl)-*L*-cysteinate (4.11)

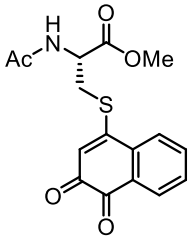

$C_{16}H_{15}NO_5S$
333.07 g/mol

Compound **4.11** was synthesized according to GP5. In an oven-dried flask equipped with a magnetic stir bar, **Tag B** (144 mg, 1.00 mmol, 1.0 equiv.) was dissolved in DMF (8 mL) and oxidized with IBX (336 mg, 1.20 mmol, 1.2 equiv.) at 0 °C. The reaction mixture was stirred and allowed to warm to room temperature to ensure complete oxidation.

In another oven-dried flask, *N*-acetyl-*L*-cysteine methyl ester (177 mg, 1.00 mmol, 1.0 equiv.) was dissolved in DMF (2 mL), and phosphate buffer (pH 7.2, 1 M, 2 mL) was added at 0 °C. The freshly prepared oxidized **Tag B** solution was then added to the cysteine-containing reaction mixture at 0 °C. After completion, the crude mixture was purified by flash column chromatography on silica gel (cyclohexane/EtOAc, 3:2), affording compound **4.11** as a red solid in 24% yield (82.3 mg, 250 µmol).

^{1}H NMR (400 MHz, DMSO) δ 8.65 (d, *J* = 7.9 Hz, 1H), 8.00 (ddd, *J* = 7.6, 1.4, 0.6 Hz, 1H), 7.83 – 7.74 (m, 2H), 7.65 (ddd, *J* = 7.6, 6.6, 2.0 Hz, 1H), 6.48 (s, 1H), 4.67 (ddd, *J* = 8.7, 7.8, 4.9 Hz, 1H), 3.70 (s, 3H), 3.58 (dd, *J* = 13.6, 5.0 Hz, 1H), 3.40 (dd, *J* = 13.6, 8.7 Hz, 1H), 1.88 (s, 3H) ppm.

^{13}C NMR (101 MHz, DMSO) δ 178.5, 175.8, 170.4, 169.7, 156.2, 135.1, 133.0, 131.2, 130.5, 128.4, 124.9, 120.4, 52.5, 50.4, 32.0, 22.3 ppm.

IR (ATR): $\tilde{\nu}$ [cm^{-1}] = 2953, 1751, 1733, 1694, 1682, 1646, 1580, 1527, 1450, 1434, 1372, 1324, 1294, 1248, 1218, 1169, 1126, 1044, 1011, 972, 943, 883, 860, 849, 806, 769, 724, 707, 660, 629.

LCMS (ESI) m/z calcd. for $C_{16}H_{15}NO_5S$ ([M+H]$^+$): 334.07, found 334.10.

R_f (CyHex/EtOAc, 1:1) = 0.40.

Methyl *N*-(*tert*-butoxycarbonyl)-*L*-alanylglycyl-S-(3,4-dioxo-3,4-dihydronaphthalen-1- yl)-*L*-cysteinate (4.12)

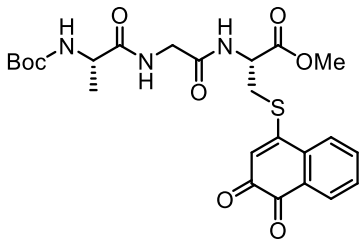

$C_{24}H_{29}N_3O_8S$
519.17 g/mol

Compound **4.12** was synthesized according to GP5. In an oven-dried flask equipped with a magnetic stir bar, **Tag B** (144 mg, 1.00 mmol, 1.0 equiv.) was dissolved in DMF (8 mL) and oxidized with IBX (336 mg, 1.20 mmol, 1.2 equiv.) at 0 °C. The reaction mixture was stirred and allowed to warm to room temperature to ensure complete oxidation.

In another oven-dried flask, **compound 7.15** (364 mg, 1.00 mmol, 1.0 equiv.) was dissolved in DMF (2 mL), and phosphate buffer (pH 7.2, 1 M, 2 mL) was added at 0 °C.

The freshly prepared oxidized **Tag B** solution was then added to the 7.15 reaction mixture at 0 °C. After completion, the crude reaction mixture was purified by flash column chromatography on silica gel (cyclohexane/EtOAc, 3:2), affording compound **4.12** as a red solid in 24% yield (125 mg, 240 µmol).

^{1}H NMR (400 MHz, MeOD) δ 8.15 – 7.45 (m, 4H), 6.45 (s, 1H), 4.77 (s, 3H), 4.17 – 3.21 (m, 8H), 1.41 (s, 9H), 1.36 – 1.30 (m, 3H) ppm.

^{13}C NMR (101 MHz, MeOD) δ 180.3, 177.4, 176.1, 171.7, 171.2, 159.9, 157.8, 136.3, 134.5, 132.4, 131.5, 129.8, 126.4, 121.0, 80.6, 79.4, 53.4, 51.9, 51.7, 49.6, 49.4, 49.2, 49.0, 48.8, 48.6, 48.4, 43.3, 33.6, 28.7, 18.1 ppm.

R_f (CyHex/EtOAc, 1:1) = 0.42.

7.9 Chapter 5: Oxidative rearrangement of tertiary allylic alcohol using an immobilized hypervalent iodine catalyst

7.9.1 Synthesis and Characterisation of Starting Materials

SP-IBS I was prepared according to our previously reported procedure.[243,245]

Stock solutions

Fmoc-Ala-OH (A, 0.51 M in DMF)

HBTU (B, 0.49 M in DMF)

DIPEA (C, 2.04 M in NMP)

Piperidine (D, 40% v/v in DMF)

Preparation of polystyrene-ethylamine gel

Polystyrene-ethylamine resin (200 µmol) was swollen in DCM (2 mL) for 10 min in a 10 mL polypropylene reactor. Five such reactions were conducted in parallel to reach a total of 1000 µmol of resin. The solvent was subsequently removed by suction using the peptide synthesizer.

Peptide coupling

Fmoc-Ala-OH (1.6 mL, 800 µmol, 4 equiv.) was added to the swollen resin. HBTU solution B (1.7 mL, 800 µmol, 4 equiv.) and DIPEA solution C (1.2 mL, 800 µmol, 4 equiv.) were added, and the mixture was vortexed for 40 min (15 s vortex, 2 min rest cycles). The solvent was removed by suction, and the resin was washed with DMF (3 × 2 mL).

Fmoc deprotection

Piperidine solution D (2.4 mL, 9.2 mmol, 48 equiv.) was added to the resin and vortexed for 3 min (15 s vortex, 1 min break). After removing the solvent by suction, a mixture of piperidine solution D (1.2 mL, 4.6 mmol, 24 equiv.) and DMF (1.2 mL) was added, and the resin was vortexed for 12 min (15 s vortex, 2 min break). The solvent was removed, and the resin was washed thoroughly with DMF (6 × 2 mL).

Theoretical loading

The theoretical loading was calculated according to equation 1:

$$\boldsymbol{theo.Loading}\left(\frac{mmol}{g}\right) = \boldsymbol{B}\left(\frac{mmol}{g}\right).\frac{1000}{\left(1000 + \left(\boldsymbol{B}\left(\frac{mmol}{g}\right).(\boldsymbol{M} - 18)\right)\right)}$$

where ***B*** represents the initial resin loading, and ***M*** is the molecular weight of the amino acid chain with protective groups.

Coupling of IBS catalyst to solid support

PC-IBS (210 mg, 600 µmol, 3 equiv.) and HATU (228 mg, 600 µmol, 3 equiv.) were combined in DMSO (2 mL), followed by DIPEA solution C (1.2 mL, 800 µmol, 4 equiv.). The mixture was vortexed for 24 h (15 s vortex, 2 min break). Afterward, the solvent was removed by suction, and the resin was washed with DMSO (4 × 2 mL) and DCM (6 × 2 mL).

Final end-capping

A mixture of DCM (2 mL) and acetic anhydride (1.89 mL, 20 mmol, 100 equiv.) was added to the resin and vortexed for 4 h. The resin was filtered by suction and washed sequentially with DMF (3 × 2 mL) and DCM (6 × 2 mL).

Determination of catalyst loading

Solid-supported catalysts I was oxidized as described previously. Preoxidized SP-IBS I (30 mol%) was added to L-(−)-borneol (4.56 mg, 29 µmol, 1 equiv.) in acetonitrile (0.2 mL, 0.15 M) and stirred at 70 °C for 18 h. The mixture was filtered, and the filtrate analyzed by GC-FID. The observed conversion was divided by the theoretical maximum (30%) to determine the actual loading in mmol/g.

Catalyst cartridge information

Catalyst cartridges were prepared following previous method.[243] Reactor volumes were determined by weighing the cartridge before and after solvent filling. The difference in mass divided by the solvent density gave the reactor volume. For clarity, the average packed-bed volumes of polystyrene-supported IBS (3.6 mL) is used throughout.

Synthesis of Tetrabutylammonium Peroxomonosulfate

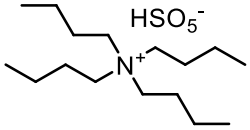

Following a modified literature procedure,[251] Oxone® (51.8 g, 169 mmol, 1.1 equiv.) was dissolved in water (519 mL, 0.3 M). Tetrabutylammonium hydrogen sulfate (52.0 g, 153 mmol, 1.0 equiv.) was added, and the mixture was stirred at room temperature for 30 min. DCM) was then added, and the phases were separated. The aqueous layer was extracted twice with DCM, and the combined organic extracts were dried over sodium sulfate and concentrated under reduced pressure. The residue was washed with hexane and dried under reduced pressure to afford tetrabutylammonium peroxomonosulfate (51.8 g, 146 mmol, 92% yield, 91% purity).

The peroxo content was determined by iodometric titration. An aqueous iodide solution (10 wt% sodium iodide in water) and an aqueous sodium thiosulfate solution (1.27 g in 50 mL water) were prepared. A sample of the synthesized tetrabutylammonium peroxomonosulfate (150 mg) was dissolved in anhydrous acetic acid (1 mL), followed by addition of the iodide solution (2 mL). The mixture was diluted with THF to a total volume of 10 mL and titrated with the sodium thiosulfate solution until the yellow color disappeared. The peroxo content was calculated from the volume of sodium thiosulfate consumed.

Sodium 2-iodo-5-methylbenzenesulfonate (5.1)

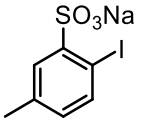

$C_7H_6INaO_3S$
319.90 g/mol

Following a previously reported method,[243] 2-amino-5-methylbenzenesulfonic acid (10.0 g, 53.4 mmol, 1.0 equiv.) was placed in an oven-dried round-bottom flask equipped with a magnetic stir bar and suspended in concentrated hydrochloric acid (20 mL, 37%, 245 mmol, 4.6 equiv.) containing crushed ice (40 g). Aqueous sodium nitrite (4.05 g, 58.8 mmol, 1.1 equiv. in 20 mL water) was added dropwise over 40 min at 0 °C, ensuring the internal temperature did not exceed 5 °C to minimize nitrous gas evolution. The resulting diazonium suspension was stirred at this temperature for an additional 40 min. Next, a solution of sodium iodide (9.61 g, 64.1 mmol, 1.2 equiv. in 20 mL water) was added gradually at 0 °C, keeping the temperature below 5 °C. After complete addition, the reaction was stirred at 0 °C for 1 h and then allowed to reach room temperature over another hour. The mixture was subsequently heated at 50 °C for 12 h. Cooling the reaction in a refrigerator for approximately 3 h led to the precipitation of a yellowish solid, which was collected by filtration and washed sequentially with cold ethanol and a cold 1:1 mixture of methanol and diethyl ether (20 mL). The filtrate was concentrated and cooled again to afford a second portion of solid, which was isolated in the same manner. The combined solids provided sodium 2-iodo-4-methylbenzenesulfonate as a yellowish solid in 50% yield (8.6 g, 26.7 mmol).

^{1}H NMR (600 MHz, DMSO) δ 7.78 – 7.71 (m, 1H), 6.86 – 6.79 (m, 1H), 2.25 (s, 1H) ppm.

^{13}C NMR (151 MHz, DMSO) δ 149.9, 140.5, 136.8, 130.6, 128.8, 89.2, 20.4ppm.

HRMS (ESI) m/z calcd. for $C_7H_6INa_2O_3S$ ($[M+H]^+$): 342.8872, found 342.8872.

Sodium 5-carboxy-2-iodobenzenesulfonate (5.2)

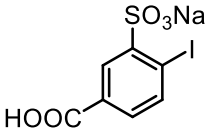

$C_7H_4INaO_5S$
349.87 g/mol

Following a reported procedure,[243] sodium hydroxide (3.15 g, 78.7 mmol, 2.4 equiv.) was dissolved in water (256 mL, 0.13 M) in an oven-dried round-bottom flask equipped with a magnetic stir bar. Sodium 2-iodo-5-methylbenzenesulfonate 2.1 (10.5 g, 32.8 mmol, 1.0 equiv.) was added, and the solution was heated to 40 °C. Potassium permanganate (15.6 g, 98.4 mmol, 3.0 equiv.) was introduced portion wise at 10 min intervals. The mixture was then heated to 75-80 °C and stirred at this temperature for 16 h. Upon completion, the reaction was quenched by adding a 1:1 mixture of methanol and water (1.1 mL) at 60 °C. The reaction mixture was cooled to 35-40 °C and filtered to remove manganese dioxide. The filtrate was acidified to pH 1 with concentrated HCl, causing precipitation of the product, which was collected by suction filtration and washed with minimal cold acetonitrile and diethyl ether. Roughly, one-third of the filtrate volume was removed under reduced pressure, and the remaining solution was cooled to 0 °C and stirred for 3-4 h. The resulting solid was collected by filtration, washed with cold acetonitrile and diethyl ether, and dried under high vacuum to afford sodium 4-carboxy-2-iodobenzenesulfonate as a fluffy white solid in 90% yield (10.3 g, 29.5 mmol).

^{1}H NMR (400 MHz, DMSO) δ 13.10 (s, 1H), 8.44 (d, *J* = 2.2 Hz, 1H), 8.02 (d, *J* = 8.0 Hz, 1H), 7.50 (dd, *J* = 8.0, 2.2 Hz, 1H) ppm.

^{13}C NMR (101 MHz, DMSO) δ 166.9, 150.7, 141.4, 130.1, 128.5, 99.7 ppm.

HRMS (APCI) m/z calcd. for $C_7H_4INa_2O_5S$ ($[M+H]^+$): 372.8614, found 372.8614.

1-Hydroxy-1λ³-benzo[d][1,2]iodaoxol-3(1H)-one (7.17)

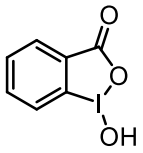

$C_7H_5IO_3$
263.93 g/mol

Following a reported procedure,[252] in a 250 mL round bottom flask, 2-iodobenzoic acid (3.00 g, 12.1 mmol, 1.0 equiv.) and oxone (8.92 g, 14.5 mmol, 1.2 equiv.) was dissolved in 60 mL water and 60 mL of dioxane, and stirred at room temperature for 1 h. The resulting solid was filtered and washed several times with ice cold water and ice-cold acetone. After drying under high vacuum, **7.17** was obtained as a solid in 80% yield (2.55 g, 9.68 mmol).

^{1}H NMR (400 MHz, DMSO) δ 8.09 – 7.92 (m, 3H), 7.84 (dd, *J* = 8.1, 1.0 Hz, 1H), 7.72 (dtd, *J* = 22.3, 7.2, 1.1 Hz, 1H) ppm.

^{13}C NMR (101 MHz, DMSO) δ 167.8, 134.5, 131.5, 131.1, 130.4, 126.3, 120.5 ppm.

IR (ATR): $\tilde{\nu}$ [cm^{-1}] = 3082, 3059, 2868, 2402, 2171, 2154, 1606, 1583, 1563, 1452, 1441, 1339, 1301, 1148, 1112, 1018, 838, 740, 695, 675, 649, 614, 582.

1-Methoxy-1l3-benzo[d][1,2]iodaoxol-3(1H)-one (7.18)

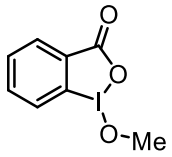

$C_8H_7IO_3$
277.94 g/mol

Following a reported procedure,[252] in a 100 mL round bottom flask, IBA (1.00 g, 4.11 mmol, 1.0 equiv.) was dissolved in 33 mL of MeOH, and MS3Å (10.0 g). stirred at 60 °C for 2 hours. MS3Å was filtered using DCM, and the solvents were then removed by evap oration. The residue was washed with hexane and filtered to remove the corresponding alcohol completely. The residue was dissolved with DCM and the extract was then filtered through filter paper to remove unreacted substrate. Removal of the solvent by evaporation gave the corresponding benziodoxole alkoxide **7.18** as a white powder.

^{1}H NMR (400 MHz, DMSO) δ 13.10 (s, 1H), 8.44 (d, *J* = 2.2 Hz, 1H), 8.02 (d, *J* = 8.0 Hz, 1H), 7.50 (dd, *J* = 8.0, 2.2 Hz, 1H) ppm.

^{13}C NMR (101 MHz, $CDCl_3$) δ 168.2, 135.2, 132.9, 131.1, 126.0, 118.7, 62.3 ppm.

IR (ATR): $\tilde{\nu}$ [cm^{-1}] = 1676, 1637, 1601, 1585, 1570, 1435, 1284, 1268, 1237, 1121, 961, 827, 740, 690, 670, 647.

Protocol for optimization studies

Batch reaction

In a 4 mL screw-cap vial equipped with a magnetic stir bar, compound 5.5 (1.0 equiv.), **SP-IBS I** (0.15 equiv.), and Oxone® (1.0 equiv., finely ground) were combined. Potassium carbonate (0.5 equiv.) and sodium sulfate (18 equiv.) were added, was dissolved in EtOAc (0.2 M, unless otherwise noted). The resulting mixture was stirred at the desired temperature for 4 h. Upon completion, the reaction mixture was filtered and diluted with EtOAc. The solvent was removed under reduced pressure, and dimethyl sulfone was added as an internal standard for NMR analysis. For isolation, the crude mixture was washed with brine, dried over sodium sulfate, and purified by column chromatography on silica gel.

Continuous flow reactions

A flow reactor packed with **SP-IBS I** was placed in a water bath preheated to 60 °C. Compound **5.5** (1.0 equiv.) was dissolved in acetonitrile, and TBA-Oxone® (nBu$_4$NHSO$_5$, 1.0 equiv.) was dissolved separately in MeCN. The two solutions were delivered using a dual syringe pump at various combined flow rates and residence times. Prior to entering the reactor, the streams were merged via a three-way valve (T-mixer), and the resulting mixture was passed through the packed bed and collected in a receiving flask. After complete passage of the reaction mixture, the reactor was flushed with acetonitrile under identical flow conditions to yield the product solution. The solution was concentrated under reduced pressure, and dimethyl sulfone (1.0 equiv.) was added as an internal standard. The reaction mixture was analyzed by ^{1}H NMR to determine the product yield.

Protocol for the reaction without TBA-Oxone®:

A flow reactor packed with preoxidized SP-IBS I (1.10 g, 0.38 mmol/g) was placed in a water bath preheated to 60 °C. Substrate **5.5** (104 mg, 0.42 mmol, 1.0 equiv.) was dissolved in MeCN or EtOAc, and the solution was delivered through the catalyst cartridge using a syringe pump at a preset flow rate. The effluent was collected in a round-bottom flask.

After complete passage of the substrate solution, the system was flushed with MeCN or EtOAc to ensure complete collection of the product. Dimethyl sulfone (1.0 equiv.) was then added as a second internal standard, and the reaction mixture was analyzed by ^{1}H NMR to quantify the product.

General procedure for Synthesis of Starting Materials (tert-Allylic Alcohols), (GP6):

An oven-dried round-bottom flask was charged with cyclohexanone (1.0 equiv.) in THF/Et_2O (0.25 M). The solution was flushed with argon and cooled to -78 °C. The organolithium reagent (1.2 equiv.) was added dropwise, and the reaction mixture was allowed to warm gradually to 0 °C and then to room temperature over 2 h. The reaction was quenched by addition of saturated aqueous NH_4Cl, and Et_2O was added. The layers were separated, and the aqueous phase was extracted with Et_2O three times. The combined organic extracts were washed with brine, dried over Na_2SO_4, filtered, and concentrated under reduced pressure. The crude residue was purified by flash column chromatography on silica gel to afford the desired product.[218,221]

Synthesis and characterisation of starting materials

1-Phenylcyclohex-2-en-1-ol (5.5)

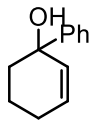

$C_{12}H_{14}O$
174.10 g/mol

The compound **5.5** was synthesized according to GP6 from 2-cyclohexen-1-one (1.00 mL, 9.81 mmol, 1.0 equiv.) and phenyl lithium (6.12 mL, 11.7 mmol, 1.0 equiv.) in THF (39 mL). The crude reaction mixture was purified by flash column chromatography on silica gel (CyHex/EtOAc = 97:3) to afford compound **5.5** as a white solid in 90% yield (1.54 g, 8.83 mmol).

^{1}H NMR (400 MHz, $CDCl_3$) δ 7.53 – 7.49 (m, 2H), 7.39 – 7.34 (m, 2H), 7.31 – 7.25 (m, 1H), 6.07 (ddd, *J* = 10.0, 4.3, 3.2 Hz, 1H), 5.82 (dtd, *J* = 10.0, 2.2, 1.0 Hz, 1H), 2.24 – 2.05 (m, 2H), 2.04 – 1.95 (m, 2H), 1.91 (dd, *J* = 10.4, 2.9 Hz, 1H), 1.87 – 1.76 (m, 1H), 1.65 (dddd, *J* = 13.6, 10.7, 5.5, 3.3 Hz, 1H) ppm.

^{13}C NMR (101 MHz, $CDCl_3$) δ 148.0, 132.3, 130.9, 128.2, 127.0, 125.6, 72.3, 39.7, 25.1, 19.3 ppm.

HRMS (APCI) m/z calcd. for $C_{12}H_{14}N_aO$ ($[M+H]^+$): 197.0938, found 197.0937.

R_f (CyHex/EtOAc, 9:1) = 0.28.

1-Butylcyclohex-2-en-1-ol (7.19)

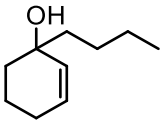

$C_{10}H_{18}O$
154.14 g/mol

Following a reported procedure, compound **7.19** was synthesized according to GP6 from 2-cyclohexen-1-one (1.00 mL, 9.81 mmol, 1.0 equiv.) and butyllithium (4.71 mL, 11.8 mmol, 1.0 equiv.) in THF (39 mL). The crude reaction mixture was purified by flash column chromatography on silica gel (CyHex/EtOAc = 95:5) to afford compound **7.19** as a white solid in 78% (1.18 g, 7.65 mmol).

^{1}H NMR (600 MHz, $CDCl_3$) δ 5.77 (dt, *J* = 9.8, 3.7 Hz, 1H), 5.60 (dd, *J* = 10.1, 2.6 Hz, 1H), 2.01 (dt, *J* = 15.6, 5.0 Hz, 1H), 1.90 (ddq, *J* = 17.7, 8.7, 2.8 Hz, 1H), 1.72 – 1.45 (m, 7H), 1.30 (qt, *J* = 7.0, 5.1 Hz, 4H), 0.89 (t, *J* = 7.0 Hz, 3H) ppm.

13C NMR (151 MHz, $CDCl_3$) δ 133.0, 129.8, 69.8, 42.2, 35.5, 25.8, 25.4, 23.4, 19.2, 14.2 ppm.

HRMS (ESI) m/z calcd. for $C_{10}H_{18}N_aO$ ($[M+Na]^+$): 177.1250, found 177.1251.

R_f (CyHex/EtOAc, 9:1) = 0.36.

1-Hexylcyclohex-2-en-1-ol (7.20)

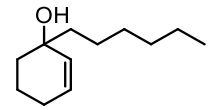

$C_{12}H_{22}O$
182.17 g/mol

Following a reported procedure, compound **7.20** was synthesized according to GP6 from 2-cyclohexen-1-one (1.00 mL, 9.81 mmol, 1.0 equiv.) and hexyllithium (5.12 mL, 11.8 mmol, 1.0 equiv.) in THF (39 mL). The crude reaction mixture was purified by flash column chromatography on silica gel (CyHex/EtOAc = 95:5) to afford compound **7.20** as a white solid (1.44 g, 7.95 mmol).

^{1}H NMR (600 MHz, $CDCl_3$) δ 5.78 (ddd, *J* = 10.1, 4.6, 3.0 Hz, 1H), 5.60 (d, *J* = 9.8 Hz, 1H), 2.02 (dd, *J* = 18.2, 5.2 Hz, 1H), 1.92 (dddt, *J* = 17.9, 8.6, 5.6, 2.8 Hz, 1H), 1.72 – 1.59 (m, 4H), 1.56 – 1.45 (m, 3H), 1.36 – 1.18 (m, 8H), 0.87 (t, *J* = 6.6 Hz, 3H) ppm.

^{13}C NMR (151 MHz, $CDCl_3$) δ 133.0, 129.8, 69.9, 42.5, 35.6, 32.0, 30.0, 25.4, 23.6, 22.7, 19.2, 14.2 ppm.

HRMS (APCI) m/z calcd. for $C_{12}H_{22}N_aO$ ($[M+Na]^+$): 205.1562, found 205.1563.

R_f (CyHex/EtOAc, 9:1) = 0.38.

1-Vinylcyclohex-2-en-1-ol (7.21)

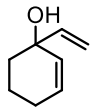

$C_8H_{12}O$
124.09 g/mol

Following a reported procedure, compound **7.21** was synthesized according to GP6 from 2-cyclohexen-1-one (1.00 mL, 9.81 mmol, 1.0 equiv.) and vinyl magnesium bromide (14.8 mL, 14.8 mmol, 1.0 equiv.) in diethyl ether (39 mL). The crude reaction mixture was purified by flash column chromatography on silica gel (CyHex/EtOAc = 9:1) to afford compound **7.21** as a white solid in 81% yield (991 mg, 7.98 mol).

^{1}H NMR (400 MHz, $CDCl_3$) δ 5.99 – 5.84 (m, 2H), 5.55 (dt, *J* = 10.0, 2.3 Hz, 1H), 5.22 (dd, *J* = 17.4, 1.4 Hz, 1H), 5.08 (dd, *J* = 10.6, 1.4 Hz, 1H), 2.11 – 1.91 (m, 2H), 1.76 – 1.66 (m, 5H).

^{13}C NMR (101 MHz, $CDCl_3$) δ 144.3, 131.1, 130.5, 113.1, 71.1, 36.5, 25.1, 19.1 ppm.

HRMS (APCI) m/z calcd. for $C_{40}H_{63}N_6O$ ($[M+H]^+$): 915.4013, found 915.4016.

R_f (CyHex/EtOAc, 9:1) = 0.20.

1-Ethynylcyclohex-2-en-1-ol (7.22)

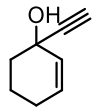

$C_8H_{10}O$
122.07 g/mol

Following a reported procedure, compound **7.22** was synthesized according to GP6 from 2-cyclohexen-1-one (1.00 mL, 9.85 mmol, 1.0 equiv.) and butyllithium (29.5 mL, 14.8 mmol, 1.5 equiv.) in THF (39 mL). The crude reaction mixture was purified by flash column chromatography on silica gel (CyHex/EtOAc = 95:5) to afford compound **7.22** as a white solid in 65% yield (782 mg, 6.40 mmol).

^{1}H NMR (400 MHz, $CDCl_3$) δ 5.83 (dt, *J* = 9.9, 3.6 Hz, 1H), 5.77 – 5.71 (m, 1H), 2.49 (s, 1H), 2.33 (s, 1H), 2.02 (qdd, *J* = 5.6, 3.1, 0.8 Hz, 3H), 1.93 – 1.85 (m, 1H), 1.83 – 1.68 (m, 2H) ppm.

^{13}C NMR (101 MHz, $CDCl_3$) δ 130.2, 87.7, 71.8, 65.1, 37.8, 24.7, 19.0 ppm.

HRMS (ESI) m/z calcd. for $C_8H_{11}O$ ($[M+H]^+$): 123.0805, found 123.0804.

R_f (CyHex/EtOAc, 9:1) = 0.27.

General Procedure for the Oxidative Rearrangement of tert-Allylic Alcohols (GP7):

Following a reported procedure,[221] Powdered Oxone® was prepared as follows. Commercially available Oxone® (Aldrich, particle size 0.2–16 µm) was mechanically reduced in particle size by vigorous stirring with a magnetic stir bar under ambient atmosphere on a Schlenk line at room temperature. After 2 h of continuous stirring, a fine powdered material was obtained with an average particle size of approximately 0.16 µm.

A mixture powdered Oxone® (353 mg, 574 µmol, 1.0 equiv.), potassium carbonate (39.6 mg, 287 µmol, 0.5 equiv.), and anhydrous sodium sulfate (1.46 g, 10.3 mmol,18 equiv.; dried under vacuum with a heat gun) were combined in ethyl acetate (0.2 M) and stirred vigorously at room temperature for 24 h.

The tert-allylic alcohol (574 µmol, 1.0 equiv.), *n*Bu_4NHSO_4 (6.80 mg, 0.02 mmol, 0.10 equiv.), and **SP-IBS I** (172 mg, 86.1 µmol, 0.15 equiv.) were then added, and the reaction mixture was heated to 60 °C. After completion, the mixture was cooled to room temperature, filtered, and the solid residue washed with EtOAc. The filtrate was concentrated under reduced pressure, and the crude material was purified by flash column chromatography on silica gel using CyHex-EtOAc as eluent to afford the desired product.

7.9.2 Synthesis and Characterisation of Products

2-Phenylcyclohex-2-en-1-one (5.6)

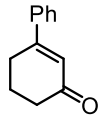

$C_{12}H_{12}O$
172.09 g/mol

Following a reported procedure, compound **5.6** was synthesized according to GP7 from **5.5** (70.0 mg, 574 µmol, 1.0 equiv.) and **SP-IBS I** (172 mg, 86.1 µmol, 0.15 equiv.) in EtOAc (2.8 mL). The crude reaction mixture was purified by flash column chromatography on silica gel (CyHex/EtOAc = 95:5) to afford compound **5.6** as a white solid in 30% yield (29.6 mg, 172 µmol).

^{1}H NMR (600 MHz, $CDCl_3$) δ 7.55 – 7.53 (m, 1H), 7.43 – 7.40 (m, 2H), 2.78 (t, *J* = 5.8 Hz, 1H), 2.49 (t, *J* = 6.7 Hz, 1H), 2.17 (p, *J* = 6.3 Hz, 1H) ppm.

^{13}C NMR (151 MHz, $CDCl_3$) δ 200.0, 159.9, 139.0, 130.1, 128.9, 126.2, 125.7, 37.4, 28.3, 23.0 ppm.

HRMS (ESI) m/z calcd. for $C_{12}H_{12}N_aO$ ($[M+H]^+$): 195.0782, found 195.0780.

R_f (CyHex/EtOAc, 9:1) = 0.40.

3-Butylcyclohex-2-en-1-one (5.7)

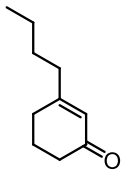

$C_{10}H_{16}O$
152.12 g/mol

Following a reported procedure, compound **5.7** was synthesized according to GP7 from **7.19** (88.5 mg, 574 µmol, 1.0 equiv.) and **SP-IBS I** (172 mg, 86.1 µmol, 0.15 equiv.) in EtOAc (2.8 mL) in 8 h. The crude reaction mixture was purified by flash column chromatography on silica gel (CyHex/EtOAc = 95:5) to afford compound **5.7** as a white solid in 40% yield (34.9 mg, 229 µmol).

^{1}H NMR (600 MHz, $CDCl_3$) δ 5.86 (t, *J* = 1.7 Hz, 1H), 2.34 (t, *J* = 6.7 Hz, 2H), 2.27 (t, *J* = 6.1 Hz, 2H), 2.20 (t, *J* = 7.7 Hz, 2H), 1.97 (p, *J* = 6.3 Hz, 2H), 1.47 (tt, *J* = 7.8, 6.2 Hz, 2H), 1.33 (m, 2H), 0.91 (t, *J* = 7.4 Hz, 3H) ppm.

^{13}C NMR (151 MHz, $CDCl_3$) δ 200.1, 166.8, 125.8, 37.9, 37.5, 29.8, 29.2, 22.9, 22.5, 13.9 ppm.

R_f (CyHex/EtOAc, 9:1) = 0.30.

3-Hexylcyclohex-2-en-1-one (5.8)

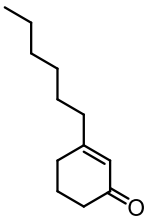

$C_{12}H_{20}O$
180.15 g/mol

Following a reported procedure, compound **5.8** was synthesized according to GP7 from **7.20** (105 mg, 574 µmol, 1.0 equiv.) and **SP-IBS I** (172 mg, 86.1 µmol, 0.15 equiv.) in EtOAc (2.8 mL) in 12 h. The crude reaction mixture was purified by flash column chromatography on silica gel (CyHex/EtOAc = 95:5) to afford compound **5.8** as a white solid in 28% yield (28.9 mg, 161 µmol).

^{1}H NMR (600 MHz, $CDCl_3$) δ 5.87 (s, 1H), 2.35 (t, *J* = 6.7 Hz, 2H), 2.28 (t, *J* = 6.1 Hz, 2H), 2.20 (t, *J* = 7.7 Hz, 2H), 1.98 (p, *J* = 6.3 Hz, 2H), 1.49 (p, *J* = 7.2 Hz, 2H), 1.34 – 1.23 (m, 10H), 0.88 (t, *J* = 6.7 Hz, 4H) ppm.

^{13}C NMR (151 MHz, $CDCl_3$) (151 MHz, $CDCl_3$) δ 200.1, 166.9, 125.8, 38.2, 37.5, 31.7, 29.8, 29.1, 27.1, 22.9, 22.7, 14.2 ppm.

HRMS (ESI) m/z calcd. for $C_{12}H_{20}N_aO$ ($[M+Na]^+$): 203.1408, found 203.1406.

R_f (CyHex/EtOAc, 9:1) = 0.30.

Abbreviations

Ac	Acetyl
AcOH	Acetic acid
ADP	Adenosine diphosphate
Ala	Alanine
APCI	Atmospheric-Pressure Chemical Ionization
Aq.	Aqueous
Ar	Aryl
Arg	Arginine
Asn	Asparagine
Asp	Aspartic acid
ATP	Adenosine triphosphate
Bn	Benzyl
Boc	tert-Butoxycarbonyl
BODIPY	Boron-dipyrromethene
BSA	Bovine serum albumin
Bu	Butyl
CAN	Ceric ammonium nitrate
Cat.	Catalyst
Cbz	Carboxybenzyl
CuAAC	Copper-catalyzed Azide–Alkyne Cycloaddition
CyHex	Cyclohexane
Cys	Cysteine
DCE	1,2-Dichloroethane
DCM	Dichloromethane

DIPEA N,N-Diisopropylethylamine

DIC N,N′-Diisopropylcarbodiimide

DMF N,N-Dimethylformamide

DMP Dess–Martin periodinane

d.r. Diastereomeric ratio

EBX Ethynylbenziodoxolone

EDC 1-Ethyl-3-(3-dimethylaminopropyl)carbodiimide

ESI Electrospray Ionization

Et Ethyl

EtOH Ethanol

Equiv. Equivalent

FITC Fluorescein isothiocyanate

Fmoc Fluorenylmethoxycarbonyl

Gln Glutamine

Glu Glutamic acid

Gly Glycine

HATU Hexafluorophosphate Azabenzotriazole Tetramethyl Uronium

HBTU O-(Benzotriazol-1-yl)-tetramethyluronium hexafluorophosphate

HCl Hydrochloric acid

HEPES 4-(2-Hydroxyethyl)-1-piperazineethanesulfonic acid

HFIP Hexafluoroisopropanol

His Histidine

HMTA Hexamethylenetetramine

HOBt 1-Hydroxybenzotriazole

HOSu *N*-Hydroxysuccinimide

HRMS High-Resolution Mass Spectrometry

h Hour

HVI Hypervalent iodine reagent

IBA 2-Iodosobenzoic acid

IBS 2-Iodoxybenzenesulfonic acid

IBX 2-Iodoxybenzoic acid

Ile Isoleucine

IR Infrared

^{i}Pr Isopropyl

Leu Leucine

LSF Late-stage functionalization

Lys Lysine

M Molar

m *Meta* (substituent orientation in phenyl ring)

MBH Morita–Baylis–Hillman

MBHA 4-Methylbenzhydrylamine

MeCN Acetonitrile

MeOH Methanol

Met Methionine

Me Methyl

MHz Megahertz

min Minute

mCPBA *meta*-Chloroperbenzoic acid

NMR Nuclear Magnetic Resonance

NMP *N*-Methyl-2-pyrrolidone

O-GlcNAc O-linked β-N-acetylglucosamine

o *Ortho* (substituent orientation in phenyl ring)

***o*-QM** *ortho*-Quinone methide

OGT O-GlcNAc transferase

p Para (substituent orientation in phenyl ring)

***p*-QM** *para*-Quinone methide

PBS Phosphate-Buffered Saline

PCC Pyridinium chlorochromate

PDC Pyridinium dichromate

PEG Poly(ethylene glycol)

Phe Phenylalanine

Ph Phenyl

PhI Iodobenzene

PIDA Phenyliodine(III) diacetate

PIFA Phenyliodine(III) bis(trifluoroacetate)

PG Protecting group

ppm Parts per million

PP Polypropylene

Pro Proline

PTM Post-translational modification

Pyl Pyrrolysine

Py Pyridine

Rf Retention factor

r.t. Room temperature

Sec Selenocysteine

Ser	Serine
SIBX	Stabilized 2-Iodoxybenzoic acid
SPAAc	Strain-Promoted Azide-Alkyne Cycloaddition
SP-IBS	Solid-phase 2-Iodoxybenzenesulfonic acid
SPPS	Solid-phase peptide synthesis
^{t}Bu	tert-Butyl
TEA	Triethylamine
TEMPO	2,2,6,6-Tetramethylpiperidin-1-oxyl
TFA	Trifluoroacetic acid
THF	Tetrahydrofuran
Thr	Threonine
TLC	Thin-layer chromatography
TMEDA	Tetramethylethylenediamine
TPC	1,3,5-Triazine-pyridine
TRIS	Tris(hydroxymethyl)aminomethane
Trp	Tryptophan
Tyr	Tyrosine
UV/Vis	Ultraviolet–Visible spectroscopy
Val	Valine
2-CTC	2-Chlorotrityl chloride resin

References

[1] J. A. Magner, *Endocrinologist* **2004**, 14, 239–244.

[2] E. Fischer, E. Fourneau, *Ber. Dtsch. Chem. Ges.* **1901**, 34, 2868–2877.

[3] R. B. Merrifield, *J. Am. Chem. Soc.* **1963**, 85, 2149–2154.

[4] R. B. Merrifield, *Recent Prog. Horm. Res.* **1967**, 23, 451–482.

[5] R. B. Merrifield, J. M. Stewart, N. Jernberg, *Anal. Chem.* **1966**, 38, 1905–1914.

[6] R. B. Merrifield, *Science* **1986**, 232, 341–347.

[7] Y. Tang, T. Nie, L. Zhang, X. Liu, H. Deng, *Cosmetics* **2025**, 12, 107.

[8] P. Fang, W.-K. Pang, S. Xuan, W.-L. Chan, K. C.-F. Leung, *Chem. Soc. Rev.* **2024**, 53, 11725–11771.

[9] A. Flissi, E. Ricart, C. Campart, M. Chevalier, Y. Dufresne, J. Michalik, P. Jacques, C. Flahaut, F. Lisacek, V. Leclère, M. Pupin, *Nucleic Acids Res.* **2020**, 48, D465-D469.

[10] M. Rother, J. A. Krzycki, *Archaea* **2010**, 2010, 1–14.

[11] L. Wang, N. Wang, W. Zhang, X. Cheng, Z. Yan, G. Shao, X. Wang, R. Wang, C. Fu, *Signal Transduct. Target. Ther.* **2022**, 7, 48.

[12] M. Liu, D. Svirskis, T. Proft, J. Loh, N. Yin, H. Li, D. Li, Y. Zhou, S. Chen, L. Song, G. Chen, W.-Y. Lu, Z. Zhang, Z. Zhou, L. Li, Y. Huang, C. Bunt, G. Sun, P. W. R. Harris, M. A. Brimble, J. Wen, *Acta Pharm. Sin. B.* **2025**, 15, 6342–6381.

[13] V. Apostolopoulos, J. Bojarska, T.-T. Chai, S. Elnagdy, K. Kaczmarek, J. Matsoukas, R. New, K. Parang, O. P. Lopez, H. Parhiz, C. O. Perera, M. Pickholz, M. Remko, M. Saviano, M. Skwarczynski, Y. Tang, W. M. Wolf, T. Yoshiya, J. Zabrocki, P. Zielenkiewicz, M. AlKhazindar, V. Barriga, K. Kelaidonis, E. M. Sarasia, I. Toth, *Molecules* **2021**, 26, 1–45.

[14] A. Henninot, J. C. Collins, J. M. Nuss, *J. Med. Chem.* **2018**, 61, 1382–1414.

[15] S. L. Schreiber, *Isr. J. Chem.* **2019**, 59, 52–59.

[16] U. A. Çevik, A. Işik, A. Karakaya, in *Computational Methods for Rational Drug Design*, ed. M. Rudrapal, Wiley **2025**, pp. 123–151.

[17] J. Lu, H. Xu, J. Xia, J. Ma, J. Xu, Y. Li, J. Feng, *Front. Microbiol.* **2020**, 11, 563030.

[18] M. Muttenthaler, G. F. King, D. J. Adams, P. F. Alewood, *Nat. Rev. Drug Discov.* **2021**, 20, 309–325.

[19] Y. Tasdemiroglu, R. G. Gourdie, J.-Q. He, *Eur. J. Pharmacol.* **2022**, 932, 175192.

[20] B. Todaro, E. Ottalagana, S. Luin, M. Santi, *Pharm.* **2023**, 15, 1648.

[21] L. R. Robinson, N. C. Fitzgerald, D. G. Doughty, N. C. Dawes, C. A. Berge, D. L. Bissett, *Int. J. Cosmet. Sci.* **2005**, 27, 155–160.

[22] H. Henseler, *GMS Interdiscip Plast Reconstr Surg DGPW* **2023**. DOI 10.3205/iprs000179.

[23] Y.-P. Hung, J.-C. Lee, C.-W. Chiu, C.-C. Lee, P.-J. Tsai, I.-L. Hsu, W.-C. Ko, *Antibiotics* **2022**, 11, 220.

[24] L. Wang, C. Zhang, J. Zhang, Z. Rao, X. Xu, Z. Mao, X. Chen, *Front. Bioeng. Biotechnol.* **2021**, 9, 748976.

[25] R. R. Sonani, S. Bianco, B. Dietrich, J. Doutch, E. R. Draper, D. J. Adams, E. H. Egelman, *Cell Rep. Phys. Sci.* **2024**, 5.

[26] K. A. Clark, B. C. Covington, M. R. Seyedsayamdost, *Nat. Chem.* **2022**, 14, 1390–1398.

[27] L. Pinheiro, C. Faustino, in *Application and Characterization of Surfactants*, ed. R. Najjar, InTech **2017**.

[28] L. A. Raedler, *Am. Health Drug Benefits* **2016**, 9, 93–96.

[29] C. Sornay, V. Vaur, A. Wagner, G. Chaubet, *R. Soc. Open Sci.* **2022**, 9, 211563.

[30] A. Yang, K. Cho, H.-S. Park, *RNA Biol.* **2018**, 15, 427–440.

[31] T. Bilbrough, E. Piemontese, O. Seitz, *Chem. Soc. Rev.* **2022**, 51, 5691–5730.

[32] G. W. Hart, M. P. Housley, C. Slawson, *Nature* **2007**, 446, 1017–1022.

[33] A. Larkin, B. Imperiali, *Biochem.* **2011**, 50, 4411–4426.

[34] D. Fass, C. Thorpe, *Chem. Rev.* **2018**, 118, 1169–1198.

[35] T. Matsumoto, T. Tanaka, A. Kondo, *Biotechnol. J.* **2012**, 7, 1137–1146.

[36] K. T.sriwong, T. Matsuda, *Org. Process Res. Dev.* **2022**, 26, 1857–1877.

[37] M. S. Robescu, T. Bavaro, *Molecules* **2025**, 30, 939.

[38] A. K. Alexander, S. I. Elshahawi, *CHEMBIOCHEM* **2023**, 24, e202300372.

[39] G. L. Holliday, J. D. Fischer, J. B. O. Mitchell, J. M. Thornton, *FEBS J.* **2011**,

[40] N. C. Goodwin, J. P. Morrison, D. E. Fuerst, T. Hadi, *ACS Med. Chem. Lett.* **2019**, 10, 1363–1366.

[41] F. Guzman, S. Barberis, A. Illanes, *Electron. J. Biotechnol.* **2007**, 10, 279–314.

[42] E. Haldón, M. C. Nicasio, P. J. Pérez, *Org. Biomol. Chem.* **2015**, 13, 9528–9550.

[43] B. T. Worrell, J. A. Malik, V. V. Fokin, *Science* **2013**, 340, 457–460.

[44] F. L. Lin, H. M. Hoyt, H. van Halbeek, R. G. Bergman, C. R. Bertozzi, *J. Am. Chem. Soc.* **2005**, 127, 2686–2695.

[45] E. Saxon, C. R. Bertozzi, *Science* **2000**, 287, 2007–2010.

[46] B. L. Nilsson, L. L. Kiessling, R. T. Raines, *Org. Lett.* **2000**, 2, 1939–1941.

[47] Y. Ding, J. P. Ting, J. Liu, S. Al-Azzam, P. Pandya, S. Afshar, *Amino acids* **2020**, 52, 1207–1226.

[48] Y. Ding, Z. T. Ball, in *Peptide Science*, ed. F. Liu, Wiley **2025**, pp. 55–86.

[49] G.-H. Feng, T.-Y. Wang, Y.-M. Li, *Chem. Commun.* **2025**, 61, 11095–11117.

[50] T. H. Kuster, T. Schnitzer, *CC* **2025**, 5, 101339.

[51] J. Rodríguez, M. Martínez-Calvo, *Chem. Eur. J.* **2020**, 26, 9792–9813.

[52] L. R. Malins, *Curr. Opin. Chem. Biol.* **2018**, 46, 25–32.
[53] C. Bottecchia, T. Noël, *Chem. Eur. J.* **2019**, 25, 26–42.
[54] D. C. Miller, S. V. Athavale, F. H. Arnold, *Nat. Synth.* **2022**, 1, 18–23.
[55] S. C. Hammer, A. M. Knight, F. H. Arnold, *Curr. Opin. Green Sustain. Chem.* **2017**, 7, 23–30.
[56] C. D. Spicer, B. G. Davis, *Nat. Commun.* **2014**, 5, 4740.
[57] O. Koniev, A. Wagner, *Chem. Soc. Rev.* **2015**, 44, 5495–5551.
[58] E. A. Hoyt, P. M. S. D. Cal, B. L. Oliveira, G. J. L. Bernardes, *Nat. Rev. Chem.* **2019**, 3, 147–171.
[59] T. Tamura, I. Hamachi, *J. Am. Chem. Soc.* **2019**, 141, 2782–2799.
[60] S. M. Hacker, K. M. Backus, M. R. Lazear, S. Forli, B. E. Correia, B. F. Cravatt, *Nat. Chem.* **2017**, 9, 1181–1190.
[61] M. Li, T. Wang, L. Chen, Z. Cui, A. Zuo, C. Wang, Y. Zhang, C. Liu, *Org. Lett.* **2025**, 27, 13140–13145.
[62] Z. He, X. Zhao, W.-Y. Gao, G. Bao, Y. Li, Q. Zuo, X. Song, L.-Y. Mou, W. Sun, R. Wang, *Sci. Adv.* **2025**, 11, eadv8712.
[63] J. Kim, B. X. Li, R. Y.-C. Huang, J. X. Qiao, W. R. Ewing, D. W. C. MacMillan, *J. Am. Chem. Soc.* **2020**, 142, 21260–21266.
[64] M.-Q. Zhang, P.-Y. He, J.-J. Hu, Y.-M. Li, *J. Pept. Sci.* **2023**, 29, e3454.
[65] J. R. Kramer, T. J. Deming, *Biomacromolecules* **2012**, 13, 1719–1723.
[66] N. Bilgin, J. C. J. Hintzen, J. Mecinović, *Chem. Commun.* **2025**, 61, 3805–3820.
[67] L. Wen, Z. Shu, L. Pan, B. Chen, G. Qu, S. Geng, Y. Yang, Y. Jiang, S. Liu, *Commun. Chem.* **2025**, 8, 69.
[68] J.-C. Tsou, C.-J. Tsou, C.-H. Wang, A.-L. A. Ko, Y.-H. Wang, H.-H. Liang, J.-C. Sun, K.-F. Huang, T.-P. Ko, S.-Y. Lin, Y.-S. Wang, *J. Am. Chem. Soc.* **2024**, 146, 33309–33315.
[69] S. Jia, D. He, C. J. Chang, *J. Am. Chem. Soc.* **2019**, 141, 7294–7301.
[70] H.-H. Li, Y. Xiao, H. Liu, X. Li, *J. Am. Chem. Soc.* **2025**, 147, 35211–35218.
[71] C. Zhang, J. Huang, S. Li, F. Huo, Y. Weng, *Eur. J. Org. Chem.* **2025**, 28, e202401214.
[72] A.-S. K. Paschke, E. J. Meeus, M. A. Masota, F. Hoffmann, N. M. Grob, B. Morandi, *J. Am. Chem. Soc.* **2026**, 148, 55–60.
[73] Y. Liu, G. Li, W. Ma, G. Bao, Y. Li, Z. He, Z. Xu, R. Wang, W. Sun, *Chem. Sci.* **2024**, 15, 11099–11107.
[74] J. Lee, M. Ju, O. H. Cho, Y. Kim, K. T. Nam, *Adv. Sci.* **2019**, 6, 1801255.
[75] N. S. Joshi, L. R. Whitaker, M. B. Francis, *J. Am. Chem. Soc.* **2004**, 126, 15942–15943.
[76] L. H. Jones, A. Narayanan, E. C. Hett, *Mol. BioSyst.* **2014**, 10, 952–969.

[77] M. Moinpour, N. K. Barker, L. E. Guzman, J. C. Jewett, P. R. Langlais, J. C. Schwartz, *Protein Sci.* **2020**, 29, 1784–1793.
[78] M. R. A. Blomberg, *Front. Chem.* **2021**, 9, 640155.
[79] A. G. Watts, I. Damager, M. L. Amaya, A. Buschiazzo, P. Alzari, A. C. Frasch, S. G. Withers, *J. Am. Chem. Soc.* **2003**, 125, 7532–7533.
[80] M. B. Maina, Y. K. Al-Hilaly, L. C. Serpell, *Front. Neurosci.* **2023**, 17, 1132670.
[81] Z. Rzepka, E. Buszman, A. Beberok, D. Wrześniok, *Postepy Hig Med Dosw* **2016**, 70, 695–708.
[82] N. Nakatsuka, A. M. Andrews, *ACS Chem. Neurosci.* **2017**, 8, 218–220.
[83] H. Maeda, N. Dudareva, *Annu. Rev. Plant Biol.* **2012**, 63, 73–105.
[84] S. Kaufman, *Biochim. Biophys. Acta* **1957**, 23, 445–446.
[85] S. Kaufman, *J. Biol. Chem.* **1957**, 226, 511–524.
[86] S. Kaufman, *J. Biol. Chem.* **1958**, 230, 931–939.
[87] S. Udenfriend, C. T. Clark, J. Axelrod, B. B. Brodie, *J. Biol. Chem.* **1954**, 208, 731–739.
[88] M. UCHIDA, S. SUZUKI, K. ICHIHARA, *Biochem.* **1954**, 41, 41–65.
[89] W. Zeng, J. Xue, H. Geng, X. Liu, J. Yang, W. Shen, Y. Yuan, Y. Qiang, Q. Zhu, *Biotechnol. Bioeng.* **2024**, 121, 799–822.
[90] Q. Zuo, J. Lu, Z. Huang, Z. Zhang, J. Yan, G. Li, S. Zhang, W. Sun, K. Hu, R. Wang, *Coord. Chem. Rev.* **2025**, 540, 216765.
[91] A. Correa, *Eur. J. Inorg. Chem.* **2021**, 2021, 2928–2941.
[92] S. Zhang, L. M. de Leon Rodriguez, F. F. Li, M. A. Brimble, *Chem. Sci.* **2023**, 14, 7782–7817.
[93] T. Long, L. Liu, Y. Tao, W. Zhang, J. Quan, J. Zheng, J. D. Hegemann, M. Uesugi, W. Yao, H. Tian, H. Wang, *Angew. Chem. Int. Ed.* **2021**, 60, 13414–13422.
[94] D. W. Romanini, M. B. Francis, *Bioconjug. Chem.* **2008**, 19, 153–157.
[95] M. Minakawa, H.-M. Guo, F. Tanaka, *J. Org. Chem.* **2008**, 73, 8669–8672.
[96] H.-M. Guo, M. Minakawa, L. Ueno, F. Tanaka, *Bioorg. Med. Chem.* **2009**, 19, 1210–1213.
[97] J. M. Hooker, E. W. Kovacs, M. B. Francis, *J. Am. Chem. Soc.* **2004**, 126, 3718–3719.
[98] T. L. Schlick, Z. Ding, E. W. Kovacs, M. B. Francis, *J. Am. Chem. Soc.* **2005**, 127, 3718–3723.
[99] H. G. Higgins, K. J. Harrington, *Arch. Biochem. Biophys.* **1959**, 85, 409–425.
[100] M. W. Jones, G. Mantovani, C. A. Blindauer, S. M. Ryan, X. Wang, D. J. Brayden, D. M. Haddleton, *J. Am. Chem. Soc.* **2012**, 134, 7406–7413.
[101] J. Zhang, D. Ma, D. Du, Z. Xi, L. Yi, *Org. Biomol. Chem.* **2014**, 12, 9528–9531.
[102] W. Liao, X. Ni, *Photochem. Photobiol. Sci.* **2017**, 16, 1211–1219.

[103] D. Alvarez-Dorta, C. Thobie-Gautier, M. Croyal, M. Bouzelha, M. Mével, D. Deniaud, M. Boujtita, S. G. Gouin, *J. Am. Chem. Soc.* **2018**, 140, 17120–17126.

[104] B. X. Li, D. K. Kim, S. Bloom, R. Y.-C. Huang, J. X. Qiao, W. R. Ewing, D. G. Oblinsky, G. D. Scholes, D. W. C. MacMillan, *Nat. Chem.* **2021**, 13, 902–908.

[105] T. C. Roberts, P. A. Smith, R. T. Cirz, F. E. Romesberg, *J. Am. Chem. Soc.* **2007**, 129, 15830–15838.

[106] D. S. Peters, F. E. Romesberg, P. S. Baran, *J. Am. Chem. Soc.* **2018**, 140, 2072–2075.

[107] J.-J. Li, T.-S. Mei, J.-Q. Yu, *Angew. Chem. Int. Ed.* **2008**, 47, 6452–6455.

[108] X. Wang, S. Niu, L. Xu, C. Zhang, L. Meng, X. Zhang, D. Ma, *Org. Lett.* **2017**, 19, 246–249.

[109] C. J. Vickers, T.-S. Mei, J.-Q. Yu, *Org. Lett.* **2010**, 12, 2511–2513.

[110] K. Maruyama, T. Ishiyama, Y. Seki, K. Sakai, T. Togo, K. Oisaki, M. Kanai, *J. Am. Chem. Soc.* **2021**, 143, 19844–19855.

[111] K. L. Seim, A. C. Obermeyer, M. B. Francis, *J. Am. Chem. Soc.* **2011**, 133, 16970–16976.

[112] T. J. Wadzinski, A. Steinauer, L. Hie, G. Pelletier, A. Schepartz, S. J. Miller, *Nat. Chem.* **2018**, 10, 644–652.

[113] N. Declas, J. R. J. Maynard, L. Menin, N. Gasilova, S. Götze, J. L. Sprague, P. Stallforth, S. Matile, J. Waser, *Chem. Sci.* **2022**, 13, 12808–12817.

[114] H. Jiang, Q. Zhang, Y. Zhang, H. Feng, H. Jiang, F. Pu, R. Yu, Z. Zhong, C. Wang, Y. M. E. Fung, P. Blasco, Y. Li, T. Jiang, X. Li, *Chem. Commun.* **2022**, 58, 7066–7069.

[115] Y. Venkata Durga Nageswar, K. Ramesh, K. Rakhi, *Front. Chem.* **2022**, 10, 841751.

[116] A. Duschek, S. F. Kirsch, *Angew. Chem. Int. Ed.* **2011**, 50, 1524–1552.

[117] X.-G. Yang, Z.-N. Hu, M.-C. Jia, F.-H. Du, C. Zhang, *Synlett* **2021**, 32, 1289–1296.

[118] F. V. Singh, S. E. Shetgaonkar, M. Krishnan, T. Wirth, *Chem. Soc. Rev.* **2022**, 51, 8102–8139.

[119] A. Yoshimura, V. V. Zhdankin, *Chem. Rev.* **2016**, 116, 3328–3435.

[120] Z. Zhang, X. Li, M. Song, Y. Wan, D. Zheng, G. Zhang, G. Chen, *J. Org. Chem.* **2019**, 84, 12792–12799.

[121] C. Hartmann, V. Meyer, *Ber. Dtsch. Chem. Ges.* **1893**, 26, 1727–1732.

[122] F. R. Greenbaum, *Am. J. Pharm.* **1936**, 108, 17–22.

[123] A. R. Katritzky, B. L. Duell, J. K. Gallos, H. D. Durst, *Magn. Reson. Chem.* **1989**, 27, 1007–1011.

[124] P. Kazmierczak, L. Skulski, L. Kraszkiewicz, *Molecules* **2001**, 6, 881–891.

[125] R. Seltzer, *FAA spurs work on explosive detection* **1990**, vol. 68, 68, 5.

[126] M. Frigerio, M. Santagostino, S. Sputore, *J. Org. Chem.* **1999**, 64, 4537–4538.

[127] S. D. Meyer, S. L. Schreiber, *J. Org. Chem.* **1994**, 59, 7549–7552.
[128] U. Ladziata, V. V. Zhdankin, *Arkivoc* **2007**, 2006, 26–58.
[129] V. V. Zhdankin, *J. Org. Chem.* **2011**, 76, 1185–1197.
[130] F. V. Singh, T. Wirth, *Chem. Asian J.* **2014**, 9, 950–971.
[131] T. Dohi, Y. Kita, *Chem. Commun.* **2009**, 2073–2085.
[132] L. McDermott, D. Aljovic, Z. G. Walters, F. Peng, R. Zhao, K. R. Campos, N. K. Garg, *Org. Lett.* **2025**, 27, 13165–13169.
[133] D. Magdziak, A. A. Rodriguez, R. W. van de Water, T. R. R. Pettus, *Org. Lett.* **2002**, 4, 285–288.
[134] M. Uyanik, T. Mutsuga, K. Ishihara, *Molecules* **2012**, 17, 8604–8616.
[135] X. Xiao, N. S. Greenwood, S. E. Wengryniuk, *Angew. Chem. Int. Ed.* **2019**, 58, 16181–16187.
[136] R. Bernini, M. Barontini, F. Crisante, M. C. Ginnasi, R. Saladino, *Tetrahedron Lett.* **2009**, 50, 6519–6521.
[137] S. Karmakar, G. Sukumar, S. Prasanthkumar, B. K. Jha, P. S. Mainkar, K. Nayani, S. Chandrasekhar, *Chem. Commun.* **2024**, 60, 3802–3805.
[138] P. Anastas, N. Eghbali, *Chem. Soc. Rev.* **2010**, 39, 301–312.
[139] J. C. Maza, D. L. V. Bader, L. Xiao, A. M. Marmelstein, D. D. Brauer, A. M. ElSohly, M. J. Smith, S. W. Krska, C. A. Parish, M. B. Francis, *J. Am. Chem. Soc.* **2019**, 141, 3885–3892.
[140] S. L. Diemer, M. Kristensen, B. Rasmussen, S. R. Beeren, M. Pittelkow, *Int. J. Mol. Sci.* **2015**, 16, 21858–21872.
[141] M. K. Meadows, E. K. Roesner, V. M. Lynch, T. D. James, E. V. Anslyn, *Org. Lett.* **2017**, 19, 3179–3182.
[142] E. Fuentes-Lemus, P. Hägglund, C. López-Alarcón, M. J. Davies, *Molecules* **2021**, 27, 1–31.
[143] Y. Cao, H. Li, *Biophys. J.* **2011**, 101, 2009–2017.
[144] S. Westermann, K. Weber, *Nat. Rev. Mol. Cell Biol.* **2003**, 4, 938–947.
[145] P. J. Hogg, *Trends Biochem. Sci.* **2003**, 28, 210–214.
[146] P. Hägglund, M. Mariotti, M. J. Davies, *Expert Rev. Proteomics* **2018**, 15, 665–681.
[147] M. J. Lobba, C. Fellmann, A. M. Marmelstein, J. C. Maza, E. N. Kissman, S. A. Robinson, B. T. Staahl, C. Urnes, R. J. Lew, C. S. Mogilevsky, J. A. Doudna, M. B. Francis, *ACS Cent. Sci.* **2020**, 6, 1564–1571.
[148] C. F. Hartman, F. Wold, *Biochem.* **1967**, 6, 2439–2448.
[149] G. T. Hermanson, *Bioconjugate Techniques*, Elsevier **2013**.
[150] S. Mädler, C. Bich, D. Touboul, R. Zenobi, *J. Mass Spectrom.* **2009**, 44, 694–706.

[151] K. Akaki, T. Mino, O. Takeuchi, *Bio Protoc.* **2022**, 12.

[152] L. Cui, Y. Ma, M. Li, Z. Wei, Y. Huan, H. Li, Q. Fei, L. Zheng, *Anal. Chem.* **2021**, 93, 4434–4440.

[153] P. Novak, G. H. Kruppa, *Eur. J. Mass Spectrom.* **2008**, 14, 355–365.

[154] A. Leitner, L. A. Joachimiak, P. Unverdorben, T. Walzthoeni, J. Frydman, F. Förster, R. Aebersold, *Proc. Natl. Acad. Sci. USA* **2014**, 111, 9455–9460.

[155] P. E. Dawson, T. W. Muir, I. Clark-Lewis, S. B. Kent, *Science* **1994**, 266, 776–779.

[156] C. S. Theile, M. D. Witte, A. E. M. Blom, L. Kundrat, H. L. Ploegh, C. P. Guimaraes, *Nat. Protoc.* **2013**, 8, 1800–1807.

[157] M. F. Bolukbasi, P. Liu, K. Luk, S. F. Kwok, A. Gupta, N. Amrani, E. J. Sontheimer, L. J. Zhu, S. A. Wolfe, *Nat. Commun.* **2018**, 9, 4856.

[158] G. T. Hermanson, *Bioconjugate Techniques*, Elsevier **2008**.

[159] H. C. Kolb, M. G. Finn, K. B. Sharpless, *Angew. Chem. Int. Ed.* **2001**, 40, 2004–2021.

[160] E. M. Sletten, C. R. Bertozzi, *Angew. Chem. Int. Ed.* **2009**, 48, 6974–6998.

[161] J. M. Thornton, *J. Mol. Biol.* **1981**, 151, 261–287.

[162] W. J. Wedemeyer, E. Welker, M. Narayan, H. A. Scheraga, *Biochem.* **2000**, 39, 4207–4216.

[163] M. Karimi, M. T. Ignasiak, B. Chan, A. K. Croft, L. Radom, C. H. Schiesser, D. I. Pattison, M. J. Davies, *Sci. Rep.* **2016**, 6, 38572.

[164] G. J. L. Bernardes, J. M. Chalker, J. C. Errey, B. G. Davis, *J. Am. Chem. Soc.* **2008**, 130, 5052–5053.

[165] D. Steinmann, O. Mozziconacci, R. Bommana, J. F. Stobaugh, Y. J. Wang, C. Schöneich, *Pharm. Res.* **2017**, 34, 2756–2778.

[166] R. L. M. van Montfort, M. Congreve, D. Tisi, R. Carr, H. Jhoti, *Nat.* **2003**, 423, 773–777.

[167] S. Ito, M. Sugumaran, K. Wakamatsu, *Int. J. Mol. Sci.* **2020**, 21, 6080–6109.

[168] M. Correia, M. T. Neves-Petersen, P. B. Jeppesen, S. Gregersen, S. B. Petersen, *PloS one* **2012**, 7, e50733.

[169] J. D. Figueroa, A. M. Zárate, E. Fuentes-Lemus, M. J. Davies, C. López-Alarcón, *RSC Adv.* **2020**, 10, 25786–25800.

[170] M. A. Ehudin, L. Senft, A. Franke, I. Ivanović-Burmazović, K. D. Karlin, *J. Am. Chem. Soc.* **2019**, 141, 10632–10643.

[171] X. Fu, J. L. F. Kao, C. Bergt, S. Y. Kassim, N. P. Huq, A. d'Avignon, W. C. Parks, R. P. Mecham, J. W. Heinecke, *J. Biol. Chem.* **2004**, 279, 6209–6212.

[172] L. B. Poole, *Free Radic. Biol. Med.* **2015**, 80, 148–157.

[173] L. Xue, I. A. Karpenko, J. Hiblot, K. Johnsson, *Nat. Chem. Biol.* **2015**, 11, 917–923.

[174] Y. Kim, H. B. Yi, K. Seo, H. S. Lee, I. Shin, *Trends Chem.* **2025**, 7, 240–254.

[175] D. N. Møller, C. Kofoed, M. B. Thygesen, K. J. Jensen, *J. Pept. Sci.* **2025**, 31, e70058.
[176] T. Hayashi, I. Hamachi, *Acc. Chem. Res.* **2012**, 45, 1460–1469.
[177] J. M. Chalker, G. J. L. Bernardes, B. G. Davis, *Acc. Chem. Res.* **2011**, 44, 730–741.
[178] J. Lotze, U. Reinhardt, O. Seitz, A. G. Beck-Sickinger, *Mol. BioSyst.* **2016**, 12, 1731–1745.
[179] S. Tuang, D. Dieppa-Matos, C. Zhang, C. R. Shugrue, P. Dai, A. Loas, B. L. Pentelute, *Chem. Commun.* **2021**, 57, 3227–3230.
[180] L. Fu, Z. Li, K. Liu, C. Tian, J. He, J. He, F. He, P. Xu, J. Yang, *Nat. Protoc.* **2020**, 15, 2891–2919.
[181] K. L. Diehl, I. V. Kolesnichenko, S. A. Robotham, J. L. Bachman, Y. Zhong, J. S. Brodbelt, E. V. Anslyn, *Nat. Chem.* **2016**, 8, 968–973.
[182] R. J. Spears, V. Chudasama, *Curr. Opin. Chem. Biol.* **2023**, 75, 102306.
[183] M. Ahangarpour, I. Kavianinia, M. A. Brimble, *Org. Biomol. Chem.* **2023**, 21, 3057–3072.
[184] Y. Liao, X. Jiang, *Explor. Drug Sci.* **2024**, 540–554.
[185] M. X. Sliwkowski, R. L. Levine, *Anal. Biochem.* **1985**, 147, 369–373.
[186] C. Zhang, E. V. Vinogradova, A. M. Spokoyny, S. L. Buchwald, B. L. Pentelute, *Angew. Chem. Int. Ed.* **2019**, 58, 4810–4839.
[187] M. D. Nolan, E. M. Scanlan, *Front. Chem.* **2020**, 8, 583272.
[188] B. Söveges, T. Imre, T. Szende, Á. L. Póti, G. B. Cserép, T. Hegedűs, P. Kele, K. Németh, *Org. Biomol. Chem.* **2016**, 14, 6071–6078.
[189] C. F. H. Allen, J. O. Fournier, W. J. Humphlett, *Can. J. Chem.* **1964**, 42, 2616–2620.
[190] C. E. Hoyle, A. B. Lowe, C. N. Bowman, *Chem. Soc. Rev.* **2010**, 39, 1355–1387.
[191] J. W. Chan, C. E. Hoyle, A. B. Lowe, *J. Am. Chem. Soc.* **2009**, 131, 5751–5753.
[192] G. Cianfoni, L. Pisano, D. M. Varouhaki, G. Centioni, A. Calcaterra, F. Ghirga, C. M. Athanassopoulos, B. Botta, S. Cammarone, P. Baiocco, D. Quaglio, *Biomacromolecules* **2026**, 27, 1024–1072.
[193] A. Michael, *J. Prakt. Chem.* **1887**, 35, 349–356.
[194] R. Zhang, B. Li, L. Dong, Z. Hu, X. Li, X. Yao, J. Zheng, A. Lin, S. Gao, T. Hang, X. Wu, Q. Chu, *Org. Lett.* **2024**, 26, 8951–8955.
[195] S. Arumugam, J. Guo, N. E. Mbua, F. Friscourt, N. Lin, E. Nekongo, G.-J. Boons, V. V. Popik, *Chem. Sci.* **2014**, 5, 1591–1598.
[196] M. C. Puljung, W. N. Zagotta, *Curr. Protoc. Protein Sci.* **2012**, Chapter 14, 14.14.1-14.14.10.
[197] Y. Kim, S. O. Ho, N. R. Gassman, Y. Korlann, E. V. Landorf, F. R. Collart, S. Weiss, *Bioconjugate Chem.* **2008**, 19, 786–791.
[198] S. B. Hansen, K. R. Andersen, *Methods Mol. Biol.* **2022**, 2446, 327–343.

[199] L. K. Chaganti, N. Venkatakrishnan, K. Bose, *Biosci. Rep.* **2018**, 38, 1–8.
[200] L. Petri, P. A. Szijj, Á. Kelemen, T. Imre, Á. Gömöry, M. T. W. Lee, K. Hegedűs, P. Ábrányi-Balogh, V. Chudasama, G. M. Keserű, *RSC Adv.* **2020**, 10, 14928–14936.
[201] J. Larson, M. Tokmina-Lukaszewska, J. Malone, E. J. Hasenoehrl, W. Kelly, X. Fang, A. White, A. Patterson, B. Bothner, *Int. J. Mol. Sci.* **2025**, 26.
[202] W. Cao, J. C. Maza, N. Chernyak, J. A. Flygare, S. W. Krska, F. D. Toste, M. B. Francis, *Bioconjugate Chem.* **2023**, 34, 510–517.
[203] A. Hameau, S. Fuchs, R. Laurent, J.-P. Majoral, A.-M. Caminade, *Beilstein J. Org. Chem.* **2011**, 7, 1577–1583.
[204] C. Hao, Y. Wang, G. Wang, Z. Zhu, *Appl. Sci.* **2020**, 10, 1134.
[205] F. A. Luzzio, *Tetrahedron* **2012**, 68, 5323–5339.
[206] C. Sell, *Perfumery Materials of Natural Origin Perfumery*, Royal Society Of
[207] P. Sundararaman, W. Herz, *J. Org. Chem.* **1977**, 42, 813–819.
[208] J. H. Babler, M. J. Coghlan, *Synth. Commun.* **1976**, 6, 469–474.
[209] A. Riahi, F. Hénin, J. Muzart, *Tetrahedron Lett.* **1999**, 40, 2303–2306.
[210] M. Shibuya, M. Tomizawa, Y. Iwabuchi, *J. Org. Chem.* **2008**, 73, 4750–4752.
[211] H. Cong, Q. Chen, Q. Geng, Z. Tao, T. Yamato, *Chin. J. Chem.* **2015**, 33, 545–549.
[212] N. R. Gade, V. Devendram, M. Pal, J. Iqbal, *Chem. Commun.* **2013**, 49, 7926–7928.
[213] P. Gao, H.-J. Chen, Z.-J. Bai, M.-N. Zhao, D. Yang, J. Wang, N. Wang, L. Du, Z.-H. Guan, *J. Org. Chem.* **2020**, 85, 7939–7951.
[214] K. C. Nicolaou, C. J. N. Mathison, T. Montagnon, *Angew. Chem. Int. Ed.* **2003**,
[215] S. Kumar, N. Ahmed, *Green Chem.* **2016**, 18, 648–656.
[216] X. Chen, Y. Zhang, H. Wan, W. Wang, S. Zhang, *Chem. Commun.* **2016**, 52, 3532–3535.
[217] S. L. Bartlett, C. M. Beaudry, *J. Org. Chem.* **2011**, 76, 9852–9855.
[218] M. Shibuya, S. Ito, M. Takahashi, Y. Iwabuchi, *Org. Lett.* **2004**, 6, 4303–4306.
[219] R. Obermüller, H. Tobisch, L. Stockhammer, M. Waser, *Org. Process Res. Dev.* **2024**, 28, 3735–3744.
[220] M. Elsherbini, W. J. Moran, *J. Org. Chem.* **2023**, 88, 1424–1433.
[221] M. Uyanik, R. Fukatsu, K. Ishihara, *Org. Lett.* **2009**, 11, 3470–3473.
[222] M. Mülbaier, A. Giannis, *Angew. Chem. Int. Ed.* **2001**, 40, 4393.
[223] W.-J. Chung, D.-K. Kim, Y.-S. Lee, *Synlett* **2005**, 2175–2178.
[224] H.-S. Jang, Y.-H. Kim, Y.-O. Kim, S.-M. Lee, J. W. Kim, W.-J. Chung, Y.-S. Lee, *J. Ind. Eng. Chem.* **2014**, 20, 29–36.
[225] Z. Lei, C. Denecker, S. Jegasothy, D. C. Sherrington, N. Slater, A. J. Sutherland, *Tetrahedron Lett.* **2003**, 44, 1635–1637.

[226] K. Bensberg, A. Gómez-Suárez, S. F. Kirsch, *Chem. Eur. J.* **2025**, 31, e202500670.
[227] G. Sorg, A. Mengel, G. Jung, J. Rademann, *Angew. Chem. Int. Ed.* **2001**, 40, 4395.
[228] A. P. Thottumkara, T. K. Vinod, *Tetrahedron Lett.* **2002**, 43, 569–572.
[229] A. Kommreddy, M. S. Bowsher, M. R. Gunna, K. Botha, T. K. Vinod, *Tetrahedron Lett.* **2008**, 49, 4378–4382.
[230] J. N. Moorthy, N. Singhal, K. Senapati, *Tetrahedron Lett.* **2008**, 49, 80–84.
[231] R. D. Richardson, J. M. Zayed, S. Altermann, D. Smith, T. Wirth, *Angew. Chem. Int. Ed.* **2007**, 46, 6529–6532.
[232] A. Y. Koposov, D. N. Litvinov, V. V. Zhdankin, M. J. Ferguson, R. McDonald, R. R. Tykwinski, *Eur. J. Org. Chem.* **2006**, 2006, 4791–4795.
[233] N. N. Reed, M. Delgado, K. Hereford, B. Clapham, K. D. Janda, *Bioorg. Med. Chem. Lett.* **2002**, 12, 2047–2049.
[234] B. M. Bizzarri, I. Abdalghani, L. Botta, A. R. Taddei, S. Nisi, M. Ferrante, M. Passacantando, M. Crucianelli, R. Saladino, *Nanomaterials* **2018**, 8, 1–13.
[235] Y.-H. Kim, H.-S. Jang, Y.-O. Kim, S.-D. Ahn, S. Yeo, S.-M. Lee, Y.-S. Lee, *Synlett* **2013**, 24, 2282–2286.
[236] J. Yoshida, Y. Takahashi, A. Nagaki, *Chem. Commun.* **2013**, 49, 9896–9904.
[237] S. Kobayashi, *Chem. Asian J.* **2016**, 11, 425–436.
[238] C. A. Hone, C. O. Kappe, *Chem. Methods* **2021**, 1, 454–467.
[239] E. M. Luteran, M. R. Aloisi, W. L. Akerley, R. D. Gilbertson, *Curr. Res. Biotechnol.* **2025**, 10, 100327.
[240] A. Naramittanakul, S. Buttranon, A. Petchsuk, P. Chaiyen, N. Weeranoppanant, *React. Chem. Eng.* **2021**, 6, 1771–1790.
[241] C. Rodríguez-Escrich, M. A. Pericàs, *Chem. Rec.* **2019**, 19, 1872–1890.
[242] N. Sugisawa, H. Nakamura, S. Fuse, *Catalysts* **2020**, 10, 1321.
[243] F. Ballaschk, S. F. Kirsch, *Green Chem.* **2019**, 21, 5896–5903.
[244] M. Tapera, A. Savvidis, C. Meysing, A. Gómez-Suárez, S. F. Kirsch, *Org. Lett.* **2026**, 28, 681–685.
[245] K. Bensberg, A. Savvidis, F. Ballaschk, A. Gómez-Suárez, S. F. Kirsch, *Chem. Eur. J.* **2024**, 30, e202304011.
[246] Y. Li, J. Li, Z. Shen, H. Kuang, Q. Zuo, G. Bao, J. Ni, W. Sun, R. Wang, *ACS Cent. Sci.* **2025**, 11, 1240–1249.
[247] S. Rajput, K. J. McLean, H. Poddar, I. R. Selvam, G. Nagalingam, J. A. Triccas, C. W. Levy, A. W. Munro, C. A. Hutton, *J. Med. Chem.* **2019**, 62, 9792–9805.
[248] P. F. Fitzpatrick, *Annu. Rev. Biochem.* **1999**, 68, 355–381.

[249] M. Falkenstein, D. Reiner-Link, A. Zivkovic, I. Gering, D. Willbold, H. Stark, *Bioorg. Med. Chem.* **2021**, 50, 116462.

[250] Z. Zhang, Z. Ding, J. Yang, Y. Zhao, Z. Zhao, C. Liu, N. Metanis, J. Zhao, *Org. Chem. Front.* **2024**, 11, 7199–7204.

[251] A. Rezaeifard, M. Jafarpour, A. Farrokhi, S. Parvin, F. Feizpour, *RSC Adv.* **2016**, 6, 64640–64650.

[252] H. China, N. Kageyama, H. Yatabe, N. Takenaga, T. Dohi, *Molecules* **2021**, 26.